Ion transport across thylakoid membranes in Chlamydomonas reinhardtii

Marcio Rodrigues Azevedo

THESE DE DOCTORAT

NNT : 2023UPASB016

université PARIS-SACLAY

Ion transport across thylakoid membranes in *Chlamydomonas reinhardtii*.

Les transports d'ions à travers la membrane du thylacoïde chez *Chlamydomonas reinhardtii*.

Thèse de doctorat de l'université Paris-Saclay

École doctorale n°567 : sciences du végétal : du gène à l'écosystème (SEVE)
Spécialité de doctorat : Biologie
Graduate School : BioSphERA,
Référent : Faculté des sciences d'Orsay

Thèse préparée dans l'unité de recherche
Biologie du Chloroplaste et Perception de la Lumière chez les Micro-algues (Sorbonne-Université, CNRS),
sous la direction de **Catherine de VITRY**, Directrice de recherche CNRS,
et le co-encadrement de **Benjamin BAILLEUL**, Chargé de recherche CNRS.

Thèse soutenue à Paris, le 20 mars 2023, par

Marcio RODRIGUES-AZEVEDO

Composition du Jury

Sébastien THOMINE Directeur de recherche, CNRS - Université Paris-Saclay	Président
Giovanni FINAZZI Directeur de recherche, CNRS - Université Grenoble	Rapporteur
Xenie JOHNSON Directrice de recherche, CEA - Université Aix Marseille	Rapporteure & examinatrice
Marion EISENHUT Research associate, UNIVERSITAT BIELEFELD - Faculty of Biology / Computational Biology	Examinatrice

université PARIS-SACLAY

ÉCOLE DOCTORALE
Sciences du végétal : du gène à l'écosystème (SEVE)

Titre : Les transports d'ions à travers la membrane du thylacoïde chez *Chlamydomonas reinhardtii*.

Mots clés : Photosynthèse, thylacoïde, *Chlamydomonas reinhardtii*, transporteurs d'ions.

Résumé : Dans la photosynthèse oxygénique, l'oxydation de l'eau par le photosystème II (PSII) est catalysée par un cluster de manganèse et la force motrice protonique (PMF) générée par le transfert d'électrons le long de la membrane du thylacoïde est dissipée principalement par l'ATP synthase du chloroplaste. Un crible basé sur la photosensibilité du PSII a été entrepris chez *Chlamydomonas reinhardtii*. Ce travail de thèse a permis l'isolation d'un mutant du principal transporteur de manganèse à travers la membrane du thylacoïde CGLD1/PAM71 et de nouveaux mutants de l'ATP synthase du chloroplaste.

Ces derniers démontrent l'exigence de l'hétérodimère AtpF-ATPG comme tige périphérique et la stabilisation de l'ARNm atpE par la protéine OPR MDE1. L'étude de la PMF à travers la membrane thylacoïde chez les mutants dépourvus de l'ATP synthase du chloroplaste révèle une voie alternative pour la dissipation de la PMF ne dépendant pas strictement de l'antiporteur échangeur proton/cation K^+ 3 (KEA3).

Title: Ion transport across thylakoid membranes in *Chlamydomonas reinhardtii*.

Keywords: Photosynthesis, thylakoid, *Chlamydomonas reinhardtii*, ion transporters.

Abstract: In oxygenic photosynthesis, light-driven oxidation of water by photosystem II (PSII) is catalyzed by a manganese cluster and the proton motive force (PMF) generated by the electron transfer along the thylakoid membrane is dissipated mainly by the chloroplast ATP synthase coupled to ATP synthesis. The screen based on light PSII photosensitivity undertook in *Chlamydomonas reinhardtii* during this PhD thesis led to the isolation of a mutant of the main manganese transporter across the thylakoid membrane CGLD1/PAM71 required for an efficient PSII donor side and of novel chloroplast ATP synthase mutants.

The latter demonstrate the requirement of AtpF-ATPG heterodimer as the peripheral stalk and the stabilization of atpE mRNA by the OPR protein MDE1. The study of the fate of the PMF across the thylakoid membrane in mutants lacking the chloroplast ATPase reveals an alternative pathway for PMF dissipation not strictly dependent on proton/cation K^+ exchange antiporter 3 (KEA3).

Autres tutelles & financements

Institut de Biologie Physico-Chimique.

Biologie du chloroplaste et Perception de la Lumière chez les Micro-algues (UMR 7141)

Centre National de la Recherche Scientifique

Sorbonne-Université

ERC
Starting Grant PhotoPHYTOMICS
ERC-2016-STG, #715579

Les Fondations Edmond de Rothschild

Labex Dynamo

Cette page a été laissée intentionnellement vide
This page was intentionally left blank

RESUME EN FRANÇAIS – ABSTRACT IN FRENCH.

Dans la photosynthèse oxygénique, la lumière permet d'activer les centres réactionnels des photosystèmes. Au niveau du photosystème II (PSII), cela se traduit par l'excitation de la paire de chlorophylles du centre réactionnel P680 le menant à un état instable, noté P680*. Elle va alors, pour retourner à un état stable, réaliser la photochimie : transférer un électron à des accepteurs d'électrons : la phéophytine puis la quinone fixe Q_A. Si elle est dans l'incapacité de le faire, la P680* va quand même pouvoir se désexciter en créant de la fluorescence ou en libérant de la chaleur.

De proche en proche, les électrons arrachés à P680 sont transportés le long de la chaine de transfert d'électrons au travers des différents complexes multiprotéiques impliqués dans la photosynthèse au sein de la membrane du thylacoïde, à savoir le PSII, le cytochrome b_6f, et le PSI, pour aboutir finalement à la formation de NADPH, ensuite utilisé par le cycle de Calvin pour fixer le dioxyde de carbone (CO_2).

L'électron initialement perdu par P680 sera ensuite restitué via l'oxydation du donneur secondaire, un résidu de tyrosine (Y_Z) de la sous-unité D1, et enfin par le cluster de manganèse Mn_4O_5Ca qui est protégé du côté luménal par trois protéines extrinsèques (PsbO, PsbP, PsbQ). Ce cluster va catalyser l'oxydation de l'eau, en libérant du dioxygène (O_2) et des protons (H^+) dans le lumen du thylacoïde.

Le transfert d'électrons à travers la membrane du thylacoïde va aussi permettre, au niveau du cytochrome b_6f, une entrée supplémentaire de protons dans le lumen, ce qui va engendrer une augmentation du gradient électrochimique de protons : la force proton motrice (PMF). Cette PMF a deux composantes : la différence de potentiel électrique à travers la membrane du thylacoïde, notée $\Delta\Psi$ et le gradient de concentration de protons, ΔpH. Le $\Delta\Psi$ va augmenter quand une molécule chargée positivement va entrer dans le lumen, et à l'inverse décroitre quand cette charge positive quitte le thylacoïde ; sur le même principe, une charge négative va faire exactement l'inverse. Ces deux composantes vont de manière combinée provoquer

l'activation de l'ATP synthase du chloroplaste, et lui permettre de générer de l'ATP en dissipant la PMF par le passage de protons du lumen vers le stroma.

L'ATP synthase, aussi appelée historiquement CF_1F_O, est un complexe multiprotéique dont les nombreuses sous-unités sont codées par des gènes d'origine multiple : soit nucléaire soit chloroplastique. De plus, l'expression des sous-unités de ce complexe codées par le génome chloroplastique est sous l'égide d'une régulation post-transcriptionnelle gouvernée par le génome nucléaire.

La régulation de la photosynthèse englobe de nombreux aspects, et de nombreux facteurs. Tout cela nécessite une orchestration minutieuse des éléments impliqués, notamment le transfert des ions à travers la membrane du thylacoïde, puisque ces derniers existent en tant que cofacteurs des nombreuses sous-unités des complexes photosynthétiques, permettant de nombreuses fonctions biologiques d'importance capitale. On peut par exemple citer les métaux comme le Mn^{2+} ou le Fe^{2+} nécessaires à la formation et au bon fonctionnement des complexes photosynthétiques, le Mg^{2+} pour la formation des pigments de chlorophylle, etc… De plus, tous ces ions sont des molécules chargées, et peuvent donc influer sur le potentiel de membrane, et ainsi moduler l'activité de tous ces processus.

Un crible de fluorescence permettant de mettre en évidence la photosensibilité du PSII a été entrepris sur des mutants de l'algue verte *Chlamydomonas reinhardtii* obtenus par mutagénèse aléatoire. Le travail réalisé lors de cette thèse a permis (1) d'isoler un mutant du principal transporteur de Mn^{2+} à travers la membrane du thylacoïde à savoir le canal ionique CGLD1, homologue de PAM71 et d'en approfondir ainsi la caractérisation. (2) de mettre en évidence de nouveaux mutants de l'ATP synthase du chloroplaste. De plus, l'étude de ces mutants d'ATP synthase a permis (3) de révéler l'existence d'une voie alternative de la dissipation de la PMF à travers le thylacoïde.

1). Le mutant photosensible *cgld1-KO* a une insertion dans le premier exon du gène cgld1, créant ainsi un décalage dans le cadre de lecture et aboutissant à une protéine tronquée. L'étude de ce mutant a permis de démontrer, par des approches

biophysiques et biochimiques notamment, que la limitation du manganèse du côté luménal du thylacoïde conduit à une hétérogénéité parmi les centres PSII. Une fraction des centres PSII ayant des clusters de manganèse pleinement fonctionnels tandis qu'une autre fraction des centres PSII présente un spectre de clusters de manganèse partiellement ou non assemblés.

Ainsi, on aurait dans ce mutant une portion de PSII pleinement actifs, capables de produire de l'oxygène alors que les PSII altérés dans les clusters de manganèse sont capables de réaliser une séparation de charge primaire sans pour autant pouvoir produire d'oxygène. En présence de DCMU, un inhibiteur du côté accepteur du PSII, le mutant montre, lors d'une illumination, une augmentation rapide de la fluorescence qu'on attribue à la fraction active de PSII, et une montée lente – par ailleurs observée chez le sauvage lors d'une carence en manganèse – attribuée à la fraction altérée des centres PSII. Cette phase lente serait due à une grande probabilité de recombinaison de charge au sein des centres altérés.

Tout cela porte à croire qu'un transport de Mn^{2+} à travers le thylacoïde malgré l'absence de CGLD1 est toujours présent. Nous suggérons que ce transfert puisse se faire par l'intermédiaire de métallochaperones du Mn^{2+} lors de leur translocation à travers la membrane du thylacoïde par la voie TAT (Twin-Arginine Translocation), qui permet le passage de protéines repliées avec leurs cofacteurs.

2). En utilisant des cribles de fluorescence et l'édition génomique via CRISPR-Cas9, plusieurs mutants de l'ATP synthase ont ainsi été isolés. Ces approches ont permis d'isoler le mutant manquant des sous-unités de l'ATP synthase du chloroplaste ; *ATPG*. Nous avons ainsi pu mettre en évidence la nécessité de l'existence de l'hétérodimère ATPG-AtpF (les sous-unités *b* et *b'* de la tige de l'ATP synthase) pour l'assemblage de l'ensemble du complexe. De plus, nous avons obtenu des mutants de *MDE1* établissant cette protéine octatricopeptidique comme un facteur essentiel dans la stabilisation des transcrits du gène chloroplastique *atpE* codant la sous-unité ε de l'ATP synthase. En effet, MDE1 se fixerait au niveau du 5'UTR de ce transcrit, et le protégerait d'une activité exonucléase 5'-3'.

Par ailleurs, nous avons croisé les mutants *atpH* et *fsth1-1* du laboratoire, mutés respectivement dans la sous-unité H du rotor et FtsH, la principale protéase des membranes du thylacoïde. Cela nous a permis de démontrer que la sous-unité transmembranaire AtpH, formant le canal à travers la membrane du thylacoïde par lequel les protons peuvent passer, s'avère être un substrat de la protéase FtsH. Cela suggère que cette protéase est significativement impliquée dans l'accumulation concertée des sous-unités de l'ATP synthase.

3). Nous avons étudié ces mutants de l'ATP synthase récemment obtenus et ceux déjà présents au laboratoire à travers des techniques de biophysique permettant l'étude de la PMF : Le potentiel électrique ($\Delta\Psi$) affecte le spectre d'absorption des pigments présents dans la membrane du thylacoïde, et cette propriété (Electro-Chromic Shift) nous permet d'analyser *in vivo* des processus photosynthétiques.

Chez des mutants dépourvus d'ATP synthase chloroplastique, nous avons été surpris d'observer un déclin rapide de PMF après des pulses de lumière intense. Cela met en évidence l'existence d'une autre voie alternative pour dissiper la PMF, différente de la translocation des protons via l'ATP synthase.

Le dernier chapitre analyse les caractéristiques biophysiques de cette voie alternative. L'étude d'un double mutant d'un transporteur de potassium (K^+) dans un contexte sans ATP synthase montre que la dissipation dépend mais n'est pas strictement dépendante de l'antiporteur échangeur proton/cation K^+ du thylacoïde (KEA3).

ABSTRACT IN ENGLISH – RÉSUMÉ EN ANGLAIS.

In oxygenic photosynthesis, light activates the reaction centers of the photosystems, which leads to photochemistry: At the level of photosystem II (PSII) this results in the excitation of the chlorophyll oh the pair of chlorophylls in the reaction center P680 leading it to an unstable state, noted P680*. In order to return back to their ground state, P680* will transfer an electron to an electron acceptor: a quinone. Step by step, electrons are transported along the electron transfer chain through the different multiprotein complexes involved in photosynthesis within the thylakoid membrane. The donor side of photosystem II (PSII) is composed of a manganese cluster consisting of manganese, oxygen and Calcium (Mn_4O_5Ca), which will catalyze the oxidation of water, releasing oxygen and protons into the thylakoid lumen. The transfer of electrons through the thylakoid membrane will also allow additional entry of protons into the lumen, which will generate an increase of the protomotive force (PMF). This PMF will be dissipated mainly by the chloroplast ATP synthase, a multiprotein complex whose subunits are encoded by genes of multiple origin: either nuclear or chloroplastic, and whose regulation is controlled by the nuclear genome.

A screen based on the photosensitivity of PSII was undertaken on mutants of the green alga *Chlamydomonas reinhardtii* obtained by random mutagenesis. The work carried out during this thesis allowed (1) the isolation and further characterization of the main Mn^{2+} transporter across the thylakoid membrane, namely the ion channel CGLD1, homologous to PAM71, (2) the identification of new mutants of the chloroplastic ATP synthase. Furthermore, the study of these ATP synthase mutants revealed (3) the existence of an alternative pathway of PMF dissipation.

1). The light-sensitive mutant *cgld1-KO*, with an insertion in the first exon of the CGLD1 gene, creating a shift in the reading frame and resulting in a truncated protein, was characterized. The study of this mutant grown in low light demonstrated, by biophysical and biochemical approaches, a heterogeneity of the manganese clusters within the PSII. A portion of the PSII centers is fully active while another fraction is only

partially active. This indicates that Mn^{2+} transport is still present. The contribution to this transport of Mn^{2+} metallochaperones translocated across the thylakoid membrane by the TAT (Twin-Arginine Translocation) pathway that allows the passage of folded proteins with their cofactors is proposed.

2). Using fluorescence screens and CRISPR-Cas9 editing, ATP synthase mutants were isolated. These approaches provided the missing mutant of the chloroplast ATP synthase subunits, *ATPG*, and showed that the AtpF-ATPG heterodimer is required as peripheral stalk. In addition, the identification of the nucleus-encoded *MDE1* gene, established this octatricopeptide protein as an essential factor in stabilizing the chloroplast-encoded *atpE* gene transcripts. Finally, the AtpH subunit was found to be a substrate for the thylakoid protease FtsH and suggests that this protease significantly contributes to the concerted accumulation of ATP synthase subunits.

(3). The study of ATP synthase mutants prompted us to explore the properties of their protomotive force (PMF) across the thylakoid membrane through biophysical techniques: The electric potential (ΔΨ) affects the absorption spectrum of the pigments present in the thylakoid membrane, and this property (Electro-Chromic-Shift) allows us to study and analyze photosynthetic processes *in vivo*.

In these mutants lacking chloroplast ATP synthase, we were able to highlight an alternative pathway to dissipate PMF. The last chapter shows the biophysical characteristics of this alternative pathway that is not strictly dependent on the thylakoid proton/ K^+ exchange antiporter (KEA3).

SOMMAIRE - TABLE OF CONTENTS

REMERCIEMENTS – ACKNOWLEDGMENTS.

Je remercie profondément Catherine, pour avoir dirigé ma thèse et avoir su me montrer et m'enseigner tant de choses sur la biochimie, la physiologie de *Chlamydomonas* et la minutie nécessaire en microbiologie. Merci à Benjamin, qui m'a montré le monde complexe et passionnant de la biophysique au laboratoire, mais aussi pour toutes nos discussions sur tout et rien (et les prêts de livres que je peux enfin lire). Je remercie absolument tous les membres du laboratoire pour avoir partagé leur immense savoir, pour tout ce que j'ai appris au cours de ces magnifiques années de thèse :

À tous mes '*jeunes*' collègues du laboratoire (les thésards et post-docs), partis ou qui resteront encore après moi, et dont la liste est trop longue pour tous les citer.

Et aussi tous les '*vieux*' qui ont partagé leur longue expérience. Un merci particulier à Francis-André Wollman et Pierre Joliot avec qui j'aurais partagé de précieux moments à discuter de biophysique, de science(s) et bien plus.

Je remercie chaleureusement tous les gens de mon entourage : famille, ami.e.s et plus qui auront été les piliers, les béquilles, les épaules, qui m'auront soutenu et supporté à tout moment de cette thèse, même les plus difficiles.

Merci aussi aux membres de mon comité de thèse, Alain, Frédéric et Pierre, qui ont été un soutien incroyablement utile et m'auront donné de très précieux conseils. À Marianne Delarue aussi, qui m'a aidé et soutenu dans toutes mes démarches liées à l'administration et le fonctionnement de l'université pour me permettre de venir à bout de cette thèse.

Finalement, un " je vous adore" couplé à un "je vous déteste", à toutes mes petites *chlamy* que j'aurais torturées, mais qui me l'auront bien rendu… malgré tout, votre belle robe verte dans vos Erlens dansants restera à jamais gravée dans ma mémoire.

Bref, un simple « Merci à tous ! *Sauf toi là-bas derrière !* »

Cette thèse a été rendue possible grâce à la bourse ministérielle de Paris-Saclay dans l'École Doctorale SEVE (ED567 - Sciences du végétal, du gène à l'écosystème), le Centre National de la Recherche Scientifique (CNRS) et Sorbonne-Université (SU) (soutiens de base de l'Unité Mixte de Recherche 7141), le programme 'Initiative d'excellence' de l'état français (Labex "DYNAMO", ANR-11-LABX-0011-01), les Fondations de Rothschild et l'ERC PhotoPHYTOMICS. Ma thèse a été subventionnée par le contrat doctoral de l'ED SEVE d'octobre 2018 à février 2022, par la fondation Edmond de Rothschild de mars à mai 2022, et par l'ERC PhotoPHYTOMICS (ERC-2016-STG grant #715579) de juin à décembre 2022 qui a subventionné principalement le travail lié au chapitre 4 par le Working Package 2 (WP2) de l'ERC.

Cette page a été laissée intentionnellement vide
This page was intentionally left blank

CHAPTER 1:

GENERAL INTRODUCTION

General Introduction

Life as we know it today probably began and developed from chemosynthetic organisms in specific niches where H_2 and organic compounds accumulated in great amounts (Lane et al., 2010; Sousa et al., 2013). It now heavily relies on oxygenic photosynthesis that can be defined as the absorption by plants, algae and cyanobacteria of light, and the conversion and storage of its energy into organic compounds such as sugars but also the creation of oxygen as a byproduct (Martin et al., 2018). The primary source of sustenance for most living organisms are these molecules, so organisms either had to produce it themselves or take it from a primary producer.

1.1 Emergence and evolution of photosynthesis

Photosynthesis, as we know it, is the result of complex and successive steps, from simple biological processes into the actual complex machinery we learned so much about over time and yet, still have so much to discover.

It is only present in 2 of the 3 fundamental domains of life, i.e. Bacteria and Eukaryota while almost none has been found in Archæa (although halobacteria perform a kind of photosynthesis *stricto sensu*, (Fuhrman et al., 2008)). It derives from an anoxygenic photosynthetic process in purple bacteria, then came the oxygenic photosynthesis which has since greatly spread and shaped the world differently (Dyall et al., 2004; Lyons et al., 2014; Sanchez-Baracaldo & Cardona, 2019) (Figure 1-1). These organisms released oxygen into the atmosphere, forcing life to adapt to these new and quite stringent conditions, as oxygenic compounds are highly reactive molecules.

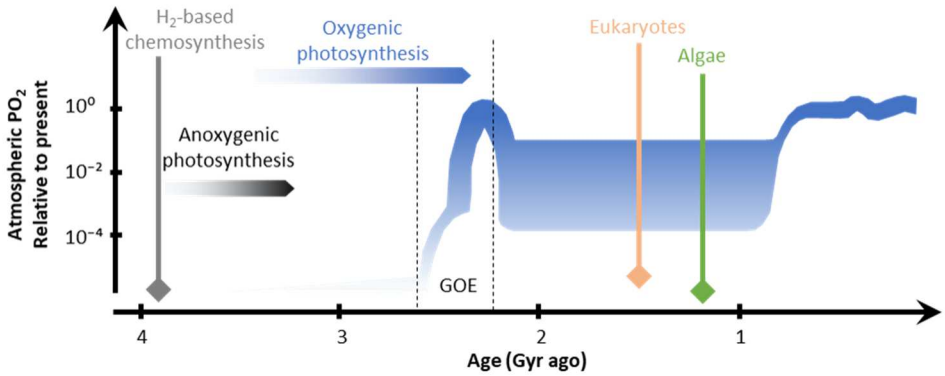

Figure 1-1 Evolution of Earth's atmospheric content through time.
Estimation of relative atmospheric partial pressure of O_2 relative to present atmospheric level. The blue form comprises highest and lowest estimations. GOE: Great oxidation event. Eukaryotes appeared ~1.5 Gya, and Algae ~1.2 Gya. Adapted from Lyons et al, 2014 and Dyall et al, 2004.

1.1.1 Anoxygenic photosynthesis

The most ancient process of photosynthesis is the anoxygenic photosynthesis in which there is no production of oxygen. These organisms take their electrons from other molecules than water (H_2 H_2S, succinate, malate…). These processes are specifically found in the bacteria domain, in organisms such as purple bacteria, green filamentous bacteria, green sulfur bacteria or heliobacteria (Hanada, 2016; Kushkevych et al., 2021). This process relies on specific pigments which are bacteriochlorophylls.

1.1.2 Oxygenic photosynthesis

Oxygenic photosynthesis (hereafter called photosynthesis) is found in bacteria and eukaryotes, and what distinguishes it from anoxic photosynthesis is that the electron to undergo the molecular process of photosynthesis comes from water, resulting in the production of oxygen as a by-product, hence the name. The first organisms to have used such mechanisms are presumed to be cyanobacteria appearing ~3 Gya in an anoxic atmosphere. The apparition of these organisms is responsible for the apparition of O_2 in the atmosphere and notably of the great oxygenation event (GOE) (*Figure 1-1*). These bacterial molecular mechanics rely heavily on pigments such as chlorophyll *a* and phycobilisomes, inserted in highly specialized protein complexes.

Prokaryotes are not the only organisms using photosynthesis: there are 3 classes of photosynthetic eukaryotes stemming from primary endosymbiosis (see below), each with different pigments:

- Viridiplantae: the green lineage comprising land plants and green algae. They contain chlorophyll *a* and chlorophyll *b*.
- Rhodophytes: the red algae, containing chlorophyll and phycobilisomes.
- Chromophytes: brown algae and diatoms that contain chlorophyll *a* and chlorophyll *c*.

Well studied and known now, photosynthesis can be simplified as:

$$CO_2 + H_2O \xrightarrow{+photons} [CH_2O] + O_2$$

This process uses the energy of light to transfer electrons from water to CO_2, the final acceptor. This reduction allows photosynthetic organisms to use CO_2 as carbon source to grow and sustain their metabolism.

1.1.3 The endosymbiotic theory and chloroplasts

Just like mitochondria came from α-proteobacteria, the chloroplasts in eukaryotes come from endosymbiosis (Margulis, 1971; Ponce-Toledo et al., 2019). An ancestral cyanobacteria entered a heterotroph eukaryotic cell (most probably through phagocytosis) and ended up as an essential organelle of the host cell. There have been several events leading to the current diversity of photosynthetic organisms (Figure 1-2):

- Primary endosymbiosis, the first event in which a eukaryote engulfed and assimilated a cyanobacteria. From this event came the Viridiplantae, the glaucophytes and the rhodophytes which form together the archaeplastida. Virtually all photosynthetic eukaryotes derive from this primary endosymbiosis, but it is to note that another independent primary endosymbiosis happened: It is the most recent event and shows the integration of a *Synechococcus*-like cyanobacteria into cercozoan amoebae from the *Paulinella* clade. (Marin et al., 2005).
- Secondary endosymbiosis, when a heterotroph eukaryote taking in a rhodophyte led to the advent of brown algae, diatoms or the euglena's ancestor.

– Tertiary endosymbiosis, when a secondary endosymbiont was engulfed and resulted in the apparition of dinoflagellates (fresh water or marine phytoplankton).

The endosymbiosis explains why the chloroplast is the subcellular location where photosynthesis takes place in photosynthetic cells. These chloroplasts are a highly specialized state of plastids, with a high content of photosynthetic pigments such as chlorophylls.

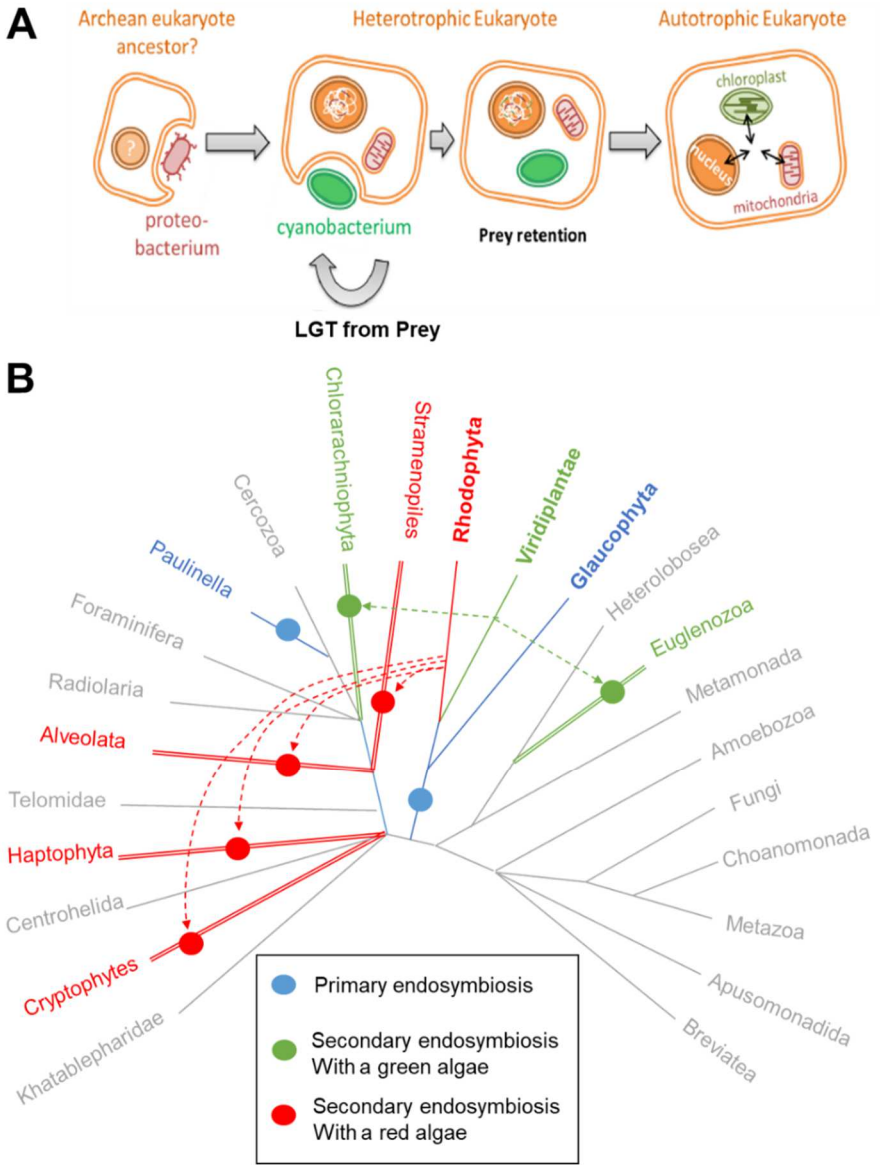

Figure 1-2 Diversity of photosynthesis.
(A) Simplified cartoon of the primary endosymbiosis event. LGT: lateral gene transfer. (B) Distribution of photosynthesis in eukaryotes with endosymbiotic events (circles). Simple lines define organisms resulting from a primary endosymbiotic event; double lines, organisms resulting from secondary endosymbiosis with dashed lines showing original lineage of secondary endosymbiosis (green or red algae); non photosynthetic organisms in grey. Adapted from Ponce-Toledo et al., 2019.

Chloroplasts are usually quite small (up to 10µm) and are encased in a double membrane envelope (for those resulting from a primary endosymbiosis; 4 membranes for most of the ones resulting from secondary endosymbiosis) separating the cytosol from the interior of the chloroplast. These membranes result from the phagocytosis and correspond to the parental cyanobacterial cell wall, viewed as prey, and the vesicular membrane of the host. The envelope is made of two sets of lipid bilayer membranes called outer and inner envelope membranes and an intermembrane space (Figure 1-3). While the outer membrane is very permeable to small molecules, the inner membrane is far more stringent and selective. Furthermore, proteins must be imported into the chloroplast, as much of the genome of the cyanobacterial progenitor of the chloroplast has been transferred to the nucleus through horizontal gene transfer. Most of these enter the chloroplast by the TOC/TIC importers (Jarvis & Soll, 2002).

The inner membrane of the envelope delimitates an alkaline compartment called the stroma in which can be found the chloroplast genome but also some of the protein, pigments, starch and lipid synthesis machineries. It is in this space that we find all necessary elements for photosynthesis: enzymes of the Calvin-Benson cycle (CBC) responsible for the so called 'dark phase' of photosynthesis, but also the thylakoids, inside which takes place the 'light phase'.

Thylakoids are flat disc-like sacs which provide an extended set of membranes sometimes stacked in supramolecular structures called grana (in land plants mostly) separated by unstacked membranes called the lamellae, or non-appressed membranes. The continuous aqueous space inside these thylakoids is called the lumen. Anchored in the membranes of the thylakoids are found the four multi-protein complexes that use the energy of light to create ATP and NADPH (Figure 1-3).

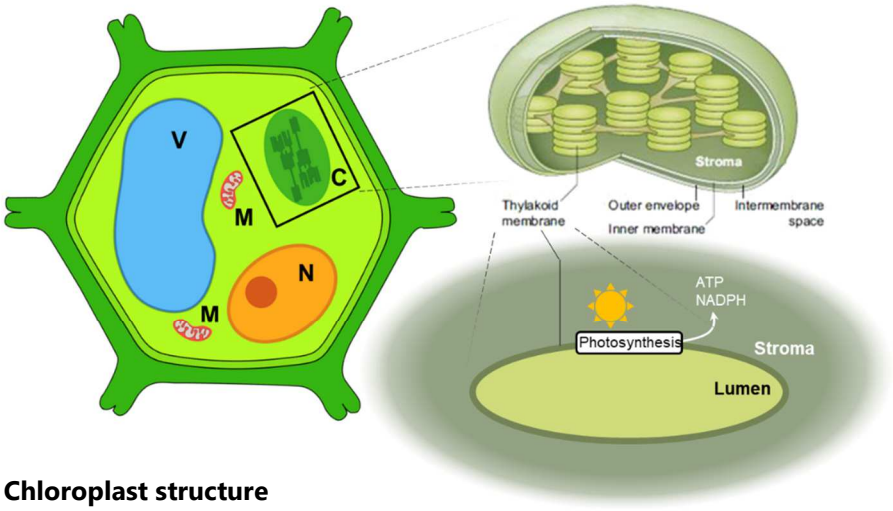

Figure 1-3 Chloroplast structure
Exploding diagram of a plant cell. With a simplified representation of higher plants' cell (left), chloroplast structure (top right) and thylakoid (bottom right) showing production of ATP and NADPH into the stroma when the photosynthetic apparatus embedded in the membrane is exposed to light.

1.2 *CHLAMYDOMONAS REINHARDTII, A LABORATORY STAR OF PHOTOSYNTHESIS STUDIES.*

Inside the Viridiplantae, we find most of land plants, organisms of great interest for humans as our primary source of nourishment and knowledge on photosynthesis. The major model organisms among land plants are *Arabidopsis thaliana and Nicotiana tabacum*.

Chlamydomonas reinhardtii (*Chlamydomonas* meaning mantle or cloak and *monas* means solitary), hereafter called *Chlamydomonas* is a small (6-10 µm) unicellular green algae from the Volvocales order inside the Chlorophyte division. It was first discovered in 1888 and has since been found in a wide set of environments (ponds, sea, marsh, volcanoes, and even snow). This genus is primarily defined by its anterior pair of flagella, a cell wall and a single chloroplast or chromatophore containing one or more pyrenoids that takes up to 75% of its volume (Harris, 2009). It also contains an eyespot that senses light. Also, their photosynthetic apparatus is very similar to the one from land plants (Wollman & Girard-Bascou, 1994). These small algae are among the laboratory stars in the study of photosynthesis, because of their single chloroplast and the amenability to genetic studies. In addition, *Chlamydomonas* is a non-obligatory photoautotroph (meaning that it can grow even with impaired photosynthesis mechanism in presence of other source of carbon such as acetate). Thus, it is a great tool to study photosynthesis mutants.

Chlamydomonas cells are easy to cultivate, store and grow (either stored at -80°C or grown on Petri dishes or liquid media at 20-25°C). They have a short generation time (around 8-10 hours) that enable quick accumulation of biological material, and their known genomes (either from nucleus, mitochondria or chloroplast) and the ease to use genomic, molecular and biochemical tools in experiments are the main reasons that make it a very useful asset to study photosynthesis.

Their capacity to grow in liquid media also enables to perform *in vivo* functional experiments to monitor photosynthesis in a wide array of conditions.

Chlamydomonas is haplobiontic as it undergoes usually an asexual vegetative life cycle in which haploid cells divide through mitosis but also a sexual reproduction where gametes from two different mating types cross. Under optimal growth conditions, cells can undergo various rounds of mitotic divisions in their mother cells' cell wall before being released in the medium. One mother cell giving place to 4 daughter cells. The culture can be grown in continuous light as usually done in our laboratory or synchronized through light and dark cycles. These haploids cells will become gametes when under nitrogen starvation. There are two mating types without any apparent differences: the plus mating type mt^+, and the minus mating type mt^- that will fuse into a meiotic diploid zygote. The zygote has no flagella and is mostly a dormant state of the species. Under light, the zygote will undergo meiosis and will release four flagellated haploid descendants that will resume the vegetative mitotic division cell cycle. (Figure 1-4).

It is of note that during the meiotic division resulting in the four descendants of the cross, all nuclear genes will be separated in a Mendelian 2:2 distribution, while the chloroplast genome will come from the mt^+ parent only (the mitochondrial genome will come from the mt^- parent). This can be very useful and informative when crossing two mutants as chloroplast mutation from mt^+ strains will automatically transfer the mutation to all descendants while the nuclear mutation from the mt^- parent will segregate in two of the four descendants thus leading to double mutants in all crosses (Figure 1-5).

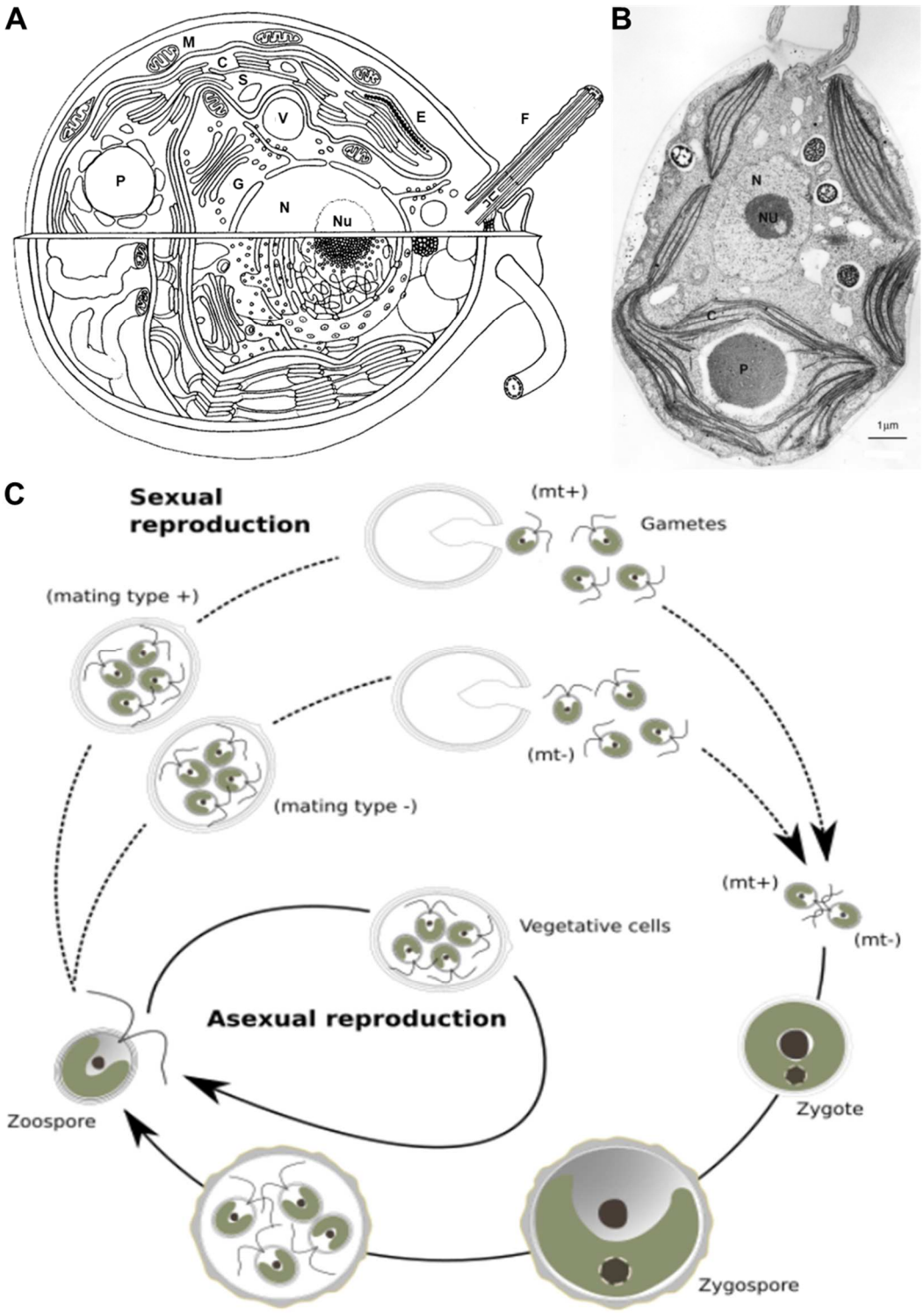

Figure 1-4 *Chlamydomonas reinhardtii*

(A) 3-D and 2-D schematic representation of C. reinhardtii cell structure. (Nickelsen & Kück, 2000). (B) Transmission electron microscopy image of median section of C. reinhardtii. (The Chlamydomonas sourcebook Vol.1: Harris et al, 2009). (C) C. reinhardtii life cycle with the different stages of the algae (Baudelet et al, 2017).

N:the central nucleus, Nu: the nucleolus, F: the two isoform flagellae, C: the cup-shaped chloroplast, E: the eyespot, P: the starch containing pyrenoid, M: the mitochondria, G: the golgi vesicle, S: starch grains, and V: the vacuoles

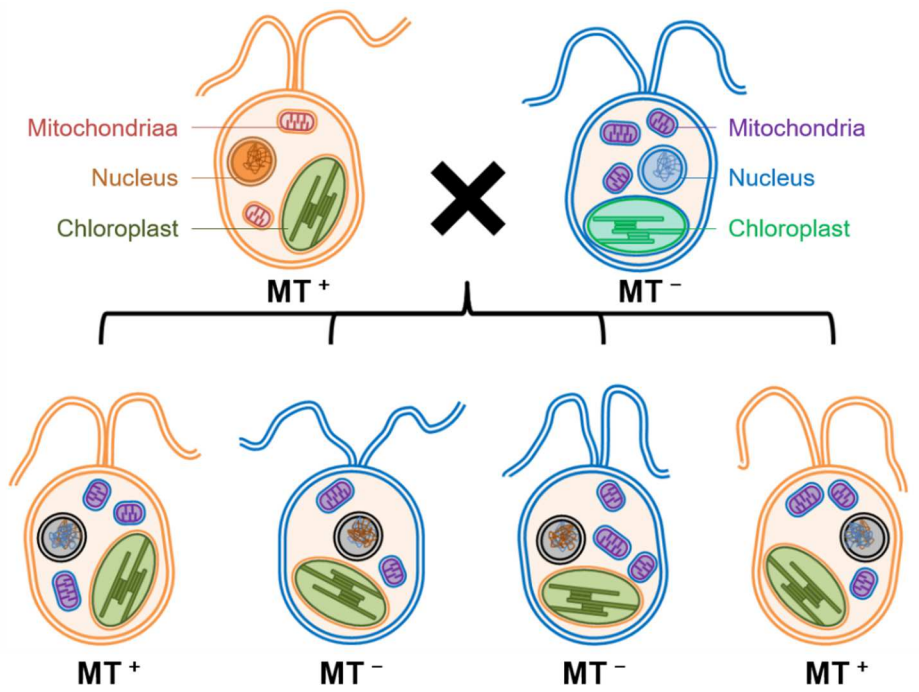

Figure 1-5 Genome segregation in sexual reproduction of *C. reinhardtii*
Schematic representation of a genetic cross of two C. reinhardtii individuals (blue, mt^+ and orange, mt^-) (From Jarrige, 2019). Upon fecundation and zygote formation, the tetrad will be composed of 2 mt^- and 2 mt^+ descendants. The progeny will get a mixture of parental nuclear genomes (blue and orange) in a segregation 2:2, but chloroplast genome will derive only from the mt^+ parent (deep green) while the mitochondrial genome will come from the mt^- parent (purple)

1.3 THE THYLAKOID PHOTOSYNTHETIC APPARATUS: THE ELECTRON TRANSFER CHAIN.

The photosynthetic chain is composed of multi-protein complexes anchored in the membrane of the thylakoid. It is composed of 4 main complexes that will convert light energy into an electron flow and a transmembrane electrochemical gradient that enables generation ATP and NADPH that will be used in metabolic processes (Figure 1-6).

These 4 complexes are known as Photosystem II (PSII), Photosystem I (PSI), cytochrome b_6f (cyt b_6f) and the ATPase/synthase (ATPase). In addition, light harvesting protein complexes (LHCI and LHCII, depending on which photosystems they are attached to) comprise a great number of pigments (mainly chlorophylls) and act as an antenna funneling the energy of photons to the core of photosystems.

1.3.1 Photosystems: the photo-activated complexes

The two photosystems in the photosynthetic machinery both work in the same way: they are big multimeric complexes, with a pair of specialized chlorophylls noted P680 at its center. The P680 can receive the energy from light and enter an excited state, noted P680*. At this point, the energy drags one chlorophyll's electron to a molecular orbital with a higher energy. Being in an unstable state, this electron will be able to get back to its original state, or ground state through three different pathways:

- The chlorophylls can translocate the high energy electron to an electron acceptor in the vicinity, a process called photochemistry. Then, a lower energy electron will be extracted from an electron donor. This transfer is possible thanks to the redox potential of the acceptor being higher than that of the excited chlorophylls' and becomes preferred over the simple decay of the energy or recombination of the electric charge.
- The energy in excess can be converted into heat (by molecular movements).
- The energy in excess can be released by emitting a photon of lower energy, with longer wavelength (fluorescence). Thus, «changes in fluorescence yield are inversely correlated with the rate of photosynthetic electron transfer (PET)» (Eberhard et al., 2008) as the lesser photochemistry, the more heat and fluorescence released.

The photosystems are linked to antennas LHCI and LHCII, which are protein complexes with a very high chlorophyll content. These work through a similar process: when chlorophylls are excited, they can release heat or fluorescence, as explained previously, but they can also transfer their energy to a neighboring chlorophyll molecule, a phenomenon called resonance energy transfer. From one to another, the chlorophylls end up delivering the energy to the reaction center in the photosystems core (Croce & van Amerongen, 2014).

1.3.2 The linear electron transfer

When P680 is excited, it transfers an electron to its immediate electron acceptor the pheophytin, which in turn reduces Q_A, a bound plastoquinone that reduces Q_B, a mobile plastoquinone. Two successive reduction steps result in the release of a plastoquinol (PQH_2) molecule that will diffuse in the thylakoid membrane. The electrons resulting from reduction of PQH_2 will be compensated by the entry of two protons from the stroma of the chloroplast. The $P680^+$ then restores its electron through oxidization of the tyrosine residue of the D1 protein of PSII called Y_Z which will be reduced in turn by the Manganese cluster thanks to the splitting of water into oxygen and protons in the lumen.

As the plastoquinol diffuses through the thylakoid membrane, it will reach a plastoquinol:plastocyanin oxidoreductase, the cytochrome b_6f. This complex will harbor many oxidoreduction steps, known as the Q-cycle which involves electron bifurcations and both reduction and oxidation of PQs into different binding sites. At the end of this complex mechanisms that will not be described here, each electron from the plastoquinol will reduce the iron-sulfur of the Rieske protein that will itself reduce cyt *f* and finally a plastocyanin. This will end up in the release of two protons in the lumen. The reduced plastocyanin will move to and reduce the oxidized special pair of PSI, P700.

PSI reduces Ferredoxin on its acceptor side after being excited by light, mostly through LHCI, its antenna. The reduced Ferredoxin will then be used to produce NADPH thanks to the Ferredoxin:$NADP^+$ oxidoreductase.

1.3.3 Cyclic electron flow

Through PSII to cytochrome b_6f to PSI, we have the linear electron flow (LEF), but there is another electron flow pathway for the photosynthetic chain: the cyclic electron flow (CEF). In this case, electrons from NADPH produced in PSI come back in the PQ pool, thus creating a loop between the cytochrome b_6f and PSI. This loop generates a higher PMF through the Q-cycle without production of NADPH enhancing ATP production (Figure 1-6).

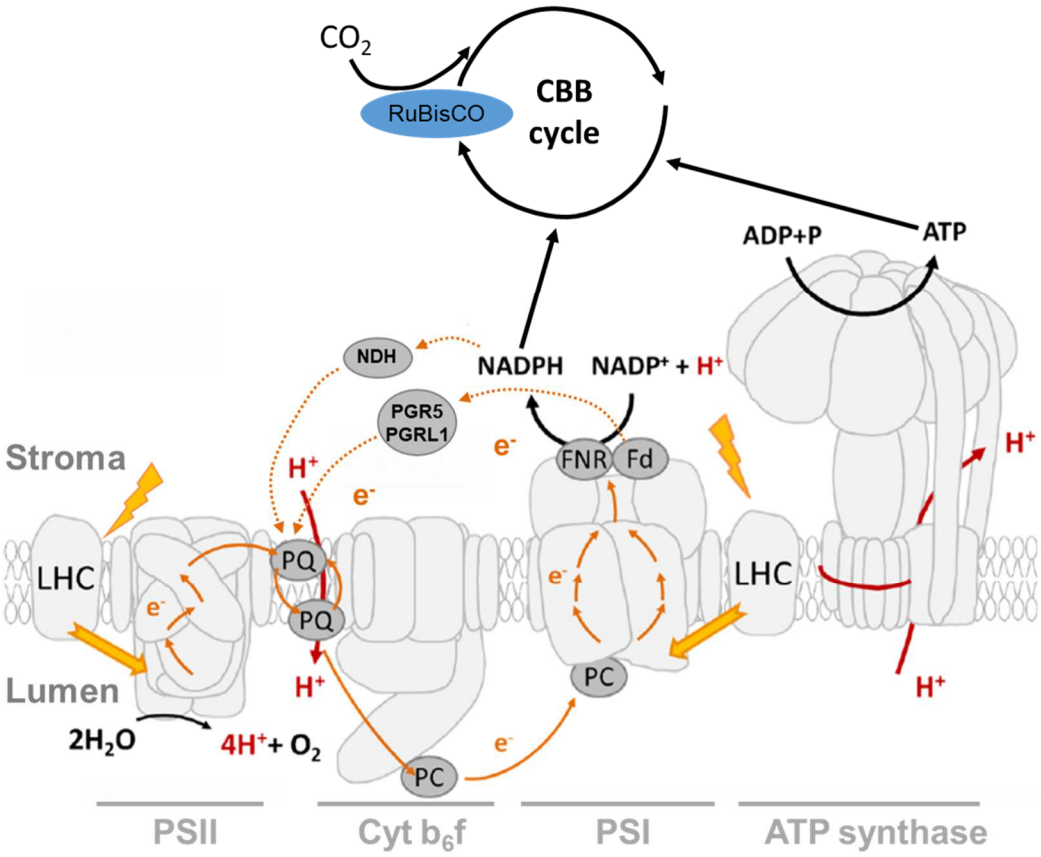

Figure 1-6 The thylakoid: the photosynthetic powerhouse

The complexes responsible for the light phase of photosynthesis are embedded in the membrane of the thylakoid. From left to right: the photosystem II (PSII), the cytochrome b_6f (cyt b_6f), the photosystem I (PSI) and the ATP synthase/ase (ATP synthase). Lightning represents illumination and yellow wide arrow excitation transmission from antennas to the reaction centers (RC) of photosystems. Orange arrows show electron pathway, full arrows show linear electron flow (LEF) and dotted arrows show specific pathways of the cyclic electron flow (CEF); red arrows show proton movements through thylakoid membrane. The electron pathway and protons passage through ATP synthase will create ATP and NADPH that will be used to fuel the Calvin cycle. Adapted from Jarrige, 2019.

1.3.4 The chemiosmotic theory and the ATPase

As was proposed in the 1960's by P. Mitchell (Mitchell, 1966), from these steps of oxidoreduction through the LEF in the photosynthetic chain result in the entry in the lumen of 3 protons per charge separation from both photosystems against the concentration gradient (ΔpH) and CEF will increase the number of H^+ entering the lumen. This will lead to an acidification of the lumen, but also to an increase of electric charge across the thylakoid membrane as protons enter and electrons leave the thylakoid (from water in the lumen to NADPH in the stroma) increasing the electrical potential ($\Delta\Psi$).

Also, Photosystems through charge separation and cyt b_6f though the Q-cycle participate in the increase of $\Delta\Psi$ (as they create a positive charge on the lumenal side and negative on the stromal side). This membrane being impermeable to protons, the electro-chemical gradient becomes a major driving force which is used by an ATP synthesizing enzyme, the ATP synthase.

This protein complex is a motor that uses the energy resulting from the accumulation of protons and electric potential, called proton-motive force (PMF, sometimes called $\Delta\mu H^+$) to turn the rotor through which protons leave the thylakoid, thus enabling the catalytic units of the ATP synthase to synthetize ATP by phosphorylation of ADP by inorganic phosphate (Pi) (Figure 1-7).

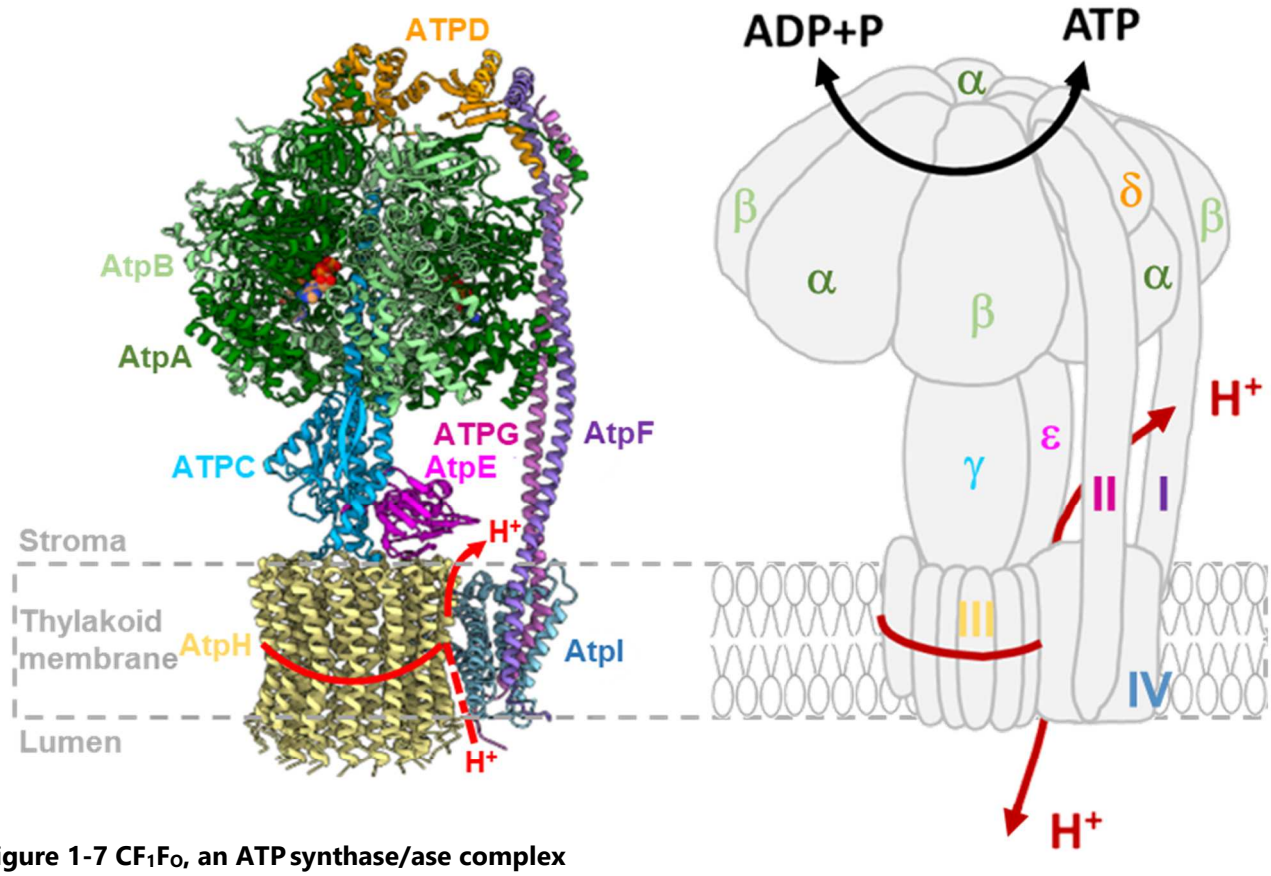

Figure 1-7 CF_1F_O, an ATP synthase/ase complex

Structural representation (left) adapted from cryo-EM map from spinach CF_1F_O (from Hahn et al, 2018) and schematic representation. Further explanation of CF_1F_O will be given in chapter 3. Proton translocation through the pore is represented as a double-headed red arrow. ATP hydrolysis or synthesis is represented as a double-headed black arrow.

This complex is reversible and able to integrate protons to the thylakoid lumen against their concentration gradient by hydrolyzing ATP into ADP + Pi. The ATPsynthase/ase will be further explained in chapter 3.

1.3.5 Benson-Calvin cycle

The production of ATP and NADPH by the 'light phase' steps will be used to fix inorganic carbon from CO_2 into sugars through the Benson-Calvin-cycle in what is called the 'dark phase' or more accurately the light-independent phase. The most important enzyme of this cycle is the ribulose bis-phosphate carboxylase/oxygenase (RuBisCO), that catalyzes addition of carbon into ribulose-1,5-bisphosphate.

1.4 REGULATION OF PHOTOSYNTHESIS

Photosynthesis involves production of radicals and highly reactive molecules (Rutherford et al., 2012). The production of reactive oxygen species (ROS) has been widely known to be detrimental to molecules, as they directly react with lipids, proteins and nucleic acids (Schmidt et al., 2016).

From the photosynthetic processes we have uncovered in the preceding pages, highly reactive molecules are produced under light. Thus, an excess of light can be harmful to the cells. This explains why processes of regulation have arisen in chloroplasts to protect the actors of photosynthesis while still maintaining an optimal yield in order to grow.

Photosynthesis is a far more complex process than what was simply depicted above, including membrane structuration of the thylakoid, interactions within the cell with other organelles such as the mitochondria or other metabolic pathways, and even with other cells and tissues (Figure 1-8). Only a few of the numerous ways of regulating photosynthesis will be presented here, we only focus on the fastest ones.

The major regulative processes within the thylakoid act directly on the excitation rate of photosystems which happens mostly in the PSII. This phenomenon is called non-photochemical quenching (NPQ) as it decreases the fluorescence yield of PSII (Horton

et al., 1996). There have been many different types of NPQ described (Eberhard et al., 2008), known as qE, qI and qT:

- qI, or photoinhibition happens when PSII reaction centers are damaged due to ROS production. They will have to be removed by proteases FtsH (Malnoë et al., 2014) in order to be later replaced after *de novo* biosynthesis.
- qT or state transition consist in the migration of phosphorylated LHCII from PSII to PSI, decreasing PSII's part in light absorption, thus enabling the electron transfer chain to avoid being clogged. (Goldschmidt-Clermont & Bassi, 2015)
- qE, or the energy-dependent quenching is the fastest of these regulatory processes and happens when pH becomes low enough to activate the Violaxanthin de-epoxidase (VDE). The formed zeaxanthin will accept the excitation from neighboring chlorophylls. The role of zeaxanthin in *Chlamydomonas* is still unclear and under debate. Also, protonation of PSII antennae residues will interfere with the pigment conformation increasing return to ground state from excited chlorophylls through heat emission. Other proteins like PsbS and LHCSR3 have been proven involved in the regulation of NPQ and LHCSR is a family of proteins that is absent in land plants but present in Chlamydomonas and other algae like diatoms (Eberhard et al., 2008).

The NPQ qE is not the only pH-dependent regulation of photosynthesis. Notably cyt b_6f slowing down constitutes a negative feedback loop resulting in another way to reduce damage to photosystems: lumen acidification reduces the rate of PQH_2 oxidation. Furthermore, the cyt b_6f is also downregulated directly by redox poise $NADP^+$/NADPH (Eberhard et al., 2008).

Interactions between organelles are of great importance upon changes in illumination conditions or when some complexes of the photosynthetic chain are impaired or inefficient. For example, during night or insufficient light illumination, ATP is translocated from mitochondrial respiration into chloroplasts (Bailleul et al., 2015; Bennoun, 1994). Of course, this is not the only cooperative exchange process between the plastids inside the cells: electron carriers and reductants produced in excess from photosynthesis are sent to mitochondria (Voon & Lim, 2019).

Thus, these organelles and specially chloroplasts have a very complex export/import array. Metabolites are not the only molecules involved, because of their importance for biological processes, « ion homeostasis in the stroma plays a major role in the regulation of the so called 'light phase' of photosynthesis» (Finazzi et al., 2015).

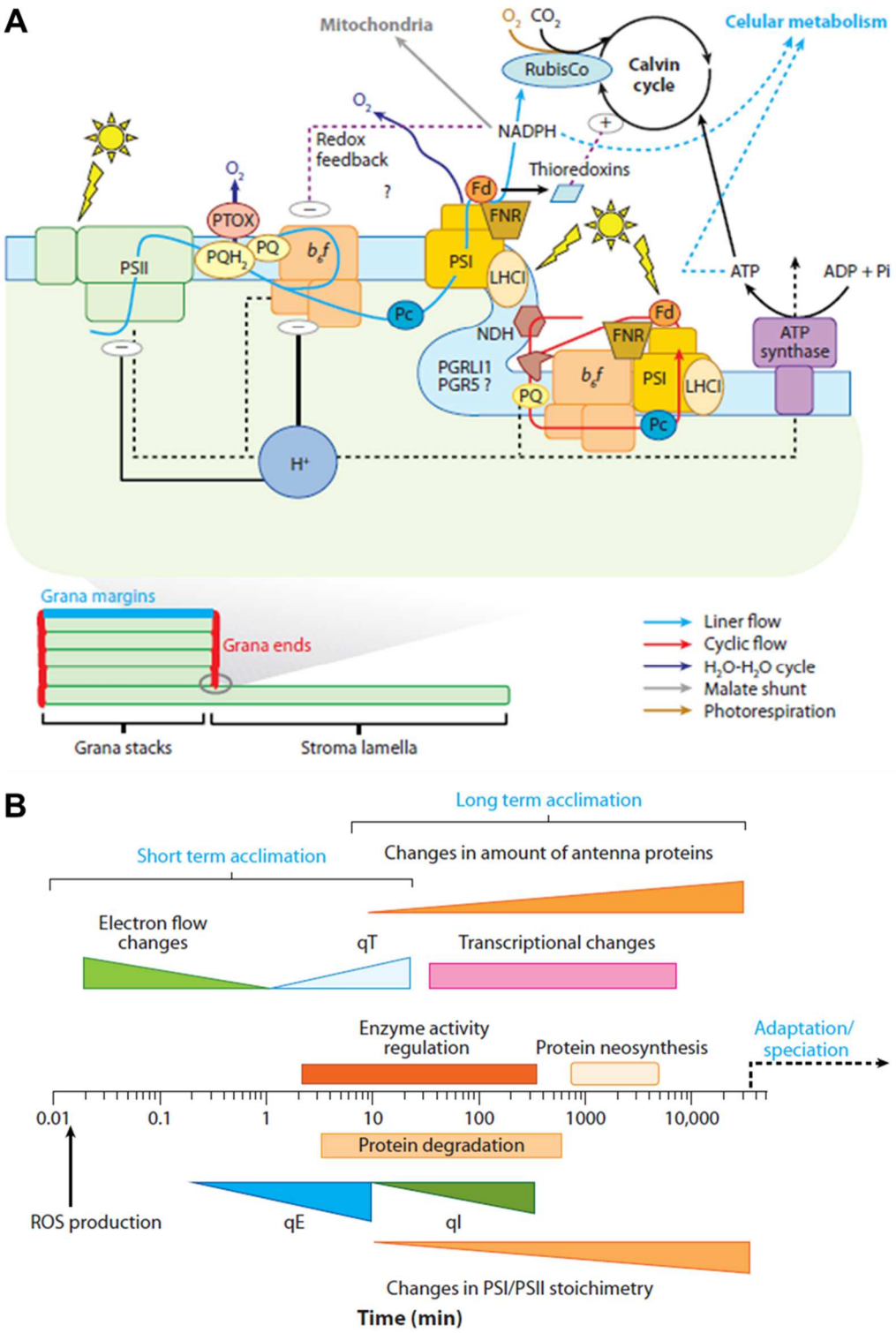

Figure 1-8 Complexity and timescale of photosynthetic regulation

(A) This figure shows the complexity of the photosynthetic electron chain and its regulation: heterogeneity of thylakoid structure with differential repartition of photosynthetic proteins through the differentiated regions (unstacked membranes and grana regions) is depicted in the lower panel. This compartmentalization is responsible to redirection of electron flow into LEF (blue) and CEF (red). Both LEF and CEF generate an electrochemical proton gradient across the thylakoid membranes (PMF), which is used for ATP synthesis. Steady-state PMF results from proton pumping by photosynthetic electron flow and proton consumption for ATP synthesis. The size of PMF is modulated by the overall metabolic state through ATP/ADP + Pi ratio. PMF also controls the rate of electron flow at the level of cyt b_6f and PSII complexes. The redox state of PSI electron acceptors, particularly the NADP/NADPH ratio, may also control cyt b_6f complex activity. Fd: ferredoxin; FNR: Fd:NADP+ reductase; Pc: plastocyanin; PQ: plastoquinone; PTOX: plastoquinone terminal oxidase; NDH: NADP:plastoquinone reductase.

(B) Here are shown short-term and long-term regulations and adaptations of light-harvesting capacity and electron flow rates. Short-term regulation also includes processes like regulation of enzymatic activities and protein-degradation mechanisms. Long-term regulation encompasses slower changes such as gene expression and protein synthesis. On longer timescales, definitive changes may happen leading to speciation process and adaptation to specific environments. (from Eberhard et al, 2008)

1.5 THE THYLAKOID, A CROSSWAY FOR METALS AND IONS.

As they do in all life processes, ions play a crucial role in metabolic and cellular functions notably as redox cofactors in complexes of the photosynthetic electron transfer transport chain. These molecules have to be imported from the media (or extracellular matrix in the case of pluricellular organisms) in a very coordinated manner as they can have tremendously different effect depending of their concentrations: ranging from micro to millimolar scale normally, they can be cytotoxic at higher levels, possibly creating ROS and other problems (Blaby-Haas & Merchant, 2017). Metallochaperones can assist metal delivery to proteins (Schmidt et al., 2020).

In the last decades, an increasing number of transporters has been discovered in the chloroplast envelopes and in the thylakoid, but we are still far from having a thorough understanding of the intricate transport net in the chloroplast. All of these transporters are transmembrane proteins that can classified in three different groups (Saier et al., 2009) and subsequent updates at https://tcdb.org/: (1) channels that transport specific molecules down their concentration gradient with no energy consumption contrary to (2) primary transporters that use directly the energy available (mostly ATP) to transport molecules, often against their concentration gradient (take for example the ATPase/synthase described in 1.3.4); the last type of transporters are (3) secondary transporters that are able to translocate molecules using the energy from the concentration gradient of other molecules, either in the same or in opposite direction, then known as symporters or antiporters respectively.

"Ions are critical for regulation of the intracellular function such as pH, volume, osmoregulation of intracellular compartments and excess can be devastating" (Marchand et al., 2018). In the case of photosynthesis, ions are of primordial importance for optimal function of each of the very complex multi-protein part of the photosynthetic apparatus presented earlier. There have been, in the last decade an astounding number of reviews on this subject (Blaby-Haas & Merchant, 2012; Finazzi et al., 2015; Marchand et al., 2018; Spetea et al., 2017; Szabò & Spetea, 2017).

We will here concentrate on the primordial transporters for the 'light phase' steps of photosynthesis.

For instance, to lightly summarize: most ions or metals are needed for osmosis, PMF regulation, overall thylakoid structuration or as cofactors for enzymes (Spetea & Schoefs, 2010): The presence of Manganese (Mn^{2+}), Calcium (Ca^{2+}) and Chloride (Cl^{-}) ions are critically important for optimal activity of the OEC (Shen, 2015). The multimeric complexes and electron carriers fixed or mobile depend highly on co-factors linked to metallic ions such as Mg/chlorophylls (light harvesting antenna, PSII P680 and PSI P700), iron (non heme Fe^{2+}; cytochrome heme irons; iron-sulfur clusters Fe_2S_2 and Fe_4S_4) at the PSII, b_6f and PSI level or copper (Cu^{2+}) in the plastocyanin complex. Also, to cope with the high oxidative environment, the chloroplast are equipped with various mechanisms to dissipate excessive oxidative stress, such as anoxidative metalloenzymes and superoxide dismutases (Aguirre & Pilon, 2015).

Imported from the media or the extracellular matrix, these molecules have to get to either the stromal or the luminal side of thylakoids to be used for photosynthesis. In order to do so, they have to pass through a set of successive barriers. The first and outer membrane is quite permeable and allows free passage of ions and metals up to the intermembrane space. Afterwards, selective passage takes place through the inner envelope of the chloroplast. Finally, if the molecule has to reach the lumen, it will have to go through the thylakoid (Figure 1-9). In this study, we will focus particularly on some transporters of the thylakoid.

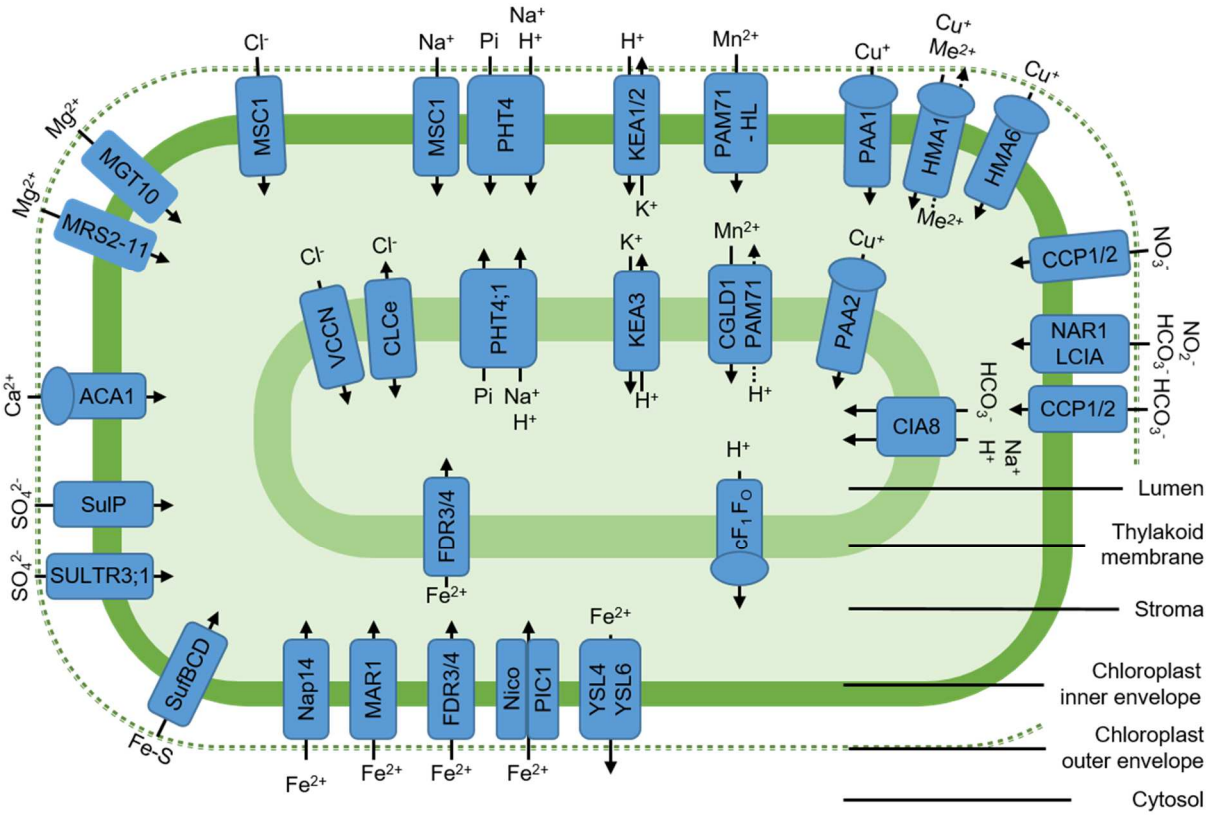

Figure 1-9 Ion transporters/channels in the chloroplast of green algae.
Transporters located in the chloroplast inner envelope (dark green) and in the thylakoid membrane (light green). As the chloroplast outer envelope (dashed line) is very permeable to most molecules, it does not have ion transporters. Transporters with ATP-related activity are represented with a round shaped cap. Adapted from Finazzi et al, 2015 and Marchand et al, 2018.

1.6 QUICK OVERVIEW AND AIM OF THIS THESIS.

In this introduction, we uncovered the general molecular mechanisms of oxygenic photosynthesis, and the importance of ions in these processes. One of the most important steps in the so-called light phase is photochemistry, where light energy is used to initiate electron flow in the photochemical electron transfer through all protein complexes embedded in the thylakoid membrane. This flow initiated by excitation of a chlorophyll pair in the photosystems is possible thanks to the redox properties of all the components of the electron chain which enable the transfer of electrons from donor to acceptor throughout the thylakoid, resulting in the generation of PMF used for ATP production, and NADPH. Many of these components depend on cofactors, and the need of many different ions. How is photosynthesis affected should one of these essential ions be missing?

For example, the oxygenic origin of this photosynthesis is due to the splitting of water into oxygen at the PSII donor site. This is possible thanks to the oxygen evolving complex (OEC) comprised of the Mn-cluster of the PSII. In this work, we focused on manganese (Mn). The knowledge of Mn intake pathway is very recent and enables further functional studies of Mn related photosynthetic processes. This metallic ion is transported through the inner envelope through CMT1 and through the thylakoid membrane by PAM71/CGLD1 (Krieger-Liszkay & Thomine, 2018). This CGLD1 transporter is the focus of the study in chapter 2.

How is Mn delivered to the OEC of PSII, and what happens to PSII when Mn becomes limiting?

Photosynthesis relies on the CF_1F_O ATP synthase for ATP production. The high-resolution structure of the complete CF_1F_O complex has been reported recently (Hahn et al. 2018), and much remains to be discovered on the assembly of this macromolecular complex.

Which subunits are required for its biogenesis, and which organellar trans-acting factors encoded in the nucleus tightly control, in a gene specific manner, the expression of plastid mRNAs encoding ATP synthase subunits?

Another question that the CF_1F_O activity raises is the becoming of the thylakoids should this proton exporter be impaired, inactive or absent. Indeed, this complex is the main dissipater of PMF, and we saw in 1.4 that excessive increase of PMF tend to decrease photosynthesis efficiency at many levels, both through regulatory mechanisms and by damage.

How is the PMF regulated in the absence CF_1F_O activity?

These questions lead my work during this thesis on ions transport across thylakoid membranes. The next chapters allowed to provide new insight into these questions, using photosynthetic mutants of the model organism *C. reinhardtii*.

References

Aguirre, G., & Pilon, M. (2015). Copper Delivery to Chloroplast Proteins and its Regulation. *Frontiers in Plant Science*, *6*, 1250. https://doi.org/10.3389/fpls.2015.01250

Bailleul, B., Berne, N., Murik, O., Petroutsos, D., Prihoda, J., Tanaka, A., Villanova, V., Bligny, R., Flori, S., Falconet, D., Krieger-Liszkay, A., Santabarbara, S., Rappaport, F., Joliot, P., Tirichine, L., Falkowski, P. G., Cardol, P., Bowler, C., & Finazzi, G. (2015). Energetic coupling between plastids and mitochondria drives CO2 assimilation in diatoms. *Nature*, *524*(7565), Art. 7565. https://doi.org/10.1038/nature14599

Bailleul, B., Cardol, P., Breyton, C., & Finazzi, G. (2010). Electrochromism : A useful probe to study algal photosynthesis. *Photosynthesis Research*, *106*(1-2), 179-189. https://doi.org/10.1007/s11120-010-9579-z

Baudelet, P.-H., Ricochon, G., Linder, M., & Muniglia, L. (2017). A new insight into cell walls of Chlorophyta. *Algal Research*, *25*, 333-371. https://doi.org/10.1016/j.algal.2017.04.008

Bennoun, P. (1994). Chlororespiration revisited : Mitochondrial-plastid interactions in Chlamydomonas. *Biochimica et Biophysica Acta (BBA) - Bioenergetics*, *1186*(1), 59-66. https://doi.org/10.1016/0005-2728(94)90135-X

Blaby-Haas, C. E., & Merchant, S. S. (2012). The ins and outs of algal metal transport. *Biochimica et biophysica acta*, *1823*(9), 1531-1552. https://doi.org/10.1016/j.bbamcr.2012.04.010

Blaby-Haas, C. E., & Merchant, S. S. (2017). Regulating cellular trace metal economy in algae. *Current Opinion in Plant Biology*, *39*, 88-96. https://doi.org/10.1016/j.pbi.2017.06.005

Buchert, F., Bailleul, B., & Joliot, P. (2021). Disentangling chloroplast ATP synthase regulation by proton motive force and thiol modulation in Arabidopsis leaves. *Biochimica et Biophysica Acta (BBA) - Bioenergetics*, *1862*(8), 148434. https://doi.org/10.1016/j.bbabio.2021.148434

Buchert, F., Konno, H., & Hisabori, T. (2015). Redox regulation of CF1-ATPase involves interplay between the γ-subunit neck region and the turn region of the βDELSEED-loop. *Biochimica Et Biophysica Acta*, *1847*(4-5), 441-450. https://doi.org/10.1016/j.bbabio.2015.01.013

Croce, R., & van Amerongen, H. (2014). Natural strategies for photosynthetic light harvesting. *Nature Chemical Biology*, *10*(7), Art. 7. https://doi.org/10.1038/nchembio.1555

Dukic, E., Herdean, A., Cheregi, O., Sharma, A., Nziengui, H., Dmitruk, D., Solymosi, K., Pribil, M., & Spetea, C. (2019). K+ and Cl− channels/transporters independently fine-tune photosynthesis in plants. *Scientific Reports*, *9*, 8639. https://doi.org/10.1038/s41598-019-44972-z

Dyall, S. D., Brown, M. T., & Johnson, P. J. (2004). Ancient Invasions : From Endosymbionts to Organelles. *Science*, *304*(5668), 253-257. https://doi.org/10.1126/science.1094884

Eberhard, S., Finazzi, G., & Wollman, F.-A. (2008). The Dynamics of Photosynthesis. *Annual Review of Genetics*, *42*(1), 463-515. https://doi.org/10.1146/annurev.genet.42.110807.091452

Finazzi, G., Petroutsos, D., Tomizioli, M., Flori, S., Sautron, E., Villanova, V., Rolland, N., & Seigneurin-Berny, D. (2015). Ions channels/transporters and chloroplast regulation. *Cell Calcium*, *58*(1), 86-97. https://doi.org/10.1016/j.ceca.2014.10.002

Fuhrman, J. A., Schwalbach, M. S., & Stingl, U. (2008). Proteorhodopsins : An array of physiological roles? *Nature Reviews. Microbiology*, *6*(6), 488-494. https://doi.org/10.1038/nrmicro1893

Genty, B., Briantais, J. M., & Baker, N. R. (1989). The relationship between the quantum yield of photosynthetic electron transport and quenching of chlorophyll fluorescence. *Biochimica et Biophysica Acta - General Subjects*, *990*(1), 87-92. https://doi.org/10.1016/S0304-4165(89)80016-9

Goldschmidt-Clermont, M., & Bassi, R. (2015). Sharing light between two photosystems : Mechanism of state transitions. *Current Opinion in Plant Biology*, *25*, 71-78. https://doi.org/10.1016/j.pbi.2015.04.009

Hahn, A., Vonck, J., Mills, D. J., Meier, T., & Kühlbrandt, W. (2018). Structure, mechanism, and regulation of the chloroplast ATP synthase. *Science (New York, N.Y.)*, *360*(6389), eaat4318. https://doi.org/10.1126/science.aat4318

Hanada, S. (2016). Anoxygenic Photosynthesis -A Photochemical Reaction That Does Not Contribute to Oxygen Reproduction. *Microbes and Environments*, *31*(1), 1-3. https://doi.org/10.1264/jsme2.ME3101rh

Harris, E. H. (2009). *The Chlamydomonas Sourcebook—Volume 1 : Introduction to Chlamydomonas and Its Laboratory Use* (Vol. 1). Academic Press.

Holt, N. E., Fleming, G. R., & Niyogi, K. K. (2004). Toward an Understanding of the Mechanism of Nonphotochemical Quenching in Green Plants. *Biochemistry*, *43*(26), 8281-8289. https://doi.org/10.1021/bi0494020

Horton, P., Ruban, A. V., & Walters, R. G. (1996). REGULATION OF LIGHT HARVESTING IN GREEN PLANTS. *Annual Review of Plant Physiology and Plant Molecular Biology*, *47*, 655-684. https://doi.org/10.1146/annurev.arplant.47.1.655

Houille-Vernes, L., Rappaport, F., Wollman, F. A., Alric, J., & Johnson, X. (2011). Plastid terminal oxidase 2 (PTOX2) is the major oxidase involved in chlororespiration in Chlamydomonas. *Proceedings of the National Academy of Sciences of the United States of America*, *108*(51), 20820-20825. https://doi.org/10.1073/pnas.1110518109

Jans, F., Mignolet, E., Houyoux, P. A., Cardol, P., Ghysels, B., Cuiné, S., Cournac, L., Peltier, G., Remacle, C., & Franck, F. (2008). A type II NAD(P)H dehydrogenase mediates light-independent plastoquinone reduction in the chloroplast of Chlamydomonas. *Proceedings of the National Academy of Sciences of the United States of America*, *105*(51), 20546-20551. https://doi.org/10.1073/pnas.0806896105

Jarrige, D. (2019). *Deciphering the « OPR code » to further assess the physiological role of OPR proteins* [Phdthesis, Sorbonne Université]. https://tel.archives-ouvertes.fr/tel-03349187

Jarvis, P., & Soll, J. (2002). Toc, tic, and chloroplast protein import. *Biochimica Et Biophysica Acta*, *1590*(1-3), 177-189. https://doi.org/10.1016/s0167-4889(02)00176-3

Joliot, P., & Delosme, R. (1974). Flash-induced 519 nm absorption change in green algae. *Biochimica Et Biophysica Acta*, *357*(2), 267-284. https://doi.org/10.1016/0005-2728(74)90066-8

Joliot, P., & Johnson, G. N. (2011). Regulation of cyclic and linear electron flow in higher plants. *Proceedings of the National Academy of Sciences*, *108*(32), 13317-13322. https://doi.org/10.1073/pnas.1110189108

Joliot, P., & Joliot, A. (2008). Quantification of the electrochemical proton gradient and activation of ATP synthase in leaves. *Biochimica et Biophysica Acta (BBA) - Bioenergetics*, *1777*(7), 676-683. https://doi.org/10.1016/j.bbabio.2008.04.010

Junesch, U., & Gräber, P. (1987). Influence of the redox state and the activation of the chloroplast ATP synthase on proton-transport-coupled ATP synthesis/hydrolysis. *Biochimica et Biophysica Acta (BBA) - Bioenergetics*, *893*(2), 275-288. https://doi.org/2

Junge, W. (1970). The critical electric potential difference for photophosphorylation. Its relation to the chemiosmotic hypothesis and to the triggering requirements of the ATPase system. *European Journal of Biochemistry*, *14*(3), 582-592. https://doi.org/10.1111/j.1432-1033.1970.tb00327.x

Kramer, D. M., Cruz, J. A., & Kanazawa, A. (2003). Balancing the central roles of the thylakoid proton gradient. *Trends in Plant Science*, *8*(1), 27-32. https://doi.org/10.1016/S1360-1385(02)00010-9

Krieger-Liszkay, A., & Thomine, S. (2018). Importing Manganese into the Chloroplast : Many Membranes to Cross. *Molecular Plant*, *11*(9), 1109-1111. https://doi.org/10.1016/j.molp.2018.07.006

Kushkevych, I., Procházka, J., Gajdács, M., Rittmann, S. K.-M. R., & Vítězová, M. (2021). Molecular Physiology of Anaerobic Phototrophic Purple and Green Sulfur Bacteria. *International Journal of Molecular Sciences*, *22*(12), 6398. https://doi.org/10.3390/ijms22126398

Lane, N., Allen, J. F., & Martin, W. (2010). How did LUCA make a living? Chemiosmosis in the origin of life. *BioEssays: News and Reviews in Molecular, Cellular and Developmental Biology*, *32*(4), 271-280. https://doi.org/10.1002/bies.200900131

Lemaire, C., & Wollman, F. A. (1989a). The chloroplast ATP synthase in Chlamydomonas reinhardtii. I. Characterization of its nine constitutive subunits. *The Journal of Biological Chemistry*, *264*(17), 10228-10234.

Lemaire, C., & Wollman, F. A. (1989b). The chloroplast ATP synthase in Chlamydomonas reinhardtii. II. Biochemical studies on its biogenesis using mutants defective in photophosphorylation. *The Journal of Biological Chemistry*, *264*(17), 10235-10242.

Li, M., Svoboda, V., Davis, G., Kramer, D., Kunz, H.-H., & Kirchhoff, H. (2021). Impact of ion fluxes across thylakoid membranes on photosynthetic electron transport and photoprotection. *Nature Plants*, *7*(7), Art. 7. https://doi.org/10.1038/s41477-021-00947-5

Lyons, T. W., Reinhard, C. T., & Planavsky, N. J. (2014). The rise of oxygen in Earth's early ocean and atmosphere. *Nature*, *506*(7488), Art. 7488. https://doi.org/10.1038/nature13068

Lyu, H., & Lazár, D. (2022). Analyzing the effect of ion binding to the membrane-surface on regulating the light-induced transthylakoid electric potential (ΔΨm). *Frontiers in Plant Science*, *13*, 945675. https://doi.org/10.3389/fpls.2022.945675

Malnoë, A., Wang, F., Girard-Bascou, J., Wollman, F.-A., & de Vitry, C. (2014). Thylakoid FtsH Protease Contributes to Photosystem II and Cytochrome b_6f Remodeling in *Chlamydomonas reinhardtii* under Stress Conditions. *The Plant Cell*, *26*(1), 373-390. https://doi.org/10.1105/tpc.113.120113

Marchand, J., Heydarizadeh, P., Schoefs, B., & Spetea, C. (2018). Ion and metabolite transport in the chloroplast of algae : Lessons from land plants. *Cellular and Molecular Life Sciences*, *75*(12), 2153-2176. https://doi.org/10.1007/s00018-018-2793-0

Margulis, L. (1971). Symbiosis and evolution. *Scientific American*, *225*(2), 48-57. https://doi.org/10.1038/scientificamerican0871-48

Marin, B., M. Nowack, E. C., & Melkonian, M. (2005). A Plastid in the Making : Evidence for a Second Primary Endosymbiosis. *Protist*, *156*(4), 425-432. https://doi.org/10.1016/j.protis.2005.09.001

Martin, W. F., Bryant, D. A., & Beatty, J. T. (2018). A physiological perspective on the origin and evolution of photosynthesis. *FEMS Microbiology Reviews*, *42*(2), 205-231. https://doi.org/10.1093/femsre/fux056

Melo, A. M. P., Bandeiras, T. M., & Teixeira, M. (2004). New Insights into Type II NAD (P) H : Quinone Oxidoreductases New Insights into Type II NAD (P) H : Quinone Oxidoreductases. *Microbiology and Molecular Biology Reviews*, *68*(4), 603-616. https://doi.org/10.1128/MMBR.68.4.603

Mitchell, P. (1966). Chemiosmotic coupling in oxidative and photosynthetic phosphorylation. *Biological Reviews of the Cambridge Philosophical Society*, *41*(3), 445-502. https://doi.org/10.1111/j.1469-185x.1966.tb01501.x

Nickelsen, J., & Kück, U. (2000). The unicellular green alga Chlamydomonas reinhardtii as an experimental system to study chloroplast RNA metabolism. *Die Naturwissenschaften*, *87*(3), 97-107. https://doi.org/10.1007/s001140050686

Nishio, J. N., & Whitmarsh, J. (1993). Dissipation of the Proton Electrochemical Potential in Intact Chloroplasts (II. The pH Gradient Monitored by Cytochrome f Reduction Kinetics). *Plant Physiology*, *101*(1), 89-96. https://doi.org/10.1104/pp.101.1.89

Peltier, G., Aro, E.-M., & Shikanai, T. (2016). NDH-1 and NDH-2 Plastoquinone Reductases in Oxygenic Photosynthesis. *Annual Review of Plant Biology*, *67*(1), 55-80. https://doi.org/10.1146/annurev-arplant-043014-114752

Ponce-Toledo, R. I., López-García, P., & Moreira, D. (2019). Horizontal and endosymbiotic gene transfer in early plastid evolution. *The New Phytologist*, *224*(2), 618-624. https://doi.org/10.1111/nph.15965

Rumberg, B., & Siggel, U. (1969). PH changes in the inner phase of the thylakoids during photosynthesis. *Die Naturwissenschaften*, *56*(3), 130-132. https://doi.org/10.1007/BF00601025

Rutherford, A. W., Osyczka, A., & Rappaport, F. (2012). Back-reactions, short-circuits, leaks and other energy wasteful reactions in biological electron transfer : Redox tuning to survive life in O2. *FEBS Letters*, *586*(5), 603-616. https://doi.org/10.1016/j.febslet.2011.12.039

Saier, M. H., Jr, Yen, M. R., Noto, K., Tamang, D. G., & Elkan, C. (2009). The Transporter Classification Database : Recent advances. *Nucleic Acids Research*, *37*(suppl_1), D274-D278. https://doi.org/10.1093/nar/gkn862

Sanchez-Baracaldo, P., & Cardona, T. (2019). On the origin of oxygenic photosynthesis and Cyanobacteria. *The New Phytologist*, *225*(4), 1440-1446. https://doi.org/10.1111/nph.16249

Schmidt, S. B., Eisenhut, M., & Schneider, A. (2020). Chloroplast Transition Metal Regulation for Efficient Photosynthesis. *Trends in Plant Science*, *25*(8), 817-828. https://doi.org/10.1016/j.tplants.2020.03.003

Schmidt, S. B., Jensen, P. E., & Husted, S. (2016). Manganese Deficiency in Plants : The Impact on Photosystem II. *Trends in Plant Science*, *21*(7), 622-632. https://doi.org/10.1016/j.tplants.2016.03.001

Schönknecht, G., Hedrich, R., Junge, W., & Raschke, K. (1988). A voltage-dependent chloride channel in the photosynthetic membrane of a higher plant. *Nature*, *336*(6199), Art. 6199. https://doi.org/10.1038/336589a0

Shen, J.-R. (2015). The Structure of Photosystem II and the Mechanism of Water Oxidation in Photosynthesis. *Annual Review of Plant Biology*, *66*(1), 23-48. https://doi.org/10.1146/annurev-arplant-050312-120129

Sousa, F. L., Thiergart, T., Landan, G., Nelson-Sathi, S., Pereira, I. A. C., Allen, J. F., Lane, N., & Martin, W. F. (2013). Early bioenergetic evolution. *Philosophical Transactions of the Royal Society of London. Series B, Biological Sciences*, *368*(1622), 20130088. https://doi.org/10.1098/rstb.2013.0088

Spetea, C., Herdean, A., Allorent, G., Carraretto, L., Finazzi, G., & Szabo, I. (2017). An update on the regulation of photosynthesis by thylakoid ion channels and transporters in Arabidopsis. *Physiologia Plantarum*, *161*(1), 16-27. https://doi.org/10.1111/ppl.12568

Spetea, C., & Schoefs, B. (2010). Solute transporters in plant thylakoid membranes : Key players during photosynthesis and light stress. *Communicative & Integrative Biology*, *3*(2), 122-129. https://doi.org/10.4161/cib.3.2.10909

Strand, D. D., Fisher, N., & Kramer, D. M. (2017). The higher plant plastid NAD(P)H dehydrogenase-like complex (NDH) is a high efficiency proton pump that increases ATP production by cyclic electron flow. *Journal of Biological Chemistry*, *292*(28), 11850-11860. https://doi.org/10.1074/jbc.M116.770792

Szabò, I., & Spetea, C. (2017). Impact of the ion transportome of chloroplasts on the optimization of photosynthesis. *Journal of Experimental Botany*, *68*(12), 3115-3128. https://doi.org/10.1093/jxb/erx063

Tester, M., & Blatt, M. R. (1989). Direct Measurement of K+ Channels in Thylakoid Membranes by Incorporation of Vesicles into Planar Lipid Bilayers 1. *Plant Physiology*, *91*(1), 249-252. https://doi.org/10.1104/pp.91.1.249

Uflewski, M., Mielke, S., Correa Galvis, V., von Bismarck, T., Chen, X., Tietz, E., Ruß, J., Luzarowski, M., Sokolowska, E., Skirycz, A., Eirich, J., Finkemeier, I., Schöttler, M. A., & Armbruster, U. (2021). Functional characterization of proton antiport regulation in the thylakoid membrane. *Plant Physiology*, *187*(4), 2209-2229. https://doi.org/10.1093/plphys/kiab135

Voon, C. P., & Lim, B. L. (2019). ATP translocation and chloroplast biology. *National Science Review*, *6*(6), 1073-1076. https://doi.org/10.1093/nsr/nwz089

Witt, H. T. (1979). Energy conversion in the functional membrane of photosynthesis. Analysis by light pulse and electric pulse methods. The central role of the electric field. *Biochimica Et Biophysica Acta*, *505*(3-4), 355-427. https://doi.org/10.1016/0304-4173(79)90008-9

Wollman, F.-A., & Girard-Bascou, J. (1994). *Une algue pour l'étude de la génétique des organites : Chlamydomonas reinhardtii*. *10*(11), 14.

Cette page a été laissée intentionnellement vide
This page was intentionally left blank

CHAPTER 2:

THYLAKOID MN2+ TRANSPORTER CGLD1 (PAM71) IS REQUIRED FOR EFFICIENT ACTIVITY OF PHOTOSYSTEM II DONOR SIDE IN CHLAMYDOMONAS REINHARDTII.

FOREWORD

Photosynthesis works thanks to photosystems, able to intake light energy and transform it into electrochemical energy by the process of photochemistry. One of those is quite important as it gave the name to oxygenic photosynthesis: photosystem II (PSII). PSII is comprised of a great number of proteins. It is organized in a reaction core comprised of 4 main proteins (D1, D2, CP43 and CP47) which is the site of the electron transfer due to photochemistry, the oxygen evolving complex that catalyzes light-driven oxidation of PSII by splitting water into O_2 and H^+, extrinsic proteins (PsbO, PsbP and PsbQ) whose role is to stabilize the OEC, and numerous other proteins responsible for diverse important roles, such as assembly, stability excitation transfer or photoprotection of the PSII core (see figure 2-1).

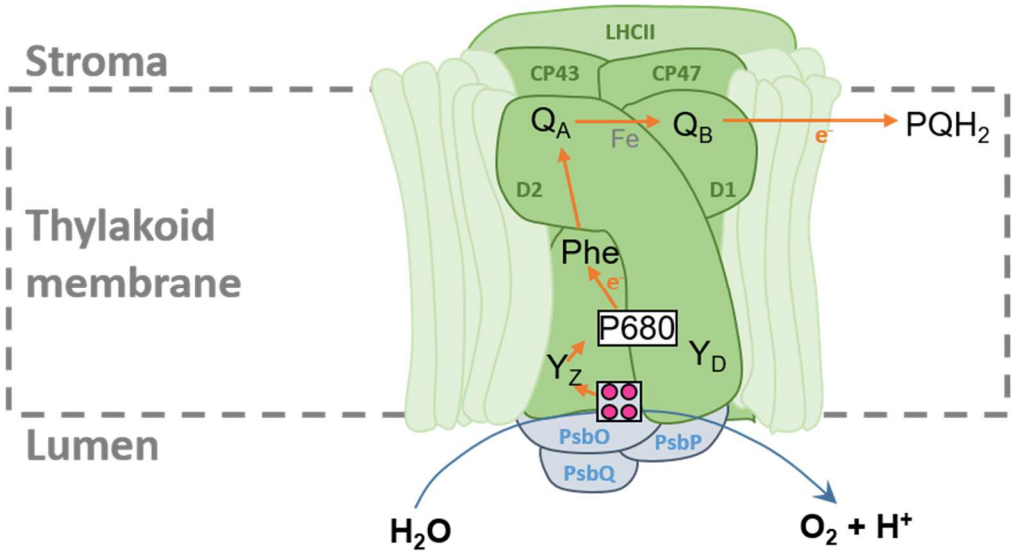

Figure 2-1 Structure of Photosystem II.
Reaction center is composed of D1, D2, CP43 and CP47. The Mn-cluster is symbolized by the square with 4 pink circles at the lumenal side of the reaction core. PsbO, PsbP and PsbQ stabilize the Mn-cluster at the lumenal side. Around the reaction core, are reprensented other PSII subunits. Antenna LHCII is represented behind PSII. The blue line representes the water splitting into O_2 and H^+. The orange arrows represent electron flow induced by photochemistry. Adapted from Hankamer et al. 1997.

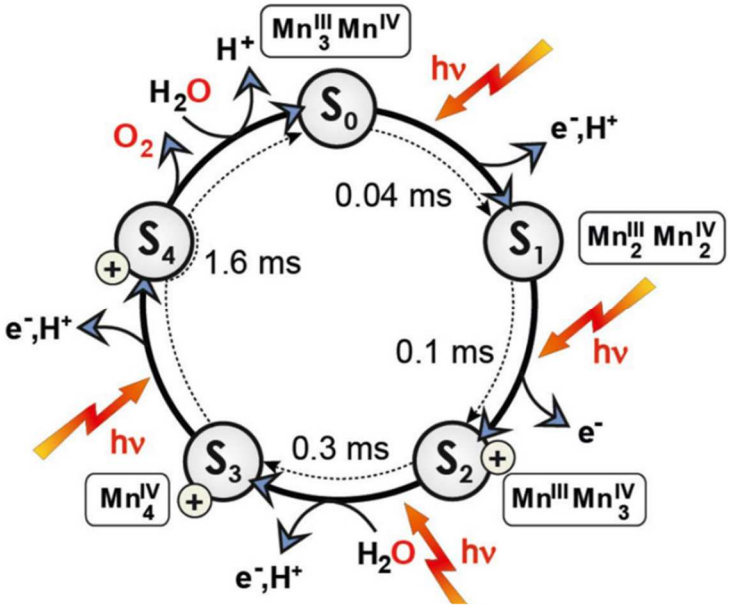

Figure 2-2 S-states cycle.
Water oxidation cycle (Kok et al. 1970, Joliot and Kok 1975) detailing the five basic S states (S0 to S4), the light-induced 1e⁻ oxidation steps and the proton release pattern (Dau and Haumann 2008), the uptake of the two substrate waters (Hillier and Wydrzynski 2008) and the Mn oxidation states (Krewald et al. 2015) (vide infra). The reaction times for the single electron oxidation steps are also indicated (Klauss et al. 2012a). Note that here the "S" stands for "state" and not for the electron spin quantum number S. From Lubitz et al. 2019. The lightning symbols show the light-dependent transitions from one state to another.

The oxygen evolving complex (OEC) stands at the lumenal side of the reaction center. This enzymatic domain consists of 4 manganese (Mn), 1 Calcium (Ca) and five oxygen (O) atoms, forming together the manganese cluster (Mn_4O_5Ca). This Mn-cluster undergoes a series of light-dependent events leading to the oxidation of H_2O molecules inside the manganese cluster, after a series of electron transfer within the reaction center resulting in reduction of Y_Z, and finally O_2 release in the lumen (see figure 2-2).

References:

Hankamer, B., Barber, J., & Boekema, E. J. (1997). STRUCTURE AND MEMBRANE ORGANIZATION OF PHOTOSYSTEM II IN GREEN PLANTS. *Annual Review of Plant Physiology and Plant Molecular Biology*, *48*, 641-671. https://doi.org/10.1146/annurev.arplant.48.1.641

Lubitz, W., Chrysina, M., & Cox, N. (2019). Water oxidation in photosystem II. *Photosynthesis Research*, *142*(1), 105-125. https://doi.org/10.1007/s11120-019-00648-3

Cette page a été laissée intentionnellement vide
This page was intentionally left blank

***

~ Research Article in preparation ~

THYLAKOID MN^{2+} TRANSPORTER CGLD1 (PAM71) IS REQUIRED FOR AN EFFICIENT PHOTOSYSTEM II DONOR SIDE IN *CHLAMYDOMONAS REINHARDTII*.

***

ARTICLE

Thylakoid Mn^{2+} transporter CGLD1 (PAM71) is required for an efficient photosystem II donor side in *Chlamydomonas* cells

Marcio Rodrigues-Azevedo[a,b], Frédéric Chaux-Jukik[a], Wojciech J Nawrocki[c,d,e], Sandrine Bujaldon[a], Catherine de Vitry[a,*]

[a] *UMR7141 CNRS-Sorbonne Université, Institut de Biologie Physico-Chimique, Paris, France*
[b] *Doctoral School of Plant Sciences (SEVE) – ED567 Université Paris-Saclay*
[c] *Biophysics of Photosynthesis, Vrije Universiteit Amsterdam, The Netherlands*
[d] *LaserLaB Amsterdam, Vrije Universiteit Amsterdam, The Netherlands*
[e] *Current address: UMR7141 CNRS-Sorbonne Université, Institut de Biologie Physico-Chimique, Paris, France*

[*] Corresponding author.

E-mail addresses: catherine.devitry@ibpc.fr (C. de Vitry)

Keywords: **Thylakoid membrane, ion transport, *Chlamydomonas reinhardtii*, manganese, CGLD1, PAM71, photosystem II, Oxygen Evolving Complex**

Abstract

Photosystem II (PSII), the water-plastoquinone oxidoreductase of oxygenic photosynthesis, comprises an oxygen-evolving manganese cluster catalyzing the light-driven oxidation of water. Manganese has to access to the lumenal side of the thylakoid membrane where the assembly of the oxygen-evolving Mn_4O_5Ca cluster takes place. Based on a PSII photosensitivity screen, we isolated a manganese transporter mutant. We examined the role of the manganese transporter CGLD1/PAM71 in the thylakoid membrane by comparing the wild-type strain and the *cgld1* mutant from *Chlamydomonas reinhardtii*, and by varying the manganese supply. We found a decreased oxygen evolution rate and a heterogeneity of PSII with accumulation of intermediates of Mn_4O_5Ca assembly when manganese becomes limiting in the thylakoid lumen. We observe a fraction of wild-type-like PSII and a fraction of partially-active PSII. The latter are capable of PSII light-induced primary charge separation, but affected in oxygen evolution, which translates into a phenotype in PSII fluorescence. A slow phase of PSII fluorescence rise in the *cgld1* mutant and in manganese-depleted wild type, but absent in the manganese-replete wild type, reflects a high rate of charge recombination in incomplete Mn_4O_5Ca centers. The presence of active oxygen evolution PSII centers in *cgld1* mutant grown under low light points to a possible manganese trans-thylakoid transfer from stroma to lumen via other cation transporters. We suggest that manganese may be delivered also by the lumenal PSII PsbP subunit (or other PsbP family members), a proposed metallochaperone for Mn^{2+}, which is translocated across the thylakoid membrane from the stroma to the lumen by the twin-arginine translocation (TAT) pathway remarkably able to translocate folded proteins with their cofactors across energy-transducing membranes.

1. Introduction

Oxygenic photosynthesis is the main bioenergetic process producing oxygen and organic matter on earth. Photosynthetic electron transfer chain in the thylakoid membrane involves four major complexes: photosystem II (PSII), cytochrome b_6 *f*, photosystem I (PSI) and ATP synthase. *The first step of this process is the light-driven oxidation of water by PSII. The PSII core is a multimeric pigment protein complex comprising the reaction center complex, the core antenna and the oxygen evolving complex.*

Light energy absorbed by photosynthesis pigments is used for photochemistry (charge separation fueling electron transport), or re-emitted by chlorophyll as fluorescence, or released as a consequence of thermal dissipation. Changes in fluorescence yield are inversely correlated with the rate of photosynthetic electron transfer (Joliot and Joliot, 1964) and this has been used in genetic analysis aimed at an investigation of the components involved in the activity of electron transport since the 1970s (Bennoun and Levine 1970). At room temperature, the variable fluorescence mainly originates from PSII with an emission peak at 690 nm, and it is particularly adapted to analyze PSII activity in vivo (Baker, 2008). The electric field generated by photosynthesis across the thylakoid membrane induces changes in the absorption by photosynthetic pigments, a phenomenon called electrochromic shift (ECS). ECS measured at (520 nm - 546 nm) is proportional to the transmembrane electric field in plants and green algae and is a powerful tool to study photosynthetic processes *in vivo* (Witt, 1979; Bailleul et al, 2010).

To investigate the biogenesis and maintenance of the photosynthetic apparatus we have used the unicellular green alga *Chlamydomonas reinhardtii* (hereafter referred to as *Chlamydomonas*) which is a reference model organism for studying photosynthesis. *Chlamydomonas* can grow on acetate as source of reduced carbon when photosynthetic activity is impaired, synthetizes chlorophyll also in the dark, has established genetics and its culture medium can be easily modified (Rochaix, 2002). We screened mutants on their PSII sensitivity after a short photo-inhibitory treatment. This approach was fruitful and led to the finding of a mutant of the thylakoid membrane

manganese (Mn) transporter CGLD1. In *Arabidopsis thaliana*, the CGLD1 orthologue PAM71 was first identified by a genetic approach (photosynthesis-affected mutant 71) as an integral thylakoid membrane protein required for efficient Mn import into the thylakoid lumen (Schneider et al, 2016), while the chloroplast Mn transporter 1 (CMT1) was found to transport Mn across the chloroplast inner envelope membrane (Eisenhut et al, 2018; Zhang et al, 2018; Krieger-Liszkay and Thomine 2018). These chloroplast Mn^{2+} transporters belong to the Uncharacterized Protein Family 0016 (UPF0016) well conserved through evolution (Demaegd et al, 2014) and are proposed to have evolved from the cyanobacterial endosymbiont (Hoecker et al, 2021). Mn supply in the thylakoid lumen has a crucial function in the PSII oxygen evolving complex, where a Mn_4O_5Ca cluster catalyzes the water-splitting reaction (Umena et al, 2011). D1 and D2 subunits of the PSII reaction center bind the main redox cofactors involved in electron transfer in PSII. Light excitation leads to the primary charge separation with an electron transferred from the chlorophyll donor P680 to the pheophytin acceptor. Subsequently, the electron is passed to the bound plastoquinone Q_A and to the mobile plastoquinone Q_B, which leaves PSII after undergoing two sequential reductions and two protonations forming the plastoquinol PQH_2. The electron hole at P680 is filled by the secondary donor the Y_Z tyrosine residue from D1 subunit, which is in turn finally rereduced by the Mn_4O_5Ca cluster. The S states denotes oxidation states of the Mn cluster involved in the storage of oxidizing equivalents in the water oxidase.

Upon high light, PSII is particularly damaged, and reaction center subunit D1 needs to be degraded and replaced by de novo synthesized D1 for a proper PSII repair. The major protease involved is this PSII repair cycle is the thylakoid FtsH protease (Kato and Sakamoto 2018; Malnoë et al, 2014). During this PSII damage and repair cycle, Mn is released when D1 is degraded and the new synthetized D1 in the PSII core will require photoactivation for the assembly of an active Mn_4O_5Ca cluster, as for the *de novo* biogenesis of PSII (Bao and Burnap,2016; Cheah et al, 2020).

Mutants lacking CGLD1 in *Chlamydomonas* or lacking PAM71 in *Arabidopsis* showed an increased PSII photosensitivity compared to wild type (Schneider et al, 2016;

Xing et al, 2017). Hereafter, we refer to the *Chlamydomonas* mutants as *cgld1* and to the *Arabidospis* mutants as *pam71*. In these studies, the *cgld1* and *pam71* mutants cultured under medium light (60 and 90 µmol photons m^{-2} s^{-1} respectively) had reduced amounts of PSII complex which hampered their characterization.

In this work, we explored PSII accumulation and activity of wild-type and *cgld1* strains grown under low light to enhance PSII accumulation and limit PSII photoinhibition. We found growth light conditions that allow wild-type level of accumulation of PSII complexes in *cgld1* mutant. We show that CGLD1 is required for efficient PSII donor side activity. We find that Mn supplementation restores in a few hours the maximal PSII yield in *cgld1* mutant while Mn depletion, induces a *cgld1*-like PSII phenotype in the wild-type strain. In *cgld1* mutant grown under low light we observe a fraction of wild-type-like PSII and a fraction of partially-active PSII. The latter are capable of PSII light-induced primary charge separation but altered in oxygen evolution and chlorophyll fluorescence. A very slow phase of fluorescence rise in presence of the inhibitor of PSII acceptor side DCMU is observed when Mn is limiting for PSII activity and is lost when the Mn cluster is destabilized by addition of an alternative electron donor to PSII (hydroxylamine). We propose a model accounting for this in PSII centers.

2. Materials and methods

2.1. Strains and growth conditions

Wild-type (t222, mt+), and mutant strains of *Chlamydomonas reinhardtii* and progeny of the cross with the interfertile species *Chlamydomonas grossii* (also known as S1-D2 or CC-2290), which has a suitable profusion of genomic polymorphisms to permit the identification of the region bearing a mutation (Rymarquis et al., 2005) were grown mixotrophically at 25°C in Tris-acetate-phosphate (TAP) medium (Harris, 1989) under continuous light (5-10 µmol photons m^{-2} s^{-1}) unless otherwise specified and collected during the exponential phase at 2 x 10^6 cells mL^{-1}. Cross was performed according to Harris (1989). The *cgld1* mutation has a modified segment of 15 bp including a 7 bp insertion (*cgld1 CCTCCACCTCCA*TCG versus WT TC-------GGCTCA) and was detected by

PCR using a forward primer 5'- CCTCCACCTCCATCGGAGAT -3' specific to the *cgld1* allele and a reverse primer a 5'- GCGTAATCGCCTTTGCCAT -3' common to wild-type and *cgld1* alleles as a 356 bp PCR product amplified only in presence of the *cgld1* mutation. The *ΔpsbA* mutant *Fud7* bears a deletion in the chloroplast gene which encodes D1 protein (Bennoun et al, 1986; de Vitry et al, 1989). The nuclear *psbO-Fud44* mutant contains a 5 kb DNA insert in the 5' region of the single *PSBO* gene and lacks PsbO/OEE1 protein (Mayfield et al, 1987a). The nuclear *psbP-BF25* mutant of the single *PSBP* gene lacks PsbP/OEE2 protein (Mayfield et al, 1987b). The nuclear *ftsh1-1* mutant expresses an inactive thylakoid FtsH protease (Malnoë et al, 2014). Tris-acetate-phosphate (TAP) medium contains 25 µM Mn^{2+} cations (Harris, 1989). TAP medium was tenfold enriched with $MnCl_2$ (Mn 10X) to contain 250 µM Mn^{2+} (Schneider et al, 2016). TAP medium depleted in Mn^{2+} was prepared without any Mn^{2+}. In case of Mn depletion, TAP grown wild-type cells were diluted hundredfold in TAP Mn deficient medium and grown for two days, then again diluted hundredfold in TAP Mn deficient medium grown for two days before fluorescence measurements. The *CGLD1* (*F28O*) mutant was generated in an effort to target and knock-out *FTSH2* by CRISPR approach. We electroporated in wild-type $t222^+$ the hygromycin resistance cassette in the presence of the Cas9 enzyme and RNA guides as described (Findinier et al, 2019). Transformants were plated on selective medium (TAP hygromycin 20 mg L^{-1}); colonies were then transferred to fresh TAP medium and grown mixotrophically in low light (5 to 10 µmol photons m^{-2} s^{-1}) for 7 days before chlorophyll fluorescence analysis (see below) and photo-inhibitory treatment (1 h at 1000 µmol photons m^{-2} s^{-1}). The *cgld1 (F28O)* mutant has an accumulation level of the thylakoid FtsH protease subunits FtsH1 and FtsH2 similar to that in wild-type (Chaux et al, 2022).

2.2. Protein isolation and immunoblot analysis

Thylakoid membranes were isolated as described (Chua and Bennoun, 1975). Before electrophoresis, proteins from whole cells or from thylakoid membranes were resuspended in 200 mM 1,4-DTT and 200 mM Na_2CO_3, solubilized in the presence of 2% SDS at 100°C for 50 s, and then spun down at 12.000 g for 15 min to remove insoluble material and subsequently analyzed. Cell or thylakoid extracts were loaded on chlorophyll basis, separated by SDS-PAGE and electro-transferred onto nitrocellulose membranes (Amersham Protran 0.1 µm NC) by semi-dry method. After semi-dry transfer, membranes were stained in Ponceau (loading control). The blot membranes were incubated separately in primary antibodies against: AtpB (that recognizes CF1 β and F1 β; Atteia et al, 1992), PSI subunit PsaD (kindly provided by Dr. Yuichiro Takahashi), and PSII subunits PsbA-D1 (Agrisera AS05084), PsbB-CP47, PsbC-CP43, PsbD-D2 (Agrisera AS06146), PsbP-OEE2 and PsbQ-OEE3. Primary antibodies were revealed by horseradish peroxidase-conjugated antibodies against rabbit IgG (n° W401B, Promega). Signals were acquired in a ChemiTouch imaging system (Bio-Rad).

2.3. Chlorophyll fluorescence measurements

Fluorescence yield changes were measured *in vivo* at room temperature, on exponentially growing cultures that were dark-adapted for at least 1 min. Three fluorescence systems were used: a home-made fluorescence setup (Rappaport et al., 2007) and a Joliot-type spectrometer (JTS-10, Biologic, Grenoble, France) on cuvettes filled with 1-3 mL of algal suspension, or a CCD camera imaging fluorometer (SpeedZen, JBeamBio, France) for measurements on plates (Johnson et al., 2009). In these set-ups, the detecting light consisted in blue pulses and the 250-ms saturating pulses were of green light (532 nm, 6200 µmol photons m^{-2} s^{-1}) or red light (619 nm, 2600 µmol photons m^{-2} s^{-1}, JTS-10). The maximal quantum yield of PSII photochemistry (F_v/F_m) was calculated as (F_m - F_0)/F_m, where F_v is the variable fluorescence, F_0 is the fluorescence level measured after dark adaptation of the cells in absence of DCMU (where the primary quinone acceptor Q_A of PSII is fully oxidized and the PSII reaction centers are in "open

state"), and F_m is the maximum fluorescence level (where the primary quinone acceptor Q_A of PSII is fully reduced and the PSII reaction centers are in "closed state"). F_m is measured shortly after the saturating light pulse (Genty et al., 1989; Baker, 2008) or at the end of a fluorescence rise induced by an actinic illumination of 135 µmol photons m^{-2} s^{-1} in the presence of 10 µM of the PSII acceptor side inhibitor 3-(3,4-dichlorophenyl)-1,1-dimethylurea (DCMU).

Time-resolved fluorescence (**Fig. 3**B) was recorded *in vivo* at room temperature with a time-correlated single-photon counting setup (FluoTime 200, PicoQuant), as described previously in (Nawrocki et al, 2021). A 10 mm by 10 mm quartz cuvette was used, and the cells were stirred using a magnetic stirrer during the measurements. Excitation was provided by a 438-nm laser working at a 10-MHz repetition rate and was set to 40 µW, unless otherwise specified, using a neutral density filter. Laser power 40 µW and 0.14 µW, and repetition rate 10 MHz and 5 MHz, were used for PSII closed state and open state measurements respectively. A long-pass optical filter was placed in front of the detector to prevent scattered light from reaching the photodiode. Detection was done at 680 ± 8 nm with 4-ps bins. DCMU (5 µM) was added to close PSII (F_m state). The instrument response function (IRF) was measured through the decay of pinacyanol iodide in methanol (6-ps lifetime). IRF obtained was 88-ps FWHM under the same conditions as sample measurements. Data analysis was done with the FluoFit software, and the decays were deconvoluted with the IRF and three exponential decay functions to yield $\tau_{average}$ values.

2.4. Electrochromic shift measurements

Cells were harvested during exponential growth (2 10^6 cells ml^{-1}) and were resuspended at a concentration of 10^7 cells ml^{-1} in minimum medium with the addition of 10% (w/v) Ficoll to prevent cell sedimentation during the measurements. The cell suspension was then vigorously stirred in a 50-ml Erlenmeyer flask for 20 min in the dark at 340 rpm to achieve aerobic conditions. Samples were also thoroughly mixed and aerated prior to absorption measurements for each wavelength probed. *In vivo* ECS

measurements (Bailleul et al, 2010) were performed by monitoring absorbance at 520 nm and 546 nm using the JTS10 spectrometer, as previously described (Bujaldon et al, 2020). The detecting and continuous lights were provided by white LEDs passing through interferential filters (520 ± 10 nm or 546 ± 6 nm) and the saturating flash by a dye laser (690 nm) pumped by a second harmonic of a neodymium-doped yttrium aluminum garnet (Nd:YAG) laser (Minilite II, Continuum). PSI and PSII charge separation capacity were calculated from changes in the amplitude of the fast phase (100 µs) of the ECS signal (at 520 nm minus at 546 nm) upon excitation with a saturating laser flash in the presence or absence of the PSII inhibitors. PSII was inhibited by 1 mM hydroxylamine and 10 µM DCMU to determine the PSI/(PSI+PSII) ratio.

2.5. Oxygen evolution measurements

For oxygen measurements (**Fig. 3**D), *Chlamydomonas* cells were washed in a 40 mM MES buffer (pH 6.5) containing 15 mM $CaCl_2$, 15 mM $MgCl_2$, 20 mM NaCl and 1 M betain and were suspended in the same buffer. Oxygen evolution of *Chlamydomonas* whole cells was measured at 25 °C by polarography using a Clark-type oxygen electrode (Hansatech) with saturating white light through infrared and water filters, adapted from (Sugiura et al, 2015). The activity was measured over a period of 1.5 minute in the presence of 1 mM 2,6-dichloro-p-benzoquinone (DCBQ) dissolved in dimethyl sulfoxide as an artificial electron acceptor of the Q_A/Q_B site. Chlorophyll concentrations were determined just after the experiment at 680 nm minus 750 nm from 550 to 750 nm spectra.

For oxygen measurements (**Fig. E** sup. mat. B), *Chlamydomonas* cells were concentrated in some TAP supernatant between 1.3 and 2.0 10^7 cells mL^{-1}. Oxygen evolution of *Chlamydomonas* whole cells was measured at 25 °C using a Clark-type oxygen electrode with various white light intensities over a period of 1.5 minute.

2.6. Sequence Analysis

Multiple sequence alignments were performed using Clustal Omega, version 1.2.4 (Sievers et al, 2011) with default parameters followed by manual editing. After

removing ambiguously aligned regions, 174 sites were retained for the phylogenetic analysis (**Fig. C** supp. mat. C). The tree was constructed using phylogenetic tree on Clustal Omega site which gives a Neibour-joining tree without distance corrections (**Fig. C** supp. mat. B). Transmembrane helix (TMH) predictions were predicted by DeepTMHMM (Hallgren et al, 2022) with manual adjustments for *Chlamydomonas* CGLD1 (**Fig. 1**C) or as indicated when amino acid residues were predicted in a TMH in at least one of the 3 sequences (**Fig. C** supp. Mat. A). *Chlamydomonas* CGLD1 structure (**Fig. 1**F) was predicted using AlphaFold (Jumper et al, 2021; Varadi et al, 2021). Sequences data of CGLD1/PAM71 related proteins used in this article can be found on Phytozome *Chlamydomonas reinhardtii* cc-4532 v6.1 (CrCGLD1, Cre02.g084350; CrCTM1A, Cre16.g660000; CrCTM1B, Cre16.g660050; and CrPML, Cre17.g731300), on Phytozome *Arabidopsis thaliana* TAIR10 (AtPAM71, At1g64150; AtCTM1, At4g13590; AtPML3, At5g36290; AtPML4: At1g25520; AtPML5: At1g68650) and on Uniprot as accession P52876 for *Synechocystis* PCC 6803 (sll0615).

3. Results

3.1. Isolation of cgld1-KO mutant

Photosensitive *Chlamydomonas* mutants were screened by chlorophyll fluorescence after a random nuclear mutagenesis by electroporation of the hygromycin resistance cassette. The *F28O* mutant isolated during this screen showed a lower maximal PSII efficiency (F_v/F_m) than in wild-type strain after 1 hour of high light as in photosensitive mutants (**Fig. 1**A). The *ftsh1-1* mutant expressing an inactive FtsH1 protein is highly sensitive to HL stress (Malnoë et al., 2014) and was used as control photosensitive strain. A cross of *F28O* mutant with the interfertile species *Chlamydomonas grossii* (also known as S1-D2 or CC-2290), showed a tetrad 2:2 segregation of the F_v/F_m phenotype indicating that the F28O phenotype was due to a single mutation in the nuclear genome (**Fig. 1**B). In addition, this cross demonstrated that the photosensitivity is not linked to the hygromycin resistance (**Fig. A** sup. mat.). To

identify the mutation, we sequenced the whole genomes of *F28O* mutant and wild-type strain on which the mutagenesis was performed (for comparison) by paired-end Illumina sequencing and mapped the reads on the genome assembly (**Fig. B** sup. mat.) according to (Bujaldon et al, 2020). Sequencing reveals a 7-bp insertion in the first exon of *CGLD1* gene (Cr02.g084350_4532.1) which causes a frameshift and an abortive stop codon in the following exon (**Fig. 1**C). The *cgld1 F28O* mutation truncates the precursor protein from 340 to 82 amino-acid residues. The CGLD1 protein is a manganese transporter across the thylakoid membrane, Mn^{2+} being required in the thylakoid lumen for the assembly of the oxygen-evolving Mn_4O_5Ca cluster of photosystem II (PSII) (**Fig. 1**D). The precursor CGLD1 protein has a targeting sequence to the thylakoid lumen comprising a hydrophobic segment ending by the AXA motif recognized by the thylakoid processing peptidase (**Fig.1**E). The mature CGLD1 protein has two repeated domains of 3 transmembrane helices (TMH) separated by a central loop and oriented in an antiparallel manner in the membrane with a highly conserved motif E-Φ-G-D-[KR]-[TS] lining the pore in THM1 and THM4 (**Fig. 1**E), as previously described for yeast homolog (Demaegd et al, 2014; Colinet et al, 2017) and as present in the *Chlamydomonas* CGLD1 structure predicted by AlphaFold (**Fig. 1**F). The sequence alignment of *Chlamydomonas* CGLD1 with *Arabidopsis* PAM71 and their homolog in *Synechocystis* shows the conservation of the mature protein (**Fig. C** sup. mat). In all the progeny of the *F28O* x S1-D2 cross, the lower F_v/F_m and the higher PSII photosensitivity were linked to the *cgld1* mutation as seen for the tetrad (**Fig. 1**B) and for other progeny strains (**Fig. D** sup. mat. A and B). Despite having some dysfunctional PSII, the *cgld1* mutant can still grow photoautotrophically under low light (**Fig. D** sup. mat. C and D).

3.2. Accumulation of PSII and primary charge separation in PSII are not reduced in the mutant

F_v/F_m is usually a proxy of PSII integrity and photochemical capacity, but F_v/F_m can also be decreased due to a low accumulation of PSII (in that case the contribution of poorly connected LHCII antenna proteins in excess and of PSI to the F_0 fluorescence

becomes significant and reduces F_v/F_m). It was therefore important to determine if the reduced F_v/F_m would be due to a decreased accumulation of PSII or to our growth conditions that allowed accumulation of altered PSII. We therefore characterized the accumulation of PSII subunits in *cgld1* mutant grown under low light (6 µmol photons m^{-2} s^{-1}) by SDS-PAGE and immunoblot analysis. Importantly, the mutant accumulated wild-type levels of PSII, PSI and ATP synthase subunits (**Fig. 2**A). Ponceau red protein staining of cell and membrane extracts on the blots before immunoblot analysis show the loading and protein migration pattern (**Fig. E** sup. mat. A). The PSII oxygen evolution enhancer 2 (OEE2), also named PsbP, is targeted across the thylakoid membrane by a twin-arginine targeting peptide (**Fig. 2**B and discussion).

The photosystem stoichiometry was further characterized by the single-turnover flash induced electrochromic shift (ECS) to detect the stoichiometry of the charge separation capacity of PSI and PSII. The fast phase (phase a, < 200 µs) of the ECS increase following a saturating laser flash corresponds to the photochemical events in the two photosystems and the amplitude of this phase is proportional to the amount of active photosystems. Inhibition of PSII activity is obtained by illuminating the sample in presence of DCMU and hydroxylamine, and the relative decrease of the fast phase amplitude is proportional to the PSI/(PSI+PSII) reaction center ratio (Bailleul et al, 2010). The same photosystem ratio was detected in the *cgld1* mutant and the wild-type strain (WT) by ECS (**Fig. 2**C), as was by immunodetection (**Fig. 2**A).

Therefore the PSII centers in the mutant strain can perform at least the light induced primary charge separation. To characterize their activity upon multiple turnovers, we further analyzed PSII function using PSII fluorescence and PSII oxygen evolution.

3.3. Lack of CGLD1 affects PSII fluorescence and oxygen production

On the one hand, the maximal quantum yield of PSII photochemistry (F_v/F_m) was calculated from steady-state data of fluorescence yield in dark-adapted cells, where F_v is the variable fluorescence (F_m - F_0), F_0 is the fluorescence of dark-adapted cells in

absence of DCMU, and F_m is the maximum of fluorescence using a saturating light pulse. This method uses strong light to induce many charge separations in (active) PSII, which rapidly leads to outcompeting the Q_A^- reoxidation by its light-driven reduction, and to reaching the F_m level. The relation between F_m and F_0 parameters - variable fluorescence F_v - is thus a proxy for the maximal quantum yield of PSII (Wientjes et al, 2013; Sipka et al, 2021). It showed at chlorophyll constant, values of 0.61 and 0.78 for *cgld1* and WT strains, respectively (**Fig. 3**A). Nonetheless, steady-state fluorescence methods, and consequently the F_v/F_m measurements, yield no information about whether F_0 or F_m levels change in the sample. On the other hand, to assess F_0 or F_m levels, we used time-resolved fluorescence in the open (F_0) and closed (F_m) state. These measurements showed that changes in both of these values contributed to the decrease of F_v/F_m, but the majority of the effect could be ascribed to the rise in F_0. Time-resolved fluorescence-based determination of F_v/F_m was in good overall agreement with the steady-state data (0.58 and 0.78 for *cgld1* and WT, respectively; see **Fig. 3**B and Fig. F sup. F).

In *cgld1* as compared to the WT, F_0 is higher and F_m lower whether measured with a saturating pulse (**Fig. 3**A), or with laser flashes in the presence of DCMU (**Fig. 3**B). However, combining the two (saturating pulse and DCMU) results in a higher F_m in the *cgld1* mutant (**Fig. 3**C). This suggests that the F_m and F_v/F_m of the mutant are underestimated with the methods in panels A and B, and that the mutant develops some particular properties when its fluorescence is measured in presence of DCMU in the light.

The consequences of the absence of CGLD1 on PSII photochemistry were measured by analyzing the rate of oxygen evolution using a Clark-type oxygen electrode. The rate of oxygen evolution for *cgld1* mutant dropped significantly compared with the WT strain (**Fig. 3**D and **Fig. E** sup. mat. B). Thus, there is a significant impact of CGLD1 on PSII activity at both maximal PSII efficiency and steady-state operational efficiency, as assessed through oxygen evolution rates in *Chlamydomonas*.

3.4. Analysis of cgld1 mutant fluorescence in presence of PSII inhibitor DCMU

To understand whether the decrease in PSII activity results from a homogenous loss of function, or from the simultaneous presence of active- and inactive RCs, we explored a broad range of experimental conditions. We measured the fluorescence yields while: 1) adding DCMU to block PSII acceptor side at Q_B site, 2) repeating the illumination to detect a possible PSII lack of recovery after the first illumination, 3) varying the dark-adaptation period to measure PSII inactivation in the dark, 4) triggering the light-dependent assembly of the Mn_4O_5Ca cluster, 5) adding DCMU and HA to destroy the Mn_4O_5Ca cluster, or 6) in comparison with mutants lacking oxygen evolution enhancer PSII subunits.

After addition of DCMU, the F_0 increases due to the Q_B^{*-} to Q_A electron transfer upon DCMU binding to the semiquinone-occupied sites (Wollman, 1978). Following even low light illumination in the presence of DCMU, the F_m is then reached quickly in the wild type, because only one electron transfer is needed to reduce Q_A. Fluorescence kinetics in presence of DCMU showed a rapid increase to a plateau in the WT strain but revealed an additional slow phase in the *cgld1* mutant of ~20% of the variable fluorescence (**Fig. 4**A). F_m was a little lower in presence than in absence of DCMU in the WT strain due to the increased fluorescence quenching upon quinone pool oxidation (Vernotte et al, 1979). The opposite was observed in the mutant, suggesting its F_m was not reached in absence of DCMU (with actinic illumination prior to the saturating pulse (**Fig. 4**A) as without (**Fig. 3**C)), at least in part of the PSII reaction centers. The *cgld1* fluorescence rise suggest a heterogeneity of PSII centers with some centers affected in the fluorescence yield kinetics (slow phase).

If this slow phase is indeed associated with an inefficient charge separation resulting from electron transfer from the donor side with a reduction of Y_Z too slow to prevent Q_A^-/Y_Z^+ back-reactions, then it is expected to disappear in the presence of an artificial donor (HA). This slow phase did disappear with addition of HA, and the fluorescence rise became similar in *cgld1* and WT strains (**Fig. 5**). This slow phase thus

corresponds to the impossibility of completely reducing Q_A in the absence of an electron source on the donor side. The only possible explanation is that the electrons coming from the donor side serve to stop the charge separation/recombination sequence that would otherwise occur between Y_Z and Q_A in the presence of DCMU. In the presence of DCMU and HA, the fluorescence rise in the WT strain was slower than in the presence of DCMU alone (with 2/3 of the rise in around 20 ms and 5 ms respectively) and the relaxation through charge recombination after the illumination was lost. These observations result from the mode of action of HA, which destroys the manganese complex of PSII, is a slower electron donor to PSII than the manganese cluster but once oxidized (oxidized HA being mobile and diffusing away from the RC in the thylakoid lumen) is not a substrate for the back-reaction with Q_A^- (Bennoun and Joliot, 1969; Joliot, 1977). After a first illumination, active PSII with Mn_4O_5Ca in wild-type re-open in a few seconds due to back reactions notably charge recombination of the $S_2Q_A^-$ state (Bennoun, 1970; Rappaport et al, 2002) while PSII lacking Mn_4O_5Ca by hydroxylamine treatment (**Fig. 5**) or some PSII altered in *cgld1* stay closed (**Fig. 4**A). In the latter, the amplitude of the slow phase corresponded to the amplitude of slowly re-opening PSII.

To further understand the properties of the slow fluorescence rise and of the recovery in affected PSII RCs, we repeated the illumination after a dark period within minutes after the first one. The wild-type strain showed a similar fluorescence kinetic upon first and second illumination, while the mutant had lost most of the slow phase and had a higher F_0 upon the second illumination (**Fig. 4**B), in agreement with only partial relaxation of the fluorescence after the first illumination (**Fig. 4**A). In the presence of DCMU, the lack of recovery of the slow phase in *cgld1* and the higher F_0 after a second illumination may be due to centers deficient in manganese with incomplete oxygen evolving center that would remain closed. When Q_A and the donor side are reduced in the presence of DCMU, if the charge released by back-reactions in the wild-type donor side cannot be released in PSII centers altered in manganese cluster and lacking of these back-reactions in the *cgld1* mutant, then closed centers are expected to appear upon dark adaptation and to disappear with photoactivation in this mutant.

To explore the effect of dark adaptation on PSII activity, we varied the dark-adaptation period prior to DCMU addition and prior to first illumination measurements. Indeed, the mutant showed after dark adaptation a larger increase of F_0 than in wild type which correlated with the loss of the slow fluorescence rise in the mutant and a slower relaxation of the fluorescence after the first illumination compared to the WT (data are normalized to F_m in **Fig. 4**C, and are compared to data non-normalized and data normalized to F_m and F_0 in **Fig. G** sup. mat.). We then tested whether low light would facilitate recovery after dark adaptation. Indeed, a few-seconds of low light after dark adaptation and prior to DCMU addition and measurement allowed recovery of most of the decrease in F_0 and of the slow phase of fluorescence rise (**Fig. H** sup. mat.). This suggests that in darkness, a slow impairment of the OEC in the *cgld1* mutant takes place which can be released by probable photoreconstitution of the Mn cluster.

We compared *cgld1* with mutants lacking subunits the oxygen evolving complex *psbO-Fud44* lacking PsbO (Mayfield et al, 1987a) and *psbP-BF25* lacking PsbP (Mayfield et al, 1987b). In absence of PsbO some of PsbP and PsbQ is found attached to the thylakoid membrane, and in absence of PsbP some of PsbO but no PsbQ is found attached to the membrane (de Vitry et al, 1989). The donor side of these strains and WT is schematized (**Fig. I** sup. mat. A). The phenotype of light induction kinetics of these donor side mutants, although having much less PSII activity than *cgld1* mutant, showed - as did *cgld1* - an F_v/F_m lower than in WT, a slow phase of rise in DCMU, and a F_m in DCMU higher than F_m without DCMU (**Fig. I** sup. mat. B).

In summary, the fluorescence experiments described above suggest a dynamic, light-dependent type of PSII donor side impairment in the *cgld1* mutant.

3.5. cgld1 mutant Mn supplementation and wild type strain Mn depletion

To study the effect of manganese concentration on PSII activity, we tested the PSII function on cells grown four days on TAP plates supplemented with 10x Mn^{2+}. Mn supplementation restored maximal PSII efficiency in our *cgld1* mutant (**Fig. 6**A). To further examine the kinetics of the restoration of photosynthesis, *cgld1* and WT strains

were grown in liquid TAP medium and transferred to TAP-supplemented medium (Mn x10) measuring PSII activity every hour. Supplementation with Mn^{2+} restored photosynthetic activity of PSII (F_v/F_m) of *cgld1* mutant within about 10 hours (**Fig. 6**B).

We then explored whether the wild-type strain upon Mn depletion would present *cgld1* symptoms. We found that Mn depleted wild type within 4 days had as *cgld1* a lower F_v/F_m, a higher F_m in presence than in absence of DCMU, and a slow phase of fluorescence rise in the presence of DCMU (**Fig. 6**C). Concerning PSII activity, the Mn depletion symptoms of the wild-type were slower to appear than the Mn supplementation restoration of *cgld1* strain.

4. Discussion

4.1. Manganese transport UPF0016 proteins in Chlamydomonas

In *Arabidopsis* five members of UPF0016 have been described. AtPAM71 protein (At1g64150) transports Mn^{2+} across the thylakoid membrane (Schneider et al., 2016). AtCMT1 protein (At4g13590) transports Mn^{2+} across the chloroplast envelope inner membrane (Eisenhut et al., 2018; Zhang et al., 2018). The three other *Arabidopsis* members of the family were named pam71-like (PML): AtPML3 (At5g36290) was located in the Golgi membrane (Yang et al., 2021), whereas AtPML4 (At1g25520) and AtPML5 (At1g68650) in the endoplasmic reticulum (ER) compartment (Hoecker et al, 2020). The cyanobacterial Mn exporter MNX/SyPAM71 (sll0615) found in the plasma and thylakoid membranes prevents accumulation of toxic levels of Mn^{2+} in the cytosol and ensures lumenal Mn^{2+} supply to PSII (Brandeburg et al, 2017; Gandini et al, 2017; Eisenhut 2020). AtCMT1, and SyPAM71 can operate in the thylakoid membrane and substitute for AtPAM71 to restore PSII efficiency, indicating that the manganese transport function is conserved between these proteins (Hoecker et al, 2021).

Chlamydomonas has four UPF0016 members. The phylogenetic tree of UPF0016 members in *Chlamydomonas, Arabidopsis* and *Synechocystis* indicates CrCGLD1 (Cre02.g084350) is an orthologue of AtPAM71, CrCMT1A (Cre16.g660000) and

CrCMTA1B (Cre16.g660050) are orthologues of AtCMT1, and CrPML (Cre17.g731300) is an orthologue of AtPML4 and AtPML5 **(Fig. C** supp. mat. B). The alignment of CrCGLD1 with AtPAM71 and SyPAM71 shows the conserved features of UPF0016 and that SyPAM71 sequence starts just before the first of the 6 transmembrane helices **(Fig. C** supp. mat. A).

4.2. Mature protein and topology of CGLD1/PAM71 in the thylakoid membrane

CGLD1/PAM71 protein is encoded by a nuclear gene, synthetized in the cytosol as a precursor with a bipartite N-terminal targeting peptide. The first targeting peptide part functions as a chloroplast import signal. The protein is imported via the translocon of the outer membrane of the chloroplast (TOC) and the translocon of the inner membrane of the chloroplast (TIC) envelope. The stromal targeting peptide is cleaved after import by the stromal processing peptidase (SPP). The second targeting peptide allows transfer through the thylakoid membrane. This thylakoid transfer sequence is cleaved by the membrane bound thylakoid processing peptidase (TPP) on the lumenal side of the membrane. A chloroplast targeting peptide was previously proposed for *Arabidopsis* PAM71 as predicted by TargetP (Schneider et al, 2016; Hoecker et al, 2020) or ChloroP (Gandini et al, 2017) but surprisingly no thylakoid lumenal transfer peptide was reported.

The well-known features of the thylakoid lumenal transfer sequence are a hydrophobic region followed by a short-chain residues, most frequently alanine residues, in position -3 and -1 positions relative to the cleavage site (Teixeira et al, 2013), and that was therefore named AXA motif. TPP cleaves not only proteins translocated to the thylakoid lumen (as PsbO, PsbP, PsbQ, plastocyanin) but also integral thylakoid membrane proteins with N-terminal localization in the lumen as cytochrome *f* (Kuras et al, 1995) and thylakoid FtsH proteases (Wang et al, 2017). We recognize all the features of thylakoid transfer sequences in CrCGLD1p (**Fig. 1**C) and AtPAM71p (**Fig. C** sup. mat.) precursor proteins. These features were also recognized by TargetP version 2 which is able to predict thylakoid lumenal transfer peptides (Almagro Armenteros et al, 2019),

and which predicts maturation sites after AXA motif for CrCGLD1p (position: 109-110. ADA-AA. Probability: 0.4605) and for AtPAM71p (position 134-135. AFA-AS. Probability: 0.8876). We propose therefore that CGLD1/PAM71 are membrane proteins matured by TPP with N-terminal localization in the lumen. Taking into account the prediction of transmembrane domains made by using DeepTMHMM (Hallgren et al, 2022) and the prediction of the localization of positively charged segments (positive basic residues in loops indicated for CGLD1 in **Fig. 1**C, 9 stromal/inside versus one lumenal) by the ''positive inside rule'' (Gavel et al, 1991), we conclude that CGLD1 has six transmembrane domains (TMH), with its N terminus and C terminus in the lumen.

Our topological model is consistent with protease treatments of Golgi vesicles from yeast that localized the acidic central loop of CGLD1 homolog GDT1 in the cytosol (Demaegd et al, 2014) and of intact thylakoid membranes from *Arabidopsis* that localized the C-terminal of PAM71 on the lumenal side of the membrane (Schneider et al, 2017). Our 6 THM model differs from their proposed 7 TMH model, the latter having an additional predicted TMH domain at the N terminus and the C terminus exposed on the opposite side of the membrane (Demaegd et al, 2014; Schneider et al, 2017). We propose that the N-terminal hydrophobic segment is part of the thylakoid lumenal transfer peptide and is absent in the CGLD1/PAM71 mature protein. Proteomic determination of the N terminus peptide or N-terminal sequencing should confirm the maturation site.

4.3. PsbP a metallochaperone for Mn^{2+}

Extrinsic proteins PsbO, PsbP, and PsbQ of PSII form a lumenal cap that protects and stabilizes the oxygen-evolving complex. Their absence greatly affects PSII activity (see very low F_v/F_m in *psbO* and *psbP* mutants in Fig. I sup. mat.). In addition, a role for PsbP to assist metal delivery as metallochaperone for Mn^{2+} in the thylakoid lumen has been proposed on the base of manganese binding to PsbP (Bondarava et al, 2005; Bondarava et al, 2007) with a structure that contains two Mn^{2+} binding sites in spinach (Cao et al, 2015). Overaccumulation of the ancestral form of PsbP, denominated CyanoP

in the *Synechocystis ΔSynPAM71* mutant, may help to alleviate the effects of increased levels of Mn^{2+} (Gandini et al, 2017). In conditions of Mn limitation for PSII assembly/repair, the accumulation of PsbP as of other PSII subunits was reduced to 50% of wild-type level in *Arabidopsis pam71* mutant grown in a 12 h day at 90 µmol photons m^{-2} s^{-1}/ 12 h night cycle (Schneider et al, 2016). PsbP accumulation was of wild-type level in *Chlamydomonas cgld1* mutant grown under 6 µmol photons m^{-2} s^{-1} (this study, **Fig. 2**A and Fig. E sup. mat.). Altogether, these results suggest that the PsbP protein may store Mn^{2+} when in excess and during the light-induced turnover of D1 in the PSII damage-repair cycle and deliver Mn during PSII assembly and upon PSII repair.

4.4. A similar PSII altered phenotype in cgld1 and pam71 mutants

The only UPF0016 mutants studied in *Chlamydomonas* are those of CGLD1. Three *cgld1* mutants have been characterized in *Chlamydomonas*: the paromomycin resistance cassette is inserted in exon 2 of the *CGLD1* gene at position +352 bp relative to the start codon in mutant *cgld1-CAL029_02_05* (Dent et al, 2015; Schneider et al, 2016), the insertion of the paromomycin cassette in mutant *cgld1-x32* caused a deletion of *CGLD1* and 4 additional genes and was compared to CGLD1 compared to complemented strains (Xing et al, 2017), and the 7-bp insertion in exon 1 at position +177 bp relative to the start codon of *CGLD1* gene caused a frameshift and an abortive stop codon (this study, **Fig. 1**C). As in the case of the *Arabidopsis pam71* mutant, the *Chlamydomonas cgld1* mutants have photosynthetic defects indicating reduced PSII function as seen by reduced F_v/F_m and O_2 evolution, which can be partially rescued by addition of Mn. In contrast to previous work, we analyze PSII activity of *cgld1* strains grown under low light to limit PSII photoinhibition and accumulate wild-type level of PSII complexes. By various spectroscopic measurements, we show that CGLD1 is required for efficient PSII donor side activity. A very slow phase of fluorescence rise in presence of the inhibitor of PSII acceptor side DCMU is observed when Mn is limiting for PSII activity, notably lost

when the Mn cluster is destabilized by addition of an alternative electron donor to PSII (hydroxylamine). We propose a model accounting for the heterogeneity in PSII centers and Mn delivery in *cgld1* mutant (**Fig. 7**).

4.5. Mn supplementation in a few hours in cgld1 mutant and alternative Mn uptake

In absence of CGLD1, we measured that addition of Mn^{2+} restored photosynthetic activity of PSII (F_v/F_m) of *cgld1* mutant within a few hours under low light (**Fig. 6**B). This indicates the presence of uncharacterized low-affinity uptake for Mn at the thylakoid membrane, in addition to the Mn recycling from PSII degradation for PSII biogenesis/repair (**Fig. 7**). It has been proposed previously that there was a transport of Mn^{2+} from the stroma to the thylakoid lumen, with lower efficiency than CGLD1, by other divalent cation transporter in the thylakoid membrane (Schneider et al, 2016).

We consider that may contribute the transport of a protein binding Mn^{2+} across the thylakoid by the chloroplast twin arginine translocation (Tat) pathway which is able to translocate folded proteins with cofactors by forming a transient translocase using the protomotive force as energy (Dabney-Smith and Storm 2014). Twin-arginine targeting peptides across the thylakoid membrane of PsbP (OEE2/PSPB1) from *Chlamydomonas* (Cre12.g550850) and *Arabidopsis* (AT1G06680) are shown in **Fig. 2**B. The PSII PsbP family contains a dozen of PsbP-like protein of the thylakoid lumen predicted addressed to the chloroplast and containing a Tat targeting peptide (in *Chlamydomonas* as in *Arabidopsis*). We suggest as candidate the PSII subunit PsbP (or other PsbP family members), a proposed metallochaperone for Mn^{2+}, translocated by the Tat pathway in higher plants (Chaddock et al, 1995) and in green alga *Chlamydomonas* (Finazzi et al, 2003).

Chlamydomonas is tolerant to excess of manganese and can store Mn^{2+} in acidic vacuoles, known as acidocalcisomes, and these Mn stores can be mobilized in Mn-deficient conditions (Tsednee et al, 2019). The standard TAP medium contains 25 µM Mn ions and manganese limitation of the wild-type *Chlamydomonas* growth occurs below 0.25 µM Mn ions with a photosynthetic function recovery within a few hours upon

addition of Mn^{2+} (Allen et al, 2007), which is consistent with our recovery time in Mn supplemented *cgld1* mutant. Proteomic results suggest that much of the *Chlamydomonas* photosynthetic apparatus remains intact under manganese limitation in line with this short recovery time (Hsieh et al, 2013). *Chlamydomonas* takes up more manganese than required when provided with 25 µM, and transfer through two rounds of dilution in TAP without manganese is required to deplete the excess stores of manganese (Allen et al, 2007). The PSII symptoms of Mn depletion in wild-type *Chlamydomonas* occurred indeed upon such transfers after several days in TAP without manganese (**Fig. 6**C).

4.6. Heterogeneity in PSII donor side activity in cgld1 mutant

Previous quantification of labeled manganese in *Arabidopsis* showed more than 80% of Mn within the chloroplast was incorporated in the thylakoid in WT and only 58% in *pam71* thylakoid fraction (Schneider et al, 2016). In our study of *cgld1* mutant grown under low light, we observe wild-type levels of PSI and PSII accumulation and capacity of charge separation (**Fig. 2**), and decreased oxygen evolution and maximal PSII efficiency with a higher F_0 (**Fig. 3**). These results together with the slow fluorescence rise in presence of DCMU (**Fig. 4**A), which is lost upon addition of alternative donor HA (**Fig. 5**), is very slowly reversible (**Fig. 4**B), and is also lost in the dark (**Fig. 4**C) but recovered by photoactivation (**Fig. H** sup. mat.) suggest the existence of a fraction of PSII centers deficient in complete tetramanganese oxygen-evolving cluster.

The photosensitivity of *cgld1* mutants also suggest that under manganese limiting conditions assembly of Mn_4O_5Ca is incomplete in part of the PSII centers; and because of incomplete water splitting machinery, photodamage occurs frequently in these affected centers. A mechanism of photoprotection during the assembly of the water-oxidizing complex of PSII has been proposed: when the manganese cluster is absent, the reduction potential of Q_A is higher by 150 mV than in the functional enzyme (Krieger et al, 1995; Johnson et al, 1995; Brinkert et al, 2016). Consequently, the free energy gap between $P680^+Q_A^-$ and $P680^+Pheo^-$ is large and the direct charge

recombination pathway ($Q_A^-/P680^+$) is favored, thereby minimizing the indirect pathway ($Pheo^-/P680^+$) and its chlorophyll $^3P680$ triplet intermediate reacting with oxygen and forming toxic singlet oxygen (Rappaport et al, 2012). The redox potential (E_m) of the plastoquinone Q_A/Q_A^- redox couple in Photosystem II (PSII) determined by redox titration in PSII membranes from spinach was around: -80 mV in active PSII, -28 mV in active PSII + DCMU, +73 mV in Mn-depleted PSII, and +123 mV in Mn-depleted + DCMU (Krieger and Rutherford, 1998). In green algae, *Chlamydomonas reinhardtii* and *Senedesmus obliquus,* PSII assembly occurs in the dark except for the manganese cluster which requires photoactivation (Rova et al, 1996; Johnson et al, 1995). In *Senedesmus obliquus,* the midpoint potential of Q_A was shifted upon photoactivation from +110 mV to -80 mV (Johnson et al, 1995). A higher Q_A/Q_A^- redox couple favors the reduction of Q_A and the reduced Q_A will increase the fluorescence level measured after dark adaptation F_0, which was reported for example after addition of DCMU (Wollman and Thorez, 1976). The deficiency in manganese of thylakoids from *Arabidopsis pam71* mutant (Schneider et al, 2016) suggests some manganese deficiency in *Chlamydomonas cgld1* mutant as well. If Mn-depleted PSII are indeed present in *cgld1* mutant, then their Q_A midpoint potential is expected to be higher and associated with higher F_0. The F_0 did increase in *cgld1* compared to WT.

The assembly of the Mn_4O_5Ca cluster requires light to induce charge separation to oxidize and strongly bind the Mn ions: a single Mn^{2+} ion is bound to a high-affinity site on D1 and is oxidized by redox-active Y_z to Mn^{3+}, upon a dark rearrangement a second Mn^{2+} ion reaches the cluster site and is oxidized to Mn^{3+}, further illumination leads to the Mn_4O_5Ca cluster (Narzi and Guidoni, 2022). After dark adaptation of *cgld1*, the F_0 increased in fluorescence traces recorded in presence of DCMU, the slow rise phase was lost, and the slow phase of relaxation increased, with larger changes than in the dark adapted wild-type. In both strains a little light reversed the phenotypes. These results are consistent with a fraction of the PSII complexes with incomplete Mn_4O_5Ca cluster in *cgld1* which fraction is unstable in the dark but recovers upon photoactivation. In the dark, release of Mn^{2+} from unstable manganese cluster intermediates raises the

reduction potential of Q_A which will tend to be reduced. Upon photoactivation, Mn^{2+} rebinding reverses the redox potential change of Q_A. These changes are reflected in the rise and decrease of F_0 levels that we observed in the two situations.

Altogether our results show that in the absence of CGLD1 (model in **Fig. 7**), the lumenal Mn becomes limiting to form the active oxygen evolution complex, the Mn_4O_5Ca cluster (PSII), and intermediates of oxygen evolving complex assembly are accumulated ($PSII_{altered}$).

Driving oxygenic photosynthesis requires manganese and is an essential process for sustaining life on Earth. Our defined conditions with an accumulation of PSII centers in a Mn deficient context are a blueprint for *in vivo* study of the oxygen evolving cluster assembly and the mechanism of Manganese homeostasis in the lumen, allowing to explore semi-functional and heterogeneous PSII variants. In addition, the *cgld1* mutant offers a background to identify additional thylakoid transporters or metallochaperones allowing the transport of manganese divalent cations from the chloroplast stroma into the lumen, and the eventual light-dependence of this process.

References

M. D. Allen, J. Kropat, S. Tottey, J. A. Del Campo, S. S. Merchant, Manganese deficiency in Chlamydomonas results in loss of photosystem II and MnSOD function, sensitivity to peroxides, and secondary phosphorus and iron deficiency. Plant Physiol. 143 (2007) 263-277.

N.R. Baker, Chlorophyll fluorescence: a probe of photosynthesis in vivo. Annu. Rev. Plant Biol. 59 (2008) 89-113.

H. Bao, R. L. Burnap, Photoactivation: the light driven assembly of the water oxidation complex of photosystem II Front. Plant Sci. 7 (2016) 578.

P. Bennoun, M. Spierer-Herz, J. Erickson, J. Girard-Bascou, Y. Pierre, R. Delosme, J.-D. Rochaix, Characterization of photosystem II mutants of *Chlamydomonas reinhardii* lacking the PSBA gene. Plant Mol. Biol. 6 (1986) 151-160.

N. Bondarava, P. Beyer, A. Krieger-Liszkay, Function of the 23 kDa extrinsic protein of Photosystem II as a manganese binding protein and its role in photoactivation. Biochim. Biophys. Acta 1708 (2005) 63-70.

N. Bondarava, S. Un, A. Krieger-Liszkay, Manganese binding to the 23 kDa extrinsic protein of Photosystem II. Biochim. Biophys. Acta 1767 (2007) 583-588.

K. Brinkert, S. De Causmaecker, A. Krieger-Liszkay, A. Fantuzzi, A. W. Rutherford, Bicarbonate-induced redox tuning in Photosystem II for regulation and protection. Proc. Natl. Acad. Sci. U.S.A. 117 (2016) 12144-12149.S. Bujaldon, N. Kodama, M. K. Rathod, N. Tourasse, S.-I. Ozawa, J. Sellés, O. Vallon, Y. Takahashi, F.-A. Wollman, The BF4 and p71 antenna mutants from Chlamydomonas reinhardtii. Biochim. Biophys. Acta 1861 (2020) 148085.

P. Cao, Y. Xie, M. Li, X. Pan, H. Zhang, X. Zhao, X. Su, T. Cheng, W. Chang, Crystal structure analysis of extrinsic PsbP protein of Photosystem II reveals a manganese-induced conformational change. Mol. Plant 8 (2015) 664-666.

A. M. Chaddock, A. Mant, I. Karnauchov, S. Brink, R. G. Herrmann, R. B. Klösgen, C. Robinson, A new type of signal peptide: central role of a twin-arginine motif in transfer signals for the ΔpH dependent thylakoidal protein translocase. EMBO J. 14 (1995), 2715-2722.

M. H. Cheah, M. Zhang, D. Shevela, F. Mamedov, A. Zouni, J. Messinger. Proc. Natl. Acad. Sci. U.S.A. 117 (2020) 141-145.

N. H. Chua, P Bennoun, Thylakoid membrane polypeptides of *Chlamydomonas reinhardtii*: wild-type and mutant strains deficient in photosystem II reaction center. Proc. Natl. Acad. Sci. U. S. A. 72 (1975) 2175-2179.

A.-S. Colinet, L. Thines, A. Deschamps, G. Flémal, D. Demaegd, P. Morsomme. Acidic and uncharged polar residues in the consensus motifs of the yeast Ca2+ transporter Gdt1p are required for calcium transport. Cell. Microbiol. 19 (2017) e12729.

D. Demaegd, A.-S. Colinet, A. Deschamps, P. Morsomme (2014) Molecular evolution of a novel family of putative calcium transporters. Plos One 9: e100851.

R. M. Dent, M. N. Sharifi, A. Malnoë, C. Haglund, R. H. Calderon, S. Wakao, K. K. Niyogi, Large-scale insertional mutagenesis of *Chlamydomonas* supports phylogenomic functional prediction of photosynthetic genes and analysis of classical acetate-requiring mutants. Plant J. 82 (2015) 337–351.

C. de Vitry, J. Olive, D. Drapier,M. Recouvreur, F.-A. Wollman, Posttranslational events leading to the assembly of photosystem II protein complex: A study using photosynthesis mutants from *Chlamydomonas reinhardtii*. J. Cell Biol. 109 (1989) 991-1006.

G. Finazzi, C. Chasen, F.-A. Wollman, C. de Vitry, Thylakoid targeting of Tat passenger proteins shows no ΔpH dependence *in vivo*. EMBO J. 22 (2003) 807-815.

E. H. Harris, The *Chlamydomonas* Sourcebook: Introduction to *Chlamydomonas* and Its Laboratory Use, Academic Press, 2009.

J. Findinier, C. Delevoye, M. M. Cohen, The dynamin-like protein Fzl promotes thylakoid fusion and resistance to light stress in *Chlamydomonas reinhardtii*. PLoS Genet 15 (2019) e1008047.

C. Gandini, S. Birkelund Schmidt, S. Husted, A. Schneider, D. Leister. The transporter SynPAM71 is located in the plasma membrane and thylakoids, and mediates manganese tolerance in *Synechocystis* PCC6803. New Phytologist 215 (2017) 256-268.

B. Genty, J.-M. Briantais, J.M., N. R. Baker, The relationship between the quantum yield of photosynthetic electron transport and quenching of chlorophyll fluorescence. Biochim. Biophys. Acta 990 (1989) 87-92.

Y. Gavel, J. Steppuhn, R. Herrmann, G. von Heijne, The 'positive-inside rule' applies to thylakoid membrane proteins. FEBS Lett. 282 (1991) 41-46.

J. Hallgren, K. D. Tsirigos, M. D. Pedersen, J. J. Almagro Armenteros, P. Marcatili, H. Nielsen, A. Krogh, O. Winther, DeepTMHMM predicts alpha and beta transmembrane proteins using deep neural networks. BioRxiV (2022) doi.org/10.1101/2022.04.08.487609

N. Hoecker, Y. Hennecke, S. Schrott, G. Marino, S. Birkelund Schmidt, D. Leister, A. Schneider, Gene replacement in Arabidopsis reveals manganese transport as an ancient feature of human, plant and cyanobacterial UPF0016 Proteins. Front. Plant Sci. 12 (2021) 697848.

S. I. Hsieh, M. Castruita, D. Malasarn, E. Urzica, J. Erde, M. D. Page, H. Yamasaki, D. Casero, M. Pellegrini, S. S. Merchant, J. A. Loo, The proteome of copper, iron, zinc, and manganese micronutrient deficiency in *Chlamydomonas reinhardtii*. Mol. Cell. Proteomics 12.1 (2013) 65-86.

G. N. Johnson, A. W. Rutherford, A. Krieger, A change in the midpoint potential

of the quinone Q_A in photosystem II associated with photoactivation of oxygen evolution. Biochim. Biophys. Acta 1229 (1995) 202–207.

X. Johnson, G. Vandystadt, S. Bujaldon, S., F.-A. Wollman, R. Dubois, P. Roussel, J. Alric, D. Béal, A new setup for in vivo fluorescence imaging of photosynthetic activity. Photosynth. Res. 102 (2009) 85-93.

P. Joliot, A. Joliot, Etude cinétique de la réaction photochimique libérant l'oxygène au cours de la photosynthèse. C. R. Hebd. Seances Acad. Sci. 258 (1964) 4622-4625.

J. Jumper, R. Evans, A. Pritzel, T. Green, M. Figurnov, O. Ronneberger, K. Tunyasuvunakool, R. Bates, A. Žídek, A. Potapenko, A. Bridgland, C. Meyer, S. A. A. Kohl, A. J. Ballard, A. Cowie, B. Romera-Paredes, S. Nikolov, R. Jain, J. Adler, T. Back, S. Petersen, D. Reiman, E. Clancy, M. Zielinski, M. Steinegger, M. Pacholska, T. Berghammer, S. Bodenstein, D. Silver, O. Vinyals, A. W. Senior, K. Kavukcuoglu, P. Kohli, D. Hassabis, Highly accurate protein structure prediction with AlphaFold. Nature 596 (2021) 583-589

Y. Kato, W. Sakamoto, FtsH protease in the thylakoid membrane: physiological functions and the regulation of protease activity. Front. Plant Sci. 9 (2018) 855.

A. Krieger, A. W. Rutherford, G. N. Johnson, On the determination of redox midpoint potential of the primary quinone electron acceptor, Q_A, in photosystem II. Biochim. Biophys. Acta 1229 (1995) 193–201.

A. Krieger-Liszkay, A. W. Rutherford, Influence of herbicide binding on the redox potential of the quinone acceptor in photosystem II: relevance to photodamage and phytotoxicity. Biochem. 37 (1998) 17339-17344.

A. Krieger-Liszkay, S. Thomine, Importing Manganese into the Chloroplast: Many Membranes to Cross. Mol. Plant 11 (2018) 1109-1111.

R. Kuras, S. Büschlen, F.-A. Wollman, Maturation of pre-cytochrome *f* in *vivo*. A site-directed study in *Chlamydomonas reinhardtii*. J. Biol. Chem. (1995) 270:27797-27803.

A. Malnoë, F. Wang, J. Girard-Bascou, F.-A. Wollman, C. de Vitry Thylakoid FtsH protease contributes to photosystem II and cytochrome b_6f remodeling in *Chlamydomonas reinhardtii* under stress conditions. Plant Cell 26 (2014) 373-390.

S. P. Mayfield, P. Bennoun, J.-D. Rochaix, Expression of the nuclear encoded OEE1 protein is required for oxygen evolution and stability of photosystem II particles in *Chlamydomonas reinhardtii*. EMBO J. 6 (1987a) 313-318.

S. P. Mayfield, M. Rahire, G. Frank, H. Zuberand, J.-D. Rochaix, Expression of the nuclear gene encoding oxygen-evolving enhancer protein 2 is required for high levels of photosynthetic oxygen evolution in *Chlamydomonas reinhardtii*. Proc. Natl. Acad. Sci. U.S.A. 84 (1987b) 749-753.

D. Narzi, L. Guidoni, Structural and dynamic insights into Mn_4Ca cluster-depleted Photosystem II. Phys. Chem. Chem. Phys. 23 (2021) 27428-27436.

W. J. Nawrocki, X. Liu, B. Raber, C. Hu, C. de Vitry, D. I. G. Bennett, R. Croce, Molecular origins of induction and loss of photoinhibition-related energy dissipation qI. Sci. Adv. 7 (2021) eabj0055

R. Porra, W. Thompson, P. Kriedemann, Determination of accurate extinction coefficients and simultaneous equations for assaying chlorophylls a and b extracted with four different solvents: verification of the concentration of chlorophyll standards by atomic absorption spectroscopy. Biochim. Biophys. Acta 975 (1989) 384-394.

F. Rappaport, D. Béal, A. Joliot, P. Joliot, On the advantages of using green light to study fluorescence yield changes in leaves. Biochim. Biophys. Acta 1767 (2007) 56-65.

J.-D. Rochaix, *Chlamydomonas*, a model system for studying the assembly and dynamics of photosynthetic complexes. FEBS Lett. 529 (2002) 34-38.

E. M. Rova, B. Mc Even, P.-O. Frederiksson, S. Styring, Photoactivation and photoinhibition are competing in a mutant of *Chlamydomonas reinhardtii* lacking the 23-kDa extrinsic subunit of photosystem II. J. Biol. Chem. 271 (1996) 28918-28924.

A. W. Rutherford, A. Osyczka, F. Rappaport, Back-reactions, short-circuits, leaks and other energy wasteful reactions in biological electron transfer: Redox tuning to survive life in O2. FEBS Lett. 586 (2012) 603-616.

L. A. Rymarquis, J. M. Handley, M. Thomas, D. B. Stern, Beyond complementation. Map-based cloning in *Chlamydomonas reinhardtii*. Plant Physiol. 137 (2005) 557-566.

A. Schneider, I. Steinberger, A. Herdean, C. Gandini, M. Eisenhut, S. Kurz, A. Morper, N. Hoecker, T. Rühle, M. Labs, U. I. Flügge, S. Geimer, S. B. Schmidt, S. Husted, A. P. Weber, C. Spetea, D. Leister, The evolutionarily conserved protein PHOTOSYNTHESIS AFFECTED MUTANT71 is required for efficient manganese uptake at the thylakoid membrane in Arabidopsis. Plant Cell 28 (2016) 892-910.

J. B. Shackleton, C. Robinson. Transport of proteins into chloroplasts. The thylakoid processing peptidase is a signal-type peptidase with stringent substrate requirements at the -3 and -1 positions. J. Biol. Chem. 266 (1991) 12152-12156.

F. Sievers, A. Wilm, D. G. Dineen, T. J. Gibson, K. Karplus, W. Li, R. Lopez, H. McWilliam, M. Remmert, J. Söding, J. D. Thompson, D. Higgins, *Fast, scalable generation of high-quality protein multiple sequence alignments using Clustal Omega*. Molecular Systems Biology 7 (2011) 539.

G. Sipka, M. Magyar, A. Mezzetti , P. Akhtar, Q. Zhu,Y. Xiao, G. Han, S. Santabarbara, J.-R. Shen, P. H. Lambrev, G. Garab, Light-adapted charge-separated state of photosystem II: structural and functional dynamics of the closed reaction center. Plant Cell 33 (2021) 1286–1302.

M. Sugiura, M. Nakamura, K. Koyama, A. Boussac, Assembly of oxygen-evolving

photosystem II occurs with the apo-cyt*b559* but the holo-cyt*b559* accelerates the recovery of a functional enzyme upon photoinhibition. Biochim. Biophys. Acta 1847 (2015) 276-285.

P. F. Teixeira, E. Glazer, Processing peptidases in mitochondria and chloroplasts. Biochim. Biophys. Acta 1833 (2013) 360-370.

M. Tsednee, M. Castruita, P. A. Salomé, A. Sharma, B. E. Lewis, S. R. Schmollinger, D. Strenkert, K. Holbrook, M. S. Otegui, K. Khatua, S. Das, A. Datta, S. Chen, C. Ramon, M. Ralle, P. K. Weber, T. L. Stemmler, J. Pett-Ridge, B. M. Hoffman, S. S. Merchant, Manganese co-localizes with calcium and phosphorus in *Chlamydomonas* acidocalcisomes and is mobilized in manganese-deficient conditions. J. Biol. Chem. 294 (2019) 17626-17641.

Y. Umena, K. Kawakami, J. R. Shen, N. Kamiya, Crystal structure of oxygen-evolving photosystem II at a resolution of 1.9 Å. Nature 473 (2011) 55-60.

M. Varadi, S. Anyango, M. Deshpande, S. Nair, C. Natassia, G. Yordanova, D. Yuan, O. Stroe, G. Wood, A. Laydon, A. Žídek, T. Green, K. Tunyasuvunakool, S. Petersen, J. Jumper, E. Clancy, R. Green, A. Vora, M. Lutfi, M. Figurnov, A. Cowie, N. Hobbs, P. Kohli, G. Kleywegt, E. Birney, D. Hassabis, S. Velankar, AlphaFold Protein Structure Database: massively expanding the structural coverage of protein-sequence space with high-accuracy models. Nucleic Acids Res. 50 (2022) 439-444.

C. Vernotte, A.-L. Etienne, Briantais, Quenching of the system II fluorescence by the platoquinone pool. Biochim. Biophys. Acta 545 (1979) 519-527.

F. Wang, Y. Qi, A. Malnoë, Y. Choquet, F.-A. Wollman, C. de Vitry, The high light response and redox control of thylakoid FtsH protease in *Chlamydomonas reinhardtii*. Mol. Plant 10 (2017) 99-114.

E. Wientjes, H. van Amerongen, R. Croce, Quantum yield of charge separation in photosystem II: functional effect of changes in the antenna size upon light acclimation. J. Phys. Chem. B 117 (2013) 11200−11208.

F.-A. Wollman, D. Thorez, Oscillation du niveau de fluorescence initiale chez Chlorelle pyrnoîdosa après préillumination, puis addition de DCMU. C. R. Acad. Sci 283, 1345-1348.

J. Xing, P. Liu, L. Zhao, F. Huang, Deletion of CGLD1 Impairs PSII and Increases Singlet Oxygen Tolerance of Green Alga *Chlamydomonas reinhardtii*. Front. Plant Sci. 8 (2017) 2154.

B. Zhang, C. Zhang, C. Liu, Y. Jing, Y. Wang, L. Jin, L. Yang, A. Fu, J. Shi, F. Zhao, W. Lan, S. Luan, Inner envelope CHLOROPLAST MANGANESE TRANSPORTER 1 supports manganese homeostasis and phototrophic growth in Arabidopsis. Mol. Plant. 11 (2018) 943-954.

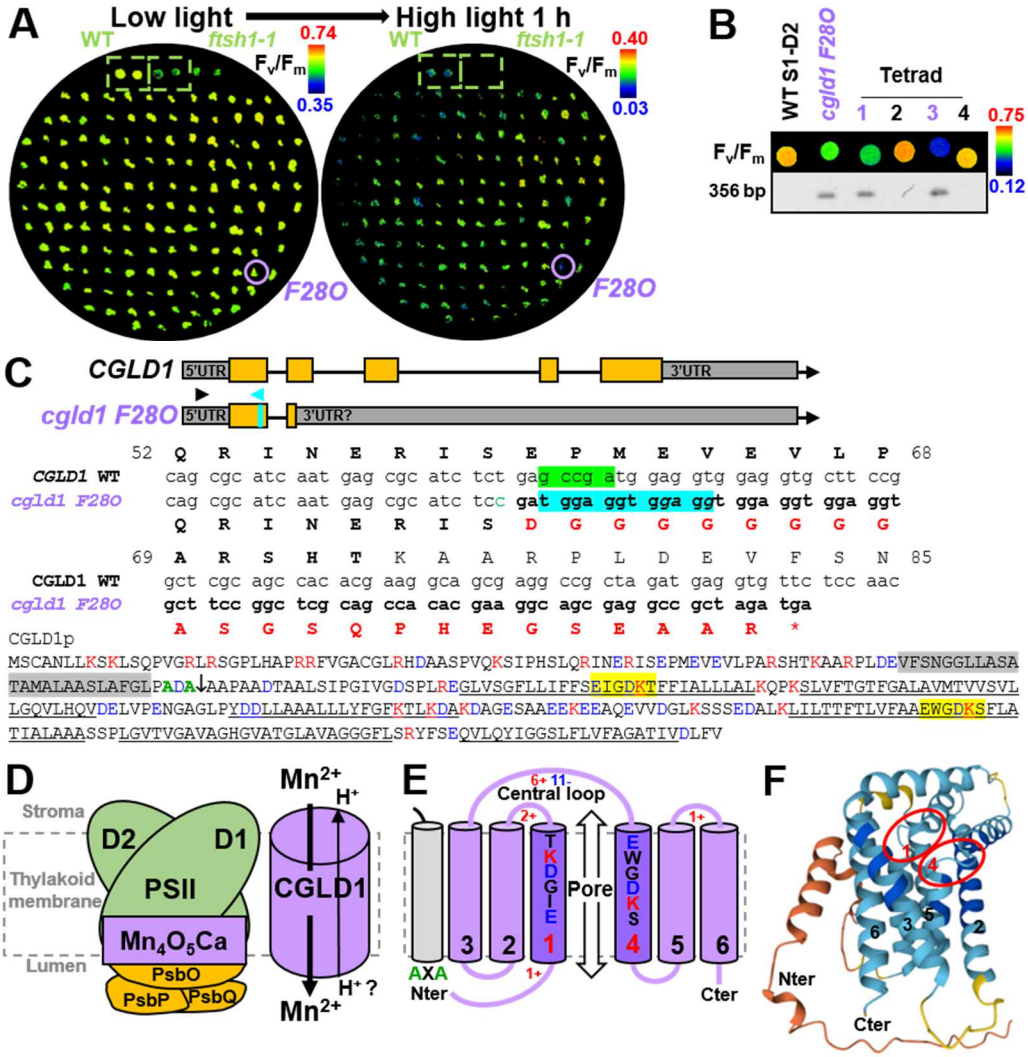

Fig. 1. Isolation and genotype of thylakoid Mn^{2+} transporter *cgld1* mutant. (A) Maximum efficiency of PSII photochemistry F_v/F_m of the plate from which *F28O* mutant was isolated, before and after high light treatment (1 h, 1000 µmol photons m^{-2} s^{-1}). Wild-type t222$^+$ (WT) and *ftsh1-1* strains as controls. (B) 2:2 cosegregation in a *F28O* X WT S1-D2 progeny tetrad of lower F_v/F_m with *F28O* mutation detected by PCR using a WT and *F28O* common primer (in (C) black arrow) and a *cgld1* specific primer (in (C) blue arrow). (C) Wild-type *CGLD1* and *cgld1 F28O* gene models: sequencing reveals 5-bp deletion (green highlighted), 12-bp duplication (blue highlighted) and a substitution (green) in 1st exon of *CGLD1* gene (Cr02.g084350_4532.1) which causes a frameshift (red) and an abortive stop codon (*). Amino-acids residues are numbered according to wild-type CGLD1 precursor protein (CGLD1p). Target peptide hydrophobic region (gray highlighted) and motif AXA (green) cleaved by thylakoid processing peptidase (TPP) on the thylakoid membrane lumenal side (↓). Transmembrane helices (TMH) underlined. Basic (red) and acidic (blue) amino-acid residues. Pore motifs (yellow highlighted). (D) Schematic PSII and CGLD1 in the thylakoid membrane. (E) CGLD1 topology model. Mature protein TMHs numbered from N- to C-terminus. Amino acid residues of the two repeated motifs within pore-lining TMH1 and TMH4. Number of basic residues (red) within mature protein loops and avidic residues (blue) within central loop. (F) CGLD1 structure predicted using AlphaFold. Confidence very high (dark blue), high (light blue), low (yellow), very low (orange). THMs are numbered as in (C). THM1 and THM4 repeated motif (circled red).

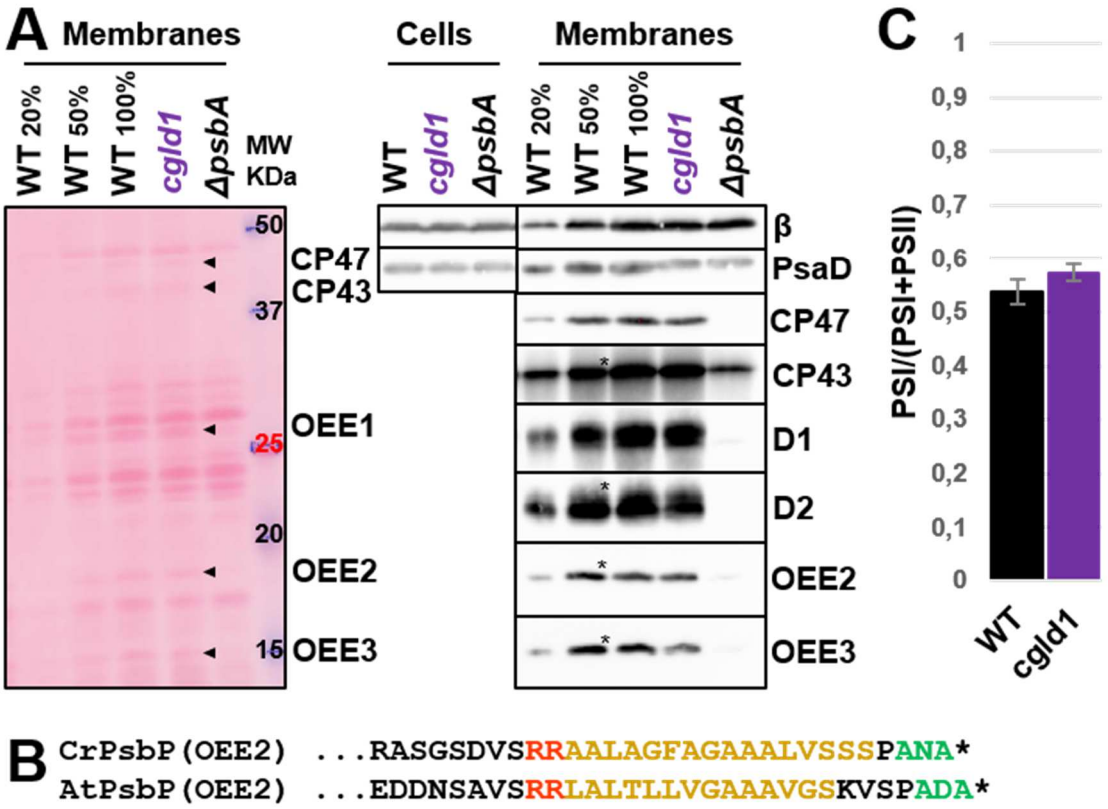

Fig. 2. The *cgld1* mutant accumulates wild-type levels of PSI and PSII. (A) Extracts of total cells and membranes of the wild type (WT), *cgld1* mutant and *ΔpsbA* mutant grown in acetate medium at 6 µmol photons m^{-2} s^{-1} were separated by SDS/PAGE and analyzed by Ponceau red protein staining (left) and by immunodetection with antibodies against chloroplast ATP synthase subunit β, PSI subunit PsaD and against PSII subunits PsbA (D1), PsbB (CP47), PsbC (CP43), PsbD (D2), PsbP (OEE2) and PsbQ (OEE3). Arrow heads indicate PSII subunits detectable by protein staining and asterisks overloading. The *ΔpsbA* mutant is used as control for PSII subunit deficiency. (B) Twin-arginine targeting peptide across the thylakoid membrane of PsbP (OEE2) from *Chlamydomonas* (Cre12.g550850) and *Arabidopsis* (AT1G06680). Twin arginine motif (red), hydrophobic region (ocher) and AXA motif (green) cleaved by the thylakoid processing peptidase. (C) Determination of PSI to PSII stoichiometry by electrochromic shift analysis (ECS) in WT and *cgld1* strains. Data represent means ± SD of six independent experiments.

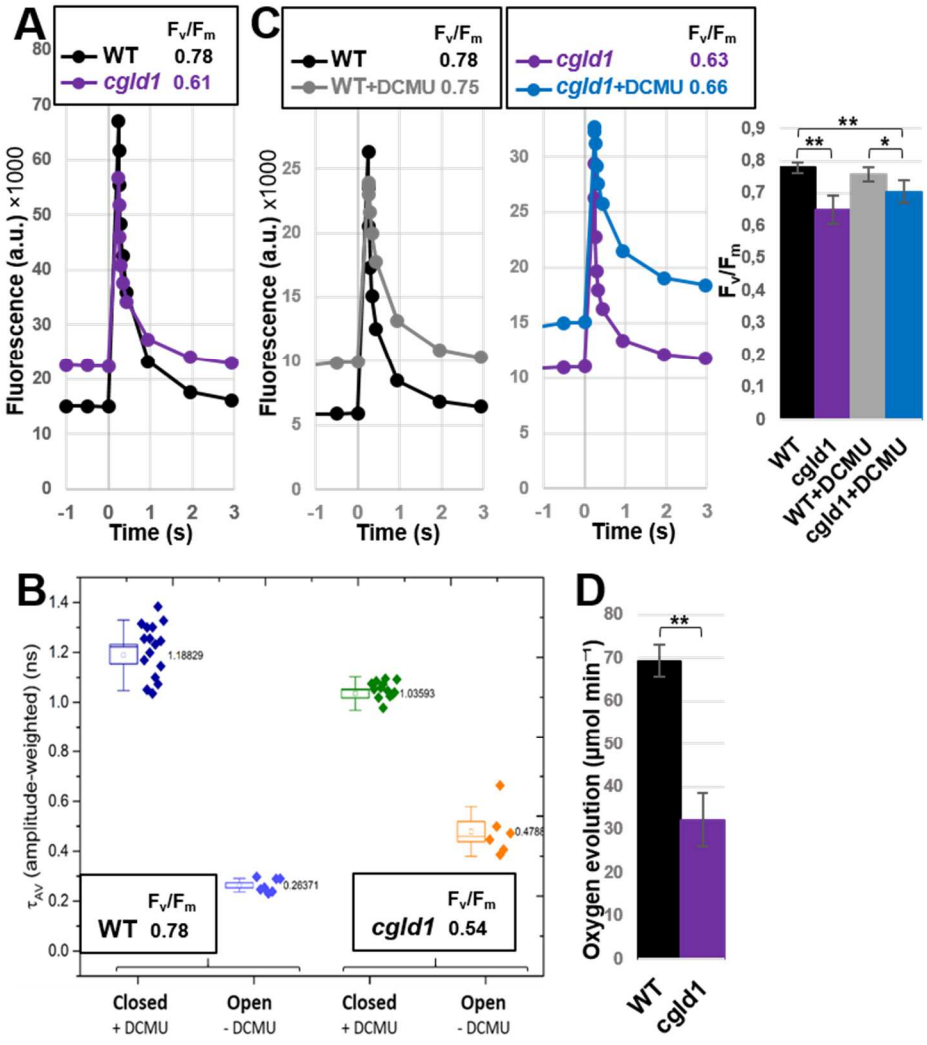

Fig. 3. Decreased maximum PSII efficiency and oxygen production in *cgld1* mutant. (A) Fluorescence kinetics induced by a 250 ms light pulse (applied at time 0, see Methods) in dark adapted cells. The maximal quantum yield of PSII photochemistry is calculated as $F_v/F_m = (F_m - F_0)/F_m$ (see Methods). (B) Time-resolved fluorescence decay. PSII closed and open centers were respectively obtained in presence and in absence of PSII inhibitor DCMU. Laser power 40 µW and 0.14 µW, and repetition rate 10 MHz and 5 MHz, were used for closed state and open state measurements respectively. Each data point corresponds to the global decay time (bi-exponential decay, see Methods) of one experiment. Three independent experimental batches of algae were tested. Box: mean (square), median (line), standard error of mean (box itself), standard deviation (whiskers). Lifetimes were free parameters of linked fitting of biological replicas of the experiment (see **Fig. E** supp. mat. for raw data example). (C) Fluorescence kinetics in presence or absence of DCMU using a saturating pulse to detect F_m. F_v/F_m data represent means ± SD of four to six independent experiments. (D) Rates of gross oxygen evolution (net oxygen production in the light minus oxygen consumption in the dark) at constant chlorophyll (DO at 680 nm minus DO at 750 nm equal to one). Data represent means ± SD of three technical replicates. *p-value < 0.05 and **p-value < 0.01 in Student's t-test.

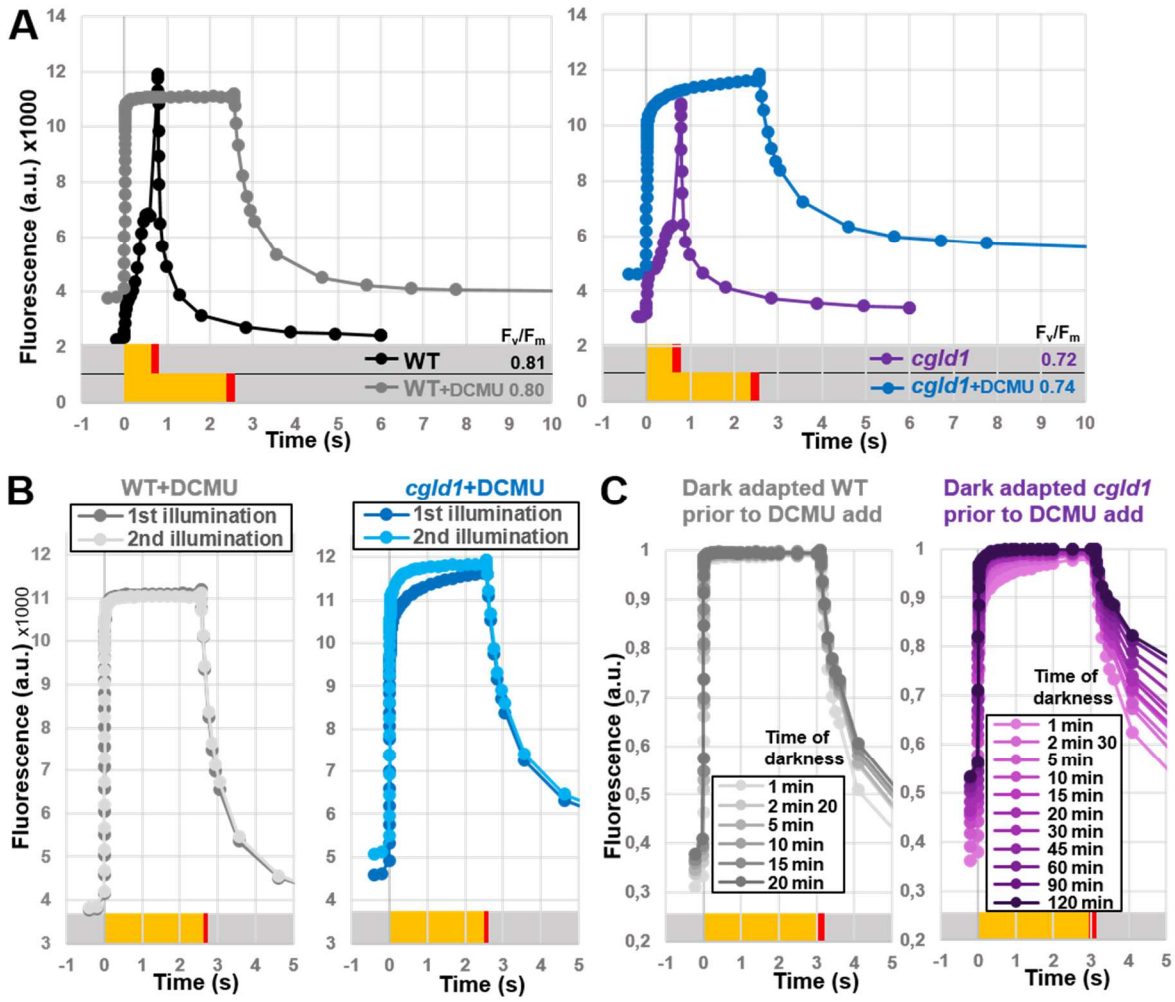

Fig. 4. Fully closed PSII (true F_m) require long illumination in the presence of DCMU in *cgld1* mutant. *cgld1* and not WT strain shows a slow phase of fluorescence rise which is lost at 2nd illumination and in the dark. WT (left panels) and *cgld1* (right panels). (A) Fluorescence kinetics in DCMU presence, or DCMU absence using a saturating pulse to detect F_m. (B) Fluorescence kinetics in DCMU presence upon the 1st and 75 sec of darkness after upon a 2nd illumination. (C) Fluorescence kinetics after various time periods of dark adaptation prior to DCMU addition and measurements, data normalized to F_m.

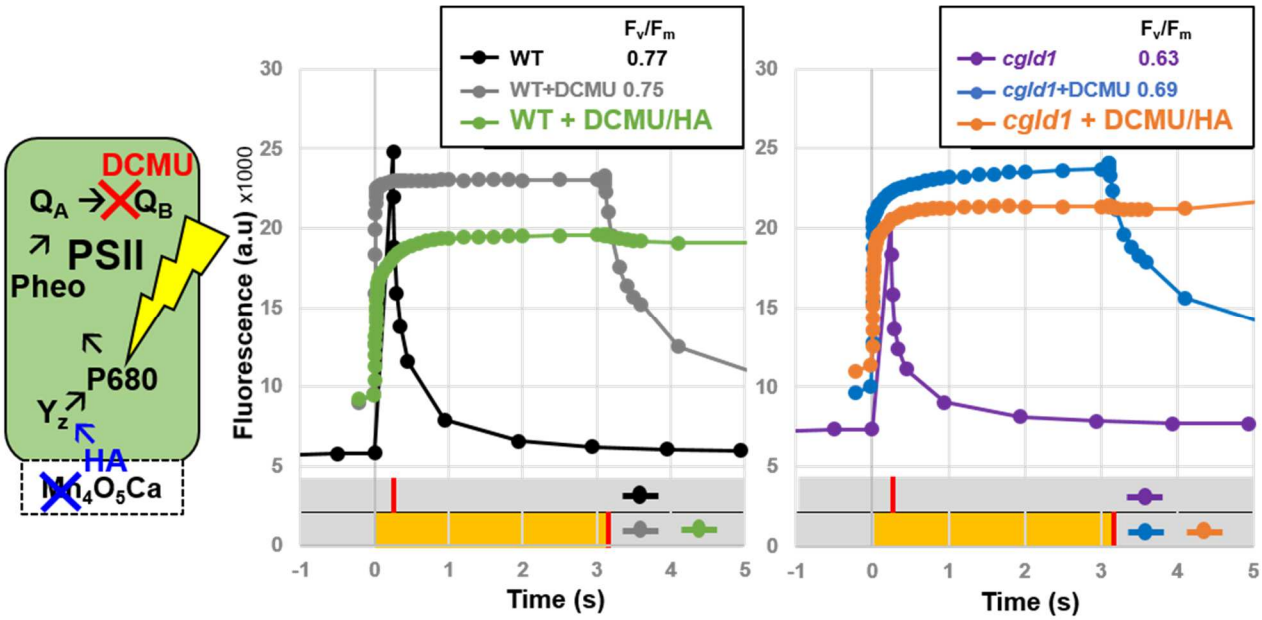

Fig. 5. Fluorescence in presence of PSII inhibitor DCMU and PSII electron donor hydroxylamine (HA). WT strain (left panels) and *cgld1* mutant (right panels). Schematic action of PSII inhibitors. DCMU is a competitive inhibitor of the quinone electron acceptor Q_B. Hydroxylamine destabilizes the Mn_4O_5Ca cluster and donates electrons to PSII donor side less efficiently than the Mn_4O_5Ca cluster. Fluorescence kinetics in presence of DCMU plus or minus HA, or in absence of DCMU using a saturating pulse to detect F_m.

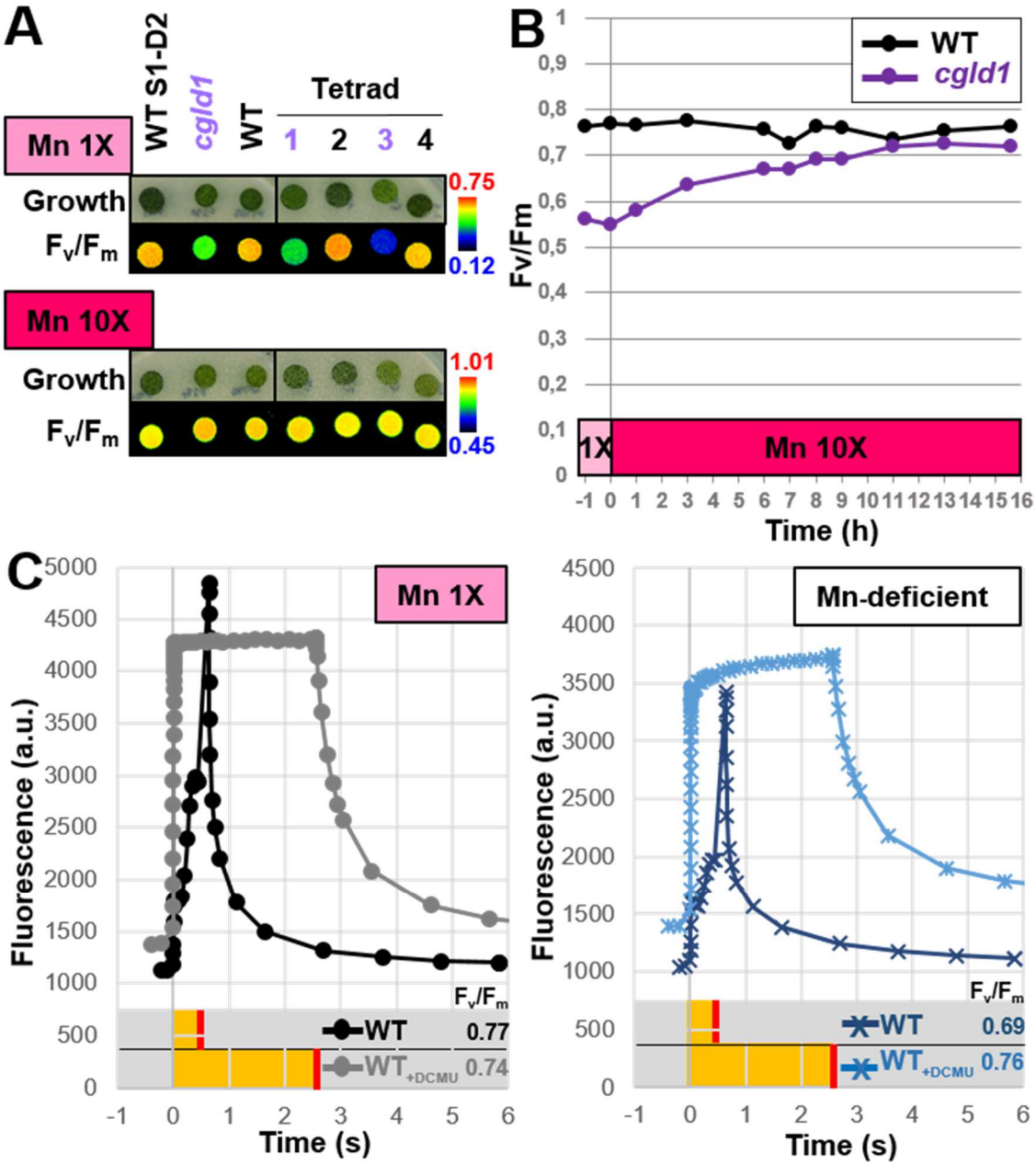

Fig. 6. Mn supplementation restores PSII activity in *cgld1* mutant, and Mn depletion decreases PSII activity in WT strain. Strains were grown under continuous illumination (6 µmol photons m^{-2} s^{-1}). (A) Parents and tetrad progeny of cross *cgld1* X WT S1-D2 and wild-type WT $t222^{+}$ (WT) were grown on solid TAP medium Mn-supplemented (Mn 10X) or not (Mn 1X). Maximal quantum yield of PSII photochemistry (F_v/F_m) was measured after 4 days of growth. (B) *cgld1* and WT cells were grown in TAP liquid medium (Mn 1X) and transferred to Mn-supplemented TAP liquid medium (Mn 10X). (C) Decreased maximum of PSII efficiency and biphasic rise of fluorescence in the presence of DCMU in wild-type strain grown in TAP medium followed by dilutions in Mn-deficient TAP liquid medium (Mn-deficient).

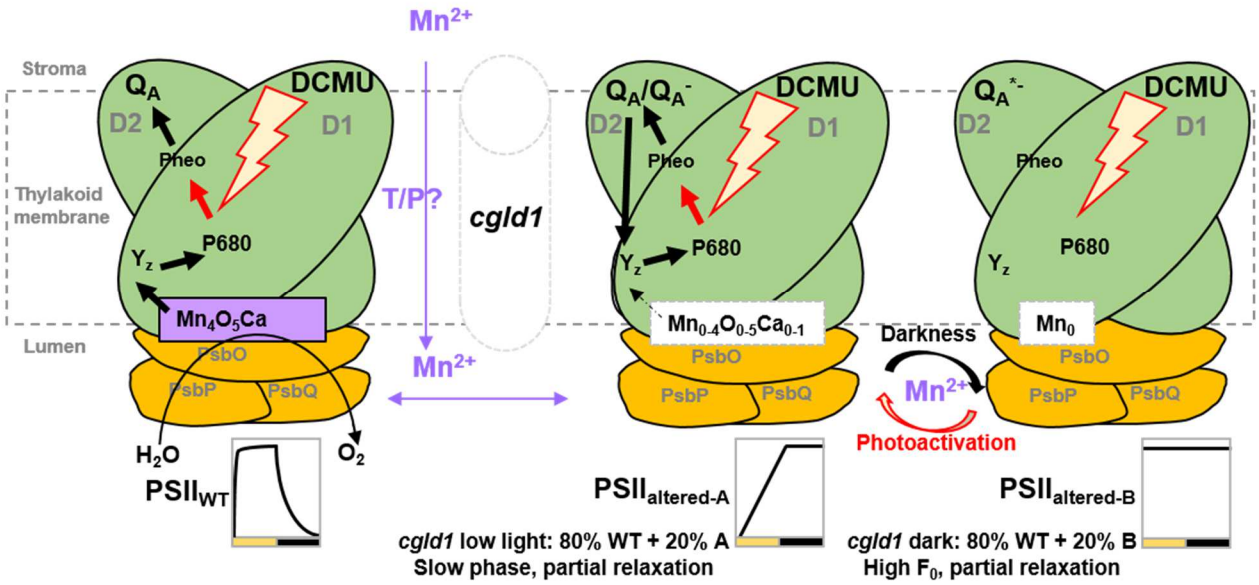

Fig. 7. Model showing heterogeneity of PSII in presence of DCMU and delivery of manganese in *cgld1* mutant. Active PSII with Mn_4O_5Ca cluster of the oxygen-evolving complex ($PSII_{WT}$). Oxygen evolution inactive PSII lacking complete Mn_4O_5Ca ($PSII_{altered}$). D1 and D2 subunits of the PSII reaction center bind the main redox cofactors involved in electron transfer in PSII. Light excitation leads to the primary charge separation with an electron transferred from chlorophyll donor P680 to pheophytin acceptor (Pheo). Subsequently, the electron is passed to the bound plastoquinone Q_A and in the presence of DCMU cannot be passed to the mobile plastoquinone Q_B. The electron hole at P680 is filled by oxidation of the secondary donor a tyrosine residue (Y_Z) from D1 subunit and finally by the Mn_4O_5Ca cluster which is shielded on the luminal side by three extrinsic proteins (PsbO, PsbP, PsbQ). When the Mn_4O_5Ca cluster is uncomplete, the reduction of Y_Z by the donor side is slow and the back reaction from the acceptor side is high ($PSII_{altered-A}$). Potentially damaging highly oxidizing components are accumulated in PSII and protective mechanisms cannot fully prevent photoinhibition. After a first illumination, active PSII with Mn_4O_5Ca will re-open in a few seconds while PSII lacking Mn_4O_5Ca (hydroxylamine treated and PSII altered) are closed in Q_A^{*-} state with a lack of fluorescence relaxation. In the dark, release of Mn^{2+} from unstable manganese cluster intermediates raises the reduction potential of Q_A which will tend to be reduced Q_A^{*-} ($PSII_{altered-B}$). Upon photoactivation, Mn^{2+} rebinding reverses the redox potential change of Q_A. Schematic kinetics of fluorescence are indicated below each PSII type. Kinetics of fluorescence measured in *cgld1* mutant correspond to ~ 80% $PSII_{WT}$ and 20% $PSII_{altered}$ ($PSII_{altered-A}$ when *cgld1* is grown in low light, $PSII_{altered-B}$ when *cgld1* is dark adapted). In the absence of CGLD1, Mn becomes limiting for the Mn_4O_5Ca cluster. Some Mn is transported in the thylakoid lumen from the stroma by alternative pathways less efficient than CGLD1 that are not yet determined, other cation transporter or Tat translocated Mn-binding members of the PSII PsbP family (↓T/P?). In addition, some Mn is delivered by Mn recycling from PSII (↔).

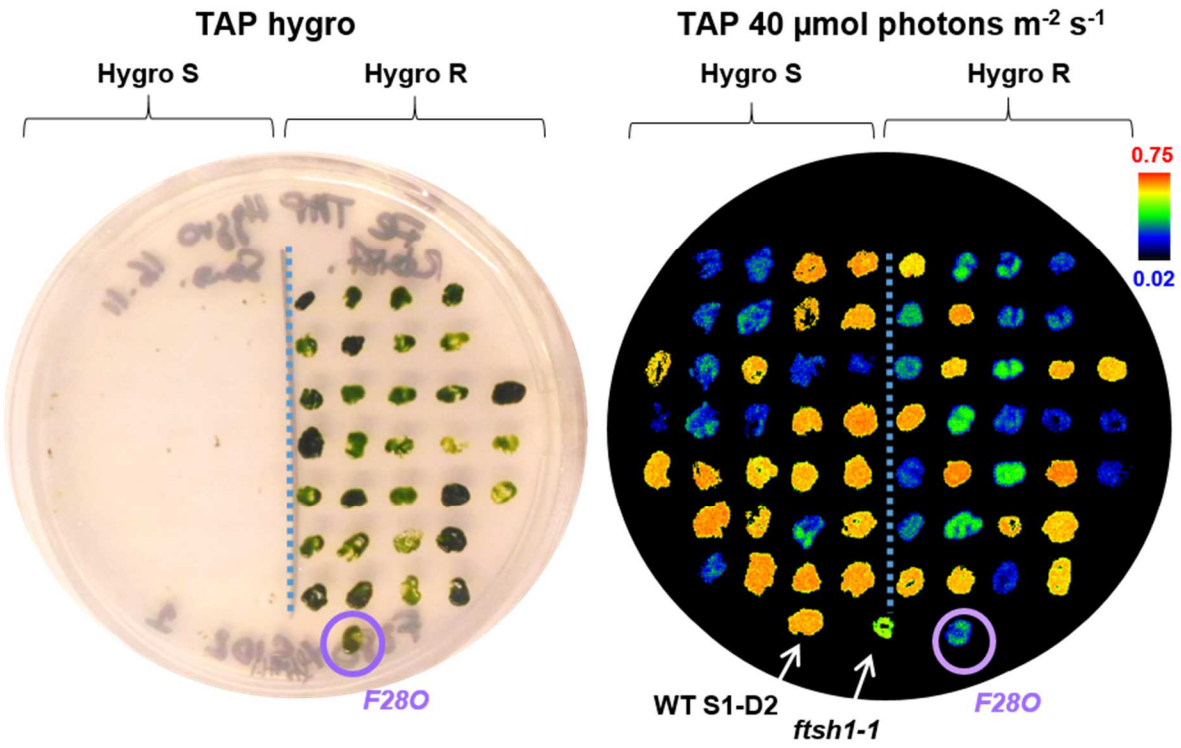

Fig. A supp. mat. Photosensitivity is not linked to hygromycin resistance. Absence of co-segregation in the progeny from the backcross of *F28O* mutant with WT S1-D2 between the hygromycin resistance (Hygro R) or sensitivity (Hygro S) and the photosensitivity observed in *F28O* mutant. Thylakoid protease mutant *ftsh1-1* is a control of PSII photosensitivity.

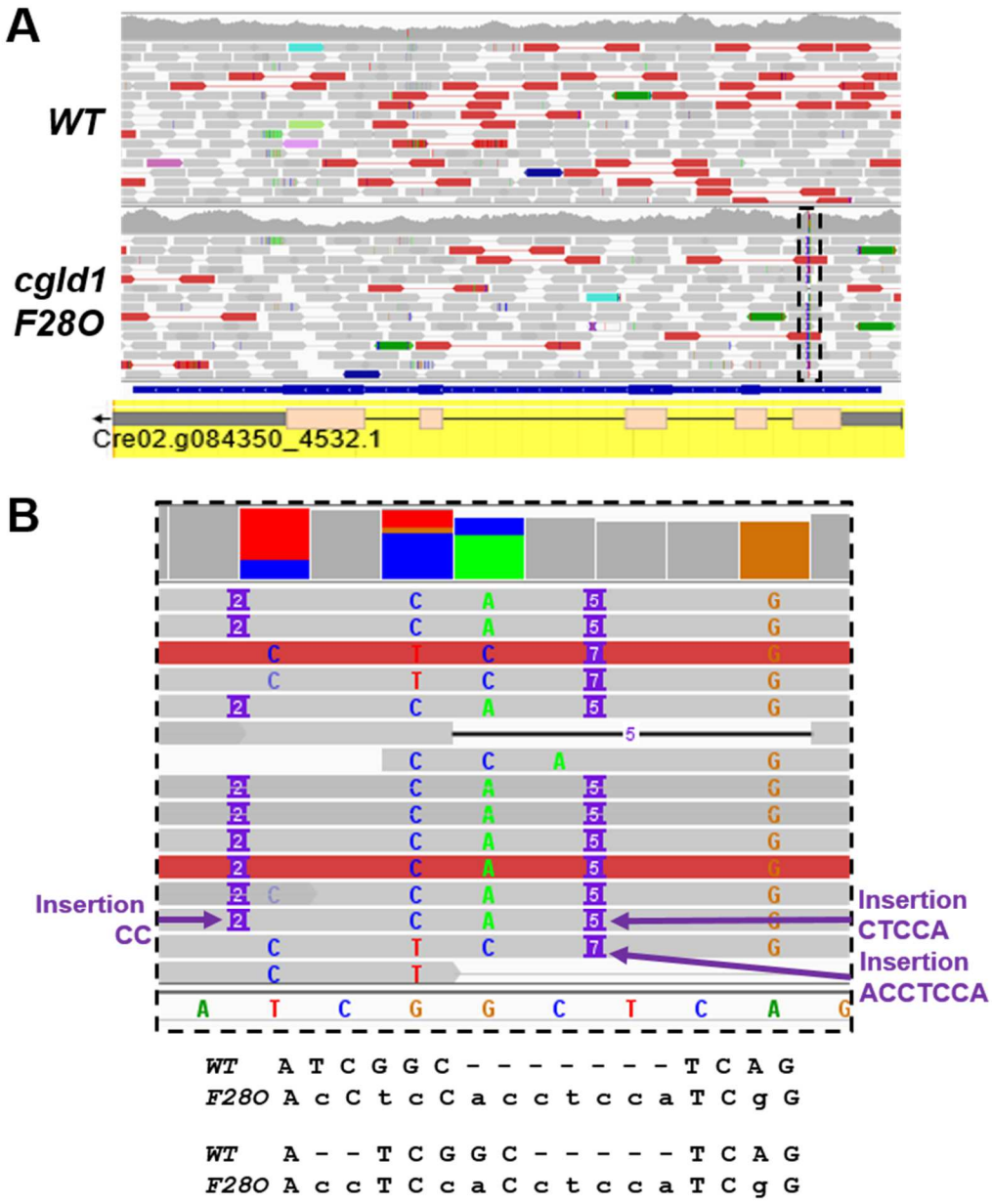

Fig. B supp. mat. Sequencing reveals a 7-bp insertion of in the *CGLD1* gene of *F28O* mutant. (A) Paired-end sequencing reads were mapped to the reference genome. Read mapping in WT (top) and *F28O* (bottom) centred on the *CGLD1* locus (Cre02.g084350). In grey, reads with both ends mapping in neighbouring areas (red and blue reads denote interspace that are longer or shorter than the usual range, respectively); in light colours, reads with ends mapping on distinct chromosomic areas. Below is shown the gene model for *CGLD1* (5'-UTR, coding sequence (CDS) and 3'-UTR). (B) Zoom on the reads showing a 7-bp insertion with 4 substitutions, or equivalent but aligned with two insertions of 5-bp and 2-bp with 3 substitutions. This mutation corresponds to a 5-bp deletion, 12-bp duplication with one substitution with a net insertion of 7-bp (as shown in **Fig. 1**C).

Fig. C supp. mat. Sequence alignment and phylogenetic tree of CGLD1/PAM71 related proteins: four in *Chlamydomonas*, 5 in *Arabidopsis thaliana* and one in *Synechocystis* PCC6803. The protein sequence alignments were generated by Clustal O (1.2.4.). (A) Alignement of *Chlamydomonas* CGLD1 (CrCGLD1) with its thylakoid membrane-localized homolog from *Arabidopsis thaliana* (AtPAM71) and its homologue from *Synechocystis* PCC6803 (SyPAM71). Amino-acids identity (*), strongly (:) and weakly (.) similar properties. Predicted target peptide hydrophobic helix (highlighted in gray) and motif AXA (green) cleaved by thylakoid processing peptidase (TPP) on the lumenal side of the thylakoid membrane (↓). Transmembrane helices (TMH) as predicted by DeepTMHMM and soluble central loop (comas) are indicated above the sequences. Two highly conserved E-Φ-G-D-[KR]-[TS] motifs (highlighted in yellow), with Φ being a hydrophobic residue. (B) Unrooted phylogenetic tree. (C) Sequence alignment of conserved segments used for neighbour-joining tree in (B). *Chlamydomonas* sequences cc-4532 v6.1: CrCGLD1, Cre02.g084350; CrCTM1A, Cre16.g660000; CrCTM1B, Cre16.g660050; and CrPML, Cre17.g731300. *Arabidopsis*: AtPAM71, At1g64150; AtCTM1, At4g13590; AtPML3, At5g36290; AtPML4: At1g25520; AtPML5: At1g68650. *Synechocystis*: sll0615.

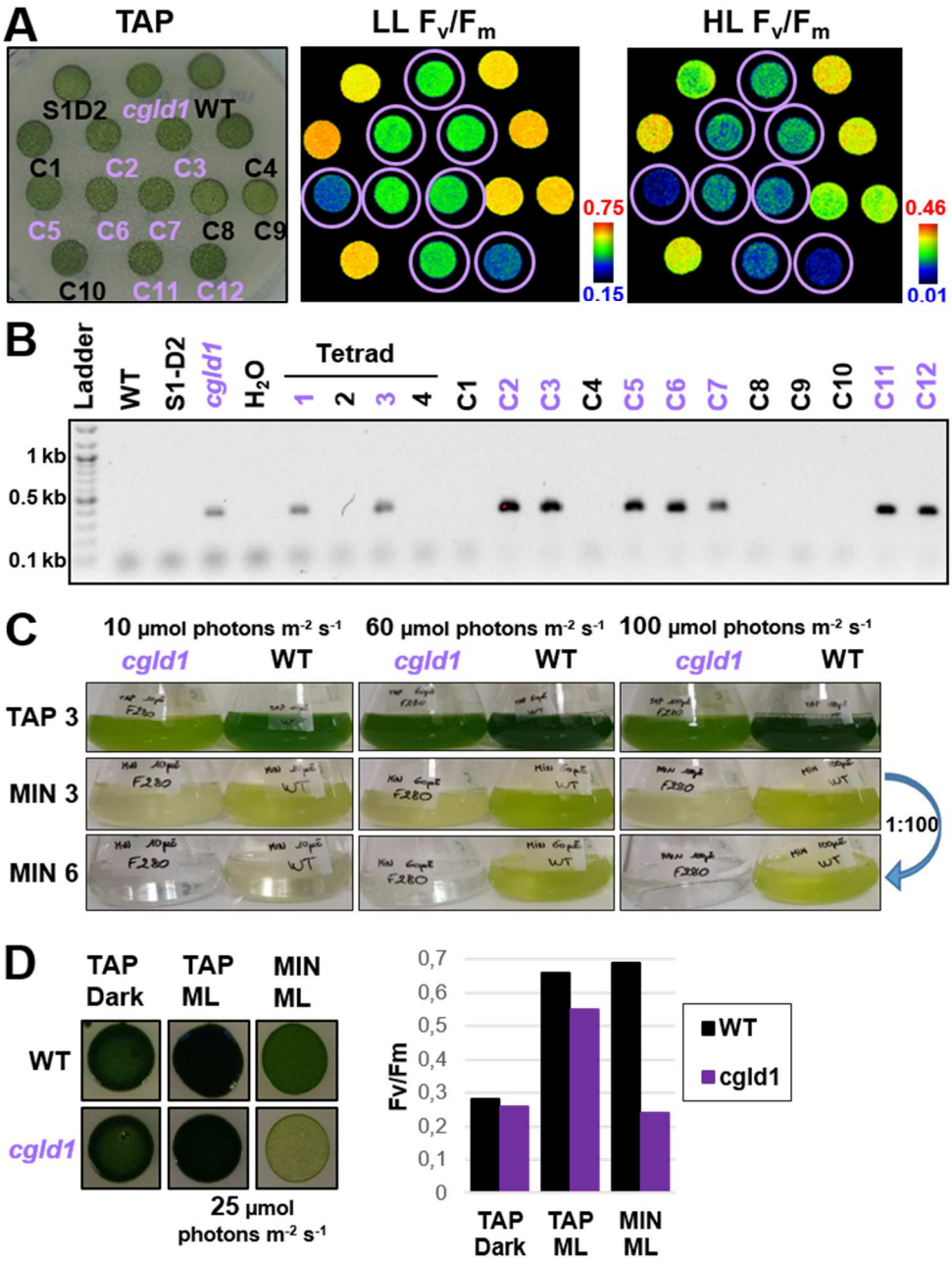

Fig. D supp. mat. The lower maximal PSII efficiency and photosensitivity are linked to the *cgld1 F28O* mutation, and the mutant despite this can still grow photoautotrophically. WT t222^{+} (WT), parents and progeny from the cross *cgld1 F28O* X WT S1-D2 (S1-D2). (A) Four days' growth on TAP medium at 6 µmol photons m^{-2} s^{-1} (LL) and fluorescence analysis (F_v/F_m) before and after 1 h high light treatment at 1000 µmol photons m^{-2} s^{-1} (HL). (B) PCR products obtained on genomic extracts using a primer specific of the *cgld1 F28O* mutation. Amplification without genomic extract (H_20) as PCR negative control. (C) Growth after inoculation of 2 10^5 cells ml^{-1} in TAP medium during 3 days (TAP 3), or photoautotrophically in minimum medium during 3 days (MIN 3) followed by 100 fold dilution and 3 additional days of growth (MIN 6) at 10, 60 and 1000 µmol photons m^{-2} s^{-1}. (D) Growth during 10 days on TAP medium plates in the dark or under 25 µmol photons m^{-2} s^{-1} (ML), or photoautotrophically on MIN medium under ML.

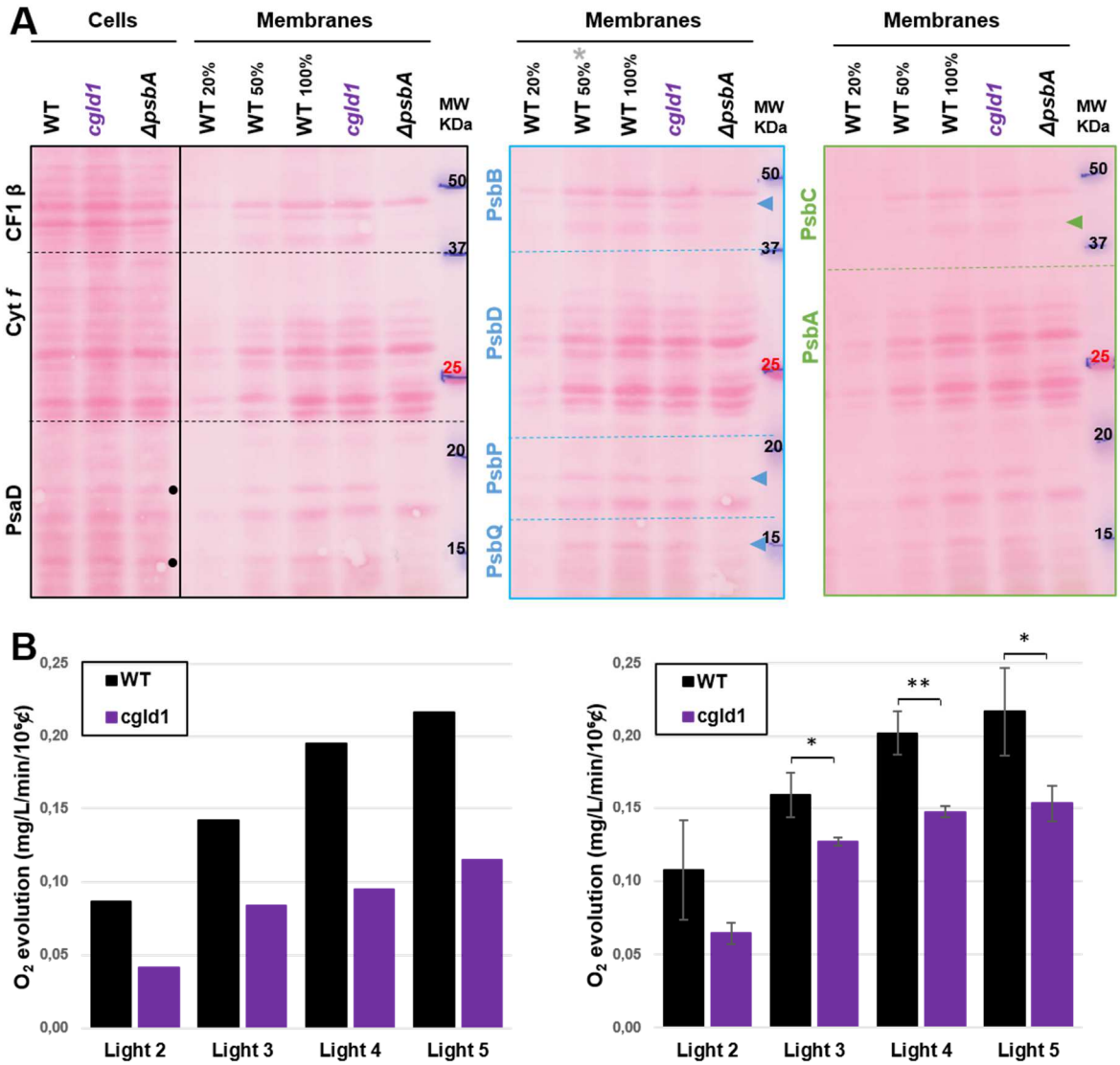

Fig. E supp. Mat. Protein accumulation and oxygen evolution. (A) Ponceau red protein staining of cell and membrane extracts separated by SDS-PAGE and electrotransfered on blots used for immunodetection in Fig. 2A. The subunits recognized by immunodetection are indicated on the left of each panel. Arrow heads indicate PSII subunits detectable by protein staining and absent in PSII deficient mutant *ΔpsaA*. The asterisk in middle panel indicates overloading of WT 50%. Oxygen evolving subunits PsbP and PsbQ are accumulated in cells (dots), and deficient in membranes of PSII deficient mutant *ΔpsaA* as detected by Ponceau red protein staining and immunodetection. (B) Rates of gross oxygen evolution (net oxygen production in the light minus oxygen consumption in the dark) at constant cell density measured in TAP medium at various light intensities without (left panel) or with changing sample (right panel) prior to each illumination. Data represent means ± SD of two or three technical replicates. *p-value < 0.05 and **p-value < 0.01 in Student's t-test.

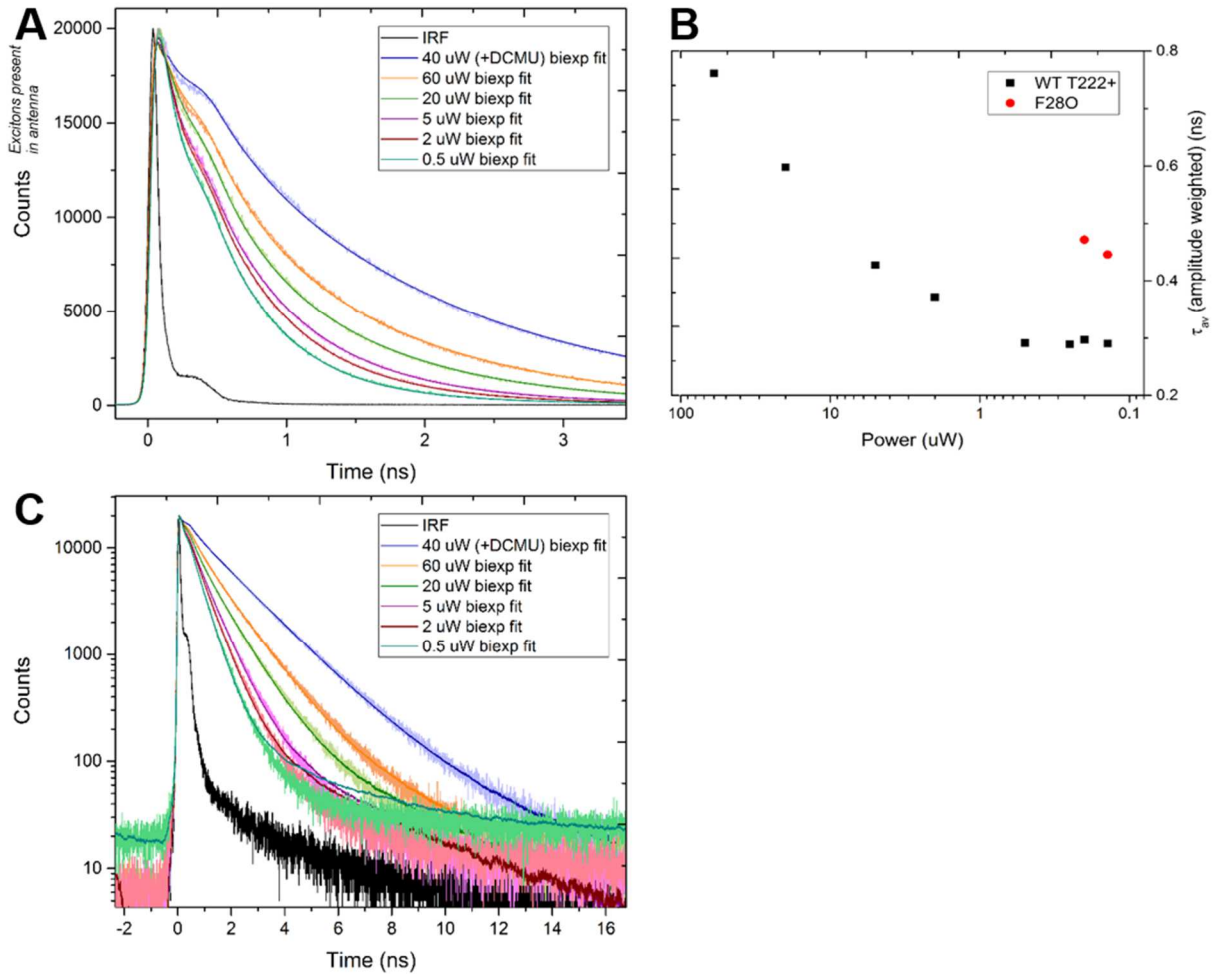

Fig. F supp. mat. Time resolved fluorescence. (A) Raw traces (light colors) and the biexponential fits (dark thin lines). (B) Open centers measurements. To keep the cells as close as possible to F_0, very low powers are used in the absence of DCMU to limit the number of laser hits within one PSII RCs before this very center oxidizes its Q_A^-. A power dependence study was performed in the WT to determine when a plateau is reached where lowering the power did not result in a lower fluorescence signal. The average lifetime from these experiments was plotted as a function of power used. IRF – instrument response function, the « baseline » of the TR fluorescence, deconvoluted upon signal fitting. Variable laser power 40 µW to 0.14 µW. Laser repetition rate 10 MHz (40 to 0.5 µW) and 5 MHz (0.2 and 0.14 µW). Excitation wavelength 438 nm. Detection wavelength 680 nm, ± 8 nm FWHM. Biexponential fit; global decay lifetime is shown. Traces for the two lowest powers, 0.2 and 0.14 µW are omitted. After this power study as concluded, the lowest power was always used for open state measurements: 0.14 µW, marked in red circle. (C) Same data as in (A), logarithmic scale used. Counts correspond to photons counted in each 4 ps bin. Note that the F_v/F_m values, calculated from the absolute lifetimes of chlorophyll fluorescence, match closely with the data from relative fluorescence yield measurements.

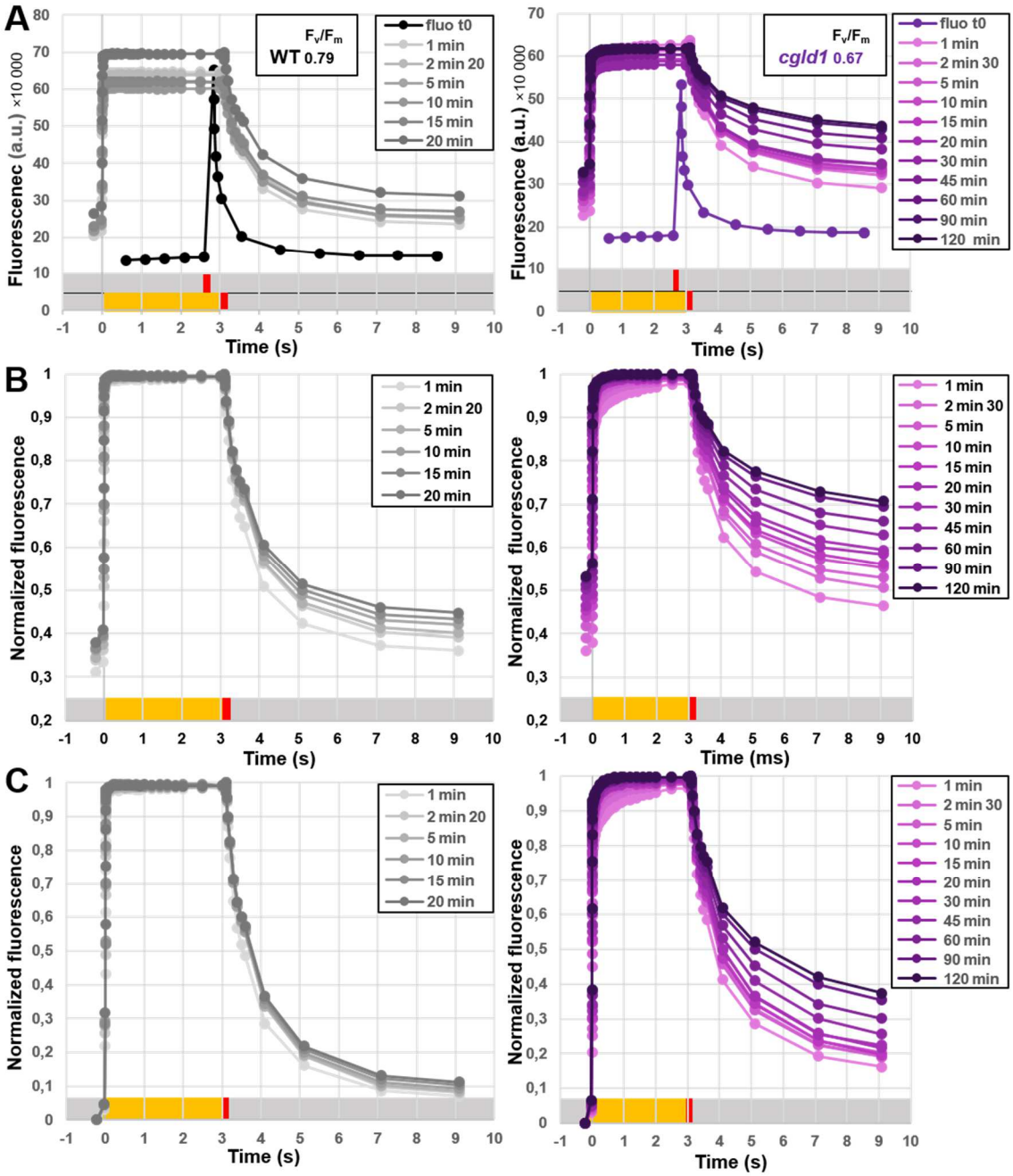

Fig. G supp. mat. Fluorescence in presence of DCMU varying the time period of dark adaptation prior to addition of DCMU. WT strain (left panels) and *cgld1* mutant (right panels). (A) Fluorescence kinetics in presence or absence of DCMU using a saturating pulse to detect F_m. (B) Data from (A) normalized to F_m. (C) Data from (A) normalized to F_m and F_0.

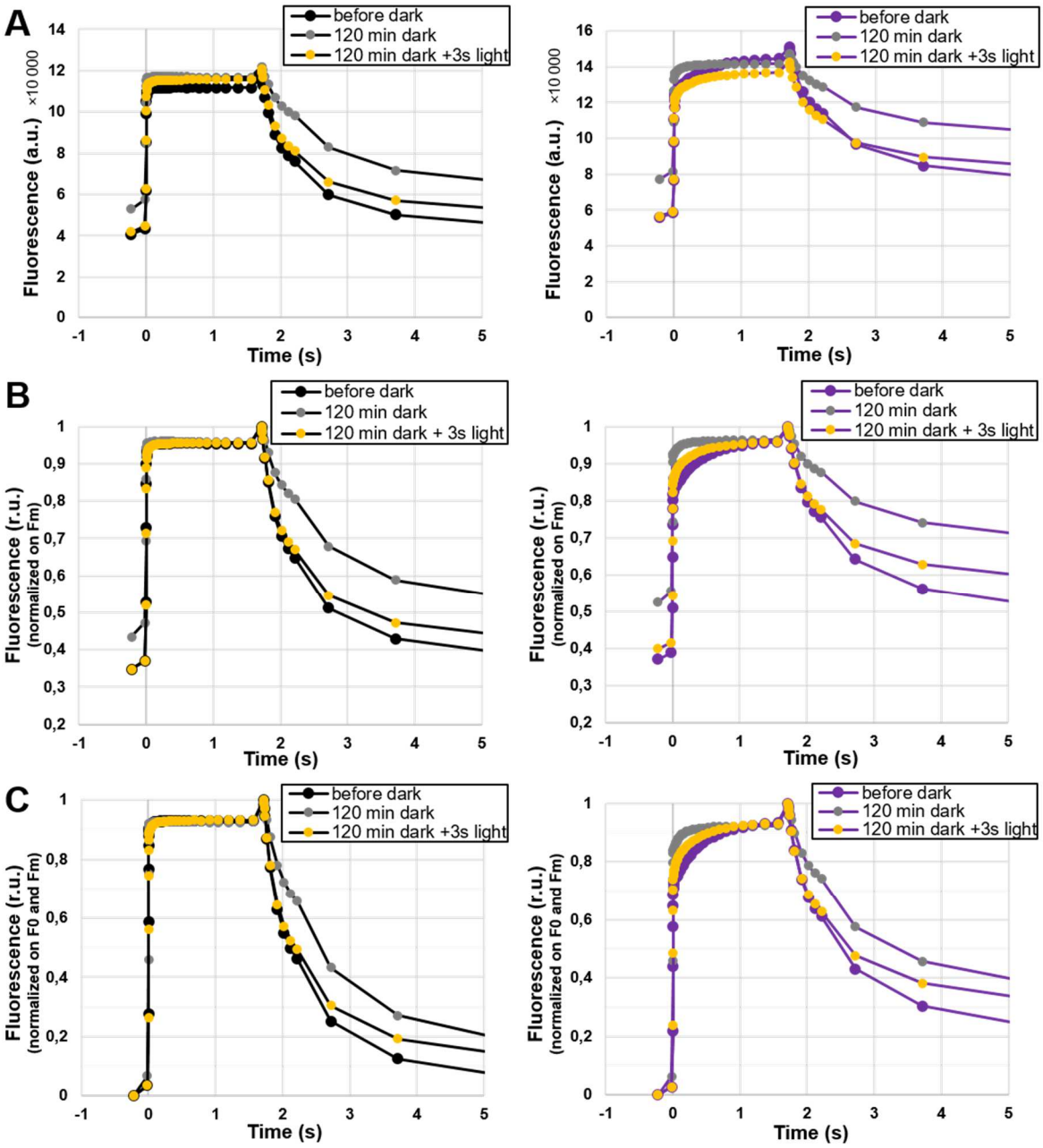

Fig. H supp. mat. Low light illumination after a 120 min period of dark adaptation restores the slow fluorescence rise in presence of DCMU in *cgld1* mutant. WT strain (left panels) and *cgld1* mutant (right panels). Comparison of fluorescence before dark, and after 120 min of dark without or with a 3 sec illumination under 3 µmol photons m^{-2} s^{-1} prior to addition of DCMU and measurement. (A) Fluorescence kinetics in presence of DCMU using a saturating pulse to detect F_m. (B) Data from (A) normalized to F_m. (C) Data from (A) normalized to F_m and F_0.

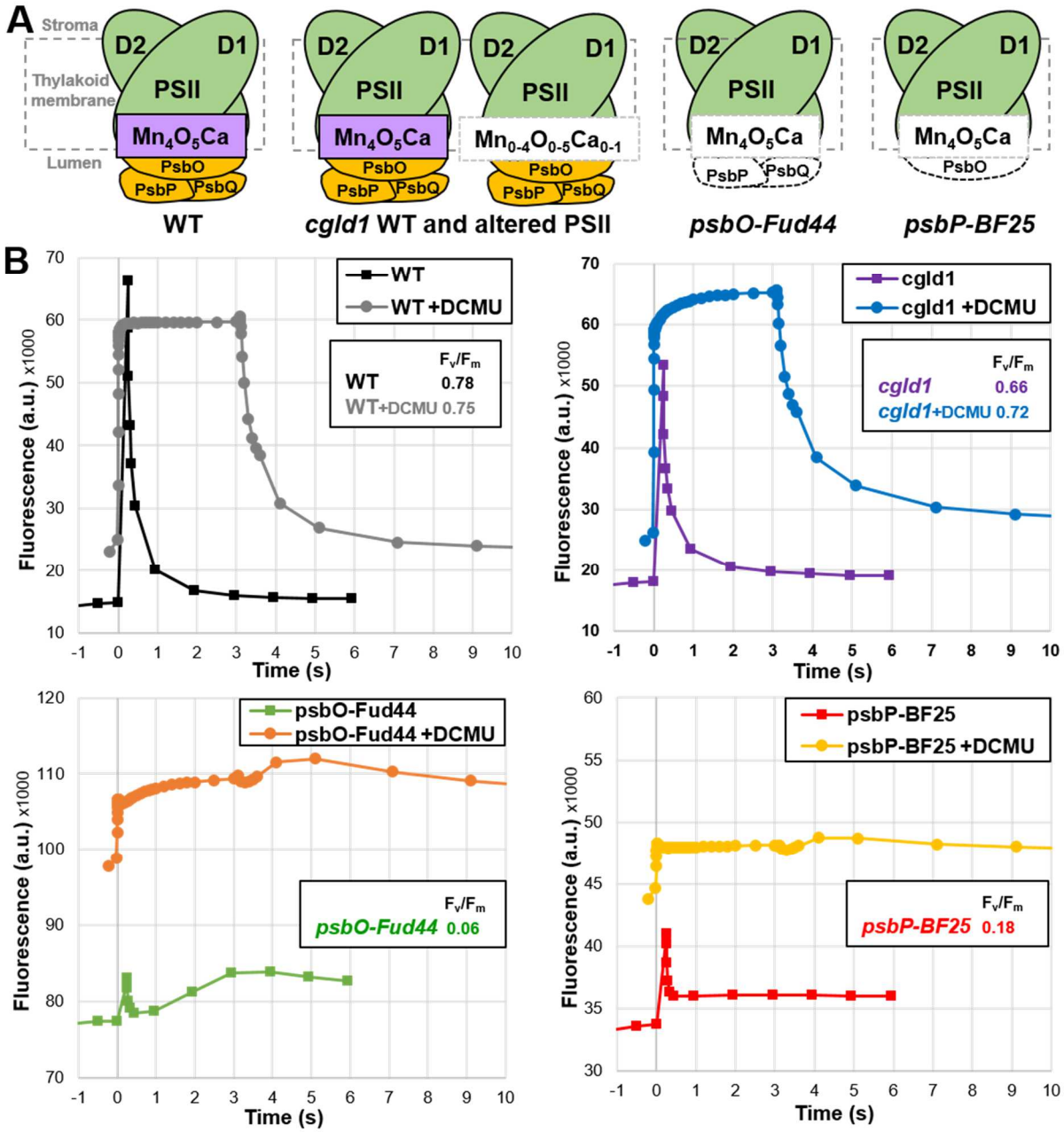

Fig. I supp. mat. Fluorescence kinetics of mutants lacking subunits of the PSII oxygen evolving site share *cgld1* characteristics. (A) Schematic PSII donor side in wild type, *cgld1*, *psbO-Fud44* lacking PsbO (OEE1), and *psbP-BF25* lacking PsbP (OEE2) strains. (B) Fluorescence kinetics of *Fud44* and *BF25* mutants show a lower F_v/F_m that in WT, and a higher F_m in presence of DCMU than in absence DCMU, and a slow phase of fluorescence.

CHAPTER 3:

CHLOROPLAST ATP SYNTHASE REQUIRES PERIPHERAL STALK SUBUNITS ATPF AND ATPG AND STABILIZATION OF *ATPE* MRNA BY OPR PROTEIN MDE1.

FOREWORD

Plants produce ATP by the chloroplast F_1F_O ATP synthase (CF_1F_O), a macromolecular machine, driven by the electrochemical proton gradient across the photosynthetic membrane, also called the protomotive force (PMF). ATP synthesis in the hydrophilic head (CF_1) is powered by the CF_O rotary motor in the thylakoid membrane. The discoveries of the chemiosmotic theory and of the rotary catalysis model have earned P. Mitchell (1978) and P. Boyer & J. Walker (1997) Nobel Prizes in chemistry. A central stalk transmits torque to the head and a peripheral stalk acts as a stator (Figure 3-1). The peripheral stalk is a heterodimer which derived from a bacterial homodimer.

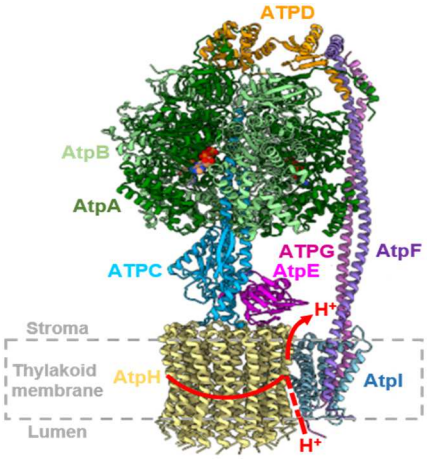

Figure 3-1 Chloroplast ATP synthase structure.
Adapted from cryo-EM map of spinach cF_1F_O (Hahn et al, 2018). cF_1 (A_3B_3CDE) extends into the stroma, whereas cF_O ($FGH_{14}I$) is embedded in the thylakoid membrane (grey). The central rotor consists of the central stalk (CE) connected to the AtpH ring. The peripheral stalk subunits (FG) of the stator are attached by AtpD to the head subunits AtpA and AtpB containing the nucleotide-binding sites. The AtpI subunit and its interface with the AtpH ring form the proton translocation pathway (arrow). The electrochemical proton gradient drives ring rotation.

A plastidial common feature is that most genes of the ancestral endosymbiont were transferred to the nucleus during evolution. Thus, the biogenesis of the photosynthetic apparatus requires the crosstalk of plastid and nuclear genomes. Photosynthetic complexes are of dual genetic origins and nuclear-encoded factors control, in a gene-specific manner, the expression of plastid mRNAs. In addition, accumulation of subunits of a photosynthetic complex is a concerted process due to two complementary mechanisms: some chloroplast-encoded subunits are controlled by epistasy of synthesis – a protein assembly-dependent control of translation, and others are rapidly degraded by proteases when they cannot assemble in a complex. The main protease in the thylakoid is the ATP-dependent FtsH protease (Figure 3-2).

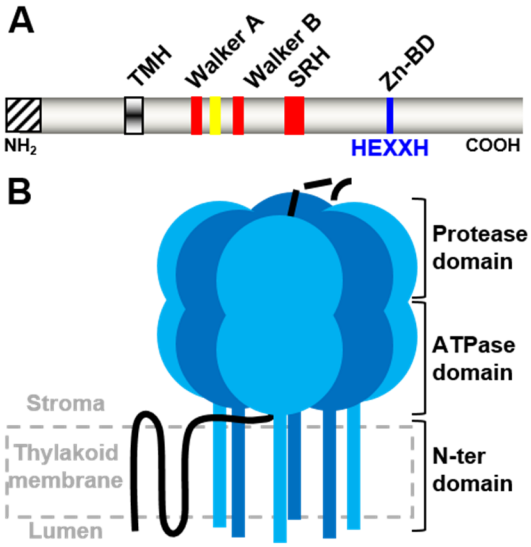

Figure 3-2 The Thylakoid FtsH structure.
(A) Linear diagram of the domain organization of the Chlamydomonas FtsH1/2 subunits with N-ter transit peptide, trans-membrane helix (TMH), ATPase Walker A and B motifs (in red), pore loop (in yellow), second region of homology (SRH) containing Arg residues required for ATP hydrolysis (one of which is substituted by Cys in *ftsh1-1* mutant), and Zn-binding domain (Zn-BD) with HEXXH motif (in blue). (B) Schematic representation of the FtsH1/2

Our study contributes to the understanding of the mechanisms that ensure the $A_3B_3CDEFGH_{14}I$ accumulation of cF_1F_O subunits in Chlamydomonas reinhardtii.

- We succeeded to engineer and characterize knock-out mutants of the peripheral stalk subunits ATPG and AtpF and of a new trans-acting factor MDE1 controlling the expression of the central stalk subunit AtpE.
- We show that neither ATPG nor AtpF homodimers can substitute for the ATPG/AtpF heterodimer peripheral stalk of chloroplast ATP synthase.
- We demonstrate that MDE1, a novel octotricopeptide repeat (OPR) protein encoded in the nucleus, promotes expression of the chloroplast-encoded subunit AtpE by binding to the atpE mRNA 5'-untranslated region.
- Concerning unassembled subunits degradation, while unassembled CF_1 subunits are substrates of the stromal ClpP protease, we identify unassembled CF_O subunits as substrates of the thylakoid FtsH protease.

References:

Hahn, A., Vonck, J., Mills, D. J., Meier, T., & Kühlbrandt, W. (2018). Structure, mechanism, and regulation of the chloroplast ATP synthase. *Science (New York, N.Y.)*, *360*(6389), eaat4318. https://doi.org/10.1126/science.aat4318

Malnoë, A., Wang, F., Girard-Bascou, J., Wollman, F.-A., & de Vitry, C. (2014). Thylakoid FtsH Protease Contributes to Photosystem II and Cytochrome *b* $_6$ *f* Remodeling in *Chlamydomonas reinhardtii* under Stress Conditions. *The Plant Cell*, *26*(1), 373-390. https://doi.org/10.1105/tpc.113.120113

Cette page a été laissée intentionnellement vide
This page was intentionally left blank

***

~ Research Article in preparation ~

CHLOROPLAST ATP SYNTHASE REQUIRES PERIPHERAL STALK SUBUNITS ATPF AND ATPG AND STABILIZATION OF *ATPE* MRNA BY OPR PROTEIN MDE1

***

ARTICLE

CHLOROPLAST ATP SYNTHASE REQUIRES PERIPHERAL STALK SUBUNITS ATPF AND ATPG AND STABILIZATION OF *ATPE* MRNA BY OPR PROTEIN MDE1

Authors: Frédéric Chaux[1,$] (0000-0003-3298-8415), Domitille Jarrige[2] (0000-0002-0633-8999), Marcio Rodrigues-Azevedo[3], Sandrine Bujaldon (0000-0003-2177-4315), Oliver D. Caspari[4] (0000-0001-8235-0503), Shin-Ichiro Ozawa[5] (0000-0001-7698-5350), Dominique Drapier, Olivier Vallon (0000-0001-8827-4927), Yves Choquet (0000-0003-4760-3397), Catherine de Vitry[$] (0000-0002-3632-1370)

Unité Mixte de Recherche (UMR) 7141, Centre National de la Recherche Scientifique (CNRS) and Sorbonne Université, Institut de Biologie Physico-Chimique, 13 rue Pierre et Marie Curie, F-75005 Paris, France

[$] corresponding authors: frederic.chaux-jukic@sorbonne-universite.fr, catherine.devitry@ibpc.fr

[1] present address: Sorbonne Université, CNRS, UMR7238, Institut de Biologie Paris-Seine, Laboratory of Computational and Quantitative Biology, 75005 Paris, France

[2] Present address: University of Strasbourg (UNISTRA), Génétique Moléculaire, Génomique, Microbiologie (GMGM), France

[3] Doctoral School of Plant Sciences (SEVE) – ED567 Université Paris-Saclay

[4] present address: Institut Pasteur, Department of Microbiology, 28 Rue du Docteur Roux, 75015 Paris, France

[5] present address: Research Institute for Interdisciplinary Science, Okayama University, Okayama, Japan.

Keywords: ATP synthase, ATPG, AtpF, organellar trans-acting factor, helical repeat protein, OPR, FtsH protease, CRISPR-Cas9, *Chlamydomonas reinhardtii*

Summary:

Chloroplast ATP synthase contains subunits of plastid and nuclear genetic origin. To investigate the coordinated biogenesis of this complex, we isolated novel ATP synthase mutants in the green alga *Chlamydomonas reinhardtii* by screening for high light sensitivity. We report here the characterization of mutants affecting the two peripheral stalk subunits *b* and *b'*, encoded respectively by *atpF* and *ATPG*, and of three independent mutants which identify the nuclear factor MDE1, required to stabilize the chloroplast-encoded *atpE* mRNA. First, whole-genome sequencing reveals a transposon insertion in the 3' UTR of *ATPG* and mass spectrometry indicates that a small amount of all eight ATP synthase subunits still accumulates in this knock-down *atpG* mutant. In contrast, knock-out *atpG* mutants were obtained by CRISPR-Cas9 gene editing and fully prevent ATP synthase function, as observed in *atpF* frame-shift mutants. Crossing with thylakoid protease mutant *ftsh1-1* identifies AtpH as FtsH1/2 substrate and suggests that this protease significantly contributes to the concerted accumulation of ATP synthase subunits. In *mde1* mutants, the absence of *atpE* transcript fully prevents ATP synthase biogenesis and photosynthesis. Using chimeric *atpE* genes to rescue *atpE* transcript accumulation, we demonstrate that MDE1, a novel octotricopeptide repeat (OPR) protein, genetically targets the *atpE* 5'UTR. In the perspective of the primary endosymbiosis (~1 Gy), the recruitment of MDE1 to its *atpE* target exemplifies a nucleus/chloroplast interplay which evolved rather recently (in the ancestor of Volvocales, ~300 My).

Significance statement:

Using screening and CRISPR-Cas9 editing, we provide the missing mutant of chloroplast ATP synthase subunits, *atpG*, and show the absolute requirement of AtpF-ATPG heterodimer as the peripheral stalk. We also identify the nuclear-encoded *MDE1* gene, establishing this octatricopeptide protein as an essential trans-acting factor in the expression of chloroplast-encoded *atpE* gene, probably widely conserved.

INTRODUCTION

In almost all living cells, ATP is mainly generated by F-type ATP synthases. These "splendid molecular machines" (Nobel prize P. D. Boyer) are multi-subunit nanomotors made of a transmembrane moiety (F_o) comprising a rotor, which is put in motion by the dissipation of the transmembrane proton gradient, and a protruding stator part, where the phosphorylation of ADP into ATP takes place in the hydrophilic head of the soluble moiety (F_1). The crucial coupling between chemiosmotic flow and phosphorylation relies both on the central stalk spinning along with the rotor, and the structuring peripheral stalk. Interestingly, chloroplast ATP synthase, as most large complexes of eukaryotes' organelles, are "genetic mosaics" since some subunits are encoded in the mitochondrial or plastid genomes and others in the nuclear genome. Organellar genomes usually harbor a limited and well-described gene content, whereas nuclear genes encoding plastid proteins require an importation system of the pre-protein from the cytosol, e.g. to the chloroplast and ultimately the thylakoid, involving targeting peptides, endopeptidases and carriers (von Heijne et al., 1989; Wollman, 2016; Garrido et al., 2020).

The subunit composition of ATP synthase is conserved between bacteria and plastids (names of the chloroplast proteins are indicated between brackets). The rotor comprises a homo-oligomer of 8 to 14 subunits *c* (AtpH) forming a barrel-like structure. One after the other, each *c* exchanges protons with stator subunit *a* (AtpI), with which it forms two half proton-channels spanning the membrane. The scrolling of *c* oligomer drives the rotation of the central stalk formed by the subunits γ (ATPC) and ε (AtpE). The central stalk asymmetrically protrudes in the cavity of the catalytic head, inducing conformational changes which fuel a 3-steps cycle: recruitment of ADP and Pi, ATP synthesis and ATP release. The head is composed of 3 α (AtpA) and 3 β (AtpB) subunits and is capped by subunit δ (ATPD). The catalytic head remains static relative to the rotor due to a peripheral stalk anchored in the membrane and bound to *a*. The peripheral stalk is

a homodimer b_2 in most bacteria and a heterodimer *bb'* (AtpF and ATPG) in cyanobacteria and thylakoids. Hence, we aimed at understanding how cells reach the complicated stoichiometry of ATP synthase ($\alpha_3\beta_3\gamma\delta\varepsilon$*abb'*$c_{8\text{-}14}$ or $A_3B_3CDEIFGH_{8\text{-}14}$).

In cyanobacteria and plants, the obtention of ATP synthase mutants is limited by its absolute requirement in both respiratory and photosynthetic chains. This limitation is overcome in the model green microalga *Chlamydomonas reinhardtii*, a facultative phototroph that can use a reduced carbon source, such as acetate, to readily grow heterotrophically in the dark, while nonetheless undergoing normal chloroplast biogenesis in the absence of photosynthesis. *C. reinhardtii* mutants have previously been isolated for each subunit of the chloroplast ATP synthase except one: *ATPG* (Drapier et al., 2007; Finazzi et al., 2009). This collection and few other nuclear mutants (whose causal mutations were not known at the time) have notably revealed that the control of subunit synthesis in the chloroplast is mainly post-transcriptional and that assembly intermediates control translation of the chloroplast-encoded subunits (Lemaire & Wollman, 1989a; Lemaire & Wollman, 1989b; Drapier et al., 1992; Drapier et al., 2007). Overall, the pleiotropic loss of all subunits in ATP synthase mutants suggests that each is required for the accumulation of the other subunits at WT level. However, differences in stability can be observed, which allow insights into how assembly of ATP-synthase complex proceeds and is regulated. Peripheral membrane CF_1 subunits α, β and γ are more stable in absence of CF_o transmembrane subunits than *vice-versa* (Lemaire & Wollman, 1989a; Lemaire & Wollman, 1989b). This concerted accumulation occurs via the control of synthesis and/or the degradation of unassembled subunits (Choquet & Wollman, 2022).

Regarding control of synthesis, the β subunit is required to activate in trans the translation of α but translation of β itself is inhibited by an oligomer of α and β in absence of γ (Drapier et al, 2007). Also, β does not bind to CF_o in absence of α. Anchoring of CF_1 to the membrane requires the peripheral stalk subunit *b* and rotor subunit *c* but not the stator subunit *a* and rotor subunit ε. Thus, the peripheral stalk appears to be required for anchoring CF_1 while *a* is recruited later to prevent proton gradient leakage

through assembly intermediates. The synthesis of ε subunit even requires the accumulation of several subunits: α, β, *b* and *c* (but not *a*) (Lemaire & Wollman, 1989a; Lemaire & Wollman, 1989b). Thylakoid membranes of Chlamydomonas accumulate very little α and β in *atpE* (*Fud17*) mutant lacking ε, pointing to its important role in the assembly/stabilization of ATP synthase (Lemaire & Wollman, 1989b; Robertson et al., 1990). Since peripheral stalk subunits AtpF and ATPG are paralogous and very similar structurally, one may question their interchangeability. The *Fud18* Chlamydomonas mutant lacking AtpF (Lemaire & Wollman, 1989b) does not accumulate ATP synthase, refuting that homodimeric ATPG may form an alternative peripheral stalk. To analyze the eventuality of homodimeric AtpF peripheral stalk, we isolated and characterized *atpG* mutants in this work.

On the other hand, chloroplast proteases rapidly degrade some subunits when they cannot assemble within a complex or when they are misfolded or damaged, e.g. in photo-inactivated photosystem II (van Wijk, 2015; Schroda and de Vitry, 2022). In contrast with the regulations regarding synthesis, few data exist regarding the role of protein degradation in the quality control of ATP synthase. Stromal ClpP protease was shown to play a role in the degradation of non-assembled CF_1 subunits (Majeran et al., 2019), and we investigate in this work the role of the major protease of the thylakoid FTSH in the degradation of ATP synthase. The nuclear *ftsh1-1* mutant expresses an inactive thylakoid FTSH protease (Malnoë et al., 2014) and has contributed to show previously that FTSH controls PSII repair, and recycling of misassembled cytochrome b_6f and LHCa (Schroda & de Vitry, 2022). To assess how degradation of unassembled subunits contributes to concerted biogenesis of ATP synthase, we crossed different chloroplast and nuclear ATP synthase mutants with the *ftsh1-1* mutant.

Nucleus-encoded factors control plastid gene expression in most cases in a gene-specific manner: the M factors fare involved in mRNA maturation and stabilization and the T factors in mRNA translation activation (Hammani et al., 2014; Wang et al., 2015). Small RNA sequencing revealed footprints at the 5' end of most transcripts, suggesting

that many of these molecular factors remain to be identified (Cavaiuolo et al., 2017). Recently, however, a few nucleus-encoded factors related to ATP synthase have been molecularly identified. The MDA1 (Viola et al., 2019) and TDA1 (Eberhard et al., 2011) proteins bind to the 5'untranslated region (UTR) of *atpA* transcript and respectively promote its maturation and stabilization and its translation. The MTHI1 protein stabilizes the *atpH* transcript and its binding to *atpH* or *atpI* 5'UTRs promotes their translation (Ozawa et al., 2020). Moreover, a gain-of-function mutation in the *NCC1* gene provokes its recruitment to the coding sequence (CDS) of *atpA* transcript and promotes its destabilization (Boulouis et al., 2015). Interestingly, all these factors are octotricopeptide repeat (OPR) proteins. In the green lineage, large helical repeat proteins contribute to post-transcriptional regulations, such as the tetratricopeptide repeat (TPR), pentatricopeptide repeat (PPR) and OPR proteins, which comprise repeats of degenerate RNA-binding motifs of 34, 35 and 38 amino-acids, respectively. Usually, recognition of the target transcript is driven by the binding of each motif to a preferred nucleotide, determined by the amino-acid properties at a given position, such as the 5th and 35th for PPR (Barkan et al., 2012; Yan et al., 2019). In *C. reinhardtii*, OPR proteins are far more numerous than PPRs, but the "OPR code" is still imprecise due to the limited identification of OPR protein/RNA target interactions.

Here, we screened transformants from random nuclear mutagenesis and present the phenotype of several new ATP synthase mutants. By whole genome sequencing we identify new mutants in two genes: *ATPG*, encoding one of the two peripheral stalk subunits, and 2 alleles of *MDE1*, encoding a novel OPR protein. Previously, the mutant strain CAL014.01.30 (Dent et al., 2005) has been named *mde1* because RNA blots and small RNA sequencing revealed altered Maturation/stabilization of complex D (ATP synthase) subunit AtpE mRNA (Cavaiuolo et al., 2017), and we also identify its previously unknown causal mutation. We provide genetic evidence that MDE1 interacts with the 5'UTR of *atpE* transcript to stabilize it. For thorough comparison, we also genotyped the previously unidentified *atpF* mutant, Fud18 (Lemaire & Wollman, 1989b) and knock-out *atpG*

mutants were obtained by CRISPR-Cas9 technology. By mass spectrometry and protein blot analysis, we show that knock down of *ATPG* decreases the accumulation of the other ATP synthase subunits, while its knock-out completely prevents it, showing that a heterodimeric AtpF-ATPG peripheral stalk is required for ATP synthase assembly. We detect an FTSH-dependent accumulation of misassembled AtpH subunit.

RESULTS

Isolation of chloroplast ATP synthase mutants by nuclear transformation

C. reinhardtii can be grown in the presence of acetate as a reduced carbon source (TAP medium) and photosynthesis mutants can be screened by chlorophyll fluorescence in a non-invasive manner (Johnson et al., 2009). The nuclear mutants *F292*, *F28N*, *E236* and *E271* presented here were obtained from a random nuclear mutagenesis and showed phenotypes of chloroplast ATP synthase mutants in growth, fluorescence and electrochromic shift (Figure 1) and protein accumulation (Figure 2).

To screen for ATP synthase mutants after the mutagenesis, cells were exposed to high light for 1 hour. In several colonies, the maximal fluorescence yield of PSII, F_V/F_M, decreased more drastically than in the wild-type (WT) strain (Figure 1A) and similarly to the control *ftsh1-1* strain which cannot fulfil PSII repair (Malnoë et al., 2014; Wang et al., 2017). We further compared the growth of our mutants on minimal (MIN) or on TAP media under increasing light intensities to that of the WT and the *mdb1* ATP synthase mutant, which lacks the nucleus-encoded maturation factor MDB1 required for the accumulation of *atpB* transcript (Drapier et al., 1992) (Figure 1B). In TAP, mutants *E271*, *F28N*, *F292* and *mdb1* could grow under moderate light (25 µmol photon m^{-2} s^{-1}), although slightly less than WT, but they were almost killed by higher light (120 µmol photon m^{-2} s^{-1}), further confirming their photosensitive phenotypes. In MIN, they were not able to grow at all, suggesting that photosensitivity in *E271*, *F28N* and *F292* mutants originate from strong impairments of photosynthesis itself, similar to the *mdb1* mutant.

In contrast, growth of mutant *E236* under moderate light was similar to that of WT and *ftsh1-1* in TAP and was not completely abolished in MIN; under higher light, *E236* exhibited slower growth than WT in TAP and full inhibition in MIN, similar to the *ftsh1-1* phenotype.

Because decreased F_V/F_M, loss of phototrophy and/or sensitivity to high light can be caused by numerous distinct mutations, among which chloroplast ATP synthase (Majeran et al., 2001), RuBisCO deficiencies (Johnson, 2011) and FTSH1 mutations, a possible defect in ATP synthase was then assessed by spectroscopy. At the onset of light, the wild-type (WT) strain reached a low level of steady-state fluorescence (F_S) within a few seconds while in mutant strains *E236*, *E271*, *F28N* and *F292*, fluorescence yield increased almost up to the maximal fluorescence yield F_M' within a few minutes (Figure 1C). This phenotype has been previously reported in mutants of the RuBisCO or of chloroplast ATP synthase (Bennoun & Chua 1976; Bennoun et al., 1980; Majeran et al., 2001; Johnson, 2011) and is attributed to the gradual appearance of a bottleneck in electron flow towards CO_2 fixation and to the build-up of very high proton gradient which down-regulates PSII photochemistry (low F_M' - F_S). Transfer of charges across the thylakoid membrane induces changes in the transmembrane electrical field which in turn affects carotenoids absorption: this so-called "electrochromic shift" (ECS) can be recorded using spectrophotometric measurements (at 520nm). In WT cells, upon illumination, activity of photosystems and cytochrome b_6f generates a transmembrane gradient, which is consumed by ATP synthase (Bailleul et al., 2010). In our four mutants, release of the ECS was much slower than in the WT (Figure 1D): decay rates in *F28N* and *E271* were similar to that of known mutants lacking essential ATP synthase genes, while in *E236* and *F292* mutants, they were slightly faster.

Accumulation of ATP synthase subunits is downregulated in mutants of *ATPG* and *MDE1* genes.

To gain insight on these mutants at the molecular level, we investigated the accumulation of RuBisCO and individual subunits of the chloroplast ATP synthase by immunodetection (Figure 2). Subunits AtpA, AtpB and AtpE (Figure 2B-D) belong to the soluble moiety (CF_1), which can assemble in the stroma (Lemaire & Wollman, 1989a; Lemaire & Wollman, 1989b), while AtpH (Figure 2D) is part of the transmembrane moiety (CF_o) (structure/function illustrated in Figure 2E-F). As controls, we used deletion mutants of chloroplastic ATP synthase genes (*ΔatpB*, *ΔatpH*, *ΔatpI*) as well as *mda1*, *mdb1* and *mrl1* nuclear mutant strains, which lack the factors required for the accumulation of chloroplast transcripts *atpA*, *atpB* (Drapier et al., 1992; Viola et al., 2019; Cavaiuolo et al., 2017) and *rbcL* (Johnson et al., 2010), respectively. Nuclear mutant strain *mrl1* serves as a control for a non-photosynthetic strain devoid of RuBisCO but unaffected in the ATP synthase. Indeed, large subunit of RuBisCO was absent in *mrl1* but accumulated similarly in the other mutant strains and in the WT, precluding that the *E236*, *E271*, *F28N* or *F292* lack RuBisCO (Figure 2A). In contrast, the levels of the four ATP synthase subunits were much lower in the four mutants than in the WT, although showing distinct patterns of accumulation, which may reflect distinct impairments in the biogenesis of ATP synthase. Subunit AtpA was detected only in *F28N* and *F292* but not in other mutant strains (Figure 2B). AtpB was absent from *mdb1* as expected, and all four mutants accumulated about one fifth (*E236* and *F292*) or less (*F28N* and *E271*) as compared to WT (Figure 2C). Traces of subunit AtpE were detected in *ΔatpH*, *E236* and *F292* but not in *ΔatpB*, *F28N* or *E271* mutants. Finally, no subunit AtpH was detected in any tested mutant (Figure 2D), in line with previous reports that AtpH is stable only when ATP synthase is fully assembled (Lemaire et al., 1988; Lemaire & Wollman, 1989a; Lemaire & Wollman, 1989b; Ketchner et al., 1995).

Altogether, this preliminary characterization indicated that the four mutants *E236*, *E271*, *F28N* and *F292* are deficient in the chloroplast ATP synthase, with *E236* being slightly leaky. They were obtained in a transformation involving the *aphVII* cassette but, in the progeny of backcross to a WT strain, the mutant phenotypes did not co-segregate with hygromycin resistance, revealing that in the four mutants the ATP synthase defect was genetically independent from the transgene insertion but rather due to other mutations. To identify these mutations, we sequenced the whole genome of the mutant strains *E236*, *F28N*, *F292* and *E271* as well as the WT strain by paired-end Illumina sequencing (Suppl. Table ST1) and took advantage of recent genome improvements (O'Donnell et al., 2020; Craig et al., 2021). We also sequenced the ATP synthase mutant *CAL014.01.30* isolated in a screen for non-photosynthetic mutants (Dent et al., 2005): this mutant lacks a maturation footprint for the *atpE* transcript and it was hence called *mde1*, but the gene coding for MDE1 had thus far not been identified (Cavaiuolo et al., 2017) (Suppl. Figure 2). We first looked for candidate mutations in genes known to be related to ATP synthase, namely nucleus-encoded subunits, assembly factors and organellar trans-acting factors (OTAFs) (Ruhle and Leister, 2015).

The mutant *E236* was found to carry a TOC1 transposon insertion in the 3'UTR of *ATPG* gene (locus Cre11.g481450), about 30 bp downstream of the stop codon (Figure 2G, top left panel; Suppl. Figure S1A). Paired-end reads mapped to distinct chromosomes, each of them corresponding to one of the many genomic locations of the *TOC1* transposon (Day & Rochaix, 1991; Kim et al., 2006). We confirmed this large rearrangement by PCR amplification (Suppl. Figure S1B) and used the 2.5 kb PCR product from the WT for complementation (see below). To compare *atpG* and *atpF* mutants, we sequenced the chloroplast *atpF* gene of the *Fud18* mutant which specifically lacks synthesis of AtpF, the other peripheral stalk subunit (Lemaire & Wollman, 1989b). We observe thymine deletion shortly after the start codon, causing a frameshift and an early stop codon (Figure 2G, top right panel; Suppl. Figure S1C).

Next, we found three distinct mutations in the 1st exon of the same gene on chromosome 8, Cre08.g358530 (version v5; in v6: Cr_08_37856.1) in three independent mutants (Figure 2G, bottom panel). As compared to the WT, the *F28N* and *E271* mutants carry a single nucleotide insertion and an insertion of 124 bp, respectively (Suppl. Figure S2A). To identify the mutation in the mutant *CAL014.01.30*, we outcrossed it to the highly polymorphic wild-type strain S1D2, pooled the progeny into either ATP synthase-deficient or wild-type phenotypes. Sequencing both pools separately revealed that *mde1* phenotype was linked to chromosome 8 left arm (Suppl. Figure S2B). More specifically, whereas the wild-type pool showed only S1D2-inherited polymorphisms in this region, we found in the ATP-synthase deficient pool a single-nucleotide insertion in the 1st exon of gene Cre08.g358530 (Suppl. Figure S2C), which could be the cause for the *mde1* phenotype of this strain (Cavaiuolo et al., 2017). To conclude, the insertions in mutants *F28N* and *CAL014.01.30* produce frame shifts, and the insertion in *E271* mutant introduces a stop codon, all leading to truncated polypeptides for Cre08.g358530 (Suppl. Figure S2D-F). The Cre08.g358530 locus is made of 5 exons and extends over 8,2 kb. It encodes a large protein of 2175 residues that contains 12 OPR repeats. Because of its length, we failed to amplify the full WT gene to complement these mutants for formal identification of Cre08.g358530 as *MDE1*. However, the three independent strains mutated in Cre08.g358530 lack the *atpE* transcript (see below) and *F28N*, *CAL014.01.30* and *E271* are likely allelic mutants of the *MDE1* gene which we therefore call *mde1-1*, *mde1-2* and *mde1-3*, respectively.

In mutant F292, we found no mutation in known ATP synthase-related genes nor in the photosynthesis "Green-cut" gene set (Merchant et al., 2007). Using the impact predictor of point mutations SnpEff (cingolani et al, 2012) and the current genome annotation, we found no difference in *F292* as compared to the WT. However, numerous *F292* reads were anchored in transposable elements (Craig et al 2021) absent in the WT: the promoter HSP70A from our transgene integrated in *Gypsy-7* and the DIRS retrotransposon *TOC1* was found in three novel loci, which together with its transposition in

the 3'UTR of *ATPG* in *E236*, suggests that *TOC1* transposition is relatively promoted during the transformation process, possibly due to stress conditions and/or DNA damage.

Altogether, we characterize the mutations in five strains. One in the CDS of the chloroplast gene *atpF* and another in the 3'UTR of the nuclear gene *ATPG*, each coding for one of the two peripheral stalk subunits of chloroplast ATP synthase (respectively subunits *b* and *b'*) and for which we investigated the impact on assembly in the next three sections. Further 3 mutants were found to carry frame-shift mutations in Cre08.g358530, which we characterize as *MDE1* in the following.

Complementation of mutant *E236* by *ATPG* gene

To formally demonstrate that photosynthesis impairment in *E236* stems from alteration of *ATPG*, we re-introduced the WT version of *ATPG* (hereafter denoted $ATPG^{WT}$) by complementation. Mutant cells were electroporated in the absence or presence of $ATPG^{WT}$, plated on minimal medium and grown under high light for selection. Clones appeared only when *E236* was transformed with $ATPG^{WT}$. Few clones were randomly chosen for further analysis (Figure 3). Complemented lines *E236::*$ATPG^{WT}$ C1 and C3 grew as well as the WT strain in absence of acetate (MIN) and under high light (Figure 3A, left panel) and restored PSII yield (Figure 3A, right panels, Figure 3B), while mutant *E236* was severely impaired. As control, we compared our mutant *E236* to the CF_o mutants *ΔatpH* and *atpF*. The decay rate of the proton gradient (Figure 3C) and accumulation of subunits AtpB, AtpH and ATPG in thylakoid membranes (Figure 3D) was restored to WT levels in the complemented strain *E236::*$ATPG^{WT}$ *C1* as compared to all mutants. Altogether, this confirms that ATP synthase impairment in *E236* originates from mutation in *ATPG* gene, providing the first mutant of subunit *b'* and the last missing among *C. reinhardtii* mutants of ATP synthase subunits (Finazzi et al., 2009). However, *E236* was less impacted in growth on MIN medium under low light and TAP medium under high light than other ATP synthase mutants such as *ΔatpH*, *atpF-Fud18*, *mdb1*, *mde1-1* and *mde1-3 (F28N* and *E271*) (Figure 1B), suggesting that the *TOC1* insertion in the 3'UTR of

ATPG may not fully prevent its expression and thus that mutant *E236* may represent a knock-down, rather than a knock-out, of *ATPG* (*E236*: *atpg-kd*).

To probe the possible accumulation of full ATP synthase at reduced levels in *atpG-kd* (*E236*), we used mass-spectrometry to quantify the protein content in cells grown in phototrophic conditions under low light (Figure 4A). Using Benjamini-Hochberg's adjustment (α=0.05), accumulation levels were significantly altered in *atpG-kd* as compared to WT for 452 (15%) of the total 3105 detected proteins, among which only respectively 3 and 18 proteins were at least twice more or twice less present in *atpG-kd* than in WT. We did not distinguish specific pathway or functional group of proteins that were up- or downregulated, except ATP synthase itself. Seven of its subunits were at least six-fold less abundant in *atpG-kd* than in the WT, i.e. AtpA, AtpB, ATPC, ATPD, AtpE, AtpF and notably ATPG. The two peripheral stalk subunits, ATPG and AtpF, were most depleted, down to ~5% of WT levels. Regarding the last two ATP synthase subunits, (i) AtpH was not detected from either WT or *atpG-kd* and (ii) AtpI was only detected in 5 of the 6 replicates from WT and not detected in any sample from *atpG-kd* (Suppl. Figure S4), probably because these two subunits are small and/or highly hydrophobic. Thus, this mutant can accumulate low levels of functional ATP synthase, allowing dissipation of part of the proton gradient (Figure 3C) to produce ATP. This supports the weak phototrophic growth and offers a better tolerance to high light than ATP synthase null mutants (Figure 1 and 3). Unfortunately, we could not detect the known nucleus-encoded ATP synthase expression factors to compare their accumulation, probably because of the low abundance of organellar trans-acting factors in cells. In conclusion, we provide evidence that *TOC1* insertion in the 3'UTR of *ATPG* gene in mutant *E236* decreases the expression level and accumulation of ATPG protein but does not abolish it, allowing the assembly of rare, functional ATP synthase complex.

Concerted accumulation of ATP synthase subunits involves proteolysis by FTSH

Since the accumulation of ATP synthase in *atpG-kd* (*E236*) is limited by the amount of ATPG subunit, we wondered whether other subunits may be produced in excess and subsequently removed by proteolysis. One candidate for such regulation by proteolysis is the thylakoid FTSH protease, a transmembrane FTSH1-FTSH2 hetero-hexamer, which degrades damaged subunit D1 during PSII repair cycle, cytochrome b_6f subunits and thylakoid membrane proteins involved in cytochrome b_6f biogenesis upon nutrient starvation or in cytochrome b_6f mutants, and LHCI antenna proteins in chlorophyll *b*-less mutants (Malnoë et al., 2011; Malnoë et al., 2014; Wei et al., 2014; Bujaldon et al., 2017; de Mia et al., 2019; Schroda & de Vitry, 2022). We thus crossed mutants of ATP synthase peripheral stalk to the *ftsh1-1* mutant, which is impaired in the processing of substrates (Malnoë et al., 2014). We observed that subunits AtpB, ATPC and AtpH accumulated in higher amounts in the double mutants *atpG-kd ftsh1-1* and *atpF ftsh1-1* as compared to single mutants *atpG-kd* and *atpF* (Figure 4B). This suggests that FTSH is involved in the elimination of soluble CF_1 and membrane CF_o ATP synthase subunits in single peripheral stalk mutants. To further test the role of thylakoid FTSH protease further, we crossed the *ftsh1-1* mutant to previously characterized CF_1 mutants (Suppl. Figure S4). We had previously observed that while the *petB* mutation H202Q (*petB** in the following) impaired accumulation of the cytochrome b_6f complex, the *ftsh1-1* mutation restored its accumulation in double mutants *petB* ftsh1-1* (Malnoë et al., 2011), e.g. the cytochrome b_6f transmembrane subunit IV (Suppl. Figure S4A). Crossing *petB* ftsh1-1* to the *atpC1* mutant did not increase accumulation of soluble subunits AtpA and AtpB but restored accumulation of the membrane subunit AtpH (Suppl. Figure S4A). In a cross between *ΔatpA* and *ftsh1-1*, the double mutant accumulated similar levels of AtpB and ATPC subunits but significantly more AtpH than the *ΔatpA* mutant (Suppl. Figure S4B). Prior studies (Drapier et al., 2007), have shown that the absence of ATPC limits the translation of AtpB while unassembled AtpB stimulates the translation of AtpA. In contrast, no assembly-mediated regulation has been shown for AtpH (Ozawa et al., 2020),

and our results suggest that AtpH level in ATP synthase mutants is largely controlled by its stability, tailored by the FTSH protease.

To completely disrupt ATPG accumulation, we developed a custom CRISPR-Cas9 protocol (see Materials and Methods and Suppl. Figure S5-S6), aiming at targeted knock-out by inserting a hygromycin resistance cassette, equipped with homology flanks, at the CRISPR-Cas9 cut site within the *ATPG* coding sequence (Suppl. Figure S5A). Transformants were screened using chlorophyll fluorescence recorded directly on selection plates under medium light, revealing a large decrease in PSII yield after 3-minutes illumination (as in Figure 1C) in ~5% of the clones in two replicate CRISPR-Cas9 transformations (Suppl. Figure S5B, left panel). To analyze the profile of mutations obtained in our approach, the regions flanking the CRISPR-Cas9 cutting site in *ATPG* were amplified in 31 putative *atpG* clones by PCR using several pairs of primers and sequenced (Suppl. Figure S5-S6-S7). Altogether, the presence of homologous regions in the co-transformation cassette ("Hygro_HR", 21 clones analyzed) allowed repair of Cas9 cut by recombination at 23 of the 42 borders; this approach notably yielded 8 mutants recombinated as expected, proving relative accuracy for knock-in (~38% of selected clones). In contrast, in the absence of homologous regions in the co-transformation cassette ("Hygro", 10 clones analyzed), it inserted in *ATPG* in only 4 mutants and small indels appeared more often in the CRISPR site ("Hygro": 3 mutants out of 10 analyzed, "Hygro_HR": 2 out of 21), suggesting that absence of HR may be very suitable to generate point mutations by imperfect NHEJ (~30% of selected clones).

All *atpG* mutants obtained by CRISPR-Cas9 approach were unable to grow on minimal media (Figure 4C), similarly to ATP synthase knock-out mutants (e.g. *ΔatpH*, *ΔatpE*, …), while *atpG-kd* could grow slightly. In immunoblot analyses of these mutants (Suppl. Figure S5H), no ATPG was detected and the level of AtpB was generally decreased to ~1/10th of the WT level. Moreover, the decay of proton gradient measured by ECS was much longer in the *atpG* mutants tested (Suppl. Figure S5I) than in the WT, similar to ATP synthase knock-out mutants rather than *atpG-kd* (*E236*) (see Figure 1 D).

Altogether, this finally demonstrates that ATPG is required for the assembly and function of chloroplast ATP synthase and ultimately for phototrophic growth, as is the other peripheral stalk subunit AtpF (Lemaire & Wollman, 1989b).

Impact of the MDE1 factor on the accumulation of *atpE* mRNA

We first observed that the accumulation of *atpA*, *atpB*, *atpH* and *atpI* transcripts in the mutants *E236*, *E271*, *F28N* and *F292* were similar to that in the WT (Suppl. Figure S8). This was also true for accumulation of *atpE* transcript in the WT and in the *Fud17* mutant strain that carries a single base deletion in the *atpE* CDS (Robertson et al., 1990) (Figure 5A). The *atpE* transcript, however was absent in the three *F28N, CAL014.01.30* and *E271* strains mutated in Cre08.g358530 identifying this protein as the *MDE1* stabilization factor for *atpE* mRNA. To further demonstrate this, we constructed a chimeric construct "*aAdE*" (Figure 5B) with the *atpE* CDS fused to the 5'UTR of the photosystem I gene *psaA*. When transformed into *mde1-1* and WT strains (control), the *aAdE* chimera replaced the endogenous *atpE* gene and restored the accumulation of *atpE* transcript (Figure 5A), at a lower size because the 5'UTR of *psaA* is shorter than that of *atpE*. This construct sustained phototrophic growth and linear electron flow (Figure 5A (bottom panels) and 5C, transformants C1 and C2 in *mde1-1* background; Suppl. Figure S9, transformants X1-X4 in *mde1-2* background and transformants #1-#4 in *mde1-3* background). This shows that ATP synthase can be restored in the absence of MDE1 when the 5'end of *atpE* is substituted by another sequence able to stabilize the downstream transcript (here 5'end from *psaA*).

The WT displays a footprint at the 5'end of the *atpE* mRNA which disappears in the *mde1-2* mutant (Cavaiuolo et al., 2017), suggesting that binding of MDE1 at this site prevents degradation of the transcript by 5'-3' exonucleases. To explore to which extent the recruitment of MDE1 on the *atpE* 5'UTR may be conserved, we analyzed the region upstream of *atpE* in representative Chlorophytes species (Figure 6A-B). The *atpE* gene is

ancestrally encoded downstream of *atpB* in the green lineage, notably in the core Chlorophyta species *U. mutabilis* and *Tetraselmis sp CCMP 881*, but it located downstream of *rps7* in most Chlorophyceae (Figure 6A, left panel). However, using motif discovery tool MEME, we found that similarity in the *atpE* 5'UTRs is mostly limited to few regions in *C. reinhardtii*, *C. incerta* and *C. schloesseri* on the one hand (blue boxes), and between *V. carteri*, *G. pectorale* and *Y. unicoca* on the other hand (orange box). Nevertheless, the MDE1 footprint found in *C. reinhardtii* (Cavaiuolo et al., 2017) corresponded to the most significant motif detected in several, but not all, Chlorophycean species from the Chlamydomonadales and Sphaeropleales orders (CS), suggesting that this target likely emerged in the ancestor of CS clade (Figure 6A, yellow box, and Figure 6B; Suppl. Figures S5-6). MDE1 orthologs were found in many genomes of the Reinhardtinia clade and in few closely related species (Figure 6A (right panel) and 6C, Suppl. Figure S10; *Gonium pectorale* was excluded from the analysis because of a local gap in the genome assembly). We compared all candidate MDE1 orthologs and detected conserved regions (Figure 6C, Suppl. Figure S10) using MEME (ungapped), GLAM2 (gap allowed) and MAST. At least 12 OPR domains were clearly identified (shown as barrel pairs). Altogether, our analyses suggest that the nuclear factor MDE1 and its specific ~20 bp target sequence upstream of *atpE* were recruited to stabilize *atpE* mRNA in the last common ancestor of Volvocales, estimated ~500 My ago (Del Cortona et al., 2020).

DISCUSSION AND PERSPECTIVES

Chlamydomonas CF_1F_O requirement for peripheral stalk subunits AtpF and ATPG

ATP synthase is the crucial converter of proton gradient potential into actual cell fuel. AtpF and ATPG both form long helices that protrude from the membrane into the stroma and form the peripheral stalk of plastid ATP synthase, derived from the bacterial b_2 homodimer. Both peripheral stalk subunits are encoded in the chloroplast in red algae (Douglas and Penny, 1999) and red algal plastid endosymbionts (Oudot-le Secq et al., 2007), in contrast to the green algae (Gallaher et al., 2018) and land plants (Malik Ghulam

et al., 2012) in which AtpF is encoded in the chloroplast and ATPG in the nucleus. Mutants of all ATP synthase subunits except ATPG were previously obtained in *Chlamydomonas* (Drapier et al., 2007; Finazzi et al., 2009). We first identified from random nuclear mutagenesis an *atpG-kd* mutant (*E236*) with a *TOC1* transposon insertion in the 3'UTR of the nuclear *ATPG* gene. As recombination is rarely homologous in the *Chlamydomonas* nuclear genome, we used CRISPR-Cas9 technology which is a powerful tool for targeted gene modification. We developed a custom CRISPR-Cas9 protocol (see Materials and Methods) to target *ATPG* gene and obtain *atpG-ko* mutants. We show that neither *atpG-ko* nor *atpF-ko* mutants can accumulate CF_1F_o ATP synthase. This requirement of both ATPG and AtpF subunits indicates that neither ATPG nor AtpF homodimers can substitute for the ATPG/AtpF heterodimer peripheral stalk of *Chlamydomonas* chloroplast ATP synthase. These newly available mutants may further be useful for structural investigation of the peripheral stalk. Indeed, recent structural study of chloroplast ATP synthase has introduced that the peripheral stalk may not only be involved in preventing CF_o-driven rotation of CF_1 but may also be animated by elastic conformational changes crucial for the energetic requirements of ATP synthesis cycle (Hahn et al., 2018). Our work opens the door to testing spring properties both by complementation assay with mutated *AtpF* and/or *ATPG*, and *de novo* generation of CRISPR-Cas9 mutants following our approach.

Transmembrane subunits of ATP synthase as thylakoid FTSH protease substrates

The FTSH proteases are embedded in membranes and are important in the removal of damaged, misfolded or misassembled membrane proteins. By considering the fate of unassembled ATP synthase subunits in *ftsh* mutants, several non-assembled ATP F_o subunits could be previously shown to be substrates of FTSH proteases in bacteria and mitochondria. The bacterial ATP synthase subunit *a* (homolog of CF_o subunit AtpI also named IV and of yeast F_o subunit Atp6) is a substrate of the homo-oligomer FtsH in *Escherichia coli* (Akiyama et al., 1996). In yeast mitochondria, the ATP synthase F_o subunits Atp6, Atp8 and Atp9 are substrates of the hetero-oligomer FTSH protease facing

the matrix (*m*-AAA) in *Saccharomyces cerevisiae* (Pajic et al., 1994; Guélin et al., 1996). The recovery of accumulation of CF_o subunit AtpH (also named III, and homolog of bacterial F_o subunit *c* and mitochondrial subunit Atp9) occurred when the thylakoid FTSH protease is inactivated by the *ftsh1-1* mutation in all ATP synthase assembly mutant tested, *atpG-kd*, *atpF* (*Fud18*), and *atpC-1* and *DatpA*, indicating that AtpH is a substrate of FTSH1/2. Our study extends the trans-membrane ATP synthase subunits as substrates of the thylakoid membrane FTSH protease.

Interplay between MDE1 factor and *atpE* mRNA

The coupling between the organelle(s) and the rest of the cell has expectedly been one of the major issues and a driver of evolution in photosynthetic eukaryotes. In *C. reinhardtii*, a recent study demonstrated that a specific 22-bp sequence in the 5'UTR of *atpE* chloroplast gene is protected by the MDE1 nuclear factor, required for atpE gene expression by preventing the degradation of its transcripts (Cavaiuolo et al., 2017). Neither the affected gene nor the mutation, however, were identified. Here, among the new mutants obtained, we have found that mutant *F28N* carries a mutation (*mde1-1*) in a gene, Cre08.g358530, that is also mutated in CAL014.01.30 (*mde1-2*) and in mutant *E271* (*mde1-3*), and we have formally established the genetic interaction between *MDE1* and the 5'UTR of *atpE*. Because we found OPR repeats in MDE1 as in numerous chloroplast-targeted RNA-binding factors (Hammani et al., 2014), we suspect that MDE1 may directly bind to the 22-bp target sequence to allow the maturation of *atpE* transcripts. The most likely scenario is the stabilisation of *atpE* mono-cistron against 5'à3' exonucleases, as exemplified for MDA1 with *atpA* (Drapier et al., 2002; Viola et al., 2019), MDB1 with *atpB* (Jarrige, 2019), MTHI1 with *atpH* (Ozawa et al., 2020), MCA1 with *petA* (Loiselay et al., 2008; Boulouis et al., 2011), etc. Further, biochemical approaches could be implemented to verify these assumptions.

Intriguingly, no such trans-acting factors are known for *aptE* among plants and bacteria. In maize, *atpE* is co-transcribed downstream of *atpB* and the absence of the nucleus-encoded factor ATP1 impairs the translation of both proteins but not the stability of *atpB*/*atpE* mRNA (Mc Cormac & Barkan, 1999). In tobacco, *atpE* start codon is located within *atpB* coding sequence but the bicistronic pre-mRNA is matured in distinct *atpB* and *atpE* mRNAs for translation (Kapoor et al., 1994). Notably, replacement of the Shine-Dalgarno (SD)-like sequence GGAG 15-18 bp upstream of *atpE* start site abolishes translation of *atpE* (Hirose & Sugiura, 2004), but replacement of the SD-like sequence (GAAG) found 19-22 bp upstream of *atpE* start site in *C. reinhardtii* is not detrimental for translation (Fargo et al., 1998). Among Chlorophytes, *atpE* gene relocated from downstream of *atpB* to downstream of *rps7* in the ancestor of Chlorophycea, yet our phylogenetic analyzes suggest that recruitment of MDE1 and its target sequence in 5'UTR of *atpE* occurred later. Has this interaction brought a selective advantage and how? Requirement of nucleus-encoded MDE1 for *atpE* expression may be beneficial to synchronizing chloroplast ATP synthase expression with the nuclear agenda, e.g. cell cycle progression, response to changes in energy or nutrient supply. In the diurnal cycle analysis (Strenkert et al., 2019), MDE1 expression level peaks sharply half an hour after light is turned on, as is typical of genes involved in chloroplast gene expression. In other conditions, MDE1 levels could contribute to a regulatory response, in the sense that, for instance, a nutrient deficiency would downregulate MDE1 level, hence shutting down the expression of *atpE*. Our characterization of the OPR protein MDE1 and its mRNA target in the phototroph-facultative model *C. reinhardtii* contributes to the knowledge of the regulation of chloroplast genes by nuclear factors. OPR proteins have tandem helical repeats that bind consecutive nucleotides with a specificity that is largely determined by the identities of amino acids at a few positions, forming an OPR code that will be progressively unraveled in the future.

Chlamydomonas reinhardtii strains, growth conditions and genetic methods

Wild-type T222+ and mutant strains of *Chlamydomonas* were grown at 25 °C in Tris-acetate-phosphate (TAP) medium, pH 7.2 or, when indicated, in minimal medium lacking acetate, pH 7.2 (Harris, 1988), under continuous low light (5 to 10 µmol photon m^{-2} s^{-1}; white light-emitting diode) unless otherwise specified. Crosses, tetrad dissection and random progeny analysis were performed according to Harris (1988). The deletion strains *ΔatpA*, *ΔatpH*, *ΔatpI,* as well as the chloroplast *atpF-Fud18* and *atpE-Fud17* mutants have been previously described (Ozawa et al., 2020; Drapier et al., 2007; Lemaire and Wollman, 1989b, Robertson et al., 1990). The nuclear *mdb1*, *mda1* and *mrl1* mutants impair *atpE*, *atpB* and *rbcL* mRNA accumulation, respectively (Drapier et al., 1992; Viola et al., 2019; Johnson et al., 2010), while the *atpC1* mutant lacks expression of the *ATPC* gene encoding the CF_1 subunit γ (Smart & Selman, 1991; Smart & Selman, 1993). The nuclear mutant *ftsh1-1* expresses an inactive thylakoid FTSH protease (Malnoë et al., 2014). Except if specified otherwise, light levels are the following: low light: 5 µmol photon m^{-2} s^{-1}, moderate light: 25 µmol photon m^{-2} s^{-1}, high light: 200 µmol photon m^{-2} s^{-1}.

Generation of ATP synthase mutants

The *F292*, *F28N*, *E236* and *E271* mutants were generated in an effort to target and knock-out *FTSH2* and *EGY1* loci by CRISPR approach. We electroporated the hygromycin resistance cassette in the presence of the Cas9 enzyme and RNA guides as described (Findinier et al., 2019). Mutants were plated on selective medium (TAP hygromycin 20 mg L^{-1}); colonies were then transferred to fresh TAP medium and grown mixotrophically in low light (5-10 µM photon m^{-2} s^{-1}) for 7 days before chlorophyll fluorescence analysis and photo-inhibitory treatment (1 h at 1000 µmol photon m^{-2} s^{-1}). Accumulation level of the thylakoid FTSH protease subunits FTSH1 and FTSH2, detected by Western blot using anti-Var2 antibody (Suppl. Figure 11), and PCR amplification of the *EGY1* targeted

region were similar in mutants and WT strain, indicating *FTSH2* and *EGY1* loci were not knocked out in the *F292*, *F28N*, *E236* and *E271* mutants.

Nucleic Acid Manipulations: DNA and Constructs

Standard nucleic acid manipulations were performed according to Sambrook et al. (1989). The primers used in this study are listed in the Supplemental Table ST4. All DNA constructs were sequenced before transformation in Chlamydomonas and introduced by biolistic transformation.

Construction of the chimeric *5'psaA-atpE* gene.

Plasmid P50 contains the 19.7 kbp Bam12 restriction fragment (Rochaix, 1978) cloned in the PUC8 vector, in an orientation that places the *psbA* gene close to the *Sma*I site of the PUC8 multiple cloning site. P50 was digested by *Hpa*I and religated on itself to generate P50-H, which in turn was digested by *Sal*I and *Eco*RV, blunted with Klenow and religated on itself to yield p50-HSE. This latter plasmid was then digested with *Bam*HI and *Hpa*I, blunted with Klenow and religated again on itself to create the p50Sh plasmid.

The chimeric 5'*psaA-atpE* gene was then generated by a two-step megaprime PCR procedure (Higuchi, 1990): primers psaA5U_F and psaAatpE_R were used to amplify a 262 bp fragment from template plasmid ps1A1 (Kück et al., 1987), while primers psaAatpE_F and atpE_PstI_R generated a 454 bp amplicon from template plasmid p50Sh. These two partially overlapping amplicons were mixed and used as templates in a third PCR reaction with the external primers psaA5U_F and atpE_PstI_R. The final amplicon (676 bp) was then digested with *Cla*I, blunted with Klenow and phenol-extracted, then digested with *Btg*I and cloned into the p50Sh vector digested by *Btg*I and *Bsa*BI to yield paAdE. The recycling 5'*psaA-aadA*$_{Exc}$ cassette, excised from plasmid p5'aA-aadA485 (Boulouis et al., 2015) by digestion with AleI and XhoI, and blunted with Klenow, was cloned into plasmid paAdE, digested by *Avr*II and blunted with Klenow, in reverse orientation with respect to *atpE*, to yield plasmid pK^{r}aAdE.

Deletion of the atpB gene.

Plasmid P-112, obtained from the Chlamydomonas Genetic Center (www.biology.duke.edu/chlamy/), contains a 5.3 kbp BamHI-EcoRI fragment from the chloroplast genome encompassing the *atpB* gene (Woessner et al., 1986), subcloned into pUC8 vector. The recycling 5'*psaA-aadA*$_{Exc}$ cassette, excised from plasmid p5'aA-aadA485 by digestion with *Ale*I and *Xho*I, and blunted with Klenow was cloned into plasmid P-112, digested with *Eco*RV and *Cla*I, itself blunted with Klenow, in direct orientation with respect to *atpB*.

Chlorophyll fluorescence analysis

We set a fast screening procedure by chlorophyll fluorescence imaging on plates with a time-resolved wide-angle camera (Johnson et al., 2009) to measure the ability to maintain PSII function upon short photo-inhibitory treatment. About 2000 random transformants were transferred to fresh TAP plates and grown for one week in permissive conditions (5 µmol photon m^{-2} s^{-1}). As a control of how thylakoid FTSH protease defect impacts fluorescence yields, we introduced the *ftsh1-1* mutant and the complemented C17strain *ftsh1-1*::pSL18-FTSH1 (Malnoë et al., 2014) as well as the untransformed WT. Using the method of weak detection pulses and saturating flash (Baker 2008), we measured on each plate (i) the basal fluorescence F_0 and the maximal fluorescence F_M in the so-called dark-adapted state, as well as (ii) transient fluorescence F' and maximal fluorescence F_M' after 5 seconds low light. The ratio F_V/F_M, where $F_V=F_M-F_0$, is the so-called maximum PSII yield and depends almost solely on PSII function (*e.g.* PSII deficient mutants show F_V/F_M close to 0); in contrast, the PSII (operating) yield Y(II), defined as $(F_M'-F')/F_M'$, decreases when photosynthetic electron flow is limited (*e.g.* PSI deficient mutants show F_V/F_M similar to WT but Y(II) close to 0 even under low light). Figure 1A exemplifies our screening procedure with F_V/F_M pictures of the plate where the mutant *E236* was isolated. Under the permissive conditions of growth (left panel: TAP, low light), the *ftsh1-1* mutant shows F_V/F_M and Y(II) (not shown) similar to WT (≈0,65). We hence discarded clones with F_V/F_M or Y(II) close to 0 under these permissive conditions

to focus on "*ftsh1-1*-like" phenotypes. To trigger the processes of damage and repair, the photo-inhibitory treatment then consisted in an exposure to 1000 µmol photon m^{-2} s^{-1} for 1 h. This resulted in a drastic decrease of F_V/F_M in *ftsh1-1* (≈0,05) mutant as compared to the moderate decrease in WT, C17 and most of the plated strains (≈0,30) (Figure 1A, right panel), as expected due to the central role of FTSH protease in PSII repair (Malnoë et al., 2014) and allowed us to identify ≈20 photosensitive clones altered in the maintenance of photosynthesis, such as the mutant *E236* (Figure 1A, white circle).

Genomics

For each strain, we ordered an Illumina sequencing technology-based NGSelect DNA data package (Eurofins, Germany), comprising the generation of a standard genomic library (DNA fragmentation, adapter ligation, size selection and amplification) and a data package of >5 million pair reads (2x151bp). From these raw data, we generated genomic sequences using open-source platform Galaxy (usegalaxy.org) as follows. Paired-end reads raw data were converted to fastq format using FASTQ groomer and their quality were confirmed using FASTQC (maximum quality scores were well maintained all over the 151bp, not shown). The genome sequences were reconstructed using the published workflow "SNP calling on paired end data" for the mapping of the paired reads against a reference *C. reinhardtii* genome sequence (that of our WT strain T222+ was generated as described in (Gallaher et al., 2015)). We visualized the genomes using IGV (software.broadinstitute.org).

The CAL014.01.30 mutant was backcrossed to the S1D2 strain and the ATP synthase-deficient and wild-type progeny were separately pooled and each pool was sequenced. Reads were aligned onto the reference genome as above. Coverage of structural variants in the two pools of progeny was calculated across a 10kb window (dots) and averaged with a sliding 100kb window (curve) using Freebayes (Garrison & Marth, 2012), version 1.2.0, default except --pooled-discrete --ploidy 2).

Protein isolation and immunoblot analysis

Thylakoid membranes were isolated as described (Chua & Bennoun, 1975). Before electrophoresis, proteins from whole cells or from thylakoid membranes were resuspended in 200 mM 1,4-DTT and 200 mM Na_2CO_3 and solubilized in the presence of 2% SDS at 100°C for 50 s. Cell or thylakoid extracts were loaded on equal chlorophyll basis, separated by SDS-PAGE and electro-transferred onto nitrocellulose membranes (Amersham Protran 0.1 µm NC) by semi-dry method. After semi-dry transfer, membranes were stained in Ponceau (loading control). Protein were immunodetected by enhanced chemiluminescence. The blot membranes were incubated separately in primary antibodies against: AtpA (Drapier et al., 1992), AtpB (that recognizes CF_1 β and F_1 β; Atteia et al., 1992), ATPC (Agrisera AS08312), AtpE (Agrisera AS101590), ATPG (Agrisera AS09457), AtpH (Agrisera AS09591), cytochrome *f* and subunit IV of cytochrome b_6f (Kuras & Wollman, 1994), *Arabidopsis* FtsH2 named Var2 (Qi et al., 2016) that recognizes FTSH1 and FTSH2 in *Chlamydomonas* (Wang et al., 2017). Primary antibodies were revealed by horseradish peroxidase-conjugated antibodies against rabbit IgG (n° W401B, Promega). Heme *f* peroxidase activity was detected on blot membranes by chemiluminescence.

RNA isolation and analysis

Total RNAs were extracted in phenol-chloroform, separated by electrophoresis on agarose gels, transferred to membrane by capillarity and UV-crosslinked. RNA gel-blot analysis for Figure 5A were performed as described previously (Drapier et al., 2002) with ^{33}P-labeled probes derived from CDSs (Eberhard et al., 2002). For Northern blots of Supplemental Figure S8, probes were produced by PCR in the presence of digoxigenin-dUTP and thereby digoxigenin-labelled. After hybridization, the membrane was incubated in the presence of anti-digoxigenin antibody containing Fab fragment conjugated to alkaline phosphatase and revealed by chemiluminescence in the presence of CDP-Star reagent (Roche). Signals were acquired in a ChemiTouch imaging system (Bio-Rad).

CRISPR-Cas9 targeted gene knockouts

A custom protocol for generation of targeted gene knockouts was set up, drawing on multiple previous studies and aiming to promote insertion at the CRISPR-Cas9 cut site of a co-transformed Hygromycin resistance cassette (Berthold et al., 2002) as a selection marker, carrying homology flanks to promote insertion at the target locus *ATPG*. Guide RNAs were designed to cut within the first exon of the target gene. Using CRISPOR-TEFOR predictor (http://crispor.tefor.net), the cutting site was chosen based on highest MIT Specificity score and lowest off-target likelihood including mismatch (Concordet & Hauessler, 2018). Per reaction, 5µg (30pmol) recombinant Cas9, 0.25µg *tracr* and 0.5µg *cr* RNAs (all from Sigma Aldrich, respectively: CAS9PROT-250UG, TRACRRNAMOD-5NMOL and SygRNA (ATPG_288nt: 5'-AAGACCUGGUUCACCCCCGU, 5nmol, modified)), giving a combined total of 0.75 µg *sg*RNA, were mixed to reconstitute the RNP complex by incubation at 37 °C for 30 minutes just before the transformation (similar to Picariello et al., 2020; Dhokane et al., 2020; Shamoto et al., 2018; Findinier et al., 2019). The Hygromycin resistance cassette was generated by PCR-amplification from plasmid *pSLHyg* by using dual-part primers (oZX119 and oZX120) containing on their 5' side 40 nucleotides homologous to the *ATPG* regions flanking the predicted Cas9 cut site ("Hygro_HR" construct). As a control, the same cassette was PCR-amplified without homology arms ("Hygro" construct, primers: oZX_062 and oZX_063). In each case, 250 ng of PCR-purified product were used per transformation reaction. Because such a cassette generally integrates randomly in the genome, we tried to enhance homologous recombination by growing the cells under a light-dark cycle (Picariello et al., 2020) of 14 h at 100 µmol photons m^{-2} s^{-1} at 25 °C versus 10 h in darkness at 18 °C (Greiner et al., 2017) in 100 ml TAP liquid culture to late exponential phase (≥4 million cells ml^{-1}), timing the transformation to fall within a 1 h window prior to subjective dusk (Angstenberger et al., 2020). We chose to use a cell-wall deficient strain (*cw15*), as removal of the cell wall had been shown to increase efficiency (Picariello et al., 2020), although efficient CRISPR/Cas9 editing has been reported in the absence of autolysin (Dhokane et al., 2020). ≥100 million cells per transformation reaction (compared to 50 million cells

(Findinier et al., 2019; Picariello et al., 2020) and 500 million cells (Dhokane et al., 2020)) were harvested by centrifugation (10 minutes, 1100 g, slow break) and resuspended in 250 µl TS40 (40 mM Sucrose in TAP), the transformation buffer used by a number of prior studies (Baek et al., 2016; Kim et al., 2020; Findinier et al., 2019; Park et al., 2020). To increase gene editing, cells were subjected to a 40 °C heat shock for 30 minutes (Greiner et al., 2017; Picariello et al., 2020; Park et al., 2020). Cells, RNP and DNA were mixed in a 4 mm electroporation cuvette and incubated on ice (Shin et al., 2016; Findinier et al., 2019; Dhokane et al., 2020; Angstenberger et al., 2020) for 5 minutes. As a control, one batch of cells was transformed in the presence of the "Hygro_HR" DNA but in absence of the RNP. To make sense of the widely varying electroporation parameters published previously, we calculated an estimate of field strength by multiplying Voltage with distance across the cuvette, and an estimate of pulse length by multiplying capacitance and resistance. An underlying consistency was revealed, with most authors using an estimated field strength between 1.5-2 kV cm^{-1} and a rough pulse length estimate of 10-15 F Ω^{-1} (Picariello et al., 2020; Shamoto et al., 2018; Findinier et al., 2019; Kim et al. , 2020; Ferenczi et al., 2017; Angstenberger et al., 2020; Shin et al., 2016). A notable exception was the use of 2.5 kV cm^{-1} and 40 F Ω^{-1} in (Dhokane et al., 2020), suggesting walled cells may be used in combination with these stronger electroporation parameters. We chose to use 1.8 kV cm^{-1} and 15 F Ω^{-1}, consistent with the two prior studies available at the time reporting the highest CRISPR-Cas9 efficiencies in wall-less cells (Findinier et al., 2019; Shamoto et al., 2018), which translates to 700 V, 50 µF and 300 Ω in our electroporation system (BioRad Gene Pulser II). Cells were subsequently transferred to 10 ml TS40 in 50 ml Falcon tubes and incubated in constant darkness (to avoid counterseleting ATP-synthase mutants) over two nights (~42 h) in the diurnal incubator (to minimize stress).

Using primers from either side of the *ATPG* gene (oZX278 and oFC584), three distinct classes of mutants could be seen. Firstly, a fragment with length similar to WT (632bp) could be amplified in 10 mutants. The second class of mutants revealed inser-

tions of at least 2.4kb, consistent with hygromycin cassette insertion. A third class consisted of a few clones that yielded no products, suggesting distinct rearrangements at *ATPG* locus. When sequencing the first class that generated WT-length fragments, four mutants carried 1-4 bp deletions in the CRISPR site (or insertion in clone 183), which should result in early stop codons and therefore truncations of the extra-membrane part of the ATPG protein. Moreover, three mutants contained DNA from various regions of the genome. As expected, the mutations are compatible with Cas9 cleavage 1-4 nucleotides upstream the PAM site (here CGG) and erroneous repair via non-homologous-end-joining (NHEJ). Note that because of our fluorescence screening, we only recovered colonies where NHEJ introduced mutations, while it probably repaired the cleaved site perfectly in many other cells. In the second class of mutants where insertion of the co-transformation cassette was suspected, we used one primer in *ATPG* and the other in the cassette to amplify and sequence the left and right regions flanking the CRISPR site. Out of the 21 analyzed clones obtained with Hygro_HR co-transformation, 8 clones transitioned from *ATPG* to the Hygro-HR cassette through the homologous regions (underlined) on both sides, exactly as expected for the repair of the CRISPR-Cas9 cut by homologous recombination. Seven other clones exhibited “clean” homologous recombination only on one of the borders, while diverse other re-arrangements occurred at the other border and in both borders of the remaining clones. We observed duplicate homologous regions without full removal of the CRISPR site (green), partial deletion of the cassette extremity, and/or integration of unrelated genomic sequences (red), suggesting NHEJ repair events involving random DNA, among which Hygro or Hygro_HR cassettes.

ACKNOWLEDGEMENTS

We thank Marion Hamon and Christophe Marchand (IBPC, Paris) for the proteomics, Matthieu Mustas and Hugo Zalzalé for help respectively with chloroplast transformation and Northern analysis. We are grateful to Justin Findinier for his detailed protocol for CRISPR-Cas9 mediated mutagenesis, to Stephan Eberhard for insightful discussions, to Cheng Xie and Richard Jumar for explaining the physics of electroporators, and to Fei Yu for antibody against *Arabidopsis* FtsH2. This work was supported by the Centre national de la Recherche Scientifique and Sorbonne Université (basic support to Unité Mixte de Recherche 7141), by the 'Initiative d'Excellence' program from the French State (Grant 'DYNAMO', ANR-11-LABX-0011-01) and by a Paris-Saclay PhD fellowship. The PhD of Marcio Rodrigues-Azevedo is supported by a Ministry's doctoral contract and registered to the Doctoral School of Plant Sciences (SEVE) – ED567 Université Paris-Saclay.

Akiyama, Y., Kihara, A. & Ito, K. (1996) Subunit a of proton ATPase F0 sector is a substrate of the FtsH protease in *Escherichia coli*. *FEBS Lett.* 399, 26-28. doi: 10.1016/s0014-5793(96)01283-5.

Angstenberger, M., de Signori, F., Vecchi, V., Dall'Osto, L. & Bassi, R. (2020) Cell synchronization enhances nuclear transformation and genome editing via Cas9 enabling homologous recombination in Chlamydomonas reinhardtii. ACS Synth. Biol. 9,2840-2850. doi: 10.1021/acssynbio.0c00390.

Atteia, A., de Vitry, C., Pierre, Y. & Popot, J.L. (1992) Identification of mitochondrial proteins in membrane preparations from Chlamydomonas reinhardtii. *J. Biol. Chem.* 267, 226–234. PMID: 1309733

Baek, K., Kim, D.H., Jeong, J., Sim, S.J., Melis, A., et al. (2016) DNA-free two-gene knockout in Chlamydomonas reinhardtii via CRISPR-Cas9 ribonucleoproteins. Sci. Rep. 6, 30620. doi.org/10.1038/srep30620 PMID: 27466170

Bailleul, B., Cardol, P., Breyton, C. & Finazzi, G. (2010) Electrochromism: a useful probe to study algal photosynthesis. *Photosynth. Res.* 106, 179-189. doi: 10.1007/s11120-010-9579-z.

Baker N.R. (2008) Chlorophyll fluorescence: a probe of photosynthesis in vivo. Annu. Rev. Plant Biol. 59, 89-113. doi: 10.1146/annurev.arplant.59.032607.092759.

Barkan, A., Rojas, M., Fujii, S., Yap, A., Chong, Y.S., Bond, C.S. & Small, I. (2012) A combinatorial amino acid code for RNA recognition by pentatricopeptide repeat proteins. *PLoS Genet.* 8, e1002910. doi: 10.1371/journal.pgen.1002910.

Bennoun, P. and Chua, N.H. (1976) Methods for the detection and characterization of photosynthetic mutants in Chlamydomonas reinhardtii. pp. 33-39. In: *Genetics and Biogenesis of Chloroplasts and Mitochondria*. Edited by Th. Buchner. Elsevier/North-Holland Biomedical Press.

Bennoun, P., Masson, A. & Delosme, M. (1980) A method for complementation analysis of nuclear and chloroplast mutants of photosynthesis in chlamydomonas. *Genetics* 95, 39-47. doi: 10.1093/genetics/95.1.39. PMID: 17249035; PMCID: PMC1214220.

Berthold, P., Schmitt, R. & Mages, W. (2002) An engineered Streptomyces hygroscopicus aph 7" gene mediates dominant resistance against hygromycin B in Chlamydomonas reinhardtii. *Protist.* 153, 401-412. doi: 10.1078/14344610260450136. PMID: 12627869

Boulouis, A., Drapier, D., Razafimanantsoa, H., Wostrikoff, K., Tourasse, N.J., Pascal, K., Girard-Bascou, J., Vallon, O., Wollman, F.-A. & Choquet, Y. (2015) Spontaneous dominant mutations in chlamydomonas highlight ongoing evolution by gene diversification. *Plant Cell* 27, 984–1001. doi: 10.1105/tpc.15.00010

Boulouis, A., Raynaud, C., Bujaldon, S., Aznar, A., Wollman, F.-A. & Choquet, Y. (2011) The nucleus-encoded trans-acting factor MCA1 plays a critical role in the regulation of cytochrome f synthesis in Chlamydomonas chloroplasts. *Plant Cell* 23, 333–349. doi: 10.1105/tpc.110.078170

Bujaldon, S., Kodama, N., Rappaport, F., Subramanyam, R., de Vitry, C., Takahashi, Y. & Wollman, F.-A. (2017) Functional accumulation of antenna proteins in chlorophyll b-less mutants of Chlamydomonas reinhardtii. *Plant Mol. Biol.* 10, 115-130. doi: 10.1016/j.molp.2016.10.001.

Cavaiuolo, M., Kuras, R., Wollman, F.-A., Choquet, Y. & Vallon, O. (2017) Small RNA profiling in Chlamydomonas: Insights into chloroplast RNA metabolism. *Nucleic Acids Res.* 45, 10783–10799. doi: 10.1093/nar/gkx668

Cingolani, P., Platts, A., Wang, L.L., Coon, M., Nguyen, T., Wang, L., Land, S.J., Ruden, D.M., Lu, X. (2012) A program for annotating and predicting the effects of single nucleotide polymorphisms, SnpEff: SNPs in the genome of Drosophila *melanogaster* strain w^{1118}; *iso-2*; *iso-3*. Fly 2012 Apr-Jun;6(2):80-92. PMID: 22728672

Choquet, Y. and Wollman, F.-A. (2022) The assembly of photosynthetic proteins. In *The Chlamydomonas Sourcebook: Introduction to Chlamydomonas and Its Laboratory Use* (Grossman, A. R. and Wollman, F.-A., eds.), Organellar and Metabolic Processes, vol. 2, Elsevier, Amsterdam, 3rd edition. Hardcover ISBN: 9780128214305.

Chua, N.H. and Bennoun, P. (1975) Thylakoid membrane polypeptides of Chlamydomonas reinhardtii: wild-type and mutant strains deficient in photosystem II reaction center. *Proc. Natl. Acad. Sci. U. S. A.* 72, 2175-2179. doi: 10.1073/pnas.72.6.2175.

Concordet, J.-P. and Haeussler, M. (2018) CRISPOR: intuitive guide selection for CRISPR/Cas9 genome editing experiments and screens. *Nucleic Acids Res.* 46, W242-W245. doi: 10.1093/nar/gky354.

Craig, R.J., Hasan, A.R., Ness, R.W. & Keightley, P.D. (2021) Comparative genomics of Chlamydomonas. Plant Cell 33, 1016-1041. doi: 101093/plcell/koab026

Day, A., Rochaix, J.-D. (1991) A transposon with an unusual LTR arrangement from Chlamydomonas reinhardtii contains an internal tandem array of 76 bp repeats. *Nucleic Acids Res.* 19, 1259-1266. doi: 10.1093/nar/19.6.1259.

De Mia, M., Lemaire, S.D., Choquet, Y. & Wollman, F.-A. (2019) Nitric oxide remodels the photosynthetic apparatus upon S-starvation in Chlamydomonas reinhardtii. *Plant Physiol.* 179, 718-731. doi: 10.1104/pp.18.01164.

Del Cortona, A., Jackson, C.J., Bucchini, F., Van Bel, M., D'hondt, S., Škaloud, P., Delwiche, C.F., Knoll, A.H., Raven, J.A., Verbruggen, H., Vandepoele, K., De Clerck, O. & Leliaert, F. (2020) Neoproterozoic origin and multiple transitions to macroscopic growth in green seaweeds. *Proc. Natl. Acad. Sci. U. S. A.* 117, 2551-2559. doi: 10.1073/pnas.1910060117.

Dhokane, D., Bhadra, B. & Dasgupta, S. (2020) CRISPR based targeted genome editing of Chlamydomonas reinhardtii using programmed Cas9-gRNA ribonucleoprotein. *Mol. Biol. Rep.* 47, 8747-8755. doi: 10.1007/s11033-020-05922-5.

Douglas, S.E. and Penny, S.L. (1999) The plastid genome of the cryptophyte alga, Guillardia theta: complete sequence and conserved syntheny groups confirm its common ancestry with red algae. *J. Mol. Evol.* 48, 238-244. doi: 10.1007/pl00006462.

Drapier, D., Girard-Bascou, J. & Wollman, F.-A. (1992) Evidence for nuclear control of the expression of the atpA and atpB chloroplast genes in Chlamydomonas. *Plant Cell* 4, 283–295. doi: 10.1105/tpc.4.3.283.

Drapier, D., Girard-Bascou, J., Stern, D.B. & Wollman, F.-A. (2002) A dominant nuclear mutation in Chlamydomonas identifies a factor controlling chloroplast mRNA stability by acting on the coding region of the atpA transcript. *Plant J.* 31, 687–697. doi: 10.1046/j.1365-313x.2002.01387.x.

Drapier, D., Rimbault, B., Vallon, O., Wollman, F.-A. & Choquet, Y. (2007) Intertwined translational regulations set uneven stoichiometry of chloroplast ATP synthase subunits. *EMBO J.* 26, 3581–3591. doi: 10.1038/sj.emboj.7601802

Dent, R.M., Haglund, C.M., Chin, B.L., Kobayashi, M.C. & Niyogi, K.K. (2005). Functional genomics of eukaryotic photosynthesis using insertional mutagenesis of Chlamydomonas reinhardtii. *Plant Physiol.* 137, 545–556. doi: 10.1104/pp.104.055244

Eberhard, S., Drapier, D. & Wollman, F.-A. (2002) Searching limiting steps in the expression of chloroplast-encoded proteins: Relations between gene copy number, transcription, transcript abundance and translation rate in the chloroplast of Chlamydomonas reinhardtii. *Plant J.* 31, 149–160. doi: 10.1046/j.1365-313x.2002.01340.x.

Eberhard, S., Loiselay, C., Drapier, D., Bujaldon, S., Girard-Bascou, J., Kuras, R., Choquet, Y. & Wollman, F.-A. (2011) Dual functions of the nucleus-encoded factor TDA1 in trapping and translation activation of atpA transcripts in Chlamydomonas reinhardtii chloroplasts. *Plant J.* 67, 1055–1066. doi: 10.1111/j.1365-313X.2011.04657.x.

Fargo, D.C., Zhang, M., Gillham, N.W. and Boynton, J.E. (1999) Shine-Dalgarno-like sequences are not required for translation of chloroplast mRNAs in Chlamydomonas reinhardtii chloroplasts or in Escherichia coli. *Mol. Gen. Genet.* 257, 271-282. doi: 10.1007/s004380050648.

Ferenczi, A., Pyott, D.E., Xipnitou, A.& Molnar, A. (2017) Efficient targeted DNA editing and replacement in Chlamydomonas reinhardtii using Cpf1 ribonucleoproteins and single-stranded DNA. Proc Natl Acad Sci U S A 114: 13567–13572. https://doi.org/10.1073/pnas.1710597114 PMID: 29208717

Finazzi, G., Drapier D. & Rappaport, F. (2009) The CF_0F_1 ATP synthase complex of photosynthesis. In *The Chlamydomonas Sourcebook Second Edition. Organella and Metabolic Processes Vol. 2.* (Stern, D., Ed.). Elsevier, Academic Press, pp. 639-670. ISBN 0080919561, 9780080919560

Findinier, J., Delevoye, C. & Cohen M.M. (2019*)* The dynamin-like protein Fzl promotes thylakoid fusion and resistance to light stress in Chlamydomonas reinhardtii. *PLoS Genet.* 15, e1008047. doi: 10.1371/journal.pgen.1008047.

Gallaher, S.D., Fitz-Gibbon, S.T., Strenkert, D., Purvine, S.O., Pellegrini, M. & Merchant, S.S. (2018) High-throughput sequencing of the chloroplast and mitochondrion of Chlamydomonas reinhardtii to generate improved de novo assemblies, analyze expression patterns and transcript speciation, and evaluate diversity among laboratory strains and wild isolates. *Plant J.* 93, 545-565. doi: 10.1111/tpj.13788.

Gallaher, S.D., Fitz-Gibbon, S.T., Glaesener, A.G., Pellegrini, M. & Merchant, S.S. (2015) Chlamydomonas genome resource for laboratory strains reveals a mosaic of sequence variation, identifies true strain histories, and enables strain-specific studies. *Plant Cell* 27, 2335-2352. doi: 10.1105/tpc.15.00508.

Garrido, C., Caspari, O.D., Choquet, Y., Wollman, F.-A. & Lafontaine, I. (2020) Evidence supporting an antimicrobial origin of targeting peptides to endosymbiotic organelles. *Cells* 9, 1795. doi: 10.3390/cells9081795.

Garrison, E. and Marth, G. (2012) Haplotype-based variant detection from short-read sequencing. *arXiv preprint arXiv:1207.3907 [q-bio.GN]*

Greiner, A., Kelterborn, S., Evers, H., Kreimer, G., Sizova, I., et al. (2017) Targeting of Photoreceptor Genes in Chlamydomonas reinhardtii via Zinc-Finger Nucleases and CRISPR/Cas9. *Plant Cell* 29, 2498–2518. https://doi.org/10.1105/tpc.17.00659 PMID: 28978758

Guélin E., Rep, M. & Grivell L.A. (1996) Afg3p, a mitochondrial ATP-dependent metalloprotease, is involved in the degradation of mitochondrially encoded Cox1, Cox3, Cob, Su6, Su8 and Su9 subunits of the inner membrane complexes III, IV and V. *FEBS Lett.* 381, 42–46. doi: 10.1016/0014-5793(96)00074-9.

Hahn, A., Vonck, J., Mills, D.J., Meier, T., Kühlbrandt, W. (2018) Structure, mechanism, and regulation of the chloroplast ATP synthase. *Science* 360, eaat4318. doi: 10.1126/science.aat4318.

Hammani, K., Bonnard, G., Bouchoucha, A., Gobert, A., Pinker, F., Salinas, T. & Giegé, P. (2014) Helical repeats modular proteins are major players for organelle gene expression. *Biochimie* 100, 141–150. doi: 10.1016/j.biochi.2013.08.031.

Harris, E.H. (1989). *The Chlamydomonas Sourcebook: A comprehensive guide to biology and laboratory use.* (San Diego: Academic Press). Elsevier, Academic Press.

von Heijne, G., Steppuhn,J. & Herrmann, R.G. (1989) Domain structure of mitochondrial and chloroplast targeting peptides. *Eur. J. Biochem.* 180, 535–545. doi: 10.1111/j.1432-1033.1989.tb14679.x.

Hirose, T. and Sugiura, M. (2004) Functional Shine-Dalgarno-like sequences for translational initiation of chloroplast mRNAs. *Plant Cell Physiol.* 45, 114-117. doi: 10.1093/pcp/pch002.

Jarrige, D. (2019) Deciphering the "OPR code" to further assess the physiological roles of OPR proteins. PhD Thesis. Sorbonne Université.

Johnson, X. (2011) Manipulating RuBisCO accumulation in the green alga, Chlamydomonas reinhardtii. Plant Mol. Biol. 76, 397-405. doi: 10.1007/s11103-011-9783-z.

Johnson, X., Vandystadt, G., Bujaldon, S., Wollman, F. A., Dubois, R., Roussel, P., Alric, J. & Béal, D. (2009) A new setup for in vivo fluorescence imaging of photosynthetic activity. *Photosynth. Res.* 102, 85-93. doi: 10.1007/s11120-009-9487-2.

Johnson, X., Wostrikoff, K., Finazzi, G., Kuras, R., Schwarz, C., Bujaldon, S., Nickelsen, J., Stern, D.B., Wollman, F.-A. & Vallon, O. (2010) MRL1, a conserved Pentatricopeptide repeat protein, is required for stabilization of rbcL mRNA in Chlamydomonas and Arabidopsis. *Plant Cell* 22, 234–248. doi: 10.1105/tpc.109.066266

Kapoor, S., Wakasugi, T., Deno, H. & Sugiura, M. (1994) An atpE-specific promoter within the coding region of the atpB gene in tobacco chloroplast DNA. *Curr Genet.* 26, 263-268. doi: 10.1007/BF00309558.

Ketchner, S.L., Drapier, D., Olive, J., Gaudriault, S., Girard-Bascou, J. & Wollman, F.-A. (1995) Chloroplasts can accommodate inclusion bodies: Evidence from a mutant of Chlamydomonas reinhardtii defective in the assembly of the chloroplast ATP synthase. *J. Biol. Chem.* 270, 15299-152306. doi: 10.1074/jbc.270.25.15299.

Kim, K.S., Kustu, S. & Inwood, W. (2006) Natural history of transposition in the green alga Chlamydomonas reinhardtii: use of the AMT4 locus as an experimental system. Genetics 173, 2005-2019. doi: 10.1534/genetics.106.058263.

Kim, J., Lee, S., Baek, K. & Jin, E.S. (2020) Site-specific gene knock-out and on-site heterologous gene overexpression in *Chlamydomonas reinhardtii* via a CRISPR-Cas9-mediated knock-in method. *Front. Plant Sci.* 11, 306. doi: 10.3389/fpls.2020.00306.

Kück, U., Choquet, Y., Schneider, M., Dron, M. & Bennoun, P. (1987) Structural and transcription analysis of two homologous genes for the P700 chlorophyll a-apoproteins in Chlamydomonas: Evidence for in vivo trans-splicing. *EMBO J.* 6, 2185–2195. doi: 10.1002/j.1460-2075.1987.tb02489.x.

Kuras, R., and Wollman, F.-A. (1994) The assembly of cytochrome b6/f complexes: An approach using genetic transformation of the green alga Chlamydomonas reinhardtii. *EMBO J.* 13, 1019–1027. doi: 10.1002/j.1460-2075.1994.tb06350.x.

Loiselay, C., Gumpel, N.J., Girard-Bascou, J., Watson, A.T., Purton, S., Wollman, F.-A. & Choquet, Y. (2008) Molecular identification and function of cis- and trans-acting determinants for petA transcript stability in Chlamydomonas reinhardtii chloroplasts. Mol. Cell. Biol. 28, 5529–5542. doi: 10.1128/MCB.02056-07

Majeran, W., Olive, J., Drapier, D., Vallon, O. & Wollman, F.-A. (2001) The light sensitivity of ATP synthase mutants of Chlamydomonas reinhardtii. *Plant Physiol.* 126, 421–433. doi: 10.1104/pp.126.1.421.

Majeran, W., Wostrikoff, K., Wollman, F.-A. & Vallon O. (2019) Role of ClpP in the biogenesis and degradation of RuBisCO and ATP synthase in Chlamydomonas reinhardtii. Plants 8, 191. doi: 10.3390/plants8070191.

Malik Ghulam, M., Zghidi-Abouzid, O., Lambert, E., Lerbs-Mache, S., Merendino, L. (2012) Transcriptional organization of the large and the small ATP synthase operons, atpI/H/F/A and atpB/E, in Arabidopsis thaliana chloroplasts. *Plant Mol. Biol.* 79, 259-272. doi: 10.1007/s11103-012-9910-5.

Malnoë, A., Wang, F., Girard-Bascou, J., Wollman, F. A. & de Vitry, C. (2014) Thylakoid FtsH protease contributes to photosystem II and cytochrome b_6f remodeling in Chlamydomonas reinhardtii under stress conditions. *Plant Cell* **26**, 373-390. doi: 10.1105/tpc.113.120121.

Malnoë, A., Wollman, F. A., de Vitry, C. & Rappaport, F. (2011) Photosynthetic growth despite a broken Q-cycle. *Nat Commun* **2**, 301. doi: 10.1038/ncomms1299.

Mc Cormac, D.J. and Barkan, A. (1999) A nuclear gene in maize required for the translation of the chloroplast atpB/E mRNA. *Plant Cell* 11, 1709-1716. doi: 10.1105/tpc.11.9.1709.

Merchant, S.S., Prochnik, S.E., Vallon, O., Harris, E.H., Karpowicz, S.J., Witman, G.B., et al. (2007) The Chlamydomonas genome reveals the evolution of key animal and plant functions. *Science* 318, 245-250. doi: 10.1126/science.1143609.

Lemaire, C., Wollman F.-A. & Bennoun, P. (1988) Proc. Natl. Acad. Sci. U. S. A. Restoration of phototrophic growth in a mutant of Chlamydomonas reinhardtii in which the chloroplast atpB gene of the ATP synthase has a deletion: an example of mitochondria-dependent photosynthesis. *Proc. Natl. Acad. Sci. U. S. A.* 85, 1344-1348. doi: 10.1073/pnas.85.5.1344.

Lemaire, C., and Wollman, F.-A. (1989a) The chloroplast ATP synthase in Chlamydomonas reinhardtii. I. Characterization of its nine constitutive subunits. *J. Biol. Chem.* 264, 10228–10234. PMID: 2524491

Lemaire, C., and Wollman, F.-A. (1989b) The chloroplast ATP synthase in Chlamydomonas reinhardtii. II. Biochemical studies on its biogenesis using mutants defective in photophosphorylation. *J. Biol. Chem.* 264, 10235–10242. PMID: 2524492

O'Donnell, S., Chaux, F., Fischer, G. (2020) Highly contiguous nanopore genome assembly of Chlamydomonas reinhardtii CC-1690. *Microbiol. Resour. Announc.* 9, e00726-20. doi: 10.1128/MRA.00726-20.

Oudot-le Secq, M.-P., Grimwood, J., Shapiro, H., Armbrust, E.V., Bowler, C. & Green, B.R. (2007) Chloroplast genomes of the diatoms Phaeodactylum tricornutum and Thaliassiosira pseudonana: comparison with other plastid genomes of the red lineage. *Mol. Genet. Genom.* 277, 427-439. doi: 10.1007/s00438-006-0199-4.

Ozawa, S.-I., Cavaiuolo, M., Jarrige, D., Kuras, R., Rutgers, M., Eberhard, S., Drapier, D., Wollman, F.-A. & Choquet, Y. (2020) The OPR Protein MTHI1 Controls the Expression of Two different subunits of ATP Synthase CFo in Chlamydomonas reinhardtii. *Plant Cell* 32, 1179-1203. doi: 10.1105/tpc.19.00770.

Pajic, A., Tauer, R., Feldmann, H., Neupert, W. & Langer, T. (1994) Yta10p is required for the ATP-dependent degradation of polypeptides in the inner membrane of mitochondria. FEBS Lett. 353, 201–206. doi: 10.1016/0014-5793(94)01046-3.

Park, R.V., Asbury, H. & Miller, S.M. (2020) Modification of a *Chlamydomonas reinhardtii* CRISPR/Cas9 transformation protocol for use with widely available electroporation equipment. *MethodsX* 7, 100855. doi: 10.1016/j.mex.2020.100855.

Picariello, T., Hou, Y., Kubo, T., McNeill, N.A., Yanagisawa, H.-A., Oda, T. & Witman, G.B., (2020) TIM, a targeted insertional mutagenesis method utilizing CRISPR/Cas9 in Chlamydomonas reinhardtii. *PLoS One* 15, e0232594. doi: 10.1371/journal.pone.0232594.

Qi, Y., Liu, X., Liang, S., Wang, R., Li, Y., Zhao, J., Shao, J., An, L., & Yu, F. (2016). A putative chloroplast thylakoid metalloprotease VIRESCENT3 regulates chloroplast development in Arabidopsis thaliana. *J. Biol. Chem.* 291, 3319–3332. doi: 10.1074/jbc.M115.681601.

Rochaix, J.-D. (1978) Restriction endonuclease map of the chloroplast DNA of Chlamydomonas reinhardtii. *J. Mol. Biol.* 126, 597-617. doi: 10.1016/0022-2836(78)90011-6.

Robertson, D., Boynton, J.E. & Gillham, N.W. (1990) Cotranscription of the wild-type chloroplast atpE gene encoding CF1/CF0 epsilon subunit with the 3′ half of the rps7 gene in Chlamydomonas reinhardtii and characterization of frameshift mutations in atpE. *Mol. Gen. Genet.* 221, 155-163. doi: 10.1007/BF00261715.

Rühle, T. and Leister, D. (2015) Assembly of F1F0-ATP synthases. *Biochim. Biophys. Acta* 1847, 849-860. doi: 10.1016/j.bbabio.2015.02.005.

Schroda, M., and de Vitry, C. (2022) Molecular chaperones, proteases, and unfolded protein responses. In *The Chlamydomonas Sourcebook: Introduction to Chlamydomonas and Its Laboratory Use* (Grossman, A. R. and Wollman, F.-A., eds.), *Organellar and Metabolic Processes, vol. 2*. Elsevier, Amsterdam, 3rd edition. Hardcover ISBN: 9780128214305.

Shamoto, N., Narita, K., Kubo, T., Oda, T. & Takeda, S. (2018) CFAP70 Is a Novel Axoneme-Binding Protein That Localizes at the Base of the Outer Dynein Arm and Regulates Ciliary Motility. *Cells* 7, 124. doi: 10.3390/cells7090124. PMID: 30158508

Shin, S.E., Lim, J.M., Koh, H.G., Kim, E.K., Kang, N.K, et al. (2016) CRISPR/Cas9-induced knockout and knockin mutations in Chlamydomonas reinhardtii. *Sci Rep* 6, 27810. https://doi.org/10.1038/srep27810 PMID: 27291619

Smart, E.J. and Selman, B.R. (1993) Complementation of a Chlamydomonas reinhardtii mutant defective in the nuclear gene encoding the chloroplast coupling factor 1 (CF1) gamma-subunit (atpC). *J. Bioenerg. Biomembr.* 25, 275-284. doi: 10.1007/BF00762588.

Smart, E.J. and Selman, B.R. (1991) Isolation and characterization of a Chlamydomonas reinhardtii mutant lacking the gamma-subunit of chloroplast coupling factor 1 (CF1). *Mol. Cell Biol.* 11, 5053-5058. doi: 10.1128/mcb.11.10.5053-5058.1991.

Strenkert, D., Schmollinger, S., Gallaher, S.D., Salomé, P.A., Purvine, S.O., Nicora, C.D., Mettler-Altmann, T., Soubeyrand, E., Weber, A.P.M., Lipton, M.S., Basset, G.J. & Merchant, S.S. (2019) Multiomics resolution of molecular events during a day in the life of Chlamydomonas. *Proc. Natl. Acad. Sci. U. S. A.* 116, 2374–2383. doi: 10.1073/pnas.1815238116.

van Wijk, K.J. (2015) Protein maturation and proteolysis in plant plastids, mitochondria and peroxisomes. *Annu. Rev. Plant Biol.* 66, 75-111. doi: 10.1146/annurev-arplant-043014-115547.

Viola, S., Cavaiuolo, M., Drapier, D., Eberhard, S., Vallon, O., Wollman, F.-A. & Choquet, Y. (2019). MDA1, a nucleus encoded factor involved in the stabilization and processing of the atpA transcript in the chloroplast of Chlamydomonas. *Plant J.* 98, 1033–1047. doi: 10.1111/tpj.14300.

Wollman, F.-A. (2016) An antimicrobial origin of transit peptides accounts for early endosymbiotic events, *Traffic*, 17, 1322–1328. doi: 10.1111/tra.12446.

Yan, J., Yao, Y., Hong, S., Yang, Y., Shen, C., Zhang, Q., Zhang, D., Zou, T. & P. Yin, (2019) Delineation of pentatricopeptide repeat codes for target RNA prediction. *Nucleic Acids Res*. 47, 3728–3738. doi: 10.1093/nar/gkz075.

Wang, F., Johnson, X., Cavaiuolo, M., Bohne, A.V., Nickelsen, J. & Vallon, O. (2015) Two Chlamydomonas OPR proteins stabilize chloroplast mRNAs encoding small subunits of photosystem II and cytochrome b6 f. *Plant J*. 82, 861–873. doi: 10.1111/tpj.12858.

Wang, F., Qi, Y., Malnoë, A., Choquet, Y., Wollman, F.-A. & de Vitry, C. (2017) The high light response and redox control of thylakoid protease in Chlamydomonas reinhardtii. *Mol. Plant* 10, 99-114. doi: 10.1016/j.molp.2016.09.012.

Wei, L., Derrien, B., Gautier, A., Houilles-Vernes, L., Boulouis, A., Saint-Marcoux, D., Malnoë, A., et al. (2014) Nitric oxide-triggered remodeling of chloroplast bioenergetics and thylakoid proteins upon nitrogen starvation in Chlamydomonas reinhardtii. Plant Cell 26, 353-372. doi: 10.1105/tpc.113.120121.

Woessner, J.P., Gillham, N.W., Boynton, J.E. (1986) The sequence of the chloroplast atpB gene and its flanking regions in Chlamydomonas reinhardtii. Gene 44, 17-28. doi: 10.1016/0378-1119(86)90038-7.

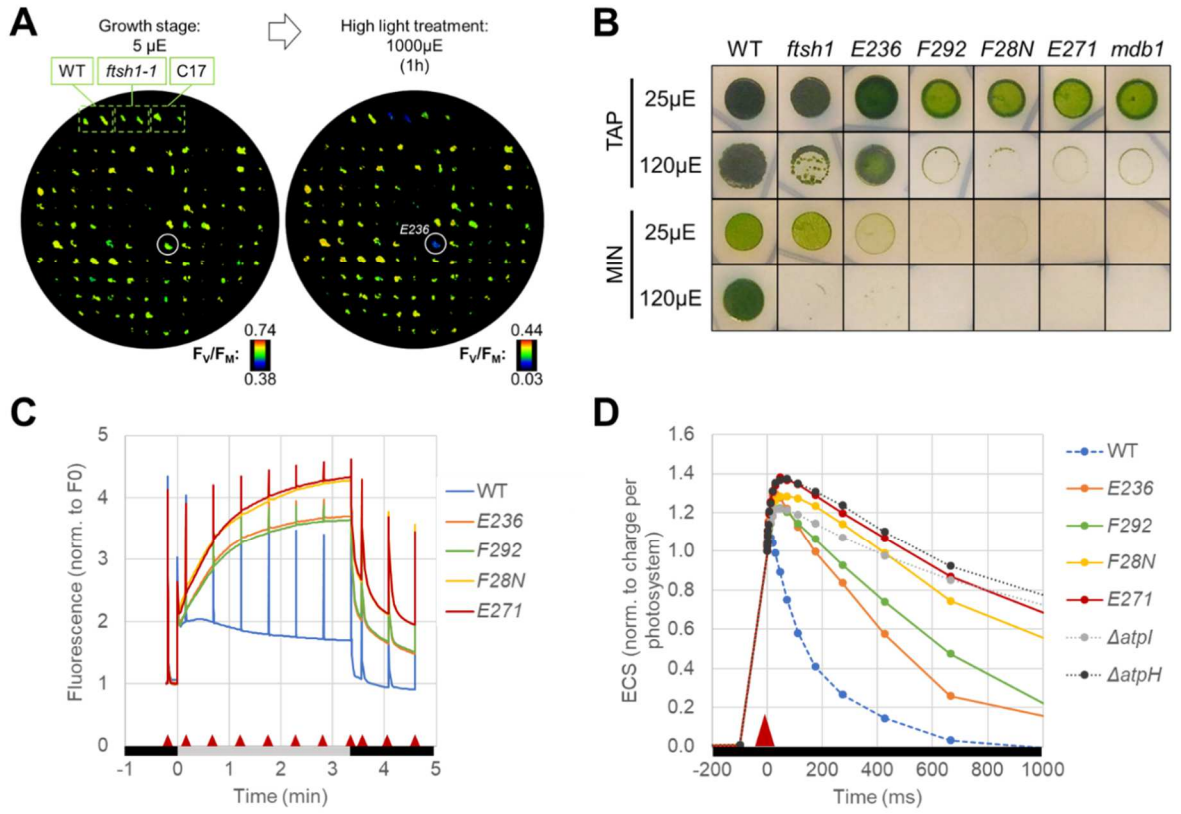

Figure 1. Isolation of chloroplast ATP synthase mutants.

A. After mutagenesis, transformants were grown mixotrophically in low light (5µM photon m^{-2} s^{-1}) for 7 days. Chlorophyll fluorescence analysis was performed before (left) and after (right) a very high light treatment (1h, 1000 µM photon m^{-2} s^{-1}). Shown is the maximum quantum efficiency of PSII photochemistry F_V/F_M for the plate from which the mutant E236 was isolated (white circle). Control strains are the wild-type (WT), ftsh1-1 mutant and complemented C17 strain. B-D. Cells were grown in dim light in TAP flasks. B. Cells were spotted onto plates containing TAP (top panels) and minimal (MIN, bottom panels) and grown for 6 days under moderate light (25 µmol photon m^{-2} s^{-1}, left panels) or high light (120 µmol photon m^{-2} s^{-1}, right panels). Control strain mdb1, ΔatpI and ΔatpI lack ATP synthase (see main text) C. Chlorophyll fluorescence kinetics were monitored in the transition from dark (black box) to moderate light (grey box). Red triangles indicate saturating pulses to estimate the PSII yield. D. Kinetics of electrochromic shift of carotenoids (ECS 520nm) upon single-turnover excitation (signal normalized to one electron.photosystem^{-1}).

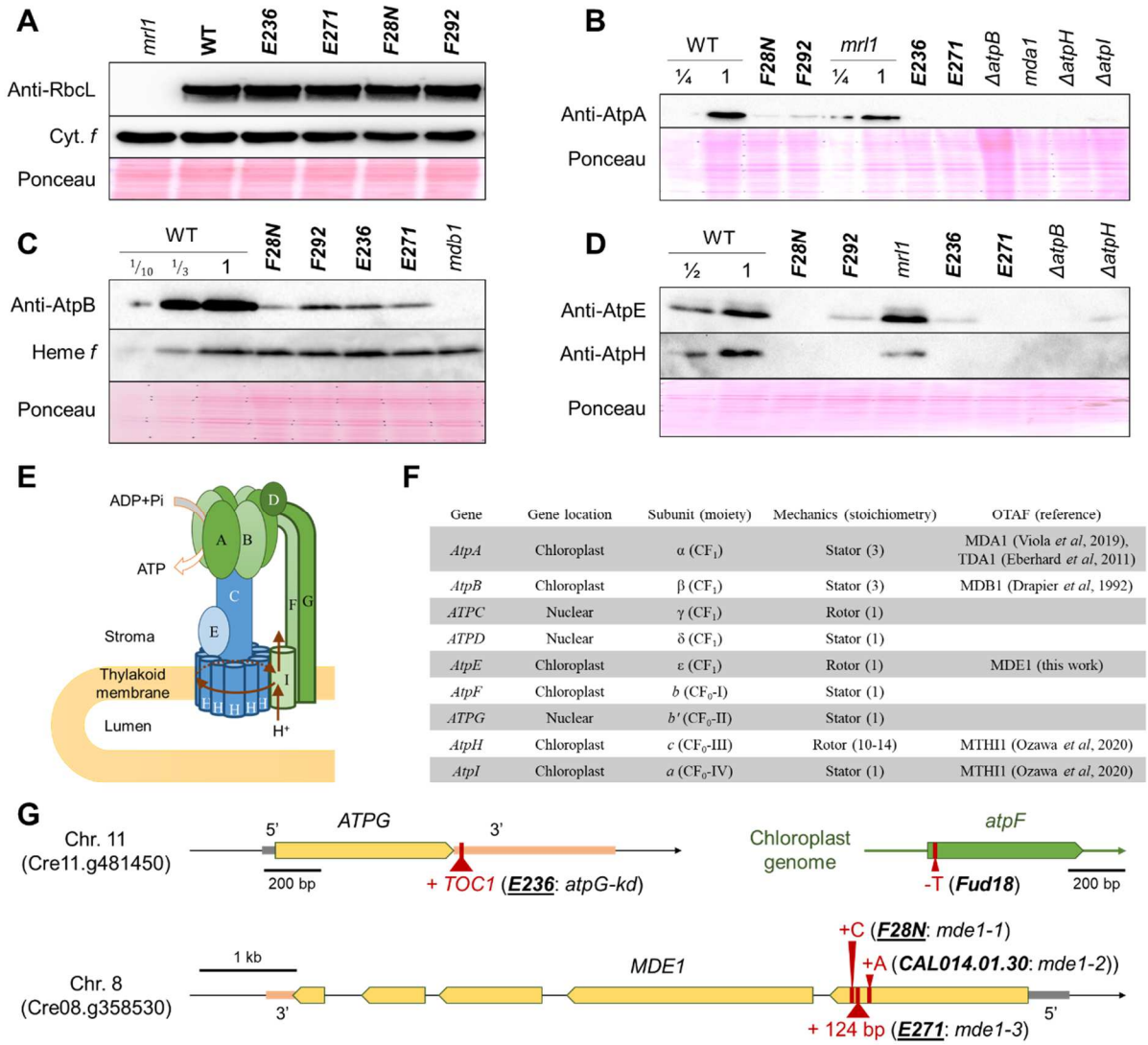

Figure 2. Impairment in accumulation of chloroplast ATP synthase and candidate causal mutations
A-D. Whole-cell proteins were analyzed by immunoblots with the indicated antibodies (RbcL: RuBisCO large subunit; AtpA, AtpB, AtpE, AtpH: ATP synthase subunits). WT was loaded in decreasing amount as indicated by fractions. The deletion strains ΔatpB, ΔatpH, ΔatpI and the nuclear mutants mda1, mdb1 and mrl1 are shown as controls (detailed in main text). Ponceau red staining, heme f and/or Cyt. f provide loading controls. E. Simplified structure/function of chloroplast ATP synthase complex. The rotor and stator subunits are shown in blue and green, respectively. Red arrows represent the flow of protons (H^+). F. Genetic and structural information regarding ATP synthase subunits. G. Diagrams of mutations detected in the mutants (bold) at the indicated loci. Nuclear genes ATPG (top left) and MDE1 (bottom) in yellow arrows (exons), 5'UTR in grey and 3' UTR in orange. Chloroplast-encoded gene atpF in green (CDS). + and - stand for insertions and deletion, respectively, as compared to WT. Mutants obtained in this work are underlined.

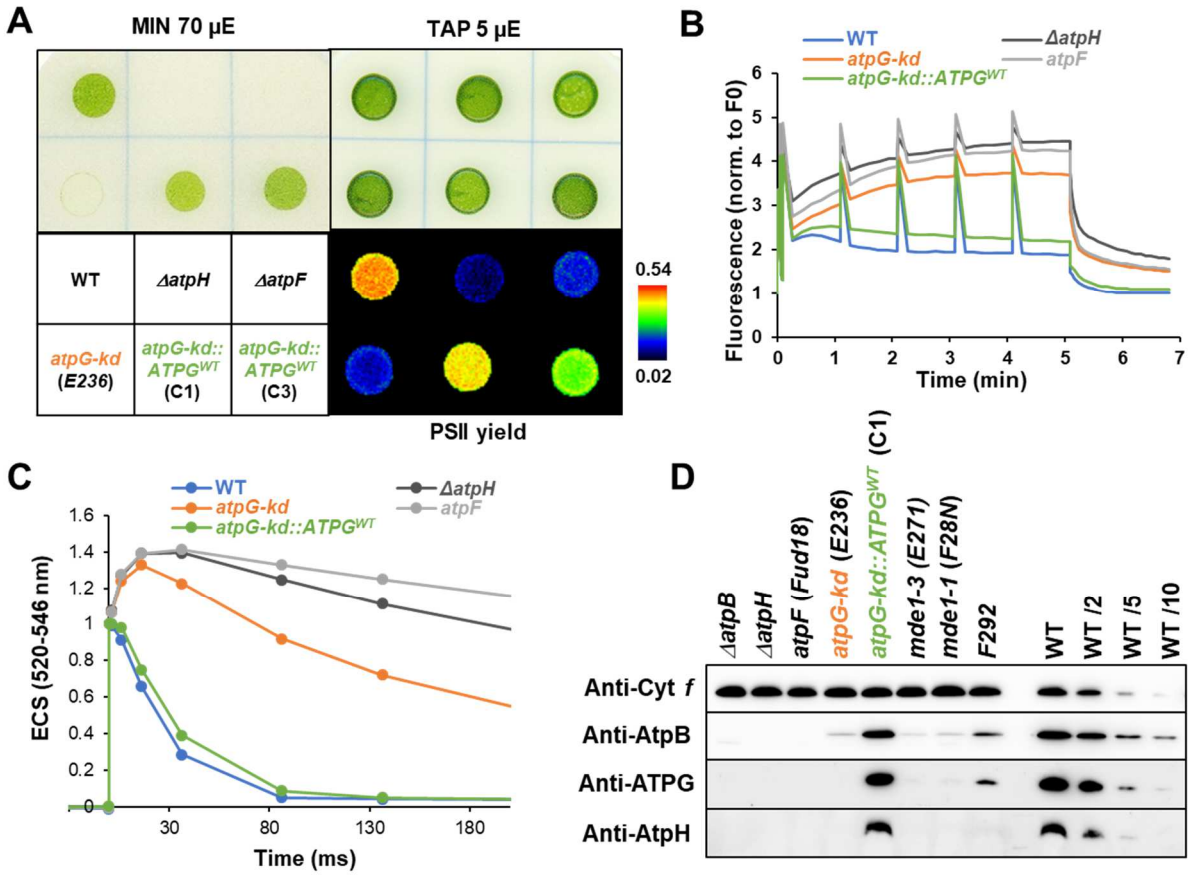

Figure 3. Photosynthesis is restored by complementing the mutant E236 with the WT version of ATPG.

A. Cells were grown phototrophically on MIN medium under moderate light (70 µM photon m^{-2} s^{-1}) or mixotrophically on TAP medium in low light (5 µM photon m^{-2} s^{-1}). PSIImaximumyield yield (F_M'-F_S)/F_M' was assessed by chlorophyll fluorescence and shown in false-color scale. B. Kinetics of chlorophyll fluorescence were monitored under moderate light. Saturating light pulses were applied every minute to reach F_M' and calculate PSII yield. C. Kinetics of electrochromic shift (ECS) of carotenoids (520nm) upon single-turnover excitation (signal normalized to photosystem charge separation). D. Thylakoid membranes were purified and content in cytochrome f (loading control) and ATP synthase subunits AtpB, ATPG and AtpH analyzed by imunoblot. Samples were loaded on equal chlorophyll basis (10 µg) together with a dilution series for the WT (1, 1/2, 1/5, 1/10).

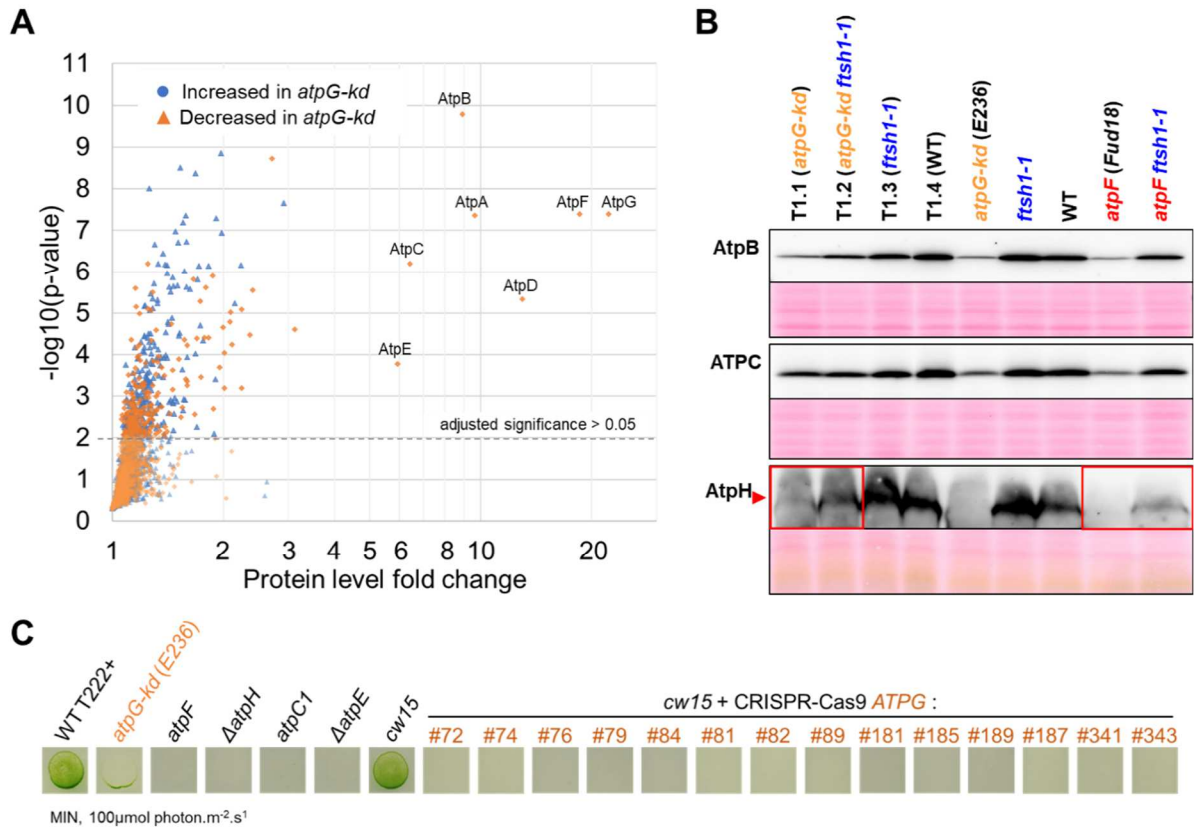

Figure 4. ATP synthase accumulation is downregulated in E236 (atpG-kd), controlled by thylakoid protease FtsH, but phototrophy is abolished in CRISPR-Cas9 atpG mutants.

A. WT and mutant E236 were grown in MIN under low light. Whole cell proteins were detected by mass spectrometry and averaged over 6 replicates to determine increased (blue triangles) or decreased (orange diamonds) levels in E236 as compared to WT (fold-change shown in log scale). Significance was assessed by unilateral t-tests (p-value shown at log scale) and adjusted according to the Benjamini-Hochberg approach. Distribution of proteins detected in less than two samples in one of the strains (no statistics available) are shown in Supplemental Figure S3. B. The mutant ftsh1-1 was crossed either to mutant atpG-kd (E236) or to mutant atpF (Fud18) and tetrads were dissected. Progeny and parental strains were grown in TAP under dim light and cell extracts were analyzed by western blot. Staining in Ponceau red as loading control. Red arrow points to the increased AtpH accumulation in double mutants combining ATP synthase and ftsh1-1 mutations as compared to single ATP synthase mutants. C. ATPG was interrupted by CRISPR-Cas9 (Supplemental Figure S5-S6-S7). Cells were grown in TAP under dim light, spotted on minimal medium (MIN) and grown for 10 days under 100 µmol photon.m^{-2}.s^{-1}.

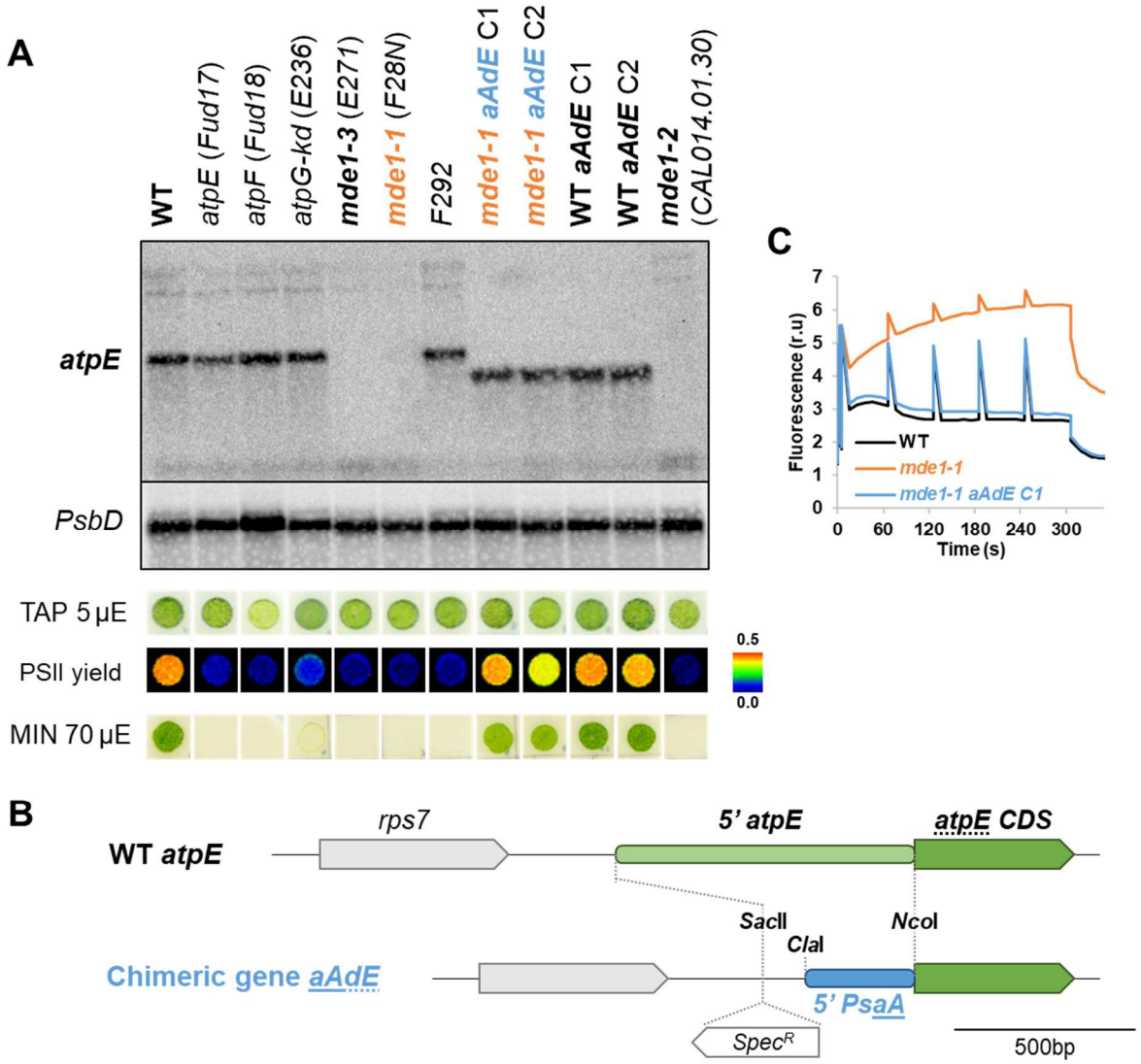

Figure 5. In absence of MDE1, accumulation of atpE transcript is restored by replacing its 5'UTR. *To restore atpE mRNA accumulation, the native atpE gene was replaced in mde1-1 mutant (F28N) and WT (control) by a chimeric transgene 5'psaA-atpE, associated with a spectinomycin resistance gene for the selection of transformed cells. Two independent transformants are shown for each genetic context (see Supplemental Figure S9 for mde1-2 and mde1-3). A. WT and ATP synthase mutant strains were grown in dim light and accumulation of transcripts atpE and PsbD (loading control) was analyzed by RNA blot. Cells were further grown in heterotrophy (TAP, 5 µmol photon m^{-2} s^{-1}) or in phototrophy (MIN, 70 µmol photon m^{-2} s^{-1}). On TAP plates, PSII yield under moderate light is shown in false-colour scale. B. Schematic representation of the aAdE chimera, where the atpE 5'-UTR has been replaced by the psaA 5'-UTR. Positions of the resistance cassette (Spec^r), inserted in the atpE orientation, and of cloning sites are shown. C. Induction kinetics of chlorophyll fluorescence in relative units (r.u.) under moderate light. Saturating light pulses were applied every minute to reach F_M'.*

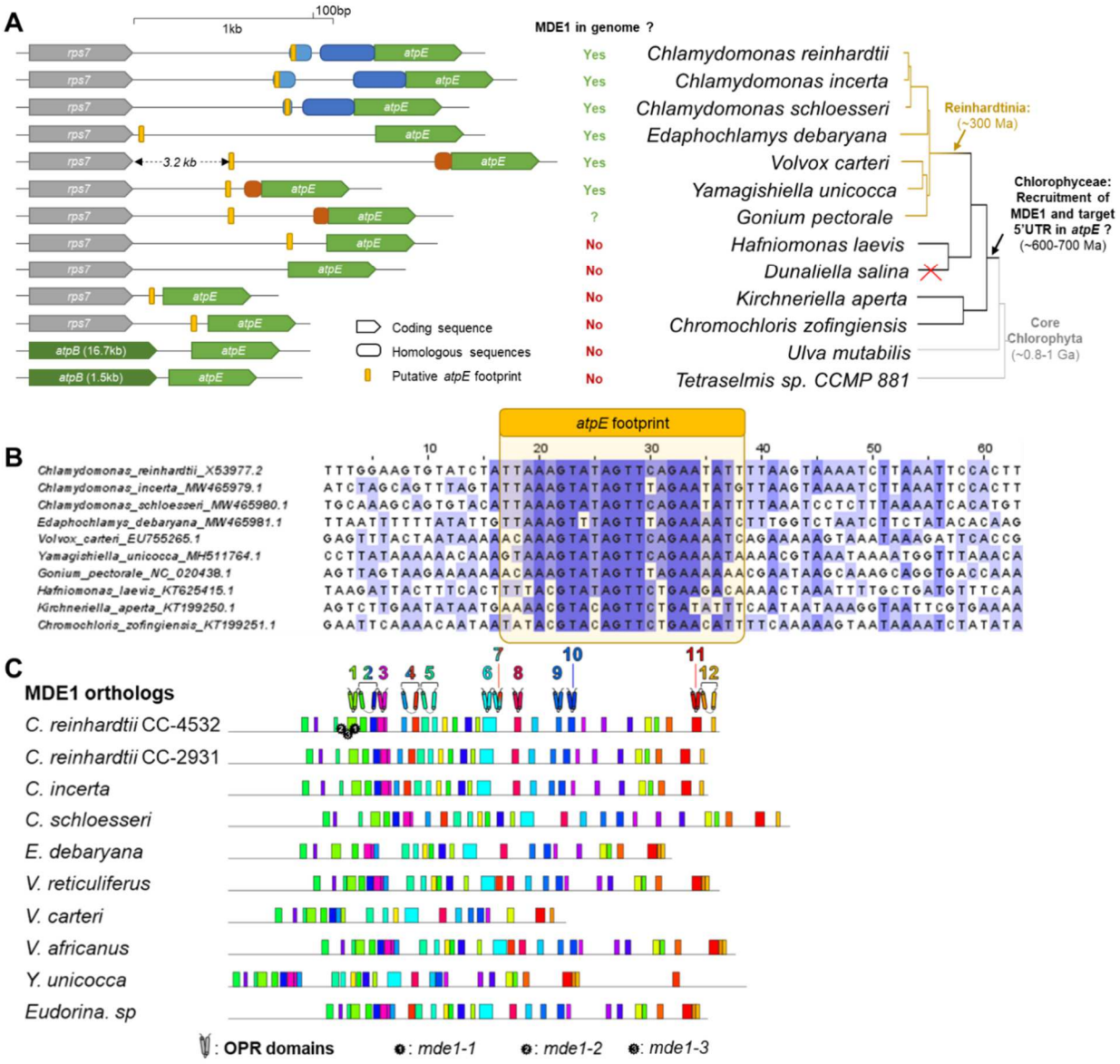

Figure 6. Conservation of atpE gene promoter and MDE1 protein in Volvocales and relatives. *A. The regions upstream of atpE were collected from chloroplast assemblies (see accession numbers in Supplemental Table ST6) and compared using BLAST. Coding sequences are shown as arrows, homologous sequences are denoted as colored boxes and possible footprints shown in yellow. Sequences are represented at scale, except intergenic region in Volvox and atpB gene in Ulva and Tetraselmis. A species-level phylogenetic tree is displayed on the left, with branch length accounting for substition frenquency among Reinhardtinia (Craig et al, 2020); longer divergence time are shown as cladogram. B. Alignment of the atpE RNA footprint from C. reinhardtii and putative homologous sequences found upstream of atpE in Volvocales. Conserved nucleotides highlighted in blue. C. Domain conservation among MDE1 orthologs was assessed using MEME (30 most probable domains, encompassing 6-100 residues, present in at least 5 species; GLAM2 was used to evidence alignment gaps in domains that are thus split by MEME). OPR domains are shown as double barrels colored according to the domain boxes. Mutated sites in mde1-1 and mde1-2 mutant strains (C. reinhardtii) shown as black stars. Multiple sequence alignment and accession numbers shown in Suppl. Figure S10 and Suppl Table ST1, respectively. Eudorina is a genus closely related to Volvox.*

SUPPLEMENTAL FIGURES

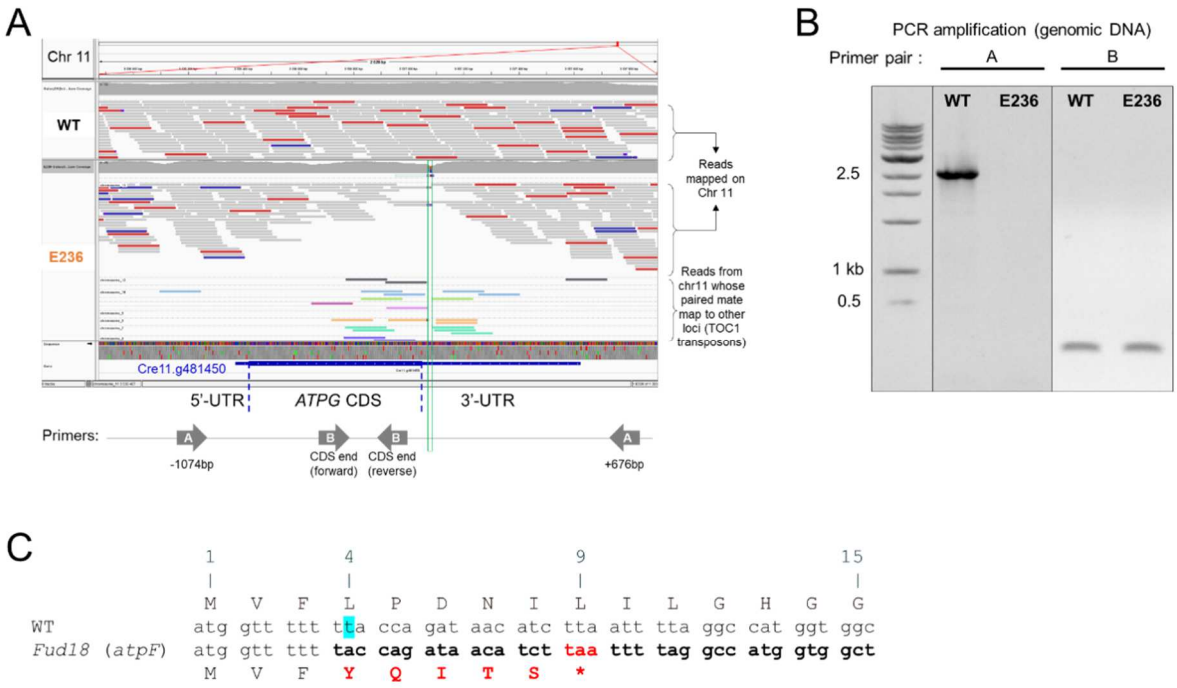

Supplemental Figure S1. Sequencing reveals the insertion of transposon TOC1 in the ATPG gene (Cre11.481450) of mutant E236 and a single-nucleotide deletion in the atpF gene of mutant Fud18. *A. Paired-end sequencing reads were mapped to the reference genome. WT (top) and E236 (bottom) reads centered on the Cre11.g481450 locus (ATPG) are shown. In grey, reads with both ends mapping in neighboring areas (red and blue reads denote interspaces that are respectively longer or shorter than usual); in light colors, reads with ends mapping on distinct chromosomic areas, in this case both chromosome 11 (Chr 11) and TOC1 transposon sequences. Below are shown the gene model for ATPG (5'UTR, coding sequence (CDS) and 3'UTR) and the position of primers used for PCR amplification (numbers stand for the distance upstream ATG start codon (-) and downstream 3'-UTR end (+). B. PCR products obtained on WT or E236 genomic extracts were separated on agarose. C. Compared to the WT atpF gene (top), the Fud18 mutant has a deletion of one T (blue) which causes a frameshift (red) and an abortive stop codon (*).*

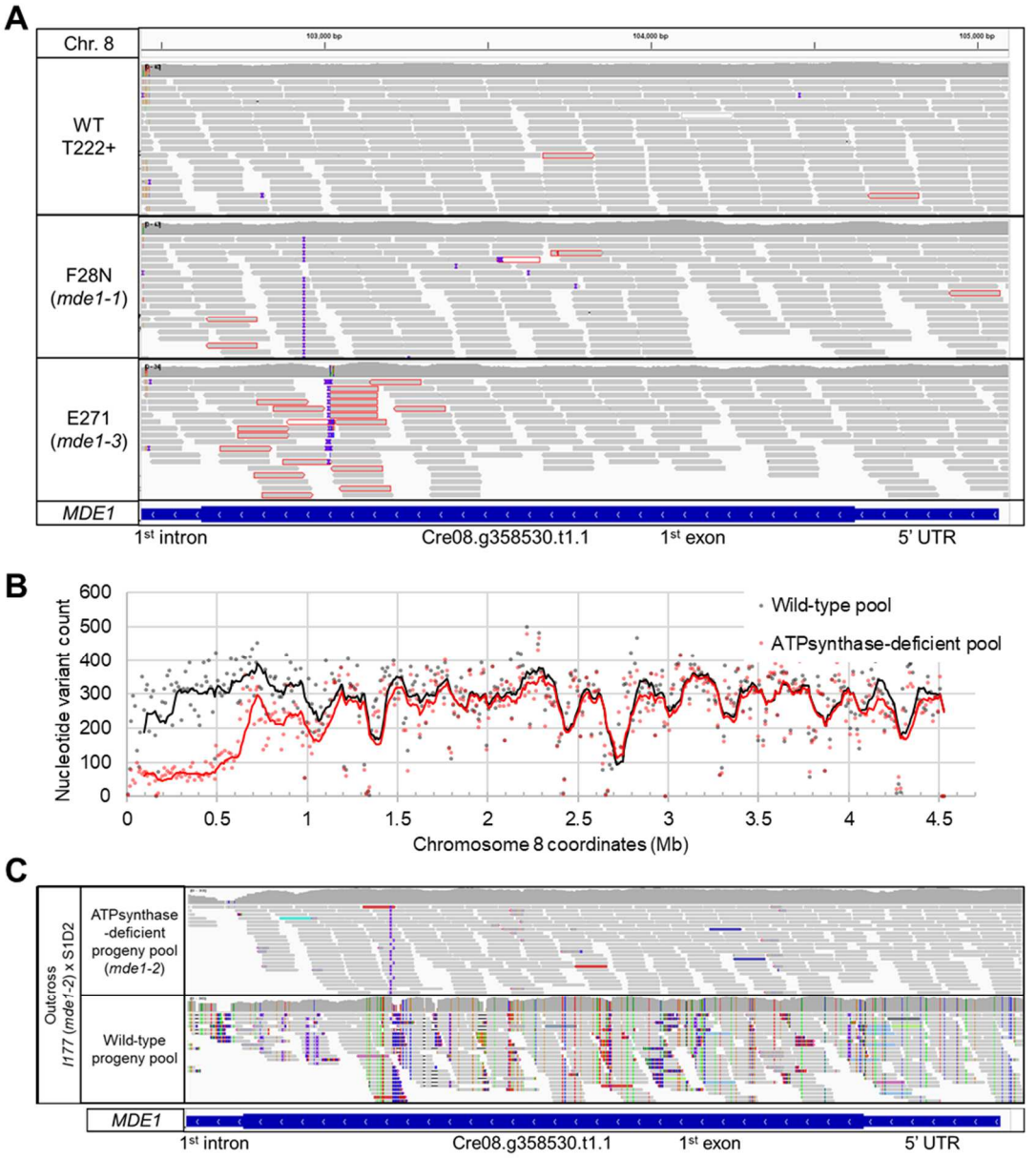
A
Chr. 8
103,000 bp
104,000 bp
105,000 bp
WT
T222+
F28N
(mde1-1)
E271
(mde1-3)
MDE1
1st intron
Cre08.g358530.t1.1
1st exon
5' UTR
B
Nucleotide variant count
600
500
400
300
200
100
0
Wild-type pool
ATPsynthase-deficient pool
0
0.5
1
1.5
2
2.5
3
3.5
4
4.5
Chromosome 8 coordinates (Mb)
C
Outcross
I177 (mde1-2) x S1D2
ATPsynthase
-deficient
progeny pool
(mde1-2)
Wild-type
progeny pool
MDE1
1st intron
Cre08.g358530.t1.1
1st exon
5' UTR
D
560
563
570
580
W E A Q A G R L M P G G G G S A A A A A M Q E E Q G E Q E
WT tgg gag gca cag gcg ggc cgg ctg atg ccc ggt ggc gga ggc ggg agc gcg gcg gcg gcg gcg atg cag gag gag cag ggg gag cag gag
F28N tgg gag gca cac ggc ggg ccg gct gat gcc cgg tgg cgg agg cgg gag cgc ggc ggc ggc ggc gat gca gga gga gca ggg gga gca gga
W E A H G G P A D A R W R R R E R G G G G D A G G A G G A G
590
600
611
G P T G R D L S N A L Y A L G L A A A A A E A A A E A E A G
WT ggg ccc acg ggt cgc gac ctg tcc aat gcc ctg tac gca cta ggt ctg gcg gcg gcg gcg gct gag gcg gca gcg gag gct gag gcg ggc
F28N ggg gcc cac ggg tcg cga cct gtc caa tgc cct gta cgc act agg tct ggc ggc ggc ggc ggc tga
G A H G S R P V Q C P V R T R S G G G G G *
E
490
500
503
509
520
A E A A G P G S A G P G A A P M R G S S S A G G S S S S S S A
WT gca gag gcg gcg ggg ccg gga tcg gcg ggg ccc ggg gca gcg ccc atg cgc ggc agt agc agc gcc gga ggc agc agc cta cag ccc cgg gcg
I177 gca gag gcg gcg ggg ccg gga tcg gcg ggg ccc ggg gca agc gcc cat gcg cgg cag tag
A E A A G P G S A G P G A S A H A R Q *
F
520
530
538
S S S S A A R S S Y G Q Q K Q Q P H V L L Q P R A A
WT agt agc agc agc gca gcc agg agc agc tac ggg cag cag aag cag cag cct cac gtg ctg cta cag ccc cgg gcg gct
E271 agt agc agc agc gca gcc agg agc agc tac ggg cag cag aag cag cag cct cac gtg ctg cga aat taa
S S S S A A R S S Y G Q Q K Q Q P H V L R N *

Supplemental Figure S2. Genotyping of F28N, CAL014.01.30 (I177) and E271 identifies mutant alleles in the 1st exon of Cre08.g358530.t1.1.

The wild-type strain (WT) T222+ and mutants F28N and E271 were sequenced using 151bp pair-ended reads. Mutant CAL014.01.30 (clone I177) was outcrossed to the polymorphic wild-type strain S1D2 and phototrophic and non-phototrophic progenies were pooled (WT and ATP synthase-deficient, respectively) and sequenced using 101bp pair-ended reads. A,C. Read mapping at the start of locus (Cre08.g358530). Insertions shown in purple. Read colors according to insert size. Consensus base in grey, SNPs in green, red, yellow and blue (A, T, G or C, respectively). Positions of 5'-UTR, 1st exon and 1st intron indicated at the bottom (minus strand). B. Nucleotide variant count across 10kb windows of chromosome 8 in pooled progenies of I177 outcross to S1D2. Lines are sliding average over 100kb. D-F. DNA sequence and translation in the WT (top) and the mutants (bottom) in the regions of 1st exon from locus Cr_08_37856.1 corresponding to residues 560-620 (D), 490-520 (E) and 516-542 (F). Insertions highlighted in blue. Numbering of amino-acids, marked in red at the frame-shift positions and premature stop codons. Surprisingly, the latter insertion contained the guide RNA scaffold for the CRISPR-Cas9 system and 21 bp of EGY1 guide RNA.

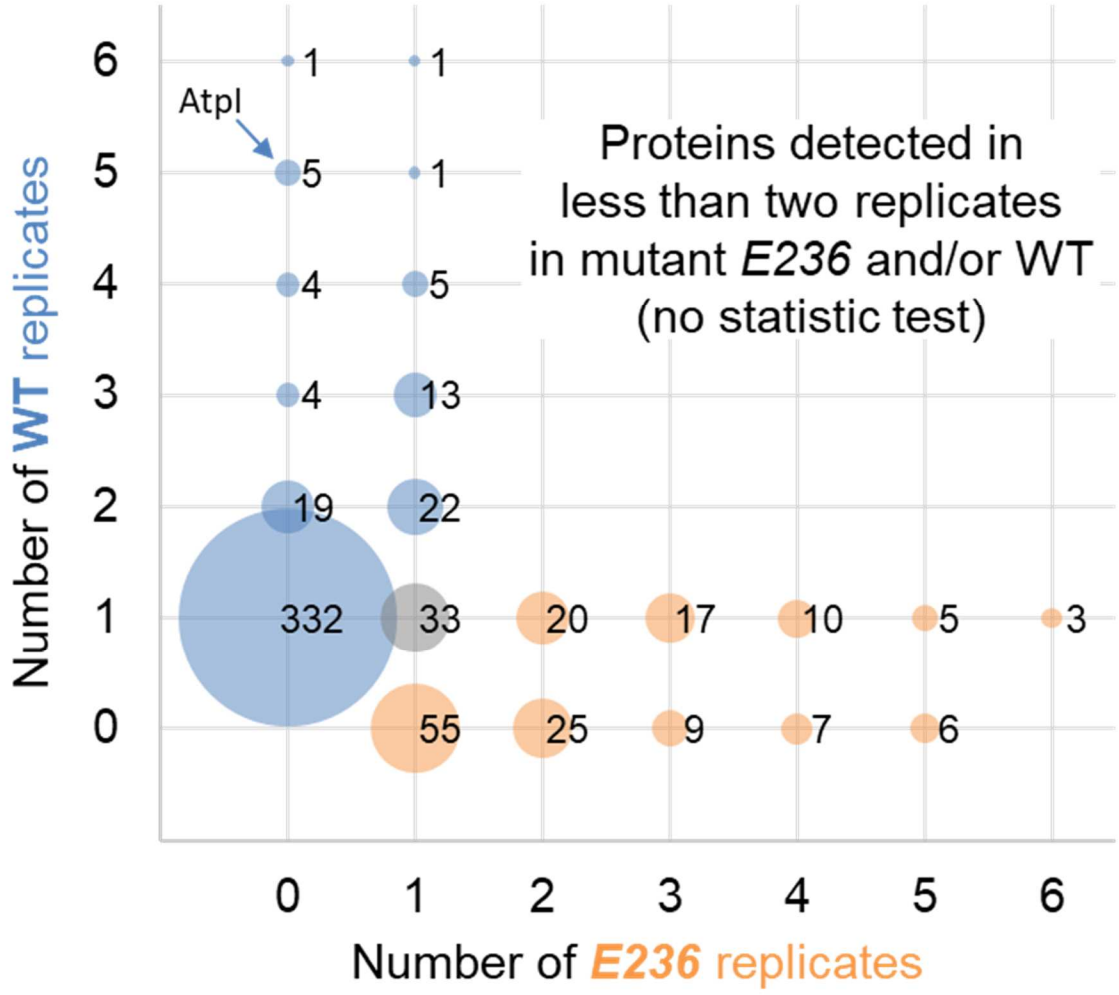

Supplemental Figure S3. Distribution of proteins detected in less than two replicates in mutant E236 and/or WT.

Number of proteins found in one to six (all) of WT replicates but less than two E236 replicates shown as blue bubbles. Number of proteins found in one to six (all) of E236 replicates but less than two WT replicates shown as orange bubbles. Proteins found in only one replicate in both strains shown in grey. (For instance, AtpI is one of the five proteins detected in five WT samples but none of the E236 samples.)

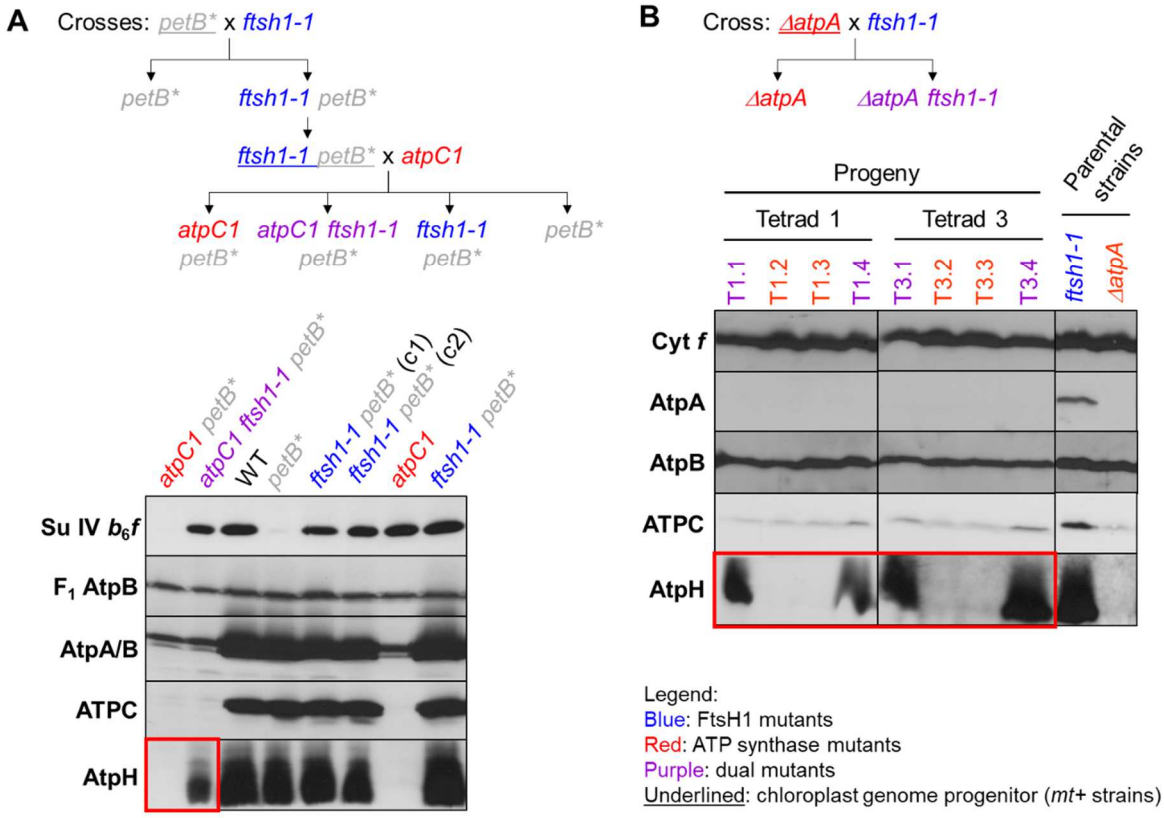

Supplemental Figure S4. Restoration of ATP synthase membrane subunit AtpH accumulation in distinct atpC1 and ΔatpA mutants by introgression of mutation in FtsH1 protease.

Single mutant strains were crossed to generate multiple mutants. The chloroplast genome is transmitted to all progeny by the mt+ strain only (underlined), notably mutations ΔatpA and petB (petB H202Q). Nuclear mutations (ftsh1, atpC1) follow Mendelian segregation. Cells were grown in dim light and analysed by western blot. A. Progeny of crosses between (i) petB* mt+ and ftsh1-1 mt- parental strains and (ii) a double mutant progeny petB* ftsh1-1 mt+ and atpC mt-. B. Two tetrads from the cross of parental strains atpA mt+ and ftsh1-1 mt-. Mitochondrial F_1 subunit ATPB (A) and cytochrome (Cyt. f) are shown as loading control.*

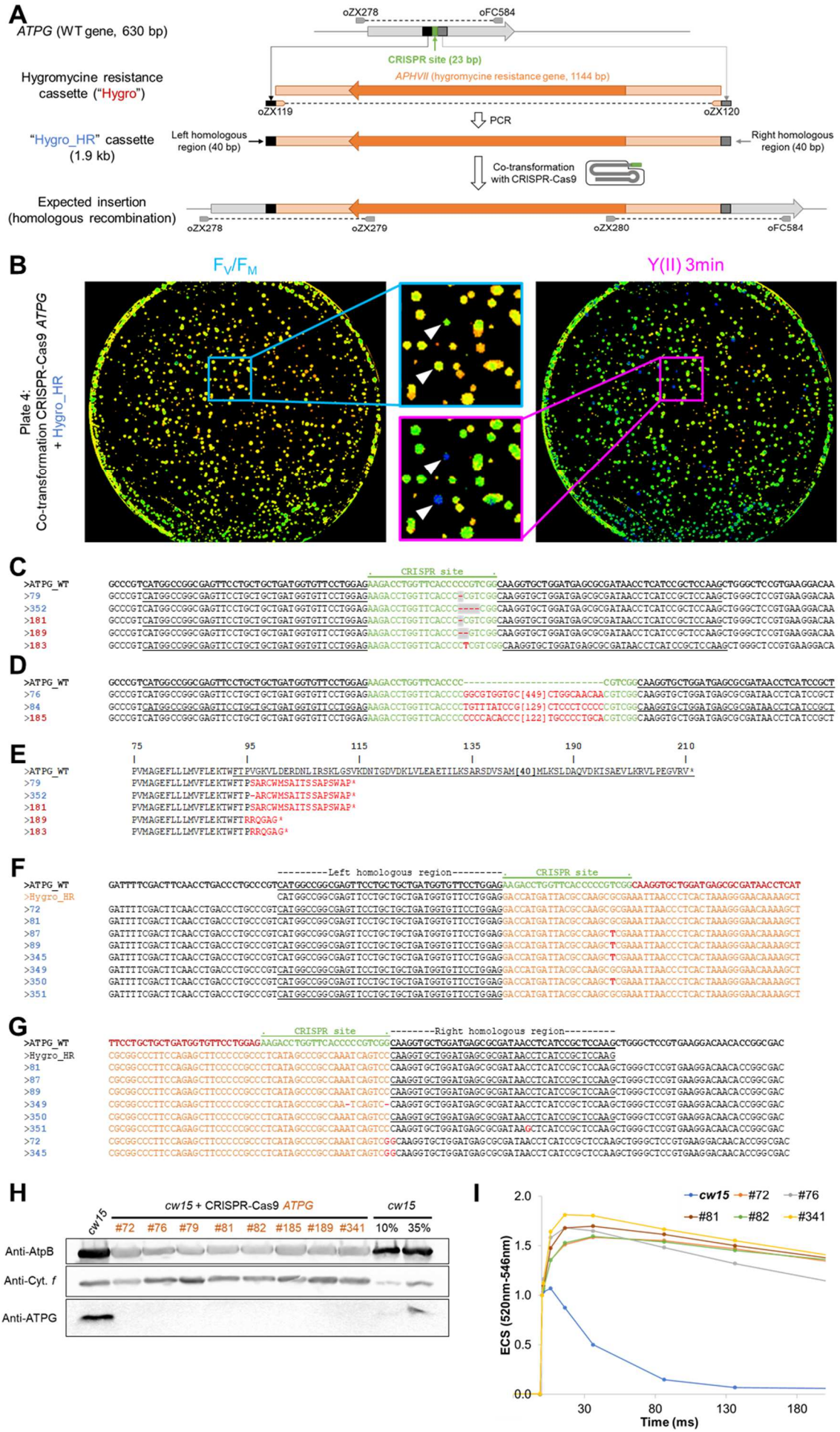
A
ATPG (WT gene, 630 bp)
oZX278
oFC584
CRISPR site (23 bp)
Hygromycine resistance cassette ("Hygro")
APHVII (hygromycine resistance gene, 1144 bp)
oZX119
oZX120
PCR
"Hygro_HR" cassette (1.9 kb)
Left homologous region (40 bp)
Right homologous region (40 bp)
Co-transformation with CRISPR-Cas9
Expected insertion (homologous recombination)
oZX278
oZX279
oZX280
oFC584
B
FV/FM
Y(II) 3min
Plate 4: Co-transformation CRISPR-Cas9 ATPG + Hygro_HR
C
CRISPR site
>ATPG_WT
>79
>352
>181
>189
>183
D
>ATPG_WT
>76
>84
>185
E
>ATPG_WT
>79
>352
>181
>189
>183
F
---------Left homologous region---------
CRISPR site
>ATPG_WT
>Hygro_HR
>72
>81
>87
>89
>345
>349
>350
>351
G
CRISPR site
--------Right homologous region---------
>ATPG_WT
>Hygro_HR
>81
>87
>89
>349
>350
>351
>72
>345
H
cw15
cw15 + CRISPR-Cas9 ATPG
cw15
#72 #76 #79 #81 #82 #185 #189 #341
10% 35%
Anti-AtpB
Anti-Cyt. f
Anti-ATPG
I
cw15 #72 #76 #81 #82 #341
ECS (520nm-546nm)
Time (ms)

Supplemental Figure S5. Analysis of CRISPR-Cas9-induced mutations of ATPG gene in NHEJ and HR clones.

A. Diagram of CRISPR-Cas9 edition of the ATPG gene. Within the WT ATPG gene (grey box), sequences used for homologous recombination (HR) are 40bp-long upstream and downstream (black and grey boxes, respectively) of the CRISPR site (green). Cells were co-transformed in the presence of the standard cassette (top panel, orange box, "Hygro") containing the hygromycin resistance gene (orange arrow). Clones which were obtained with Hygro-no-HR are shown in dark red in panels C-E. Alternatively, cells were co-transformed in the presence of a resistance cassette flanked on both sides by 40bp homologous regions (obtained by PCR amplification using overhang primers (oZX119 and oZX120), to be used as a repair template (medium panel, "Hygro_HR"). Clones obtained using Hygro_HR are shown in blue in panels C-G. Bottom panel depicts expected repair of the CRISPR-Cas9 cut in the case of homologous recombination between ATPG gene and the Hygro_HR cassette, which conserves both HR regions and replaces the 23bp CRISPR site by the full resistance cassette. Primers used to probe insertion are shown as grey arrows and amplification products as dotted lines. B. The cell-wall less strain cw15 was edited and plated for selection on hygromycin. After 10 days, chlorophyll fluorescence kinetics were recorded directly on selection medium. False-color images display PSII maximum yield (left panel and pink inset) and PSII yield at 3 minutes under medium light (right panel and blue inset). White arrows indicate two blue colonies, putatively ATP synthase deficient (see Supplemental. Figure S6). C-G. Alignments of sequences obtained in a subset of clones (see Supplemental. Figure S7 for other clones). C-D. Alignments of genomic sequences obtained using both primers in ATPG (oZX278 and oFC584). As compared to the WT sequence (in bold), single-nucleotide deletions are depicted by the symbol " - " and insertions are shown in red (numbers between brackets indicate the amount of nucleotides not displayed). E. Partial amino-acid sequences of ATPG (full protein: 209 AA) in the WT (bold) and the deletion mutants from C. Mutated residues and premature stop codons (*) due to frame-shifts shown in red. F-G. Alignments of genomic sequences obtained using forward primer in ATPG and reverse primer in the co-transformation cassette (F: oZX278+oZX279, left border; G: oZX280+oFC584, right border). WT sequence shown in bold, insertions shown in red (numbers between brackets indicate the amount of nucleotides not displayed). Deletions as compared to the hygromycin cassette are indicated between brackets. Homologous regions are underlined, CRISPR site is shown in green. H. Cells were grown in dim light and analyzed by western blot. I. Kinetics of electrochromic shift (ECS) of carotenoids (520nm) upon single-turnover excitation (signal normalized to one electron.photosystem^{-1}).

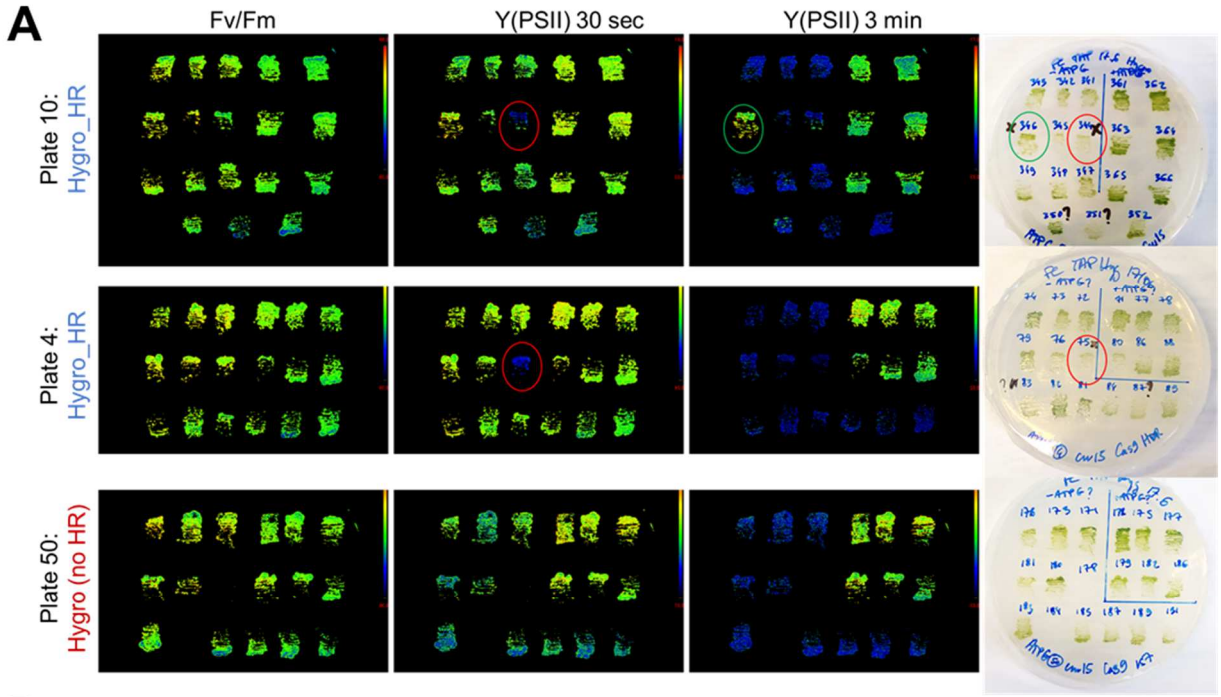
A
Fv/Fm
Y(PSII) 30 sec
Y(PSII) 3 min
Plate 10: Hygro_HR
Plate 4: Hygro_HR
Plate 50: Hygro (no HR)

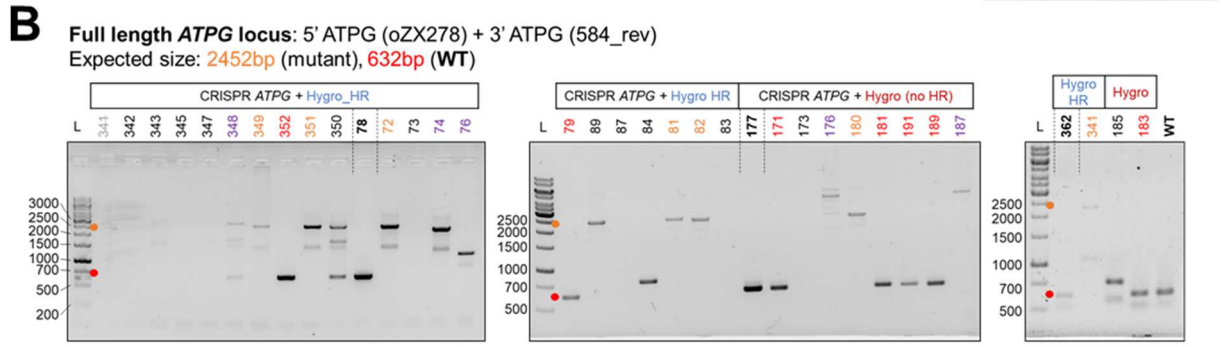
B
Full length ATPG locus: 5' ATPG (oZX278) + 3' ATPG (584_rev)
Expected size: 2452bp (mutant), 632bp (WT)
CRISPR ATPG + Hygro_HR
CRISPR ATPG + Hygro HR
CRISPR ATPG + Hygro (no HR)
Hygro HR
Hygro
WT

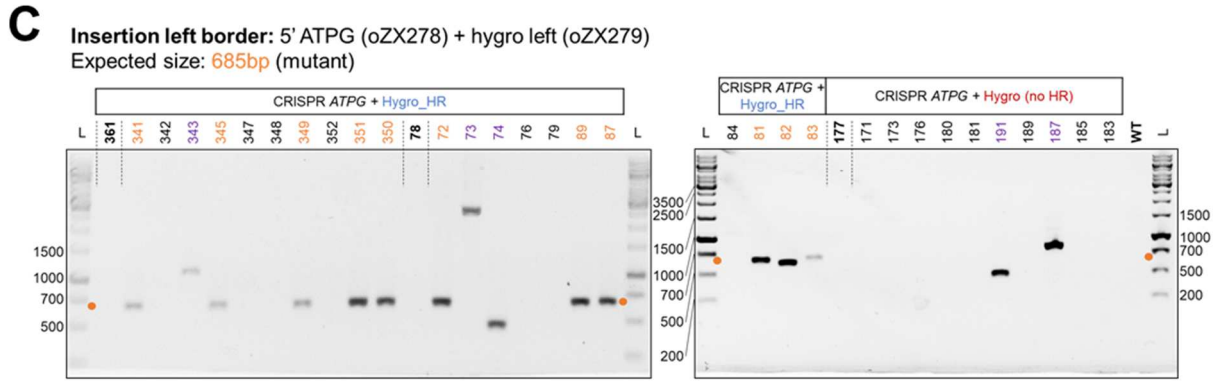
C
Insertion left border: 5' ATPG (oZX278) + hygro left (oZX279)
Expected size: 685bp (mutant)
CRISPR ATPG + Hygro_HR
CRISPR ATPG + Hygro HR
CRISPR ATPG + Hygro (no HR)
WT

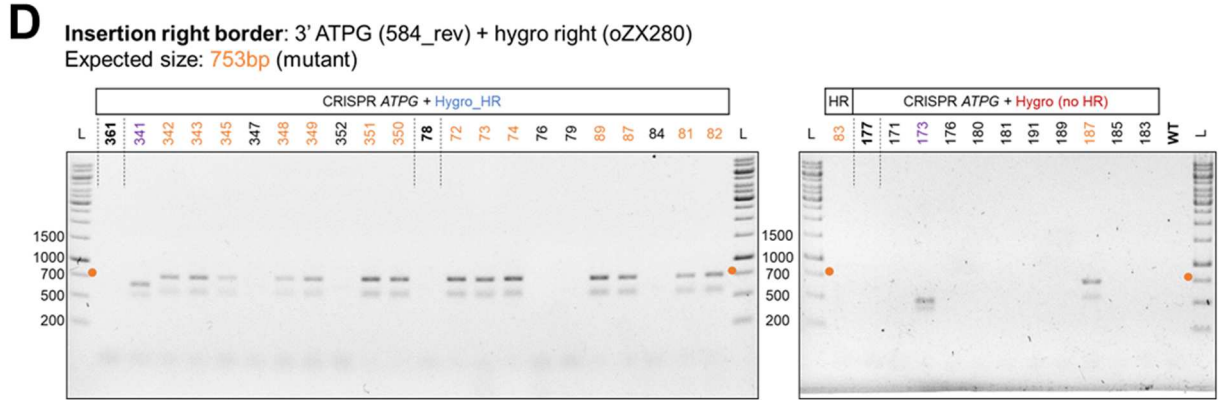
D
Insertion right border: 3' ATPG (584_rev) + hygro right (oZX280)
Expected size: 753bp (mutant)
CRISPR ATPG + Hygro_HR
HR
CRISPR ATPG + Hygro (no HR)
WT

Supplemental Figure S6. Steps 2 and 3 in CRISPR-Cas9 workflow: second phenotyping and PCR genotyping of putative atpG mutants obtain by CRISPR-Cas9 edition.

31 candidate ATP synthase-deficient clones and 18 wild-type clones were collected from different plates after CRISPR-Cas9 edition of ATPG gene, were plated on TAP and grown under dim light. A. Chlorophyll fluorescence kinetics were recorded for clones edited in the presence of resistance cassette containing homologous regions (upper and median panels, "Hygro_HR") or in absence of homologous regions in the cassette ("Hygro", lower panels). False-color images display PSII maximum yield (left panels) and PSII yield at 30 seconds (center panel) and 3 minutes (right panels) under medium light. ATP synthase-deficient phenotype was confirmed, except for candidates indicated by green and red circles that are respectively wild-type and deficient in electron flow (null PSII yield within seconds, indicative of a Cyt. b_6f or PSI mutation). B-D. PCR amplification in putative atpG mutants and control lines (bold). L: ladder. Orange: expected mutant fragment lentgh; red: WT fragment length; purple: atypical fragment length. B. Full length locus using ATPG primers (oZX278 and 584_rev). C. 5′ side of ATPG ("Left border") using forward and reverse primers in ATPG (oZX278) and cassette (oZX279), respectively. D. 3′ side of ATPG ("Right border") using forward and reverse primers in cassette (oZX280) and ATPG (584_rev), respectively.

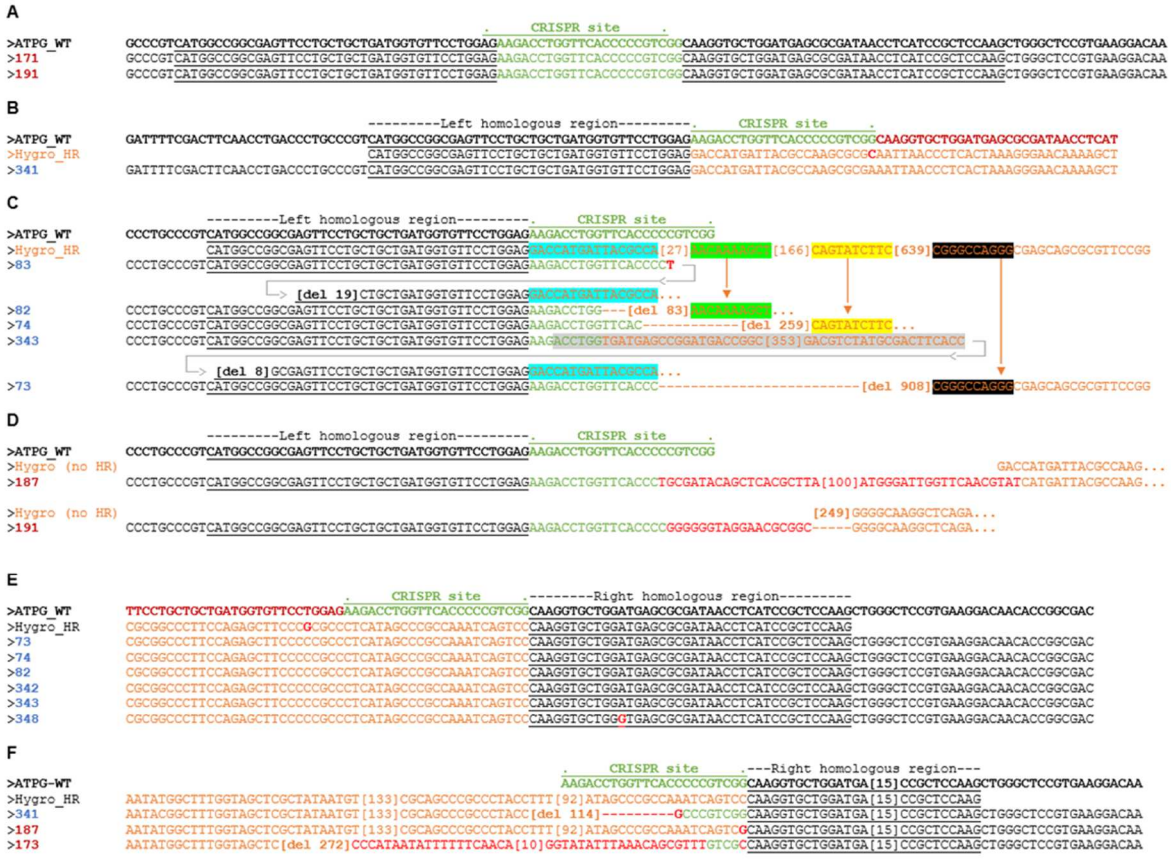

Supplemental Figure S7. Analysis of CRISPR-Cas9-induced mutations of ATPG gene in supplemental clones.

Alignments of sequences obtained in the clones excluded from Supplemental Figure S5. WT sequence shown in bold, insertions shown in red (numbers between brackets indicate the amount of nucleotides not displayed). Deletions as compared to the hygromycine cassette are indicated between brackets. Homologous regions are underlined, CRISPR site is shown in green. A. Alignments of genomic sequences obtained using both primers in ATPG (oZX278 and oFC584). Surprisingly, clones 171 and 191 were not mutated as compared to the WT, maybe due to mixed colonies (see a distinct product obtained in clone 191 in panel C). B-F. Alignments of genomic sequences obtained using forward primer in ATPG and reverse primer in the co-transformation cassette. B-D. Left border (oZX278+oZX279). E-F. Right border (oZX280+oFC584). In C., grey arrows indicate duplicates of the flanking HR sequences, inserted by NHEJ repair rather than homologous recombination. Highlighted sequences and vertical arrows show alignments between various regions of the cassette and the flanking sequences of indicated clones. The sequence highlighted in grey (clone 343) is a part of the hygromycin cassette integrated in the reverse orientation.

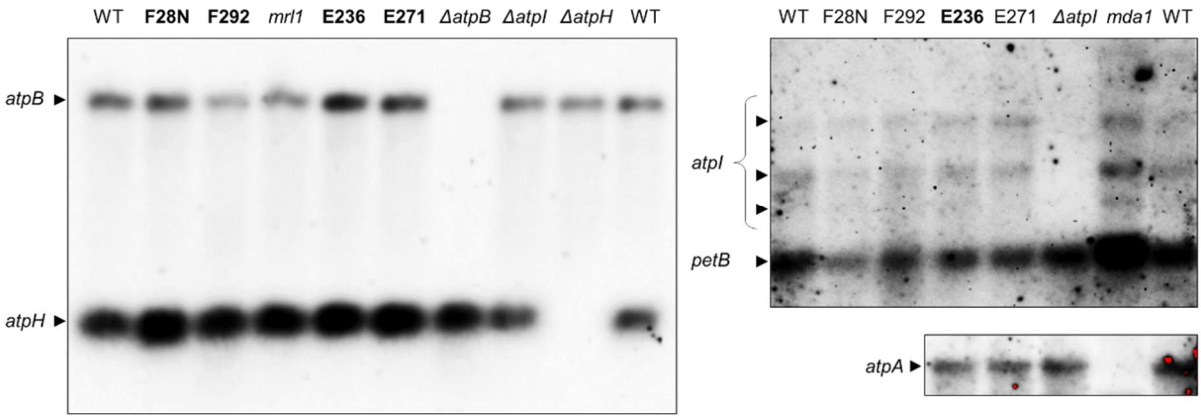

Supplemental Figure S8. Northern blot analysis of chloroplast-encoded ATP synthase transcripts atpA, atpB, atpH and atpI.

Cells were grown TAP under low light and harvested in exponential phase. Total RNAs were extracted and the indicated transcripts were detected using digoxigenin-labelled probes. Several forms are detected for atpI transcript (arrows). The petB transcript serves as loading control. Deletion mutants (ΔatpB, ΔatpH and ΔatpI) and nuclear mutants (mrl1 and mda1) as controls.

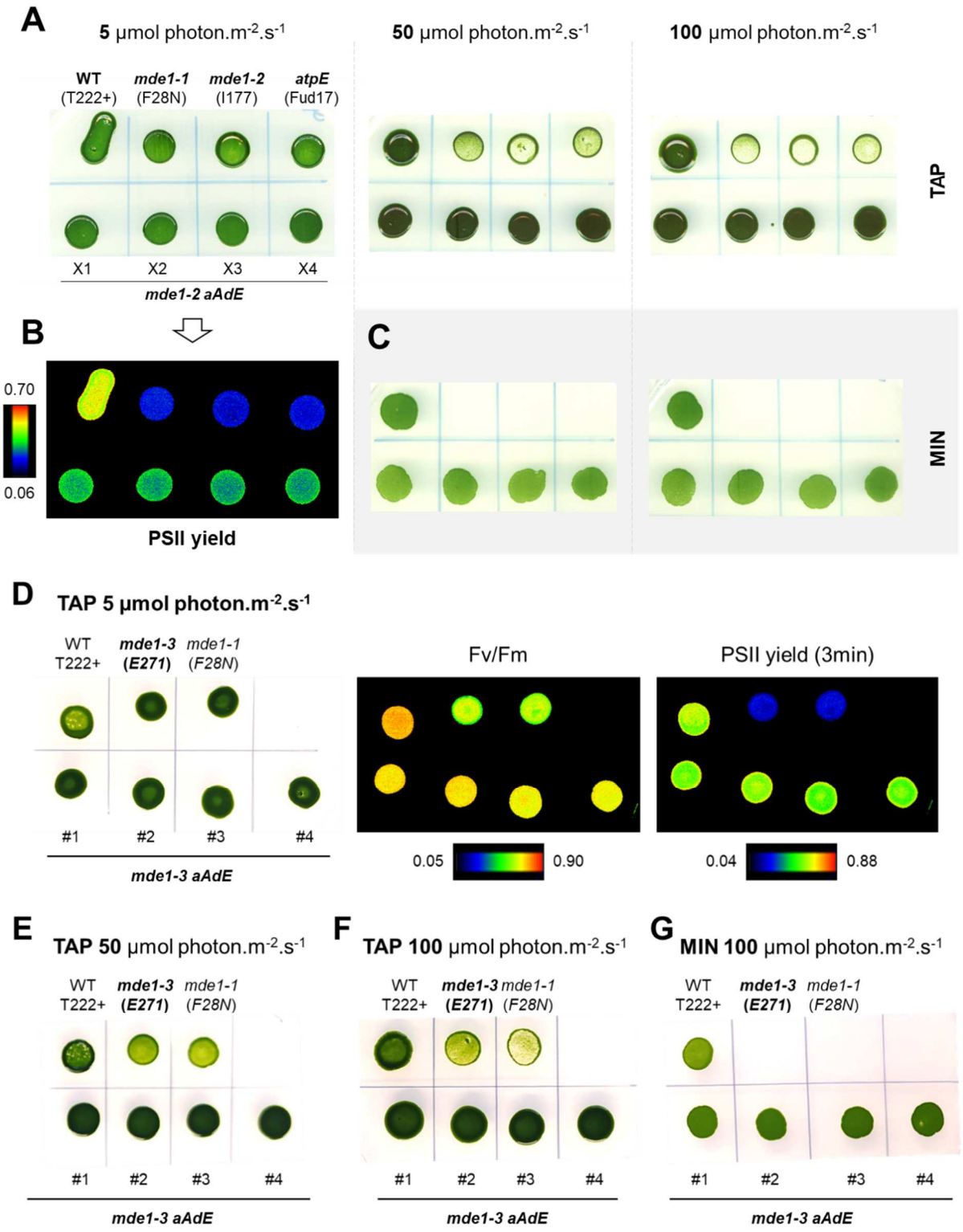

Supplemental Figure S9. Restoration of ATP synthase in mde1-2 and mde1-3 mutant backgrounds by replacement of atpE 5'-UTR

Mutant strains mde1-2 (CAL014.01.30) (panels A-C) and mde1-3 (E271) (panels D-G) were transformed with the aAdE cassette (see Figure 5B) and selected on spectinomycin-containing TAP medium. Control strains are the WT and the mde1-1 (F28N) and atpE (Fud17) mutants. A, D, E, F. Heterotrophic growth (TAP) under very dim light (5 µmol photon m^{-2} s^{-1}) and moderate light intensities (50-100 µmol photon m^{-2} s^{-1}). B. PSII yield under moderate light is shown in false-color scale. C and G. Growth test in phototrophy (MIN, 50-100 µmol photon m^{-2} s^{-1}).

Supplemental Figure S10. Conservation of OPR domains in MDE1 orthologs. (in attachment)
Sequences were aligned using MAFFT and conservation annotated using Boxshade (dark and light blue, low and high conservation, respectively). CM: conserved motifs, OPR: octotricopeptide repeat.

A

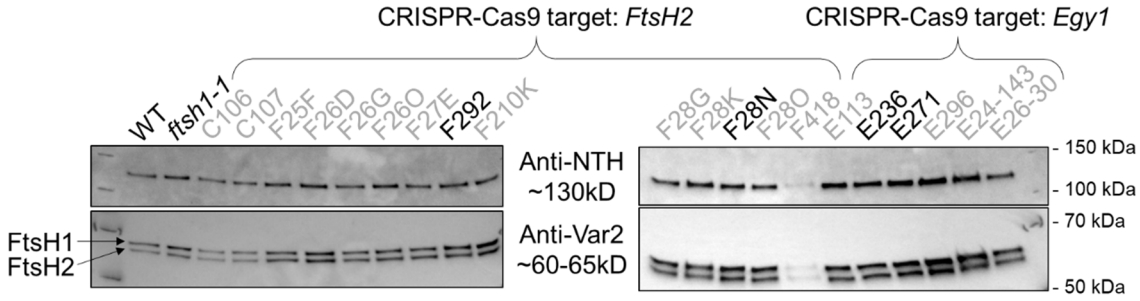

B

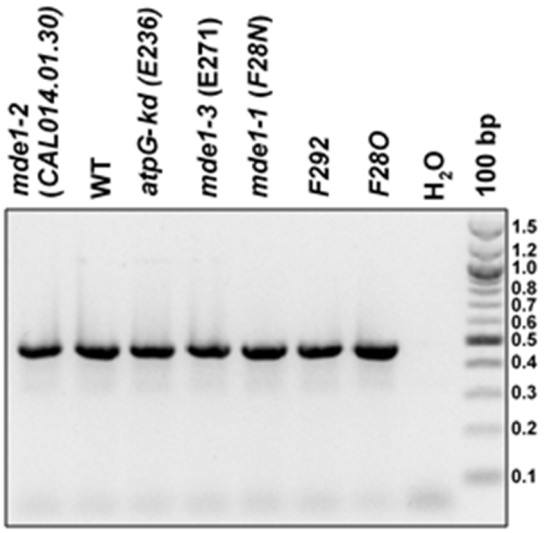

Supplemental Figure S11. Preliminary characterization of transformants.
A. Western blot analysis using antibody anti-Var2 (FtsH1 and Ftsh2 subunits). Anti-NTH as loading control. B. PCR using EGY1-S1 (5'-TGCACGATGCCATAGAGCG-3') and EGY1-A1 (5'-CATGTCCTCCTTGTCCAGC-3') primers framing the EGY1 target site of CRISP-Cas9 amplifies a product of 484 bp indicating the absence of insertion of the hygromycin resistance cassette in this site in transformants as in wild-type strain.

Organism	MDE1 orthologs
C. incerta	GenBank: KAG2424474.1
C. schloesseri	GenBank: JAEHOD010000076.1 *
E. debaryana	GenBank: KAG2482198.1
V. carteri	NCBI Ref Seq: XM_002949805.1
Y. unicocca	GenBank: GCA_003116995.1 *
G. pectorale	GenBank: KXZ40818.1
Eudorina sp.	GenBank: GCA_003117195.1 *
***C. reinhardtii* (CC-4532)**	Phytozome: Cre08.g358530_4532.1.p
***C. reinhardtii* (CC-2931)**	CC2931.v1C.fa *°
V. reticuliferus	GenBank: GIL80257.1
V. africanus	GenBank: GIL54847.1

Supplemental Table ST1. Accession number for sequences used in Figure 6 and Suppl. Fig. S10.
** indicates manual annotation of MDE1 from genome sequence. ° : genome available at https://raba.ibpc.fr/home/ovallon@ibpc.fr/Briefcase/Chlamy_genomes (Chaux-Jukic et al., 2021)*

SRA	Strain
xxx	T222+ (WT)
xxx	*E236* (*atpG-kd*)
xxx	*F28N* (*mde1-1*)
xxx	*E271* (*mde1-3*)
xxx	*F292*
xxx	WT progeny (WT S1D2 x *I177*)
xxx	ATP synthase-deficient progeny (WT

Supplemental Table ST2. Sequencing datasets

We use the updated library of C. reinhardtii repeats and transposable elements (Craig et al., 2020)

PCR primers	Sequence
atpH-dig-FW	AACCCTATCGTAGCTGCTGC
atpH-dig-RV	ACTAGACCGTAAATTGTTAA
atpB-dig-FW	CACGGTGGTGTTTCTGTATT
atpB-dig-RV	TTACGCTTTGTGCAGAATCA
petB-dig-FW	GCTGTTATTTTAGGTATGGC
petB-dig-RV	GATGCGTTGTAAATAGTGTT
atpE_probe_RV	TGTGTTGATCTCCAATATTGTTTC
atpE_probe_FW	GGGTTAGCCTTTAAGCGCGGTA
atpI_FW	TGGAGTTCCTAATACTGCTAAAGCTA
atpI_RV	ATGGAACAAGCGCAACAAGAAC
PsbD	(Rochaix, 1978; Eberhard et al., 2002)

Supplemental Table ST3. Oligonucleotides used to amplify the probes used for northern blot analyses.

The atpA probe was a 1372 EcoRI-PacI subfragment of the plasmid patpA2 (Ketchner et al., 1995).

Primer	Sequence	Target location
oZX_278	CACACCACCACCTAGGACAG	5'-UTR ATPG
584_rev	CTGATCTTGTCAACCTGGG	3'-UTR ATPG
oZX_279	CTTCACCGATCCGGAGGAAC	Cassette AphVII (outward)
oZX_280	CAGGCTCGCGTAGGAATCAT	Cassette AphVII (outward)
oZX_062	GACCATGATTACGCCAAGCG	Cassette AphVII (inward)
oZX_063	GGACTGATTTGGCGGGCTAT	Cassette AphVII (inward)
oZX_119	CATGGCCGGCGAGTTCCTGCTGCTGATGGTGTTCCTGGAGGACCATGATTACGCCAAGCG	Cassette AphVII (inward)
oZX_120	CTTGGAGCGGATGAGGTTATCGCGCTCATCCAGCACCTTGGGACTGATTTGGCGGGCTAT	Cassette AphVII (inward)
psaA5U_F	CGCATCGATACGAATACACATATGGT	5'UTR *PsaA* (plasmid *ps1A1*)
psaAatpE_R	AATAGAAATTTGTAAACTCATGGATTTCTCCTTATA	5'UTR *PsaA* (plasmid *ps1A1*)
psaAatpE_F	TTATTATAAGGAGAAATCCATGAGTTTACAAATTTC	*atpE* (plasmid *p50Sh*)
atpE_PstI_R	GCGCTGCAGTTAAATTTTTTTAAGTACTTTTACAA	*atpE* (plasmid *p50Sh*)

Supplemental Table ST 4. PCR primers list.
Overhang sequences highlighted. Partially overlapping sequences in underlined.

Division	Class (subclass)		Order	Family (Clade)	Genus/Species
Chlorophyta	**Chlorophyceae**	**CS clade**	**Chlamydomonadales (Volvocales)**	**Chlamydomonadaceae (Reinhardtinia > Metaclade-C)**	**Chlamydomonas reinhardtii**
					Chlamydomonas incerta
					Chlamydomonas schloesseri
					Edaphochlamys debaryana
				Chlamydomonadaceae (Reinhardtinia > TGV clade)	Colemanosphaera angeleri
					Gonium pectorale
					Yamagishiella unicocca
					Eudorina cylindrica
					Pleodorina starii
					Volvox carteri
				Chlamydomonadaceae	Oogamochlamys gigantea
					Carteria cerasiformis
					Chlamydomonas leiostraca
					Chlamydomonas applanata
				Dunaliellaceae	Hafniomonas laevis
					Spermatozopsis similis
					Dunaliella salina
				Phacotaceae	Phacotus lenticularis
				Pleurastraceae	
				Characiochloridaceae	
				Chlorococcaceae	
			Sphaeropleales	Bracteacoccaceae	Bracteacoccus aerius
					Bracteacoccus giganteus
				Chromochloridaceae	Chromochloris zofingiensis
				Hydrodictyaceae	Lacunastrum gracillimum
					Stauridium tetras
					Pseudopediastrum integrum
					Pseudopediastrum boryanum
					Hydrodictyon reticulatum
					Pediastrum angulosum
					Pediastrum duplex
				Neochloridaceae	Chlorotetraedron incus
					Neochloris aquatica
				Selenastraceae	Raphidocelis subcapitata
					Kirchneriella aperta
				Scenedesmaceae	Acutodesmus
					Pectinodesmus
					Coelastrella saipanensis
					Tetradesmus obliquus
				Radiococcaceae	
				Mychonastaceae	
				Pseudomuriellaceae	
				Sphaeropleaceae	
		Chlorophyceae (OCC clade)	Chaetopeltidales		
			Oedogoniales		
			Chaetophorales		
		Chlorosarcinales			
		Chlorophyceae incertae sedis			Jenufa
		Chlorophyceae incertae sedis		Treubariaceae	
	Mamiellophyceae		Mamiellales	Bathycoccaceae	Ostreococcus
	Chlorodendrophyceae		Chlorodendrales	Chlorodendraceae	Tetraselmis
	Ulvophyceae		Ulvales	Ulvaceae	Ulva mutabilis

Supplemental Table ST 5. *Distribution of presence (orange background) or absence (grey background) of homology with C. reinhardtii footprint if the 5'UTR atpE. See sequence sites in Supplemental Table ST 6.*

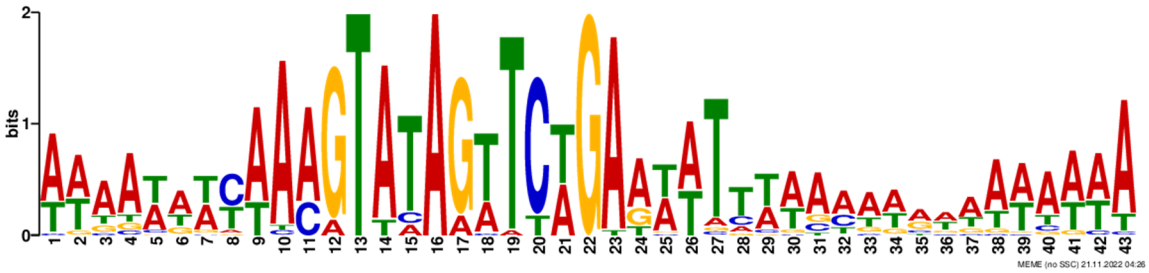

Name	*p*-value		Sites		
Pseudopediastrum_integrum_NC_037921.1	1.04e-17	TAAA TAATTT	AAAATAACAAAGTATAGATCTGAGTTTT TAACAAGTAAAAAAA		TTATT AAATT
Pseudopediastrum_boryanum_MF276983.1	9.02e-17	TTAAT AATTT	AAAATTACAAAGTATAGATCTGAGTTTT TAACAAGTAAAAAAA		TTATT AAATT
Pediastrum_angulosum_MF276978.1	3.09e-16	TTAAT TATTT	AAAATTACAAAGTATAGATCTGAGTTTT TAACAAGTAAAAATA		TTATT AAATT
Hydrodictyon_reticulatum_KY114065.1	3.09e-16	TTAAT GATTT	AAAATTACAAAGTATAGATCTGAGTTTT TAACAAGTAAAAATA		TTATT AAATT
Pediastrum_duplex_MF276981.1	4.12e-16	TTAA AGATTT	AAAATAGCAAAGTATAGATCTGAGTTTT TAACAAGTAAAAATA		TTATT AAAAT
Volvox_africanus_NC_039755.1	1.27e-14	TAAG TTACTA	ATAAAAACAAAGTATAGTTCAGAAAATC AAAAAAAAGTAAATA		AAAA AACACA
Volvox_carteri_EU755265.1	3.56e-14	GAGT TTACTA	ATAAAAACAAAGTATAGTTCAGAAAATC AGAAAAAGTAAATAA		AGAT TCACCG
Stauridium_tetras_NC_037923.1	5.25e-14	TTTTT AACTT	AAAATAAGAAAGTATAGATCTGAGTTTT TAACAAGTAAAAATA		TTAT GAAATC
Pleodorina_starrii_JX977846.1	5.25e-14	AAAC TTCCTA	ATAAAAACAAAGTATAGTTCAGAAAATC AAAAACGTAAATAAA		GATT TACGAC
Eudorina_cylindrica_MH161345.1	1.80e-11	TAAA TTGCTA	TTAAAACCAAAGTATAGTTCAGAAAATA AAAATTATATAAAAA		TTTAT TTTAT
Chlamydomonas_reinhardtii_X53977.2	7.55e-11	TTTGG AAGTG	TATCTATTAAAGTATAGTTCAGAATATTT TAAGTAAAATCTTA		AATT CCACTT
Chlorotetraedron_incus_KT199252.1	8.45e-11	ATTTT TATAG	AATAATTTAACGTATAGTTCTGAATTTTT TAACAAGTAAATAT		TTAT AAAAAA
Yamagishiella_unicocca_MH511764.1	1.06e-10	CCTTA TAAAA	AACAAAGTAAAGTATAGTTCAGAAAATA AAACGTAAATAAAAT		GGTT TAAACA
Neochloris_aquatica_KT199248.1	1.82e-10	TA	AAAAAGTCTAAGTATAGCTCTGATTTTTA ACAAGTAAATTAAA		AAAT TTAATT
Chlamydomonas_incerta_MW465979.1	10e-9	ATCT AGCAGT	TTAGTATTAAAGTATAGTTTAGAATATGT TAAGTAAAATCTTA		AATT CCACTT
Colemanosphaera_angeleri_NC_045893.1	46e-9	CTCG GACTGC	AAACAAATACAGTATAGTTCAGAAAATT ATTTATAAAATATTA		TAGA CATAAA
Chlamydomonas_schloesseri_MW465980.1	91e-9	TGCA AAGCAG	TGTACATTAAAGTATAGTTCAGAATATTT TAAATCCTCTTTAA		AATC ACATGT
Carteria_cerasiformis_KT625420.1	97e-9	AAGA GCAAAA	AAGTATACTACGTATAGTTCTGATTATTT TCTTTACCTTAATA		AGAG CCAGCT
Lacunastrum_gracillimum_NC_037918.1	24e-9	TGAA GAACTT	TATATCACAAAGTATAGAACTGAGTTTTT TAACAAGTAAAAAT		ATTA TCAAAT
Coelastrella_saipanensis_NC_042181.1	53e-9	TAAA ATACCA	AATATATCTACGTACAATTCTGATTATTA ACAAGTAAAATTAA		ATTTT TTTTT
Bracteacoccus_giganteus_KT625421.1	35e-9	ATAA TTGAGC	TTGAATTTTACGTATAGTTCTGAAAAGCG AGTTTATGGTAAAA		AACT AAATAT
Kirchneriella_aperta_KT199250.1	09e-9	AGTC TTGAAT	ATAATGAAAACGTACAGTTCTGATATTT CAATAATAAAGGTAA		TTCGT GAAAA
Gonium_pectorale_NC_020438.1	09e-9	AGTT AGTAAG	AAAAAAACAAAGTATAGTTTAGAAAAA ACGAATAAGCAAAGCA		GGTG ACCAAA
Chromochloris_zofingiensis_KT199251.1	03e-8	GAAT TCAAAA	CAATAATATACGTACAGTTCTGAACATTT TCAAAAAGTAATAA		AATC TATATA
Spermatozopsis_similis_NC_042251.1	76e-8	TGGT CAAAGT	ATGATGTCAAAATTAAAATCAGAAATTT TAGAAGCTTATAAAA		AGAA TGGTGT
Bracteacoccus_aerius_KT199254.1	04e-8	AAAA CTCTTG	TGAGATTTTACGTATAGTTCTGAAAAAC ACGTTTGCGGTAAAA		ATTA AAGATT
Dictyochloris_fragrans_MG778289.1	48e-8	CGGT CAAAAT	ATGATATCAAAATTAAAATCAGAAATTT TAGAAGCATACAAAA		AAAC TGGAAT
Edaphochlamys_debaryana_MW465981.1	96e-7	TTAAT TTTTT	ATATTGTTAAAGTTTAGTTTAGAAAATCT TTGGTCTAATCTTC		TATA CACAAG
Hafniomonas_laevis_KT625415.1	93e-7	TAAG ATTACT	TTCACTTTTACGTATAGTTCTGAAGACAA AACTAAATTTTGCT		GATG TTTCAA
Phacotus_lenticularis_KT625422.1	66e-5		TTAGGGTTTTAATAAAATTTAGTAAATG ATAATAGATTTGATA		TAGT TAAAAA

Supplemental Table ST 6. *Sites of homology with C. reinhardtii footprint if the 5'UTR atpE. MEME settings: ZOOPS (Zero or one site per sequence), Minimum Motif Width: 10, Maximum Motif Width: 50.*

CHAPTER 4:

AN ALTERNATIVE PATHWAY TO CF_1F_O-ATPASE FOR RAPID DISSIPATION OF THE PROTON MOTIVE FORCE IN *CHLAMYDOMONAS REINHARDTII*

FOREWORD

While studying the biogenesis of chloroplast ATP synthase, we monitored in mutants deficient in ATP synthase the electro-chemical shift (ECS) modification of the absorption spectrum of specific pigments caused by changes of this electric field ($\Delta\Psi$) which is a powerful tool for the analyze photosynthetic processes *in vivo*. We were surprised to find in absence of CF_1F_O ATP synthase an alternative dissipation pathway of the PMF after a pulse of intense light. We decided to characterize this intriguing pathway.

As André Verméglio mischievously says: « *Attention, on n'est jamais à l'abri d'une découverte » (« Beware, we are never safe from a discovery »)*.

Furthermore, this could be the onset of a powerful tool to study the regulation of PMF: «Recently it has become clear that regulation of PMF plays a major role in rapidly adjusting photosynthesis to changes in light intensity» (Armbruster et al, 2017). Up until now, there have been many regulations unveiled to explain how PMF is regulated, and the fastest way to counter-effect the fast effects of PMF on photosynthesis is the entry or exit of charged ions through the thylakoid membrane called counterions. On one hand, export of protons from the lumen to the stroma will decrease the ΔpH fraction of the PMF. On the other hand, export of positively charged ions or import of negatively charged ions will decrease the $\Delta\Psi$ component of PMF.

One notable transporter is KEA3, a K^+/H^+ antiporter in the thylakoid membrane that will reduce ΔpH without reducing the potential difference through the thylakoid. Other important transporters are anion importers such as the voltage gated VCCN1 or the CLCe Cl^- importers. These two ion transporters have been proposed as PMF regulators very early (Schönknecht et al., 1988; Tester & Blatt, 1989) and have since been studied for their participation in the PMF regulation in different conditions as reviewed in numerous articles in recent years (Dukic et al., 2019; Finazzi et al., 2015; Li et al., 2021; Lyu & Lazár, 2022; Marchand et al., 2018; Spetea et al., 2017; Szabò & Spetea, 2017). Of

course, Cl^- are not the only anions that enter the chloroplast and could play a role in the regulation of PMF, we could think of transporters of anions such such as bicarbonate HCO_3^- or phosphate $H_2PO_4^-$.

References

Armbruster, U., Correa Galvis, V., Kunz, H.-H., & Strand, D. D. (2017). The regulation of the chloroplast proton motive force plays a key role for photosynthesis in fluctuating light. *Current Opinion in Plant Biology*, *37*, 56-62. https://doi.org/10.1016/j.pbi.2017.03.012

Dukic, E., Herdean, A., Cheregi, O., Sharma, A., Nziengui, H., Dmitruk, D., Solymosi, K., Pribil, M., & Spetea, C. (2019). K+ and Cl− channels/transporters independently fine-tune photosynthesis in plants. *Scientific Reports*, *9*, 8639. https://doi.org/10.1038/s41598-019-44972-z

Finazzi, G., Petroutsos, D., Tomizioli, M., Flori, S., Sautron, E., Villanova, V., Rolland, N., & Seigneurin-Berny, D. (2015). Ions channels/transporters and chloroplast regulation. *Cell Calcium*, *58*(1), 86-97. https://doi.org/10.1016/j.ceca.2014.10.002

Li, M., Svoboda, V., Davis, G., Kramer, D., Kunz, H.-H., & Kirchhoff, H. (2021). Impact of ion fluxes across thylakoid membranes on photosynthetic electron transport and photoprotection. *Nature Plants*, *7*(7), Art. 7. https://doi.org/10.1038/s41477-021-00947-5

Lyu, H., & Lazár, D. (2022). Analyzing the effect of ion binding to the membrane-surface on regulating the light-induced transthylakoid electric potential (ΔΨm). *Frontiers in Plant Science*, *13*, 945675. https://doi.org/10.3389/fpls.2022.945675

Marchand, J., Heydarizadeh, P., Schoefs, B., & Spetea, C. (2018). Ion and metabolite transport in the chloroplast of algae: Lessons from land plants. *Cellular and Molecular Life Sciences*, *75*(12), 2153-2176. https://doi.org/10.1007/s00018-018-2793-0

Schönknecht, G., Hedrich, R., Junge, W., & Raschke, K. (1988). A voltage-dependent chloride channel in the photosynthetic membrane of a higher plant. *Nature*, *336*(6199), Art. 6199. https://doi.org/10.1038/336589a0

Spetea, C., Herdean, A., Allorent, G., Carraretto, L., Finazzi, G., & Szabo, I. (2017). An update on the regulation of photosynthesis by thylakoid ion channels and transporters in Arabidopsis. *Physiologia Plantarum*, *161*(1), 16-27. https://doi.org/10.1111/ppl.12568

Szabò, I., & Spetea, C. (2017). Impact of the ion transportome of chloroplasts on the optimization of photosynthesis. *Journal of Experimental Botany*, *68*(12), 3115-3128. https://doi.org/10.1093/jxb/erx063

Tester, M., & Blatt, M. R. (1989). Direct Measurement of K+ Channels in Thylakoid Membranes by Incorporation of Vesicles into Planar Lipid Bilayers 1. *Plant Physiology*, *91*(1), 249-252. https://doi.org/10.1104/pp.91.1.249

***

~ Research Article in preparation ~

An alternative pathway to CF_1F_O-ATPase for rapid dissipation of the proton motive force in *Chlamydomonas reinhardtii*

***

ARTICLE

An alternative pathway to CF_1F_O-ATPase for rapid dissipation of the proton motive force in *Chlamydomonas reinhardtii*

Marcio Rodrigues-Azevedo[a,b], Frédéric Chaux[a,c], Pierre Joliot[a], Francis-André Wollman[a], Catherine de Vitry[a,*], Benjamin Bailleul[a,*]

[a] *UMR7141 CNRS-Sorbonne Université, Institut de Biologie Physico-Chimique, Paris, France*

[b] *Doctoral School of Plant Sciences (SEVE) – ED567 Université Paris-Saclay*

[c] *UMR7238 CNRS-Sorbonne Université, Institut de Biologie Paris-Seine, Paris, France*

[*] Corresponding authors.

E-mail addresses: bailleul@ibpc.fr (B. Bailleul), catherine.devitry@ibpc.fr (C. de Vitry)

Keywords: **Chloroplast ATP synthase, Electrochromic shift, Electrochemical proton gradient, *Chlamydomonas*, KEA3, photosynthesis, thylakoid membrane.**

Abstract

Comparison of a chloroplast CF_1F_O-ATP synthase mutant (*ΔatpH*) and the wild-type (WT) strain in the green alga *Chlamydomonas reinhardtii* revealed an alternative pathway to dissipate the electrochemical proton gradient ($\Delta\mu H^+$) across the thylakoid membrane in the absence of CF_1F_O. Following a single turnover saturating flash, the $\Delta\mu H^+$ dissipation is 10 times slower in the absence than in the presence of CF_1F_O, consistent with the coupling of proton transfer across the membrane to the synthesis of ATP. Strikingly, after a pulse of intense light, we observed close-to-WT maximum rate of charge transfer across the thylakoid in the CF_1F_O deficient mutant (rate constant of approximately 40 s^{-1} vs 50 s^{-1} in the WT). This alternative pathway in the absence of CF_1F_O deactivates with a time constant of approximately 50 ms. It activates within tens of ms above a threshold close to the $\Delta\mu H^+$ threshold corresponding to proton leakage through CF_1F_O rotor - defining the maximum reachable $\Delta\mu H^+$ - in the WT. Unexpectedly, we detected dark-adapted $\Delta\mu H^+$ across the thylakoid in the absence of CF_1F_O, indicating that CF_1F_O-driven hydrolysis of ATP produced by mitochondrial respiration is not the only source of $\Delta\mu H^+$ in the dark in *Chlamydomonas reinhardtii*. Further analysis of *Chlamydomonas* mutants deficient in the thylakoid H^+/K^+ antiporter KEA3 showed that the alternative pathway is regulated by (but not strictly dependent on) KEA3. The loss of heterotrophy in the *KEA3 ΔatpH* highlights the crucial photoprotective role of this alternative pathway and the importance of its good entanglement with other ion channels in the thylakoid.

1. Introduction

The transfer of electrons along the photosynthetic chain is coupled to a transmembrane transfer of protons, from the stroma to the luminal space of the thylakoids. This promotes the generation of an electrochemical proton gradient ($\Delta\mu H^+$) across the thylakoid membrane, which comprises a proton gradient component (ΔpH) and an electric field component ($\Delta\Psi$) and plays a crucial role in photosynthesis (Mitchell, 1966). The proton motive force (PMF), which is the $\Delta\mu H^+$ divided by the Faraday

constant, is often used to express the sum of the electric and osmotic components with the unit of a membrane potential. The osmotic component of the PMF participates in the regulation of the electron transfer through photoprotection in photosystem II (Holt et al., 2004; Kramer et al., 2003) and the photosynthetic control of the turnover of the cytochrome b_6f (Joliot & Johnson, 2011; Nishio & Whitmarsh, 1993; Rumberg & Siggel, 1969). According to the chemiosmotic theory (Mitchell, 1966), $\Delta\mu H^+$ across the photosynthetic membrane provides the energy source for ATP synthesis by the chloroplast ATP synthase CF_1F_O. ATP synthesis in the CF_1 hydrophilic head is powered by the CF_O rotary motor in the thylakoid membrane. Other ion channels, such as KEA3 or VCCN1 (Uflewski et al., 2021) can participate in the dissipation of the $\Delta\mu H^+$ or in changes in its composition but their rates are considered to be slow compared to the CF_1F_O ATPase (Lemaire & Wollman, 1989a).

The presence of the thylakoid transmembrane electric field ($\Delta\Psi$) induces changes in the absorption properties of some of the photosynthetic pigments embedded in the thylakoid membrane, a phenomenon called electro-chemical shift (ECS). ECS is a powerful tool for the study of photosynthetic processes (Bailleul et al., 2010; Witt, 1979), in particular the probing of PMF *in vivo* or the activity of the CF_1F_O. *In vivo* studies of CF_1F_O activity have mainly relied on the kinetics of ECS after a single turnover flash of light. This kinetics displays three phases: (i) phase *a* takes place in less than 100 µs and corresponds to the electric field generated by photochemistry in photosystem II (PSII) and photosystem I (PSI), (ii) phase *b* takes place in ~10 ms and corresponds to the proton pumping activity of the cytochrome b_6f and (iii) phase *c*, which typically occurs in the 10 ms to 1 s range, reflects the dissipation of the PMF generated across the thylakoid by both previous phases. The last *c* phase is largely dominated by the movement of protons from the lumen to the stroma through the CF_1F_O ATPase and has long been used to quantify the activity of the latter *in vivo* (Buchert et al., 2021; Joliot & Delosme, 1974; Joliot & Joliot, 2008; Junge, 1970; Lemaire & Wollman, 1989b).

More recently, ECS kinetics following high light multiple turnover pulses (Buchert et al., 2021; Joliot & Joliot, 2008), together with resolved CryoEM structures (Hahn et al.,

2018), successfully confirmed the regulations of the CF_1F_O previously observed *in vitro* (Junesch & Gräber, 1987) and highlighted new ones. The activity of the complex is redox regulated, thanks to a cysteine couple in the γ-subunit interacting with the torque-transmitting βDELSEED-loop (Buchert et al., 2015). The activity of the CF_1F_O in its oxidized form (the situation in the dark-adapted cells used in this work) depends in two ways on the magnitude of the $\Delta\mu H^+$. $\Delta\mu H^+$ is the substrate of CF_1F_O of course, but it also regulates the rate constant of the enzyme itself. Below a $\Delta\mu H^+$ threshold, hereafter called ATPase activation threshold ($\Delta\mu H^+_{activation}$ in (Buchert et al., 2021)), the CF_1F_O is shut down, which can be visualized as a very slow (hundreds of ms to s) relaxation of the ECS signal. Above this threshold, ECS relaxation is rapid and almost entirely due to the proton movement through the ATPase coupled with ATP synthesis (Junesch & Gräber, 1987). The maximum attainable $\Delta\mu H^+$ under light is constrained by a second $\Delta\mu H^+$ threshold, the nature of which is not fully understood. A plausible hypothesis is that this second threshold corresponds to the movement (leakage) of protons through the CF_O rotor without coupling to ATP synthesis (Joliot & Joliot, 2008).

Whatever its nature, this second threshold (called $\Delta\mu H^+_{leak}$ in (Buchert et al., 2021)) is another absolute reference for the $\Delta\mu H^+$ and therefore allows an absolute quantification of the $\Delta\mu H^+$, according to a protocol which is best explained by a simple analogy: the unknown water volume in an opaque bottle can be estimated as the difference between the loading capacity of the bottle minus the amount of water that needs to be added until the water overflows (Buchert et al., 2021). Using such protocol, it was shown that a $\Delta\mu H^+$ exists in the dark in plants (Joliot & Joliot, 2008) and diatoms (Bailleul et al, 2015) that is strictly dependent on ATP produced in the mitochondria. The current model is that the chloroplast CF_1F_O ATPase hydrolyses the ATP imported from the mitochondria into the chloroplast until thermodynamic equilibrium is reached between $\Delta\mu H^+$ and [ATP]/[ADP][P], i.e. rates of ATP synthesis and ATP hydrolysis are equal. The presence of $\Delta\mu H^+$ in the dark was also shown in the green alga *Chlorella sorokiniana* (Finazzi & Rappaport, 1998) but other electrogenic pumps have been proposed to participate to its generation, in addition to CF_1F_O (Bennoun, 1994).

In this work, we decided to study the fate of $\Delta\mu H^+$ in a *Chlamydomonas reinhardtii* mutant lacking the chloroplast CF_1F_O ATPase. *Chlamydomonas reinhardtii* is a unicellular non-obligatory phototroph model organism suitable for the isolation of mutants lacking chloroplast CF_1F_O. In *Chlamydomonas*, the lack of the AtpH subunit, which constitutes the central ring of the CF_O rotor, leads to a pleiotropic loss of the other CF_1F_O subunits, as illustrated by the *ac46* mutant which does not express chloroplast-encoded AtpH subunit (Lemaire and Wollman, 1989; Majeran et al, 2001). Here, we used the *ΔatpH* mutant, which has a deletion of *AtpH* gene (Ozawa et al, 2020) and loses the whole CF_1F_O ATPase, to answer three specific questions. First, we wanted to test whether the $\Delta\mu H^+$ in the dark in *Chlamydomonas* is strictly dependent on the hydrolysis by CF_1F_O of ATP produced in the mitochondria, implying that $\Delta\mu H^+$ in the dark in the CF_1F_O mutant would be zero. Second, we wanted to challenge the idea that the maximum attainable $\Delta\mu H^+$ was given by the threshold of proton leakage through CF_O rotor. We reasoned that, if this hypothesis is true, the maximum attainable $\Delta\mu H^+$ in a mutant lacking CF_1F_O can only be higher than in the WT. A similar breakdown voltage in the two strains would on the contrary rule out this explanation and plead for the involvement of another molecular actor or process. Finally, we wanted to investigate the response of thylakoids to light stress in the absence of the main $\Delta\mu H^+$ sink. Does generation of large $\Delta\mu H^+$ by long pulses of intense light in the absence of CF_1F_O lead to irreversible damage such as loss of thylakoid integrity? To answer those questions, we measured the ECS kinetics induced by light perturbations (laser flash or intense light pulses of different durations) in the *ΔatpH* mutant and in the WT and investigated the fate of the light-induced PMF. Surprisingly, this study reveals and characterizes an alternative mode of PMF dissipation in the absence of chloroplast ATPase, which could be a photoprotective mechanism under physiological conditions where CF_1F_O activity is impaired.

2. Materials and methods

2.1. Strains and growth conditions

Wild-type (t222, mt^+), CC-5325 (cw15, mt^-), CF_1F_O deficient mutant (*ΔatpH* mt^+), *kea3* knockout (*kea3,* mt^-), and cross progeny strains of *Chlamydomonas reinhardtii* were grown mixotrophically at 25°C in Tris-acetate-phosphate (TAP) medium (Harris, 1989) under continuous light (5-10 µmol photons m^{-2} s^{-1}). Cross was performed according to Harris (1989). CC-5325 and *kea3* (KEA3 knockout LMJ.RY0402.115298) were obtained from the CLiP collection at the *Chlamydomonas* culture collection (Li et al, 2016; Li et al, 2019). The *APHVIII* cassette insertion in *KEA3* locus was tested by PCR using primers 5'-GCTCGACTTTCTCACGTTCC-3' and 5'-GCTGCAATAAACCTGGGCTA-3' (leading to an amplification product 1115 bp in absence of insertion) and by paramomycin resistant growth on TAP plates containing 10 µg mL^{-1} paramomycin. For biophysical measurements, cells were concentrated by centrifugation and resuspended in their growth medium (supplemented with 10% w/v Ficoll to prevent cell sedimentation) and kept under continuous light (5-10 µmol photons m^{-2} s^{-1}) at least 30 min before measurements.

2.2. Protein isolation and immunoblot analysis

Thylakoid membranes were isolated as described (Chua and Bennoun, 1975). Before electrophoresis, proteins from whole cells or from thylakoid membranes were resuspended in 200 mM 1,4-DTT and 200 mM Na_2CO_3 and solubilized in the presence of 2% SDS at 100°C for 50 s. Cell or thylakoid extracts were loaded on chlorophyll basis, separated by SDS-PAGE and electro-transferred onto nitrocellulose membranes (Amersham Protran 0.1 µm NC) by semi-dry method. After semi-dry transfer, membranes were stained in Ponceau (loading control). The blot membranes were incubated separately in primary antibodies against: AtpA (Drapier et al, 1992), AtpB (that recognizes $CF_1\beta$ and $F_1\beta$; Atteia et al, 1992), ATPC (Agrisera AS08312), AtpE (Agrisera AS101590), ATPG (Agrisera AS09457), AtpH (Agrisera AS09591). Primary antibodies were revealed by horseradish peroxidase-

conjugated antibodies against rabbit IgG (n° W401B, Promega). Signals were acquired in a ChemiTouch imaging system (Bio-Rad).

2.3. Photosynthesis measurements

Spectrometric measurements of ECS were performed in an absorption difference (Joliot-type) spectrometer (JTS-10, Biologic, Grenoble, France). Cells were harvested during exponential growth at a concentration of 2-5 10^6 cells/mL, centrifuged (3000 rpm, 5min, room temperature) and resuspended at a concentration of 1-2 10^7 cells/mL in its supernatant with Ficol to avoid cell sedimentation during measurements. Cells were kept under agitation in low light (5-10 µmol photons m^{-2} s^{-1}) for at least 30 minutes to promote optimal oxygenation of cells, until measurement in 1cm square plastic cuvettes. ECS signals were measured as the difference between absorbance transients at 520 nm and 546nm, to eliminate contributions from oxidized-minus-reduced signals from cytochrome *f* and, to a minor extent, P700, as well as signals related to light scattering. For the detecting pulses, we used a white led (Luxeon; Lumileds) and interferential filters at 520 ± 6 nm and 546 ± 6 nm (Schott, Mainz, Germany). The single turnover (6 ns) laser flashes and multiple turnover (few ms) pulses of high light were provided by a dye laser at 690 nm and a crown of red leds at 619 nm respectively. BG39 cut-off filters from Schott (Mainz, Germany) were placed in front of the photodiodes. Cells were thoroughly mixed and aerated before absorption measurements for each wavelength probed to allow aerobic conditions. Anoxic conditions were obtained by adding 20 mM glucose and 2 mg ml^{-1} glucose oxidase in a cuvette filled (4 mL) with the sample cell filled to the brim and closed with a cap and kept one minute in the dark prior to measurement. All ECS measurements are normalized to the fast increase of the ECS (520 - 546 signal) induced by the saturating laser flash. This fast increase, usually called *a* phase, represents the contribution of the photosystems. Since the extent of the *a* phase is proportional to the amount of active photosystems, this normalization allows to express the transmembrane electric field probed with ECS (520 - 546 signal) in positive charges in the lumen per photosystem.

For chlorophyll *a* fluorescence measurements (Supplementary Fig. 1), the JTS-10 was equipped with a white probing led (Luxeon; Lumileds) for the detecting pulses and a blue filter (470 nm) was put on the white light pulses. A LPF650 + RG 665 cut-off filter from Schott (Mainz, Germany) was placed on the measuring photodiode and a BG39 filter from Schott (Mainz, Germany) on the reference side. Quantum yield of PSII in light-adapted samples (Φ_{PSII}) was calculated as described in (Genty et al., 1989): $\Phi_{PSII} = (F_m' - F_{stat})/F_m'$, where F_{stat} is the fluorescence of the sample adapted to the actinic light and Fm' the fluorescence when a saturating pulse is applied on light-adapted sample.

For PSI measurements (Supplementary Fig. 1), the redox state of the PSI primary donor (P_{700}) was calculated as the difference between the absorption changes kinetic at 705 nm. The signal was corrected with the absorption changes kinetics at 735 nm, to eliminate spectrally flat contributions due to diffusion and plastocyanin. Data was normalized to the equivalent signal when 100% P700 was oxidized after a saturating pulse in the presence of the PSII inhibitor DCMU.

3. Results

To investigate the role of the chloroplast CF_1F_O ATPase in establishing the physiological limit for $\Delta\mu H^+$ and the dark value of $\Delta\mu H^+$, we used the *ΔatpH* mutant of the green alga *Chlamydomonas reinhardtii* lacking the CF_1F_O ATPase. The immunodetection of CF_1F_O subunits in membrane extracts of the *ΔatpH* mutant confirmed the pleiotropic loss of CF_1F_O ATP synthase subunits (**Fig. 1**A and **Fig. 1**B). As previously reported (Lemaire and Wollman 1989), the absence of CF_1F_O resulted in a 10-fold slower relaxation of the ECS after a single turnover saturating flash (see Methods) compared to the WT (**Fig.** 1C). In agreement with the coupling between generation of $\Delta\mu H^+$ and synthesis of ATP, the slow relaxation of its electric component indicates that $\Delta\mu H^+$ is no longer consumed by the ATP synthase in the *ΔatpH* mutant (**Fig. 1**C). All ECS data in the following will be normalized to the fast phase of the flash-induced ECS kinetics and will be expressed as positive charges per PS (see Methods). We will consider

in this manuscript, as in (Büchert et al, 2021), that changes in ECS, which strictly speaking inform about changes of Δψ, also measure changes in PMF for laser flashes or short pulses of <30ms which do not generate ΔpH.

3.1 An alternative pathway dissipates proton motive force in the absence of CF_1F_O ATPase

Secondly, we applied a multiple turnover pulse of high light to determine the physiological limit of the $\Delta\mu H^+$ in the absence of CF_1F_O. The maximum increase in ECS induced by the pulse in the *ΔatpH* mutant (expressed as positive charges per photosystem, see Methods) greatly exceeds that of the wild-type (**Fig. 1**D). In the WT, the maximum value is about 4 positive charges per PS, i.e. four times the value obtained after a single turnover flash. The monophasic rapid decay of the ECS after the pulse, completed in less than 100 ms, is in line with an active CF_1F_O and indicates that the $\Delta\mu H^+$ in the dark (baseline) is above $\Delta\mu H^+_{activation}$. In the absence of CF_1F_O, the maximum value is more than twice as high (~9 positive charges per PS). Strikingly and unexpectedly, we also observed a very rapid phase of Δψ decay at the end of the 30 ms high light pulse in the *ΔatpH* mutant. The rate constant of this fast phase of charge transfer across the thylakoid in the absence of CF_1F_O (~42 s^{-1}) was close to that of wild-type (~59 s^{-1}) revealing an unexpected alternative pathway of PMF dissipation (**Fig. 1**D). After this rapid decay phase completed in less than 100 ms, the relaxation to baseline (dark-adapted value) requires a very slow second phase that exhibits a time constant similar to that measured after the single turnover flash.

3.2 Analysis of maximum and dark PMF in wild-type and ΔatpH mutant

Before characterizing this new alternative valve, we estimated that the experiment shown in **Fig. 1**D was not sufficient to definitely validate the model proposed by Joliot & Joliot (2008) of a proton leak through the CF_O rotor determining the maximum $\Delta\mu H^+$. This hypothesis implies that the *absolute* $\Delta\mu H^+$ in the *ΔatpH* mutant exceeds the maximum and unsurpassable $\Delta\mu H^+_{leak}$ in the presence of CF_1F_O (in the WT). However, we only measured values *relative* to the unknown baseline value in **Fig. 1**D, i.e. the already $\Delta\mu H^+$ present in the dark before the light pulse in oxic conditions. At this stage,

it is not possible to exclude that this baseline varies between the WT and the mutant, since CF_1F_O can generate $\Delta\mu H^+$ from ATP hydrolysis in the dark. If the dark $\Delta\mu H^+$ in the WT is higher than the one of the *ΔatpH* mutant by 5 positive charges per PS (i.e. the difference between the amplitudes of the pulse-induced ECS increase in the *ΔatpH* mutant and the WT, 9 and 4 positive charges per PS, respectively), this would mean that the maximum attainable value is the same in the two strains and would argue for another actor setting this value, present in both strains. In oxic conditions in the dark, the $\Delta\mu H^+$ is strictly dependent on the mitochondrial respiratory process which is virtually the only source of ATP (Bennoun, 1994; Bailleul et al, 2015). To compare the absolute values of $\Delta\mu H^+$ in the two strains, we decided to carry out the same experiment in anoxia. Anoxia causes the cessation of mitochondrial ATP production, which is linked to the stromal pool of ATP in the chloroplast (Bennoun, 1994). At thermodynamic equilibrium, the absence of stromal ATP suppresses $\Delta\mu H^+$ in the dark (**Fig. 2**A). Note that, in turn, when $\Delta\mu H^+$ reaches values below the previously discussed threshold value ($\Delta\mu H^+_{activation}$, see Introduction) CF_1F_O is shut down, resulting in slow ECS relaxation (Junge 1970). The very slow rate of ECS decay after a single turnover saturating flash in the wild-type strain (~2 charges PS^{-1} s^{-1} vs 22 charges PS^{-1} s^{-1} under oxic conditions, **Fig. 2**B) confirmed dark $\Delta\mu H^+$ suppression in wild-type. Similar rates were found in the *ΔatpH* mutant (~0.5 charges PS^{-1} s^{-1} vs 2 charges PS^{-1} s^{-1} under oxic conditions, **Fig. 2**B).

From anoxic conditions ensuring that the $\Delta\mu H^+$ in the dark is as close to absolute zero as possible (i.e. the opaque bottle is empty in our analogy), it becomes possible to determine the maximum attainable $\Delta\mu H^+$ (i.e. the loading capacity of the bottle) in absolute values. In WT, the maximum ECS increase during a 30 ms light pulse in anoxia, which represents the maximum attainable value, is approximately 7 charges PS^{-1} (**Fig. 2**C), whereas it was about 4 charges PS^{-1} in oxia (**Fig. 1**D). This indicates that a $\Delta\mu H^+$ of approximately 3 charges PS^{-1} pre-exists the pulse in the dark and is suppressed in the absence of oxygen, consistent with its generation by CF_1F_O -driven hydrolysis of respiratory produced ATP. The maximum attainable value in anoxia fixes the $\Delta\mu H^+_{leak}$ at ~7 charges PS^{-1}. After the pulse, the ECS decay shows two distinct phases: a fast phase

completed in less than 100 ms and a slow phase with a time constant of ~2 s^{-1}. The transition between those two phases (extrapolation of the slow phase), which represents the transition from an active to an inactive CF_1F_O, occurs at $\Delta\mu H^+_{activation}$ ~3 charges PS^{-1}.

In the absence of CF_1F_O, the maximum attainable value was found to be almost twice as high in the CF_1F_O deficient mutant (~12 charges PS^{-1}, **Fig. 2**D) than in the wild-type strain (~7 charges PS^{-1}, **Fig. 2**C), validating unambiguously that the $\Delta\mu H^+_{leak}$ in the wild-type is determined by the CF_1F_O itself. The comparison of the maximum attainable value under oxic and anoxic conditions in the *ΔatpH* mutant is also very instructive. Surprisingly, the maximum ECS increase in anoxia is about 3 charges PS^{-1} higher than in oxia (**Fig. 2**D), which highlights a dark $\Delta\mu H^+$ of about 3 charges PS^{-1} similar to WT. This clearly excludes the current model that the $\Delta\mu H^+$ present in the dark under oxic conditions is strictly dependent on ATP hydrolysis by CF_1F_O. In the absence of CF_1F_O, another O_2-dependent (or ATP-dependent) electrogenic process may generate such $\Delta\mu H^+$ (see Discussion). In the *ΔatpH* mutant, the ECS decay after the pulse displays two distinct phases in both oxia and in anoxia, a slow phase with a time constant ≤ 2 s^{-1} similar to what was observed after a single turnover flash and an unexpected rapid phase completed in less than 100ms. The analysis of the rapid phase of ECS decay gave rate constants for the charge dissipation of approximately 42 and 31 s^{-1} in oxia and anoxia respectively, very close to the rates of charge dissipation by CF_1F_O in the WT (approximately 59 and 36 s^{-1} in oxia and anoxia respectively).

3.3 Characterization of the alternative PMF dissipator

The surprising observation of phase of ECS decay after a strong light pulse in the absence of CF_1F_O prompted us to characterize the properties of this alternative PMF dissipation valve. We first thought that since such a rapid decay occurs after multiple turnover pulses but not after single turnover flashes (**Fig. 1 &2**), there must be a light-dependent activation of this process. We wondered how long the light pulse must last or how high the $\Delta\Psi$/PMF must reach before this

alternative pathway activates. We varied the duration of the light pulse from 1 ms to 150 ms (keeping the same intensity) under oxic and anoxic conditions (**Fig. 3**A left or right panel, respectively).

During the light pulses, the ECS increases up to a maximum value (after ~25 ms in oxia, after ~35 ms in anoxia) then decreases. The decrease in the electric field across the membrane reflects both the slowing of the proton input related to PSI and PSII photochemistry (see Supplementary **Fig. 1**) and the acceleration of the rate of the alternative pathway, as illustrated by the acceleration of the post-illumination decay in the dark. The steady state value of the ECS (nearly reached after 150 ms of high light pulse) indicates that the rate of electric field generation by PSII, PSI and cytochrome b_6f is compensated by the activity of this alternative valve. The rate of the alternative pathway can best be studied during post-illumination relaxation of the ECS. For short pulses (<10ms), ECS relaxation takes longer than 1 s and did not show a clear fast phase. The slow phase was then compatible with the electric permeability of the thylakoid measured on a single turnover flash. For longer pulses allowing the ECS to reach the maximum value (~25 ms in oxia, after ~35 ms in anoxia), the total ECS relaxation still lasts more than 1 s but a fast phase appears, which even dominates the relaxation for pulses between 50 and 150 ms.

To better characterize the amplitude and rate of this fast phase that we attribute to an unknown PMF valve, we fitted all the experimental ECS decay kinetics in the dark with by a bi-exponential function (Supplementary **Fig. 2** and Supplementary **Fig. 3**, R^2 > 0.99 for all the fits). Since the slow phase is homothetic between all the curves (Supplementary **Fig. 2** and Supplementary **Fig. 3**), we shared the same rate constant for the slow phase whatever the pulse duration (**Fig. 3**C), which implies that the slow phase is a constitutive process whose rate constant is not regulated. The fast phase varied in amplitude and rate constant. We found that the rate constant of the fast phase representing the alternative valve increased from 0 to 40-50 s^{-1} (**Fig. 3**C) and its maximum amplitude increased from 0 to approximately 4 positive charges PS^{-1} (**Fig. 3**B)

for 50 ms pulses, both in oxia and anoxia. In total, the data show that the maximum value for the rate constant of the alternative pathway is 40-50 s^{-1}, close to the maximum value of the rate constant for the CF_1F_O (~60 charge s^{-1}, see **Fig. 1**). The delay between the high light pulse duration required for full activation of the alternative pathway (~50 ms, **Fig. 3**C) and that required for the maximum pulse amplitude (25 - 35 ms, **Fig. 3**A/B) suggests that the activation of this alternative pathway is not immediate but requires few tens of milliseconds. To confirm that the phenotype observed in the *ΔatpH* mutant is linked to the absence of CF_1F_O and not to the side effects of the mutation, we analyzed 3 other mutants carrying a deletion (or altered in translation) of other subunits of the CF_1F_O (F54 affected in TDAI, translation factor of *atpA*; Fud50, harboring a deletion in the chloroplastic atpB gene; Fud18, altered in the chloroplastic *atpF* gene). All of these mutants showed pleiotropic loss of other CF_1F_O subunits and all exhibited behavior similar to that of *ΔatpH* mutant in anoxic conditions (Supplementary **Fig. 4**). Flash-induced ECS decay was very slow (rate constant of 2-3 s^{-1}) in all mutants and acceleration of ECS decay above a threshold indicates the presence of an alternative PMF valve with maximum rate constants ranging from 35 to 60 s^{-1}. The same analysis was performed on the WT (see Supplementary **Fig. 5** and Supplementary **Fig. 6** for oxic and anoxic conditions, respectively) and indicated that the maximum rate constant for the active CF_1F_O was very similar as the one of the alternative PMF valve: 45-60 s^{-1}.

3.4 Analysis of the alternative pathway deactivation

We also wanted to determine how long it takes for the alternative pathway to turn off once the PMF relaxes back to its dark-adapted value. To test this, we used a high light pulse of 50 ms or more to allow strong activation of the alternative valve and a rapid relaxation of ECS to baseline. Once the ECS relaxed, we added a single turnover laser flash at different times after the end of the pulse (**Fig. 4**A). The decay rate of the flash-induced transmembrane electric field provided us with an estimate of the alternative valve activity. By doing so, only the time after light pulse varied, all other things being equal. We observed that, as long as the flash was applied less than 200 ms

after the light offset, the decay rate was significantly faster than for a single turnover flash applied in darkness (**Fig. 4**B). The rate constants of post-flash ECS decay (see legend of **Fig. 4**B) decrease mono-exponentially with time between pulse and laser flash (**Fig. 4**C). The half-life of the rate constant decay kinetics was estimated as 68 ± 4 ms, which we attribute to the deactivation time of the alternative valve.

3.5 Analysis of the alternative pathway in KEA3 knock-out mutants

The thylakoid membrane localized proton/cation K^+ exchange antiporter 3 (KEA3) that exchanges proton with potassium across the thylakoid can modulate the two components of the PMF, the proton gradient (ΔpH) and the electric field (ΔΨ), in *Arabidopsis* (Armbruster et al, 2014; Kuntz et al, 2014; Wang et al, 2017; Wang and Shikanai, 2019; Correa Galvis et al, 2020) and in diatoms (Seydoux et al, 2022). In doing so, it plays an important role in optimizing photosynthesis since the osmotic component (ΔpH) is the master regulator of both photoprotection in photosystem II and photosynthetic control of cytochrome b_6f turnover (Kramer et al, 2003).

We obtained *kea3 ΔatpH* double mutants in *Chlamydomonas*, by crossing the nuclear insertion knock-out *kea3* (mt^-) mutant with the chloroplast *ΔatpH* (mt^+) mutant. The chloroplast inheritance being uniparental by the mt^+ parent, all the cross progeny possessed the *ΔatpH* mutation. As the *APHVIII* cassette inserted in the *KEA3* gene confers paromomycin resistance, we identified the *kea3* {*ΔatpH*} double mutants in the progeny by the absence of PCR amplification in the 1 kb region at the *KEA3* locus when the cassette is inserted (**Fig. 5**A) and by growth resistance to paromomycin (**Fig. 5**B) which was correlated. As expected, tetrad 1 exhibited a 2:2 Mendelian segregation of *kea3* nuclear mutation. Double *kea3 ΔatpH* mutants (T1.1 and T1.2) and single *ΔatpH* mutants (T1.4 and parental strain *ΔatpH*) were used to quantify the alternative valve activity (T1.3 could not grow on acetate in the dark and was discarded from analysis). Using the same protocol as in **Fig. 3**, we extracted the fast phase associated with the alternative valve and analyzed its amplitude and rate constant as a function of high light pulse duration, under oxic conditions (**Fig. 5**C/D). As expected, the parental strain *ΔatpH*

and T1.4 achieved similar activation of the alternative valve (k ~ 40 s^{-1} for 50 ms pulses, **Fig. 5**C) and same maximum amplitude of the fast phase (4.5-5 positive charges PS^{-1} for pulses of 30ms, **Fig. 5**D). Fast phase characteristics were very similar between the two double mutants (T1.1 and T1.2) but showed significant differences with the single mutants. Although the maximum amplitude was similar between the double and single mutants, the maximum rate constant for the fast phase (15-25 s^{-1}) was significantly lower. In addition, the alternative valve activation was significantly slowed with the maximum rate constant and amplitude only being reached for 50 and 80 ms pulses, respectively. Interestingly, in the presence of CF_1F_O, KEA3 did not have significant influence on the fate of the PMF, as illustrated by the similar ECS decay kinetics between the *kea3* single mutant and the wild type used to generate it (CC-5325, Supplementary **Fig. 7**). Those results indicate that KEA3 greatly influences the activity of the alternative PMF valve identified in this work. However, KEA3 does not seem to be strictly required for the activation of this alternative PMF dissipation since the maximum rate constant measured in the double *kea3 ΔatpH* mutants is 10-fold higher than that measured after a single turnover flash.

To determine the importance of KEA3 and alternative valve activities on the fitness of *Chlamydomonas*, we decided to test the growth and photosensitivity of single and double mutants. As expected, the *ΔatpH* parental strain and progeny could not grow under phototrophic conditions (MIN medium) but all strains were able to grow in the presence of acetate (TAP medium) under low light (6 µmol photons m^{-2} s^{-1}) (**Fig. 5**B). Under higher irradiance (30 µmol photons m^{-2} s^{-1}), both double mutants T1.1 and T1.2 died indicating that the presence of KEA3 is crucial for survival in the absence of CF_1F_O (**Fig. 5**B). We propose that the crucial role of KEA3 is to regulate the alternative valve described here in order to avoid intense PMF formation that would otherwise cause irreversible damage to the thylakoids, which might be relevant in physiological conditions that alter CF_1F_O activity or promote its degradation.

4. Discussion

In this work, an alternative PMF dissipation valve was evidenced by the existence of a rapidly decaying phase of the membrane potential generated across CF_1F_O-devoid thylakoids after intense light pulses of more than 20-30 ms. Despite the large number of CF_1F_O mutants generated over the past few decades, such a phenomenon has not been reported, which could be the consequence of the almost exclusive use of ECS measurements based on single turnover laser flash for the *in vivo* characterization of CF_1F_O activity. This work illustrates the limit of such an approach and argues for the use of ECS measurements following multiple turnover pulses of strong light, as has been done previously in leaves (Joliot and Joliot, 2008; Buchert et al, 2021) and in *Chlamydomonas* (Buchert et al, 2017). Only this approach makes it possible to describe all the phases of electric (or proton) permeability of the thylakoid membranes, how the ion and proton movements depend on the value of PMF. Pulse-induced ECS measurements can also determine where physiological $\Delta\mu H^+$ lies in a given condition relative to (absolute) threshold values of $\Delta\mu H^+$, all of which are key values around which the following discussion will be structured.

4.1 When $\Delta\mu H^+$ is between 0 and $\Delta\mu H^+_{activation}$

When $\Delta\mu H^+$ is below the threshold for activation of the (oxidized) CF_1F_O ATPase, the ECS decay displays a slow phase with lasting several hundred milliseconds or a few seconds. This slow phase can only be observed when the CF_1F_0 is in its oxidized state, which is the dark physiological situation in plants; in the reduced state, the ATPase never enters an inactive mode and the ECS kinetics after a light pulse displays a monophasic decay (Buchert et al, 2021). The biphasic ECS decays we collected from anaerobic WT and *ΔatpH* mutant indicate that the CF_1F_O is also in the oxidized state in dark-acclimated *Chlamydomonas*. The slow phase below $\Delta\mu H^+_{activation}$ is best observed (and the constant rate associated to leak of protons across the thylakoid membrane is best estimated) in physiological situations ensuring that $\Delta\mu H^+$ is as close to absolute zero as possible. In plants, such situation was first approached by the use of antimycin A, an inhibitor of the

cytochrome bc_1 (complex III) of the respiratory electron transfer chain (Joliot & Joliot, 2008). Recently, it was shown that this treatment was not sufficient to fully suppress the dark $\Delta\mu H^+$ due to the remaining activity of the alternative oxidase AOX. Using a combination of antimycin A and SHAM to completely inhibit respiration or using thylakoid uncouplers cleared all $\Delta\mu H^+$ in the dark (Buchert et al, 2021). Here, we decided to use anaerobic treatment to arrive at the situation where the $\Delta\mu H^+$ in the dark is close to zero in *Chlamydomonas*. It should be noted that the absence of O_2 does not automatically mean that the production ATP in the cell is stopped: the fermentation pathways can supply ATP in anaerobic conditions and lead to a $\Delta\mu H^+$ generation in the dark (Joliot & Joliot, 1989; Finazzi & Rappaport, 1998). However, the experiments here were performed right after the anoxia was reached, whereas fermentation pathways typically take hours to express (Joliot & Joliot 1989). We therefore believe that no ATP-driven or O_2-driven electrogenic pump across the thylakoids is at work in the anoxic conditions we studied, although we cannot exclude that an electrogenic network of ion channels, independent of ATP and O_2, is at work and provides residual $\Delta\mu H^+$. In plants, the electric permeability of the lipid bilayer was considered negligible and the slow ECS decay at low $\Delta\mu H^+$ was interpreted as the consequence of 2-3 % of CF_1F_O remaining active (in its reduced form?) below the activation threshold $\Delta\mu H^+_{activation}$. The measured rate constants of the slow phase of ECS decay in this work support this view (**Fig. 2**B/C). Indeed, in the absence of CF_1F_O, the rate constant of ECS decay was about 0.5 s^{-1}, 1.5 s^{-1} lower than the value in the WT (~2 s^{-1}) and this difference is compatible with the activity of 3% active CF_1F_O since the maximum rate constant of the CF_1F_O measured in the WT was ~50 s^{-1} (see Supplementary **Fig. 5** and Supplementary **Fig. 6**).

4.2 Relative values of dark $\Delta\mu H^+$ and $\Delta\mu H^+_{activation}$

Under oxic conditions, the slow phase described in the previous section is not observed in the WT (**Fig. 1**C/D), indicating that the dark-acclimated $\Delta\mu H^+$ is greater than or equal to the $\Delta\mu H^+_{activation}$ threshold. Based on the difference between the amplitude of the pulse-induced ECS in oxia and anoxia, we estimated the dark $\Delta\mu H^+$ in the WT to

be approximately 3 charges PS^{-1}. The amplitude of the slow phase of ECS decay in the WT under anoxic conditions (**Fig. 1**C and Supplementary **Fig. 6**) suggests that the $\Delta\mu H^{+}_{activation}$ threshold is between 2 and 3 charges PS^{-1}. This means that under oxic conditions the ATP imported from mitochondrion makes it possible to generate a $\Delta\mu H^{+}$ just sufficient to activate the CF_1F_O ATPase in *Chlamydomonas*. This is in agreement with recent reports and could be due to a different regulation of the CF_1F_O in *Chlamydomonas* compared to plants (Lando & Buchert, 2022). In plants, the dark $\Delta\mu H^{+}$ is suppressed in conditions of pharmacological inhibition of the respiratory electron transfer chain or absence of its substrate O_2 in anaerobic conditions. This led to the current model (**Fig. 2**A) where the generation of such a $\Delta\mu H^{+}$ in the dark strictly depends on the hydrolysis by CF_1F_O of ATP produced outside of the chloroplast. Comparison of WT and *ΔatpH* mutant goes against this model since a similar dark $\Delta\mu H^{+}$ can be generated in the absence of CF_1F_O. This suggests the presence of another electrogenic pump which can replace CF_1F_O in its electrogenic role and whose activity is suppressed in the absence of O_2. It is tempting to propose that chlororespiration is such O_2-dependent electrogenic pump. Chlororespiration is a minimal respiratory pathway in the thylakoid membrane that involves both the oxidation of plastoquinols (PQH2) by the plastid terminal oxidase (PTOX) (Diner and Mauzeral, 1973) and the reduction of plastoquinones by a NAD(P)H dehydrogenase (Sazanov *et al.*, 1998). Chlororespiration is O_2-dependent and, in plants, participates to the generation of $\Delta\mu H^{+}$ in the dark through the proton pumping activity of the type I NAD(P)H dehydrogenase (Trouillard et al, 2012). *Chlamydomonas* has a chlororespiratory pathway (Nawrocki et al, 2015 ; Bennoun, 1982) which involves two expressed PTOX enzymes, PTOX2 being the main oxidase with a rate ~10 fold faster than PTOX1 (Houille-Vernes et al., 2011) and a monomeric NAD(P)H dehydrogenase 2 (NDA2) (Jans et al., 2008) which plays the same PQ reducing role as the plant NDH-1. NDA2 is a membrane-bound monomeric enzyme located on the stromal side of the membrane and is not electrogenic (Peltier et al., 2016) ; (Melo et al., 2004) unlike NDH-1 (Strand et al., 2017). Although chlororespiration was initially proposed to generate an electrochemical proton gradient in

Chlamydomonas, this model was later disproven because of the lack of electrogenicity of NDA2 and the position of both PTOX and NDA2 on the stromal side of the thylakoid (Bennoun, 1994). For this reason, the suppression of dark $\Delta\mu H^+$ in anaerobiosis probably does not arise from an O_2-requirement for the alternative pump, but rather from an indirect role of O_2. Obvious candidates for such generation of dark O_2-dependent $\Delta\mu H^+$ in the *ΔatpH* mutant would be other types of ATPases embedded in the thylakoid membranes. The thylakoid copper-transporting P-type ATPase HMA8 found in plant thylakoids would be a good candidate but no homolog is found in *Chlamydomonas* (Migeon et al, 2010). Since ATPases use ATP as a substrate and ATP production is suppressed in the dark under anoxic conditions, this would easily explain the O_2-dependence of the dark $\Delta\mu H^+$ in the absence of CF_1F_O. Note that once the thermodynamic equilibrium is reached in the dark, the electrochemical gradient associated with the pumped ion (whether it is Cu^{2+}, H^+ or another) would be given by the ratio [ATP]/[ADP][P], regardless of the nature of the ATPase. This is consistent with the similar $\Delta\mu H^+$ measurement in the dark in the WT and the *ΔatpH* mutant. Interestingly, such an ATP-driven electrogenic pump was already postulated in the green alga *Chlorella sorokiniana* (Rappaport et al, 1999). In the case of *Chlorella sorokiniana*, this pump was suggested to have a specificity for ions other than protons (Rappaport et al, 1999). Many transporters in the thylakoid – including ATPases – are probably awaiting discovery.

4.3 When $\Delta\mu H^+$ is between $\Delta\mu H^+_{activation}$ and $\Delta\mu H^+_{leak}$

Regardless of the relative importance of CF_1F_O and alternative ATP-driven electrogenic pumps in the process, it is clear that $\Delta\mu H^+$ across the thylakoid occurs in the dark as long as cellular ATP is not suppressed. Under oxic conditions, the cellular ATP pool is mainly produced by mitochondrial respiration but ATP is also produced by fermentative processes provided cells are placed under anoxic conditions for long periods of time. When this dark $\Delta\mu H^+$ is less than $\Delta\mu H^+_{activation}$, the ECS decay following a light perturbation (representing dissipation of the PMF) displays both a fast phase

(CF_1F_O activated) and a slow phase (CF_1F_O inactivated). When this dark $\Delta\mu H^+$ is greater than $\Delta\mu H^+_{activation}$, the ECS decay shows a monophasic decrease. In this work, we have measured monoexponential ECS decays after light pulses or flashes and estimated the rate constant of the ECS decay due to activated ATPase to be approximately 50 s^{-1}. Since the maximum amplitude of the fast phase of ECS decay was approximately 4 in the WT, this gives a maximum rate of ~200 protons s^{-1} transferred from lumen to stroma through activated ATPases at the offset of a 30-50 ms high light pulse. The maximum amplitude of the fast phase is another important parameter. As discussed previously (Joliot & Joliot, 2008), this maximum amplitude is set by two absolute limit values for the $\Delta\mu H^+$: the threshold of activation/inactivation of the CF_1F_O, $\Delta\mu H^+_{activation}$, and a threshold identified as a rapid proton leakage across the thylakoid, $\Delta\mu H^+_{leak}$. Both threshold values were shown to be absolute $\Delta\mu H^+$ references because they both responded to $\Delta\psi$ and ΔpH (Joliot & Joliot, 2008).

Three possibilities have been proposed for the origin of this fast phase above a threshold $\Delta\mu H^+$, (i) opening of specific membrane channels, (ii) leakage/slip of protons through the CF_O rotor but not coupled to ATP synthesis (when the rate of synthesis at the level of CF_1 complex has reached its maximum value while the rotational speed of the CF_O rotor still increases), (iii) an unlikely increase in the activity of ATPase. In this work, we used a strain deficient in CF_1F_O to challenge the hypothesis of a proton leak through the CF_O rotor. The observation that the maximum achievable $\Delta\mu H^+$ in the *ΔatpH* mutant was approximately 70% higher than in WT (~12 vs ~7 positive charges PS^{-1}) validates this model. It is important to note that the absolute values of $\Delta\mu H^+$ are expressed as positive charges PS^{-1} after normalizing by the ECS increase due to a saturating laser flash (see Methods). The possibility of providing such internal calibration is undoubtedly a practical aspect of ECS methodology (Mathiot & Alric, 2021). However, this makes the comparison between independent samples more complicated: we cannot reject the possibility that the concentration of photosystems in the thylakoid is slightly different in one sample and another. In our case, this means that the ratio of the absolute

$\Delta\mu H^+_{leak}$ (expressed in kJ mol^{-1}) between the *ΔatpH* mutant and WT could be slightly different from 1.7 (12/7) if the photosystem density varied between the two strains.

4.4 When $\Delta\mu H^+$ exceeds $\Delta\mu H^+_{leak}$

As shown in plants (Joliot & Joliot, 2008; Buchert et al, 2021), it is possible to reach $\Delta\mu H^+$ slightly higher than $\Delta\mu H^+_{leak}$ by using extremely high light pulses. In that case, a very rapid phase of small amplitude in the ECS decay is observed until the $\Delta\mu H^+$ reaches $\Delta\mu H^+_{leak}$ which represents the proton leak through CF_O. The situation is extremely different in the absence of CF_1F_O. At high PMF, we observed in the *ΔatpH* mutant a rapid PMF dissipation valve that can reach ECS decay rates of 40 s^{-1}, close to the rate constant associated to active CF_1F_O in the WT. It is difficult to define the threshold of activation/inactivation of this alternative valve during the pulse-induced ECS increase. However, the break in the ECS kinetics during the ECS relaxation is evident (**Fig. 3**A). The amplitude of the slow phase is always between 5 and 6 charge PS^{-1} for long pulses (**Fig. 3**B), which indicated that the alternative valve inactivates when the $\Delta\mu H^+$ reaches such values. These values are just below the $\Delta\mu H^+_{leak}$ which represents the maximum value of $\Delta\mu H^+$ in the WT (~7 charges PS^{-1}). This means that the proton leakage through CF_O (observed only in the WT) would activate at slightly higher $\Delta\mu H^+$ than the alternative valve (observed only in the *ΔatpH* mutant). It is an open question whether this alternative valve is present or absent in the WT. One could imagine that the molecular actor necessary for the alternative valve is only expressed (or over-expressed) in the absence of CF_1F_O. It is also possible that it is present in the WT but the proton leak through CF_O short-circuits the activity of this alternative valve. Regardless of their co-existence or not, we believe that the proton leak through CF_O and the alternative valve identified in this work represent two "security valves" which protect the thylakoid integrity and photosynthesis function by avoiding harmful consequences due to excessive PMF.

The nature of the alternative valve is the most intriguing question. We speculate that the alternative valve could be a single actor (**Fig. 6**, left panel), a network of ion channels (**Fig. 6**, middle panel) or a non-enzymatic process determined by the electric permeability of the lipid bilayer (breakdown voltage, **Fig. 6**, right panel). The simplest molecular model would be that a major ion transporter not strictly dependent on KEA3 is activated above the threshold $\Delta\mu H^+$ in absence of CF_1F_O. As the thylakoid membrane encompasses numerous ion channels, transporters and pumps (Spetea et al, 2017; Marchand et al, 2018), a model involving several of them in the PMF alternative decay would be likely (**Fig. 6**, middle panel). This is in line with the role of the K^+/H^+ exchanger KEA3. We observed that the fast dissipation pathway across the thylakoid membrane is not strictly dependent on KEA3. It is however regulated by KEA3 since the amplitude and rate constant of the fast phase were lower in the double mutants *kea3 ΔatpH* than in the single *ΔatpH* mutants (**Fig. 5**C/D). Another possibility is that the activation of the dissipation pathway above a threshold results from a reversible and transient membrane permeabilization/poration due to the excessive accumulation of protons (**Fig. 6**, right panel). Major structural changes were shown to result from the light-induced PMF in the absence of chloroplast ATP synthase activity in *Chlamydomonas* with considerable swelling of the thylakoids already apparent after 30 min of moderate light (70 µmol photons m^{-2} s^{-1}) and prevented by adding uncouplers (Majeran et al, 2001). Little is known about how thylakoid membrane integrity is maintained. In cyanobacteria, mutations in VIPP1 hydrophobic residues caused extreme thylakoid swelling under high light and it was proposed that VIPP1 plays an essential role in lipid binding and resisting stress-induced damage (Gupta et al, 2021). Combining nuclear mutations leading to deficiencies in candidate ion channels with the chloroplast *ΔatpH* mutation, will allow us in the future to learn more about the nature of this alternative valve, which for the moment remains a mystery.

Acknowledgements

B.B. and M.R.A. acknowledge funding from the ERC Starting Grant PhotoPHYTOMICS (ERC-2016-STG grant #715579). M.R.A. obtained a Ministry's doctoral contract and is registered to the Doctoral School of Plant Sciences (SEVE) – ED567 Université Paris-Saclay. This work was also supported by the Centre national de la Recherche Scientifique and Sorbonne Université (basic support to Unité Mixte de Recherche 7141) and by the 'Initiative d'Excellence' program from the French State (Grant DYNAMO, ANR-11-LABX-0011-01).

References

Aguirre, G., & Pilon, M. (2015). Copper Delivery to Chloroplast Proteins and its Regulation. *Frontiers in Plant Science*, *6*, 1250. https://doi.org/10.3389/fpls.2015.01250

Bailleul, B., Berne, N., Murik, O., Petroutsos, D., Prihoda, J., Tanaka, A., Villanova, V., Bligny, R., Flori, S., Falconet, D., Krieger-Liszkay, A., Santabarbara, S., Rappaport, F., Joliot, P., Tirichine, L., Falkowski, P. G., Cardol, P., Bowler, C., & Finazzi, G. (2015). Energetic coupling between plastids and mitochondria drives CO2 assimilation in diatoms. *Nature*, *524*(7565), Art. 7565. https://doi.org/10.1038/nature14599

Bailleul, B., Cardol, P., Breyton, C., & Finazzi, G. (2010). Electrochromism : A useful probe to study algal photosynthesis. *Photosynthesis Research*, *106*(1-2), 179-189. https://doi.org/10.1007/s11120-010-9579-z

Baudelet, P.-H., Ricochon, G., Linder, M., & Muniglia, L. (2017). A new insight into cell walls of Chlorophyta. *Algal Research*, *25*, 333-371. https://doi.org/10.1016/j.algal.2017.04.008

Bennoun, P. (1994). Chlororespiration revisited : Mitochondrial-plastid interactions in Chlamydomonas. *Biochimica et Biophysica Acta (BBA) - Bioenergetics*, *1186*(1), 59-66. https://doi.org/10.1016/0005-2728(94)90135-X

Blaby-Haas, C. E., & Merchant, S. S. (2012). The ins and outs of algal metal transport. *Biochimica et biophysica acta*, *1823*(9), 1531-1552. https://doi.org/10.1016/j.bbamcr.2012.04.010

Blaby-Haas, C. E., & Merchant, S. S. (2017). Regulating cellular trace metal economy in algae. *Current Opinion in Plant Biology*, *39*, 88-96. https://doi.org/10.1016/j.pbi.2017.06.005

Buchert, F., Bailleul, B., & Joliot, P. (2021). Disentangling chloroplast ATP synthase regulation by proton motive force and thiol modulation in Arabidopsis leaves. *Biochimica et Biophysica Acta (BBA) - Bioenergetics*, *1862*(8), 148434. https://doi.org/10.1016/j.bbabio.2021.148434

Buchert, F., Konno, H., & Hisabori, T. (2015). Redox regulation of CF1-ATPase involves interplay between the γ-subunit neck region and the turn region of the βDELSEED-loop. *Biochimica Et Biophysica Acta*, *1847*(4-5), 441-450. https://doi.org/10.1016/j.bbabio.2015.01.013

Croce, R., & van Amerongen, H. (2014). Natural strategies for photosynthetic light harvesting. *Nature Chemical Biology*, *10*(7), Art. 7. https://doi.org/10.1038/nchembio.1555

Dukic, E., Herdean, A., Cheregi, O., Sharma, A., Nziengui, H., Dmitruk, D., Solymosi, K., Pribil, M., & Spetea, C. (2019). K+ and Cl− channels/transporters independently fine-tune photosynthesis in plants. *Scientific Reports*, *9*, 8639. https://doi.org/10.1038/s41598-019-44972-z

Dyall, S. D., Brown, M. T., & Johnson, P. J. (2004). Ancient Invasions : From Endosymbionts to Organelles. *Science*, *304*(5668), 253-257. https://doi.org/10.1126/science.1094884

Eberhard, S., Finazzi, G., & Wollman, F.-A. (2008). The Dynamics of Photosynthesis. *Annual Review of Genetics*, *42*(1), 463-515. https://doi.org/10.1146/annurev.genet.42.110807.091452

Finazzi, G., Petroutsos, D., Tomizioli, M., Flori, S., Sautron, E., Villanova, V., Rolland, N., & Seigneurin-Berny, D. (2015). Ions channels/transporters and chloroplast regulation. *Cell Calcium*, *58*(1), 86-97. https://doi.org/10.1016/j.ceca.2014.10.002

Fuhrman, J. A., Schwalbach, M. S., & Stingl, U. (2008). Proteorhodopsins : An array of physiological roles? *Nature Reviews. Microbiology*, *6*(6), 488-494. https://doi.org/10.1038/nrmicro1893

Genty, B., Briantais, J. M., & Baker, N. R. (1989). The relationship between the quantum yield of photosynthetic electron transport and quenching of chlorophyll fluorescence. *Biochimica et Biophysica Acta - General Subjects*, *990*(1), 87-92. https://doi.org/10.1016/S0304-4165(89)80016-9

Goldschmidt-Clermont, M., & Bassi, R. (2015). Sharing light between two photosystems : Mechanism of state transitions. *Current Opinion in Plant Biology*, *25*, 71-78. https://doi.org/10.1016/j.pbi.2015.04.009

Hahn, A., Vonck, J., Mills, D. J., Meier, T., & Kühlbrandt, W. (2018). Structure, mechanism, and regulation of the chloroplast ATP synthase. *Science (New York, N.Y.)*, *360*(6389), eaat4318. https://doi.org/10.1126/science.aat4318

Hanada, S. (2016). Anoxygenic Photosynthesis -A Photochemical Reaction That Does Not Contribute to Oxygen Reproduction. *Microbes and Environments*, *31*(1), 1-3. https://doi.org/10.1264/jsme2.ME3101rh

Harris, E. H. (2009). *The Chlamydomonas Sourcebook—Volume 1 : Introduction to Chlamydomonas and Its Laboratory Use* (Vol. 1). Academic Press.

Holt, N. E., Fleming, G. R., & Niyogi, K. K. (2004). Toward an Understanding of the Mechanism of Nonphotochemical Quenching in Green Plants. *Biochemistry*, *43*(26), 8281-8289. https://doi.org/10.1021/bi0494020

Horton, P., Ruban, A. V., & Walters, R. G. (1996). REGULATION OF LIGHT HARVESTING IN GREEN PLANTS. *Annual Review of Plant Physiology and Plant Molecular Biology*, *47*, 655-684. https://doi.org/10.1146/annurev.arplant.47.1.655

Houille-Vernes, L., Rappaport, F., Wollman, F. A., Alric, J., & Johnson, X. (2011). Plastid terminal oxidase 2 (PTOX2) is the major oxidase involved in chlororespiration in Chlamydomonas. *Proceedings of the National Academy of Sciences of the United States of America*, *108*(51), 20820-20825. https://doi.org/10.1073/pnas.1110518109

Jans, F., Mignolet, E., Houyoux, P. A., Cardol, P., Ghysels, B., Cuiné, S., Cournac, L., Peltier, G., Remacle, C., & Franck, F. (2008). A type II NAD(P)H dehydrogenase mediates light-independent plastoquinone reduction in the chloroplast of Chlamydomonas. *Proceedings of the National Academy of Sciences of the United States of America*, *105*(51), 20546-20551. https://doi.org/10.1073/pnas.0806896105

Jarrige, D. (2019). *Deciphering the « OPR code » to further assess the physiological role of OPR proteins* [Phdthesis, Sorbonne Université]. https://tel.archives-ouvertes.fr/tel-03349187

Jarvis, P., & Soll, J. (2002). Toc, tic, and chloroplast protein import. *Biochimica Et Biophysica Acta*, *1590*(1-3), 177-189. https://doi.org/10.1016/s0167-4889(02)00176-3

Joliot, P., & Delosme, R. (1974). Flash-induced 519 nm absorption change in green algae. *Biochimica Et Biophysica Acta*, *357*(2), 267-284. https://doi.org/10.1016/0005-2728(74)90066-8

Joliot, P., & Johnson, G. N. (2011). Regulation of cyclic and linear electron flow in higher plants. *Proceedings of the National Academy of Sciences*, *108*(32), 13317-13322. https://doi.org/10.1073/pnas.1110189108

Joliot, P., & Joliot, A. (2008). Quantification of the electrochemical proton gradient and activation of ATP synthase in leaves. *Biochimica et Biophysica Acta (BBA) - Bioenergetics*, *1777*(7), 676-683. https://doi.org/10.1016/j.bbabio.2008.04.010

Junesch, U., & Gräber, P. (1987). Influence of the redox state and the activation of the chloroplast ATP synthase on proton-transport-coupled ATP synthesis/hydrolysis. *Biochimica et Biophysica Acta (BBA) - Bioenergetics*, *893*(2), 275-288. https://doi.org/2

Junge, W. (1970). The critical electric potential difference for photophosphorylation. Its relation to the chemiosmotic hypothesis and to the triggering requirements of the ATPase system. *European Journal of Biochemistry*, *14*(3), 582-592. https://doi.org/10.1111/j.1432-1033.1970.tb00327.x

Kramer, D. M., Cruz, J. A., & Kanazawa, A. (2003). Balancing the central roles of the thylakoid proton gradient. *Trends in Plant Science*, *8*(1), 27-32. https://doi.org/10.1016/S1360-1385(02)00010-9

Krieger-Liszkay, A., & Thomine, S. (2018). Importing Manganese into the Chloroplast : Many Membranes to Cross. *Molecular Plant*, *11*(9), 1109-1111. https://doi.org/10.1016/j.molp.2018.07.006

Kushkevych, I., Procházka, J., Gajdács, M., Rittmann, S. K.-M. R., & Vítězová, M. (2021). Molecular Physiology of Anaerobic Phototrophic Purple and Green Sulfur Bacteria. *International Journal of Molecular Sciences*, *22*(12), 6398. https://doi.org/10.3390/ijms22126398

Lane, N., Allen, J. F., & Martin, W. (2010). How did LUCA make a living? Chemiosmosis in the origin of life. *BioEssays: News and Reviews in Molecular, Cellular and Developmental Biology*, *32*(4), 271-280. https://doi.org/10.1002/bies.200900131

Lemaire, C., & Wollman, F. A. (1989a). The chloroplast ATP synthase in Chlamydomonas reinhardtii. I. Characterization of its nine constitutive subunits. *The Journal of Biological Chemistry*, *264*(17), 10228-10234.

Lemaire, C., & Wollman, F. A. (1989b). The chloroplast ATP synthase in Chlamydomonas reinhardtii. II. Biochemical studies on its biogenesis using mutants defective in photophosphorylation. *The Journal of Biological Chemistry*, *264*(17), 10235-10242.

Li, M., Svoboda, V., Davis, G., Kramer, D., Kunz, H.-H., & Kirchhoff, H. (2021). Impact of ion fluxes across thylakoid membranes on photosynthetic electron transport and photoprotection. *Nature Plants*, *7*(7), Art. 7. https://doi.org/10.1038/s41477-021-00947-5

Lyons, T. W., Reinhard, C. T., & Planavsky, N. J. (2014). The rise of oxygen in Earth's early ocean and atmosphere. *Nature*, *506*(7488), Art. 7488. https://doi.org/10.1038/nature13068

Lyu, H., & Lazár, D. (2022). Analyzing the effect of ion binding to the membrane-surface on regulating the light-induced transthylakoid electric potential (ΔΨm). *Frontiers in Plant Science*, *13*, 945675. https://doi.org/10.3389/fpls.2022.945675

Malnoë, A., Wang, F., Girard-Bascou, J., Wollman, F.-A., & de Vitry, C. (2014). Thylakoid FtsH Protease Contributes to Photosystem II and Cytochrome *b* $_6$*f* Remodeling in *Chlamydomonas reinhardtii* under Stress Conditions. *The Plant Cell*, *26*(1), 373-390. https://doi.org/10.1105/tpc.113.120113

Marchand, J., Heydarizadeh, P., Schoefs, B., & Spetea, C. (2018). Ion and metabolite transport in the chloroplast of algae : Lessons from land plants. *Cellular and Molecular Life Sciences*, *75*(12), 2153-2176. https://doi.org/10.1007/s00018-018-2793-0

Margulis, L. (1971). Symbiosis and evolution. *Scientific American*, *225*(2), 48-57. https://doi.org/10.1038/scientificamerican0871-48

Marin, B., M. Nowack, E. C., & Melkonian, M. (2005). A Plastid in the Making : Evidence for a Second Primary Endosymbiosis. *Protist*, *156*(4), 425-432. https://doi.org/10.1016/j.protis.2005.09.001

Martin, W. F., Bryant, D. A., & Beatty, J. T. (2018). A physiological perspective on the origin and evolution of photosynthesis. *FEMS Microbiology Reviews*, *42*(2), 205-231. https://doi.org/10.1093/femsre/fux056

Melo, A. M. P., Bandeiras, T. M., & Teixeira, M. (2004). New Insights into Type II NAD (P) H : Quinone Oxidoreductases New Insights into Type II NAD (P) H : Quinone Oxidoreductases. *Microbiology and Molecular Biology Reviews*, *68*(4), 603-616. https://doi.org/10.1128/MMBR.68.4.603

Mitchell, P. (1966). Chemiosmotic coupling in oxidative and photosynthetic phosphorylation. *Biological Reviews of the Cambridge Philosophical Society*, *41*(3), 445-502. https://doi.org/10.1111/j.1469-185x.1966.tb01501.x

Nickelsen, J., & Kück, U. (2000). The unicellular green alga Chlamydomonas reinhardtii as an experimental system to study chloroplast RNA metabolism. *Die Naturwissenschaften*, *87*(3), 97-107. https://doi.org/10.1007/s001140050686

Nishio, J. N., & Whitmarsh, J. (1993). Dissipation of the Proton Electrochemical Potential in Intact Chloroplasts (II. The pH Gradient Monitored by Cytochrome f Reduction Kinetics). *Plant Physiology*, *101*(1), 89-96. https://doi.org/10.1104/pp.101.1.89

Peltier, G., Aro, E.-M., & Shikanai, T. (2016). NDH-1 and NDH-2 Plastoquinone Reductases in Oxygenic Photosynthesis. *Annual Review of Plant Biology*, *67*(1), 55-80. https://doi.org/10.1146/annurev-arplant-043014-114752

Ponce-Toledo, R. I., López-García, P., & Moreira, D. (2019). Horizontal and endosymbiotic gene transfer in early plastid evolution. *The New Phytologist*, *224*(2), 618-624. https://doi.org/10.1111/nph.15965

Rumberg, B., & Siggel, U. (1969). PH changes in the inner phase of the thylakoids during photosynthesis. *Die Naturwissenschaften*, *56*(3), 130-132. https://doi.org/10.1007/BF00601025

Rutherford, A. W., Osyczka, A., & Rappaport, F. (2012). Back-reactions, short-circuits, leaks and other energy wasteful reactions in biological electron transfer : Redox tuning to survive life in O2. *FEBS Letters*, *586*(5), 603-616. https://doi.org/10.1016/j.febslet.2011.12.039

Saier, M. H., Jr, Yen, M. R., Noto, K., Tamang, D. G., & Elkan, C. (2009). The Transporter Classification Database : Recent advances. *Nucleic Acids Research*, *37*(suppl_1), D274-D278. https://doi.org/10.1093/nar/gkn862

Sanchez-Baracaldo, P., & Cardona, T. (2019). On the origin of oxygenic photosynthesis and Cyanobacteria. *The New Phytologist*, *225*(4), 1440-1446. https://doi.org/10.1111/nph.16249

Schmidt, S. B., Eisenhut, M., & Schneider, A. (2020). Chloroplast Transition Metal Regulation for Efficient Photosynthesis. *Trends in Plant Science*, *25*(8), 817-828. https://doi.org/10.1016/j.tplants.2020.03.003

Schmidt, S. B., Jensen, P. E., & Husted, S. (2016). Manganese Deficiency in Plants : The Impact on Photosystem II. *Trends in Plant Science*, *21*(7), 622-632. https://doi.org/10.1016/j.tplants.2016.03.001

Schönknecht, G., Hedrich, R., Junge, W., & Raschke, K. (1988). A voltage-dependent chloride channel in the photosynthetic membrane of a higher plant. *Nature*, *336*(6199), Art. 6199. https://doi.org/10.1038/336589a0

Shen, J.-R. (2015). The Structure of Photosystem II and the Mechanism of Water Oxidation in Photosynthesis. *Annual Review of Plant Biology*, *66*(1), 23-48. https://doi.org/10.1146/annurev-arplant-050312-120129

Sousa, F. L., Thiergart, T., Landan, G., Nelson-Sathi, S., Pereira, I. A. C., Allen, J. F., Lane, N., & Martin, W. F. (2013). Early bioenergetic evolution. *Philosophical Transactions of the*

Royal Society of London. Series B, Biological Sciences, *368*(1622), 20130088. https://doi.org/10.1098/rstb.2013.0088

Spetea, C., Herdean, A., Allorent, G., Carraretto, L., Finazzi, G., & Szabo, I. (2017). An update on the regulation of photosynthesis by thylakoid ion channels and transporters in Arabidopsis. *Physiologia Plantarum*, *161*(1), 16-27. https://doi.org/10.1111/ppl.12568

Spetea, C., & Schoefs, B. (2010). Solute transporters in plant thylakoid membranes : Key players during photosynthesis and light stress. *Communicative & Integrative Biology*, *3*(2), 122-129. https://doi.org/10.4161/cib.3.2.10909

Strand, D. D., Fisher, N., & Kramer, D. M. (2017). The higher plant plastid NAD(P)H dehydrogenase-like complex (NDH) is a high efficiency proton pump that increases ATP production by cyclic electron flow. *Journal of Biological Chemistry*, *292*(28), 11850-11860. https://doi.org/10.1074/jbc.M116.770792

Szabò, I., & Spetea, C. (2017). Impact of the ion transportome of chloroplasts on the optimization of photosynthesis. *Journal of Experimental Botany*, *68*(12), 3115-3128. https://doi.org/10.1093/jxb/erx063

Tester, M., & Blatt, M. R. (1989). Direct Measurement of K+ Channels in Thylakoid Membranes by Incorporation of Vesicles into Planar Lipid Bilayers 1. *Plant Physiology*, *91*(1), 249-252. https://doi.org/10.1104/pp.91.1.249

Uflewski, M., Mielke, S., Correa Galvis, V., von Bismarck, T., Chen, X., Tietz, E., Ruß, J., Luzarowski, M., Sokolowska, E., Skirycz, A., Eirich, J., Finkemeier, I., Schöttler, M. A., & Armbruster, U. (2021). Functional characterization of proton antiport regulation in the thylakoid membrane. *Plant Physiology*, *187*(4), 2209-2229. https://doi.org/10.1093/plphys/kiab135

Voon, C. P., & Lim, B. L. (2019). ATP translocation and chloroplast biology. *National Science Review*, *6*(6), 1073-1076. https://doi.org/10.1093/nsr/nwz089

Witt, H. T. (1979). Energy conversion in the functional membrane of photosynthesis. Analysis by light pulse and electric pulse methods. The central role of the electric field. *Biochimica Et Biophysica Acta*, *505*(3-4), 355-427. https://doi.org/10.1016/0304-4173(79)90008-9

Wollman, F.-A., & Girard-Bascou, J. (1994). *Une algue pour l'étude de la génétique des organites : Chlamydomonas reinhardtii*. *10*(11), 14.

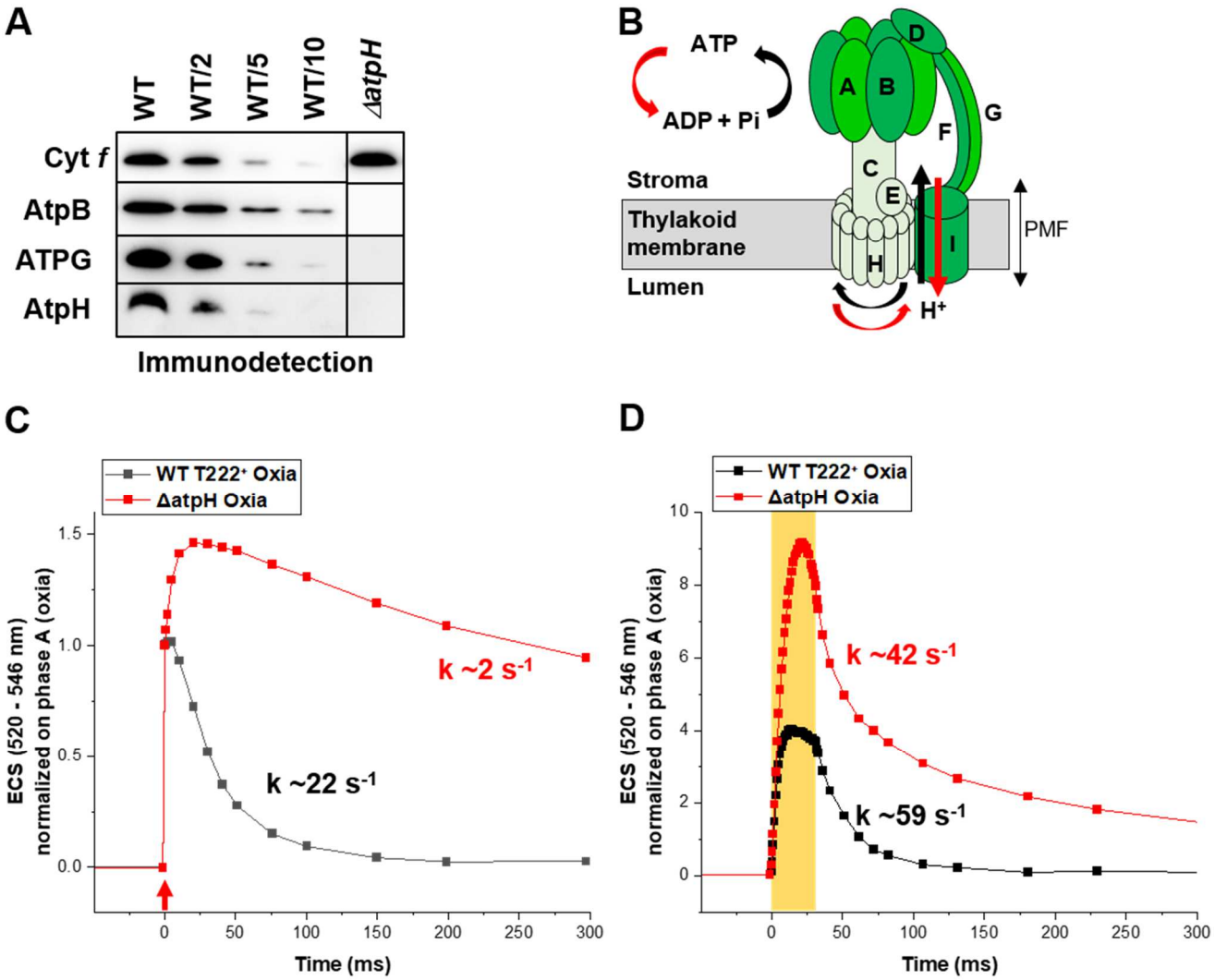

Figure 1: An alternative pathway to dissipate PMF across the thylakoid in the absence of CF_1F_O ATPase/synthase. (A) Pleiotropic loss of chloroplast (CF_1F_O) ATPase subunits in the *ΔatpH* mutant. Wild-type (WT) and *ΔatpH* mutant thylakoid membrane extracts were probed with antibodies against ATPase subunits (AtpB, ATPG and AtpH) and cytochrome *f* (Cyt *f*, as loading control). (B) Schematic structure of chloroplast (CF_1F_O) ATPase complex with rotor (in light green) and stator (in dark green). CF_1F_O catalyzes both ATP synthesis (black arrows) and ATP hydrolysis (red arrows) as a function of the transmembrane proton motive force (PMF, black two-headed arrow) and the ration [ATP]/[ADP][P]. (C-D) Light-induced ECS kinetics (520–546 nm) after a single turnover saturating flash (C, red arrow) and after a 30 ms saturating pulse (D, yellow box) in WT T222$^+$ (black) and *ΔatpH* mutant (red) under oxic conditions. The rate constant of the fast phase of ECS decay (positive charges PS^{-1} s^{-1}) is indicated next to each ECS kinetics.

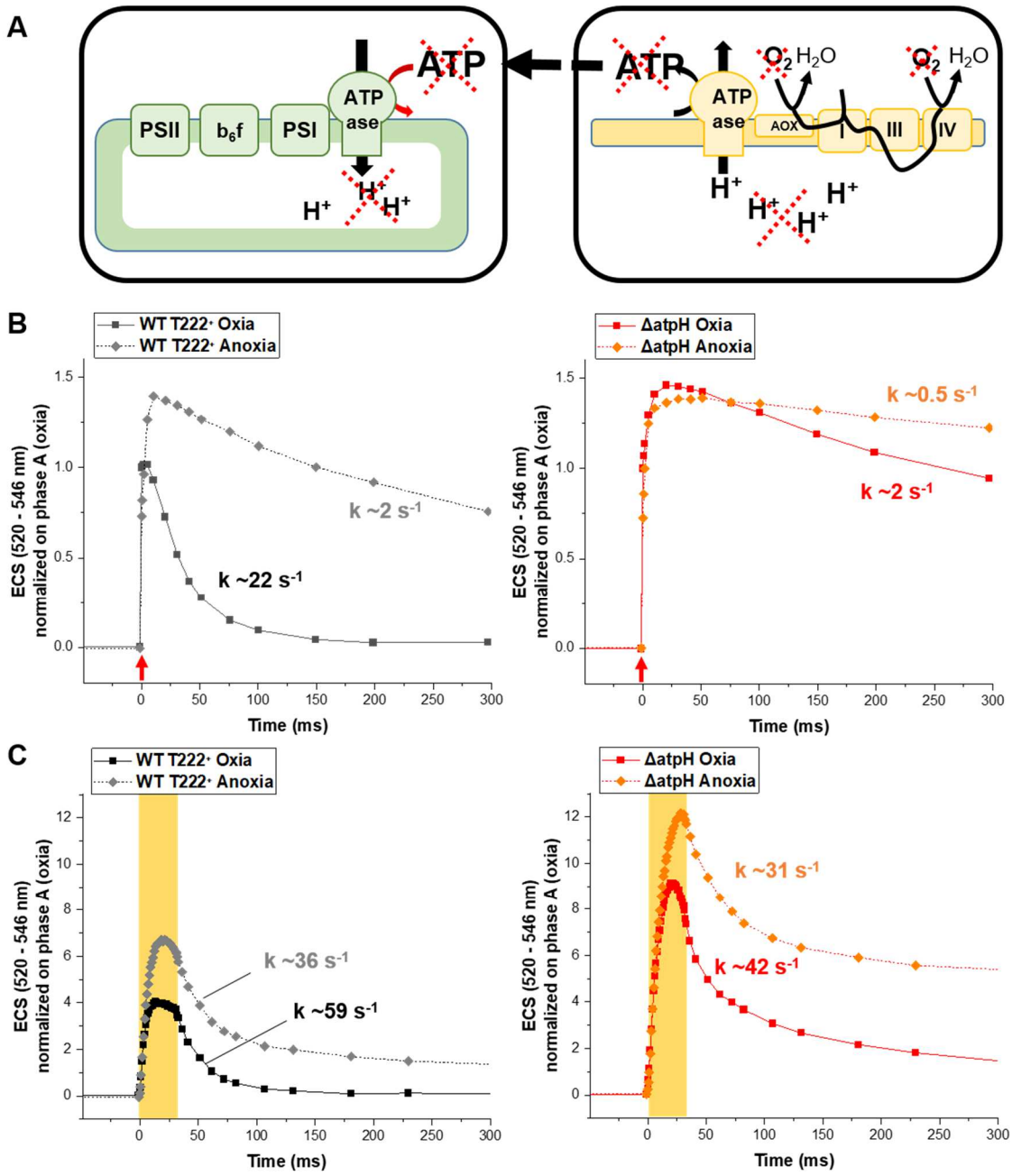

Figure 2: Maximum and dark PMF in the CF_1F_O ATPase mutant and the WT.

(A) Tested model of energetic interactions between mitochondria (right) and chloroplast (left) in WT *C. reinhardtii* in the dark. The red crosses represent the effect of anoxia: the lack of oxygen stops the respiratory electron transfer and the production of PMF in the mitochondrion, which in turn stop the production of ATP, its export to the chloroplast and its hydrolysis by CF_1F_O. Thin black arrows: respiratory electron flow in oxia. Thick black arrow: ATP synthesis/hydrolysis by chloroplastic and mitochondrial ATPases. Black dotted line: putative ATP/ADP exchange pathway between organelles. ATPase, ATPase/synthase; PSI, photosystem I; PSII, photosystem II; b_6f, cytochrome b_6f; I/III/IV, respiratory complexes I, III and IV); AOX, alternative oxidase. (B) ECS kinetics induced by a single turnover flash (red arrow) in WT (black for oxia, gray for anoxia) and *ΔatpH* mutant (red for oxia, orange for anoxia). (C) ECS kinetic induced by illumination with a 30 ms long saturating pulse (yellow box) in WT (black for oxia, gray for anoxia) and *ΔatpH* mutant (red for oxia, orange for anoxia). A representative sample shown. Rate constant of decay (charges PS^{-1} s^{-1}) is shown next to each ECS kinetics.

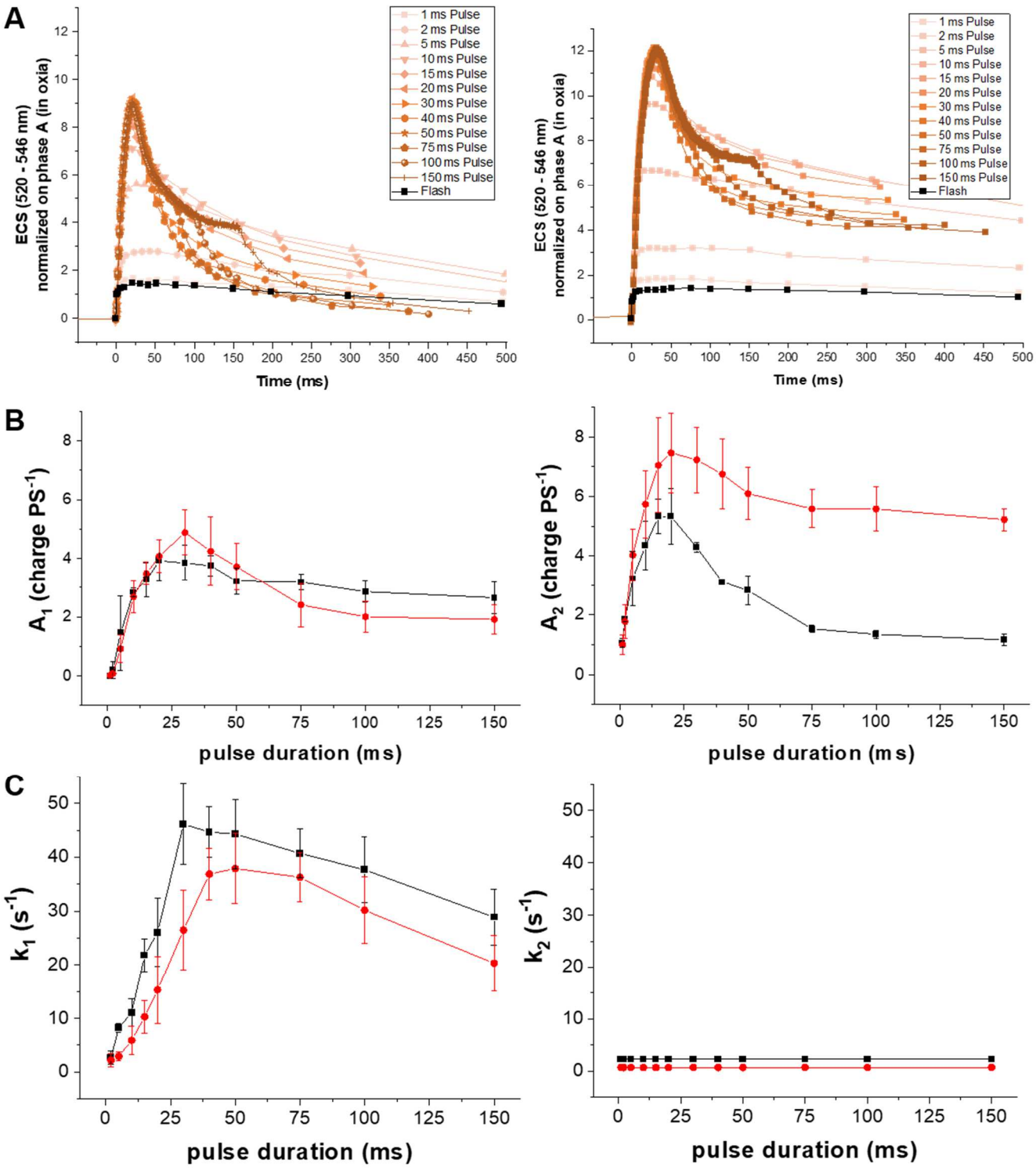

Figure 3: Maximum rate of the alternative pathway from analysis of ECS kinetics induced by pulses of different durations.

(A) ECS kinetics of *ΔatpH* mutant exposed to high light pulses of 1-150 ms or single turnover flash (black curve) in oxia (left panel) and anoxia (right panel). The experimental post-illumination ECS decays are shown as a scatter while the lines represent the extrapolation of the data with a bi-exponential decay function ($y = A_1.e^{(-k1.t)} + A_2.e^{(-k2.t)} + y_0$), where y_0 is the offset, A_1 and A_2 are the amplitudes of the fast and slow phases, respectively and k_1 and k_2 are the rate constants of the fast and slow phases, respectively. Such extrapolations, where the same t_2 value was shared for all curves, gave very good agreement with experimental data with $R^2 > 0.99$ for all fits (see Supplementary Fig 2 and 3). (B) Amplitudes of the fast phase (A_1, left) of the bi-exponential decay, representing the alternative pathway, and of the slow phase (A_2, right) in oxia (black) and anoxia (red). (C) Rate constants of the fast phase (k_1, left) and slow phase (k_2, right, shared between all curves within one condition) in oxia (black) and anoxia (red). Error bars are standard deviation; n≥ 3.

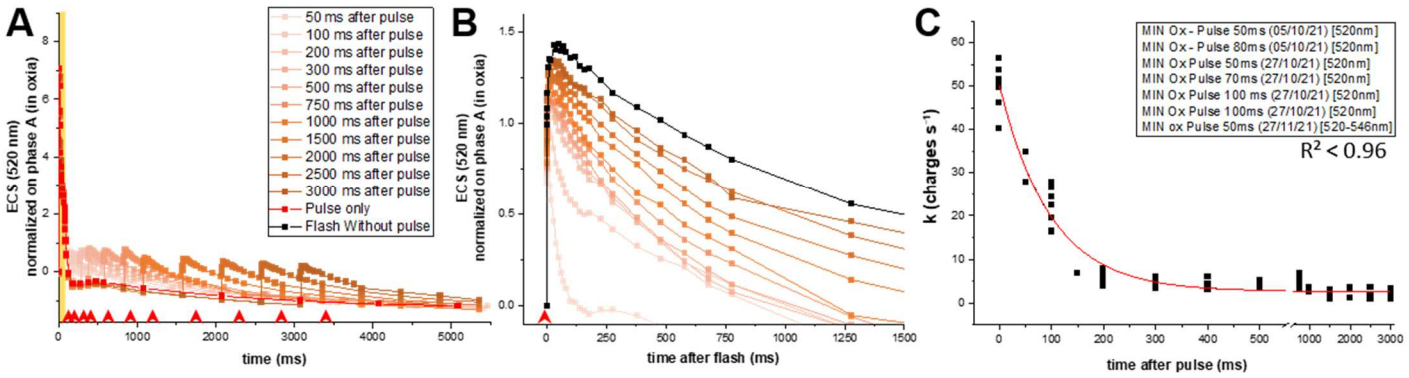

Figure 4: The alternative dissipation pathway turns off in hundreds of ms.
(A) ECS kinetics of *ΔatpH* exposed to an 80 ms pulse (yellow box) followed by a single turnover flash (red arrows) 50-3000 ms after the end of the pulse. Experiments have been carried out in oxia in minimum medium. (B) Each ECS kinetics was then shifted so that the origin was at the time the flash fired. ECS decays from experiment shown in (A) were fitted with a bi-exponential function for each flash. (C) The decay rates of the fast phase were plotted against the time between the pulse and the flash. A mono-exponential function was used to fit the data (n=7).

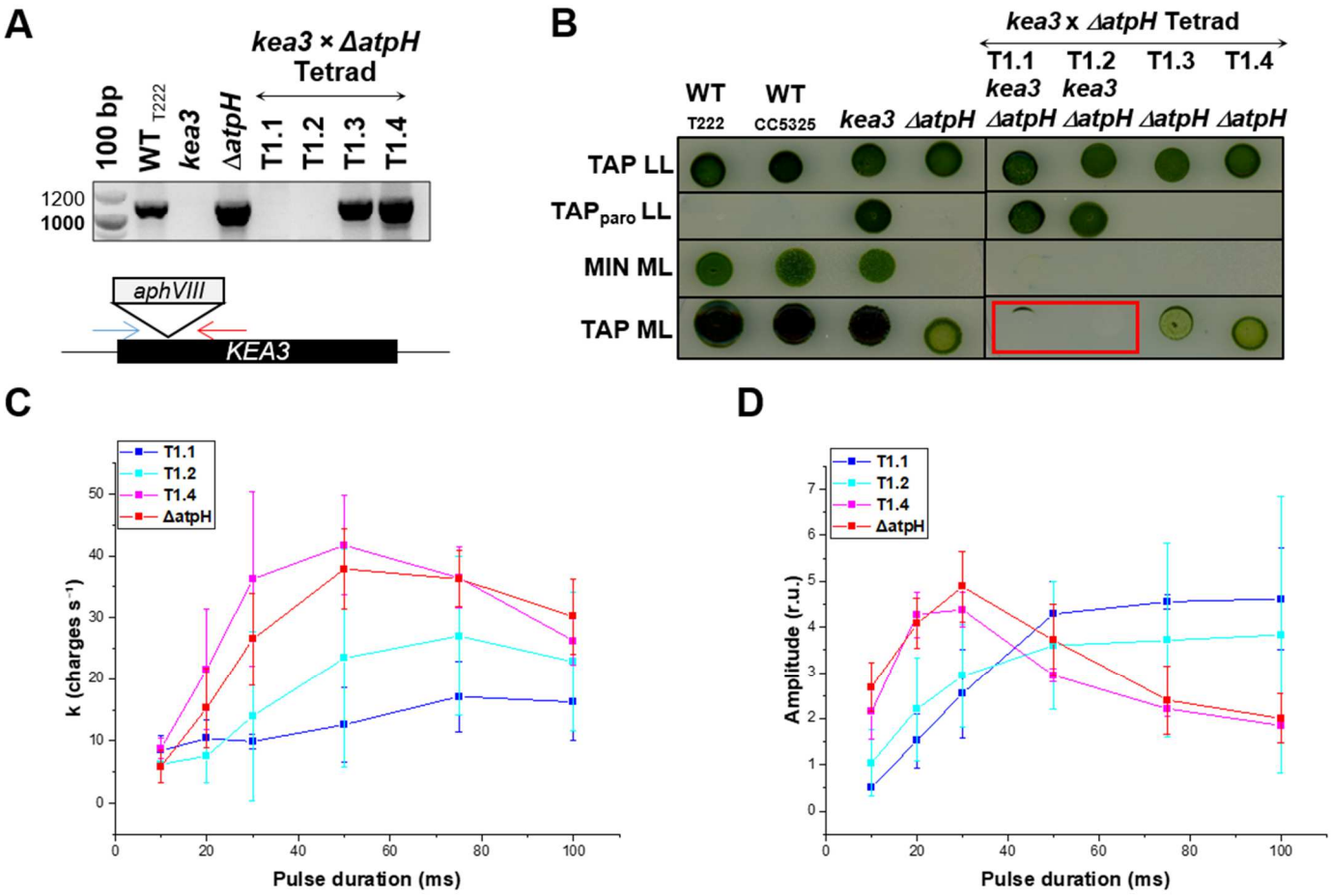

Figure 5: KEA3 is not strictly required but regulates the alternative PMF dissipation in the absence of chloroplast CF_1F_O ATPase.

Genotyping of a tetrad resulting from the crossing of the nuclear insertion mutant *kea3* (mating type -) and the chloroplast mutant *ΔatpH* (mating type +) and isolation of the double mutants *kea3* {*ΔatpH*}. (A) PCR analysis and model of the PCR product of the KEA3 locus (1115 bp). The presence of bands corresponds to the wild-type allele and the absence to the insertion of the paromomycin resistance cassette (aphVIII) with a 2:2 Mendelian tetrad segregation. Forward (blue) and reverse (red) primers are shown in the model. (B) Growth and photosensitivity assay on the single *ΔatpH* mutant, the single *kea3* mutant, their respective wild-types, T222 and CC5325, and tetrad progeny. 2:2 Mendelian tetrad segregation of nuclear *kea3* mutation allowed growth in the presence of paramomycin conferred via the insertion of the aphVIII cassette (TAP_{paro} LL); uniparental mt^+ transmission of chloroplast *ΔatpH* mutation to all tetrad progeny prevented growth on minimal medium (MIN ML). All strains grew on medium containing acetate under low light (6 µmol photons m^{-2} s^{-1}, TAP LL) but growth of double *kea3 ΔatpH* mutants (red framed) were very affected under medium light (30 µmol photons m^{-2} s^{-1}, TAP ML). (C-D) Fast phase analysis of ECS decay as a function of the high light pulse duration (protocol as in **Fig. 3** anoxia). The rate constant k (C) and amplitude (D) of the fast phase were measured under anaerobic conditions. Error bars are standard deviation; n ≥ 3.

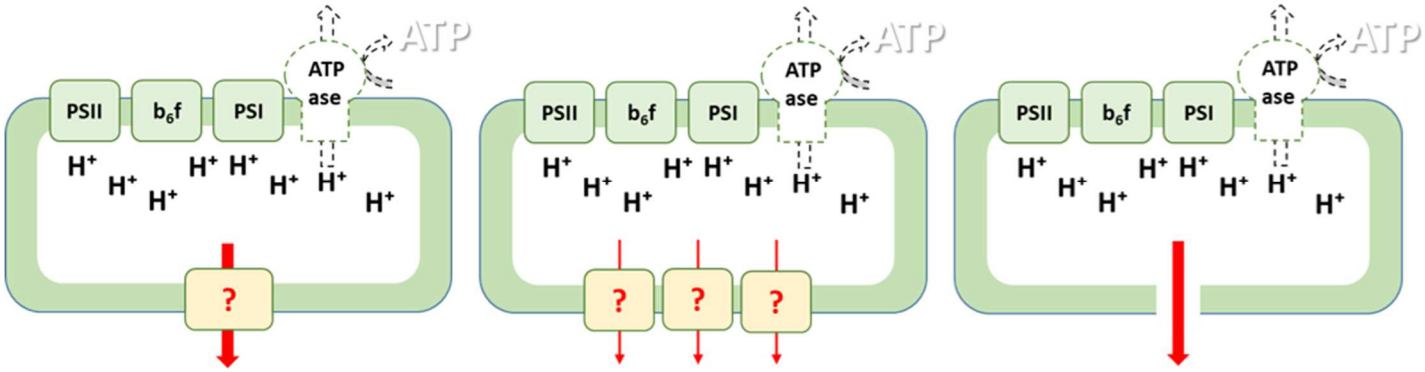

Figure 6: Molecular model for the alternative dissipation pathway.
In the absence of CF_1F_O ATPase/synthase, protons or other charges may be expelled from thylakoid lumen by one single actor (left panel), by a variety of different ion channels acting in synergy (middle panel) or through a non-enzymatic leak of ions or protons determined by the intrinsic electric permeability of the lipid bilayer (right panel).

SUPPLEMENTAL FIGURES

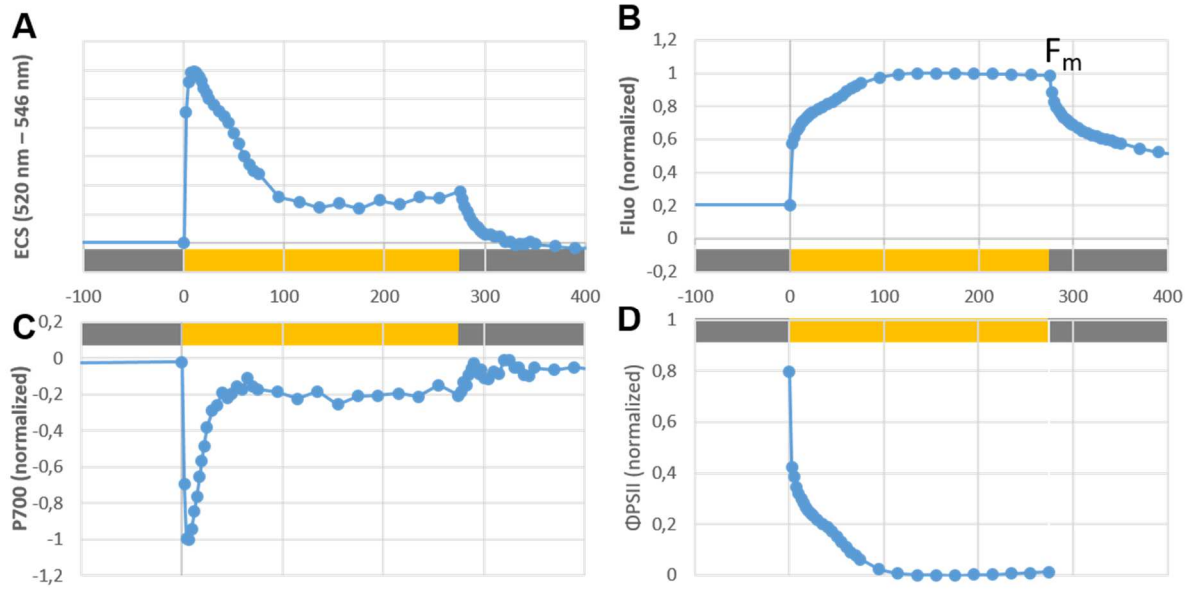

Supplementary Figure 1. Evolution of photochemistry and transthylakoid electric field during high light pulses.
ECS (A), chlorophyll fluorescence (B) and P700 (C) were followed (see Methods) during a 275 ms pulse of high light. (D) Photochemical yield of PSII was calculated from fluorescence values in (B) considering Fm as the asymptotic fluorescence value at the end of the high light pulse.

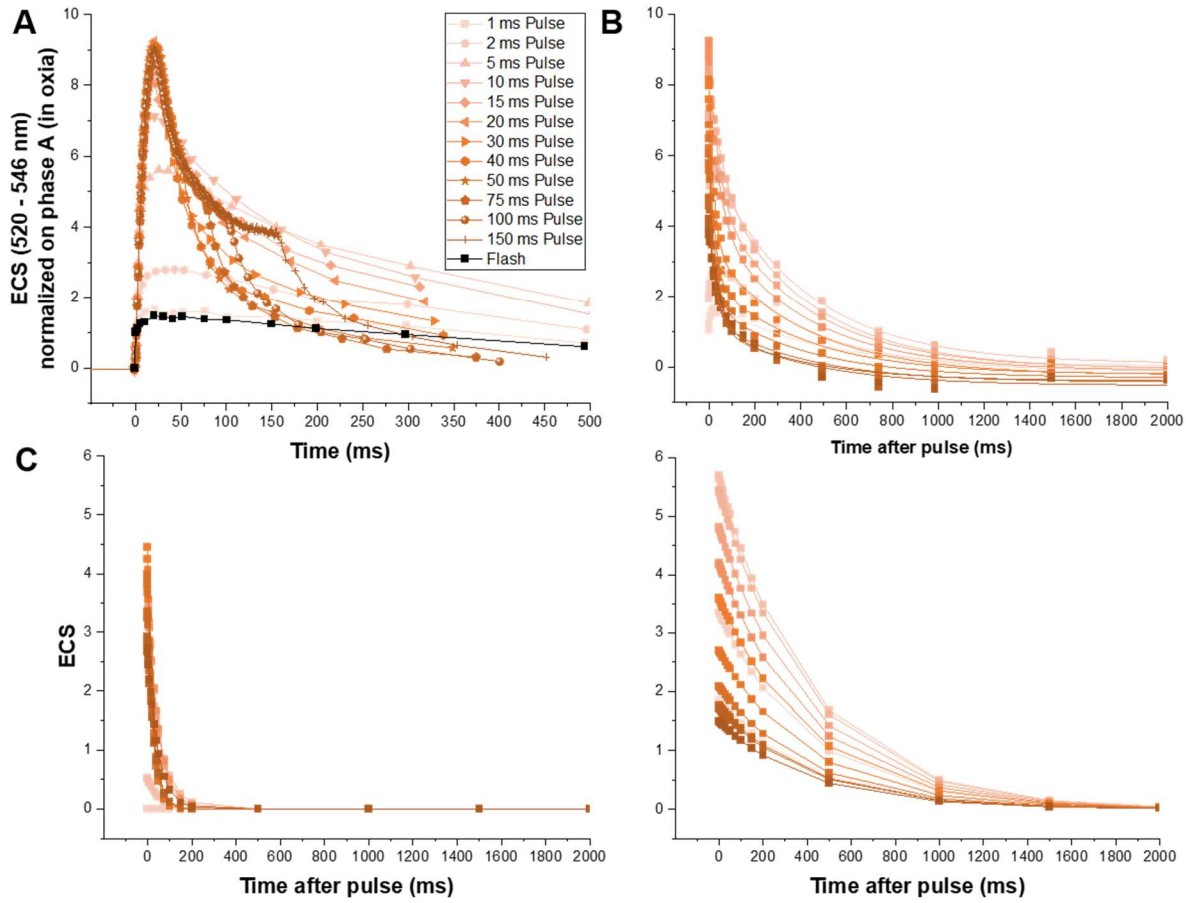

Supplementary Figure 2: Probing the PMF dependency on light pulse duration in oxia.
(A) ECS kinetics of *ΔatpH* mutant exposed pulses 1 to 150 ms long and to a single turnover flash under oxic conditions. (B) The experimental data of post-illumination ECS decays were plotted (scatter) and mathematically fitted (line) with a bi-exponential decay function $y = A_1.e^{(-k1.t)} + A_2.e^{(-k2.t)} + y_0$ with $R^2 > 0{,}99$ for all fits. Because of the homothetic decay of the slow phase, k_2 was shared for all fits. (C) Fast (left panel) and slow (right panel) phase reconstitution for each pulse duration, calculated from parameters obtained from the fits in (B).

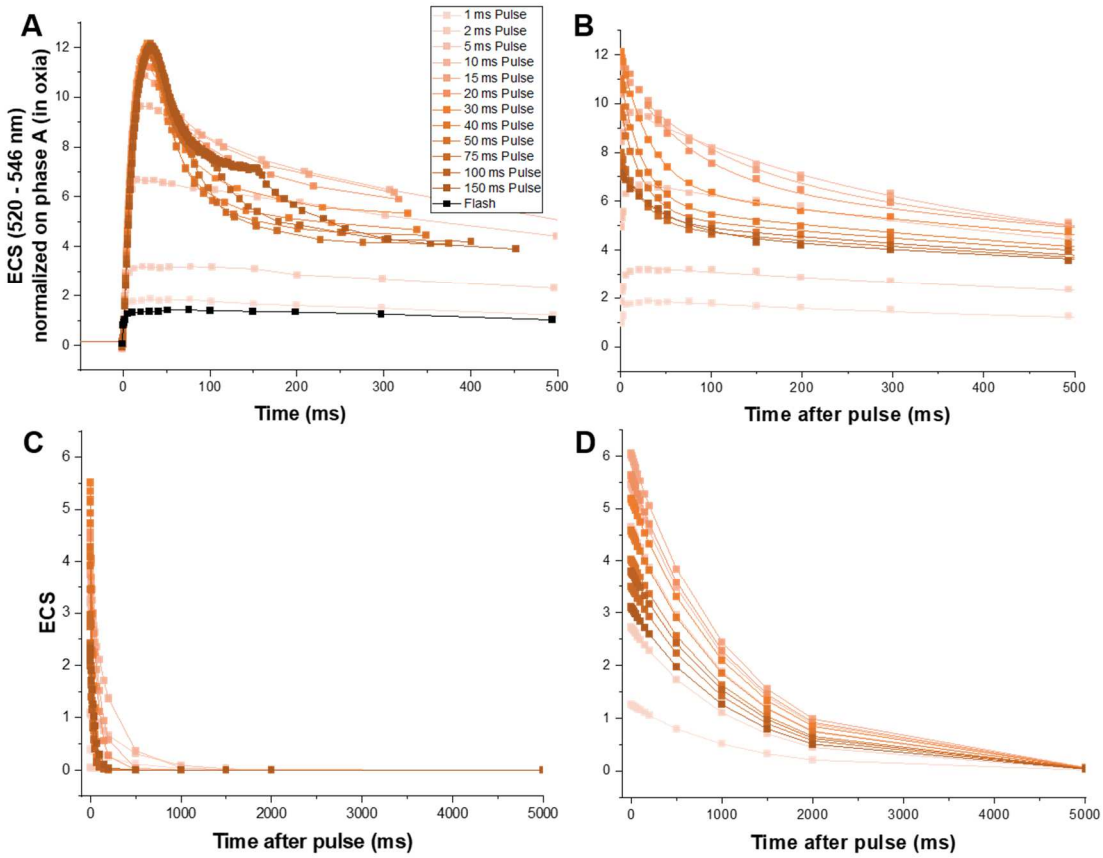

Supplementary Figure 3: Probing the PMF dependency on light pulse duration in anoxia.

(A) ECS kinetics of *ΔatpH* mutant exposed pulses 1 to 150 ms long and to a single turnover flash under anoxic conditions. (B) The experimental data of post-illumination ECS decays were plotted (scatter) and mathematically fitted (line) with a bi-exponential decay function $y = A_1.e^{(-k1.t)} + A_2.e^{(-k2.t)} + y_0$ with $R^2 > 0{,}99$ for all fits. Because of the homothetic decay of the slow phase, k_2 was shared for all fits. (C-D) Fast (C) and slow (D) phase reconstitution for each pulse duration, calculated from parameters obtained from the fits in (B).

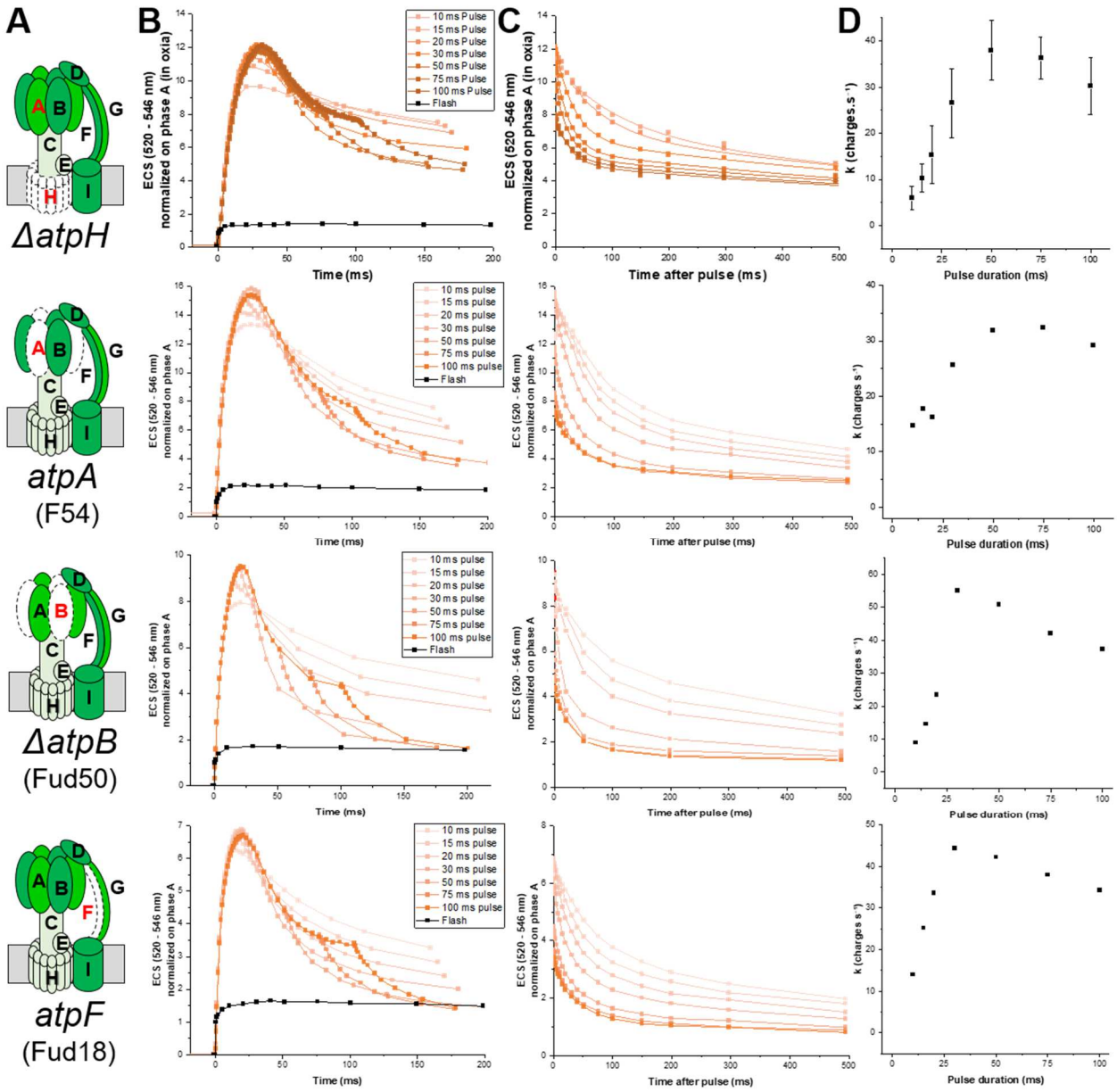

Supplementary Figure 4: Alternative PMF dissipation in different CF_1F_O mutants.

(A) Model of CF_1F_O showing the affected subunit (white and dashed) in the mutant. Note that if one subunit is absent, the complex does not assemble due to concerted accumulation. From top to bottom: *ΔatpH* as shown in **Fig.3**; *F54* affected in *TDAI*, translation factor of *atpA*; *Fud50*, harboring a deletion in the chloroplastic *atpB* gene; *Fud18*, altered in the chloroplastic *atpF* gene. (B) ECS kinetics of the CF_1F_O mutants exposed to 10-100 ms long pulses (oranges gradient) and single turnover flash (black) in strongly reduced conditions (anoxia). (C) Post-illumination ECS decays kinetics of the 4 CF_1F_O mutants after pulses from 10-100 ms. (D) fast phase decay rates were plotted from fits with a bi-exponential decay function of post-illumination ECS decays.

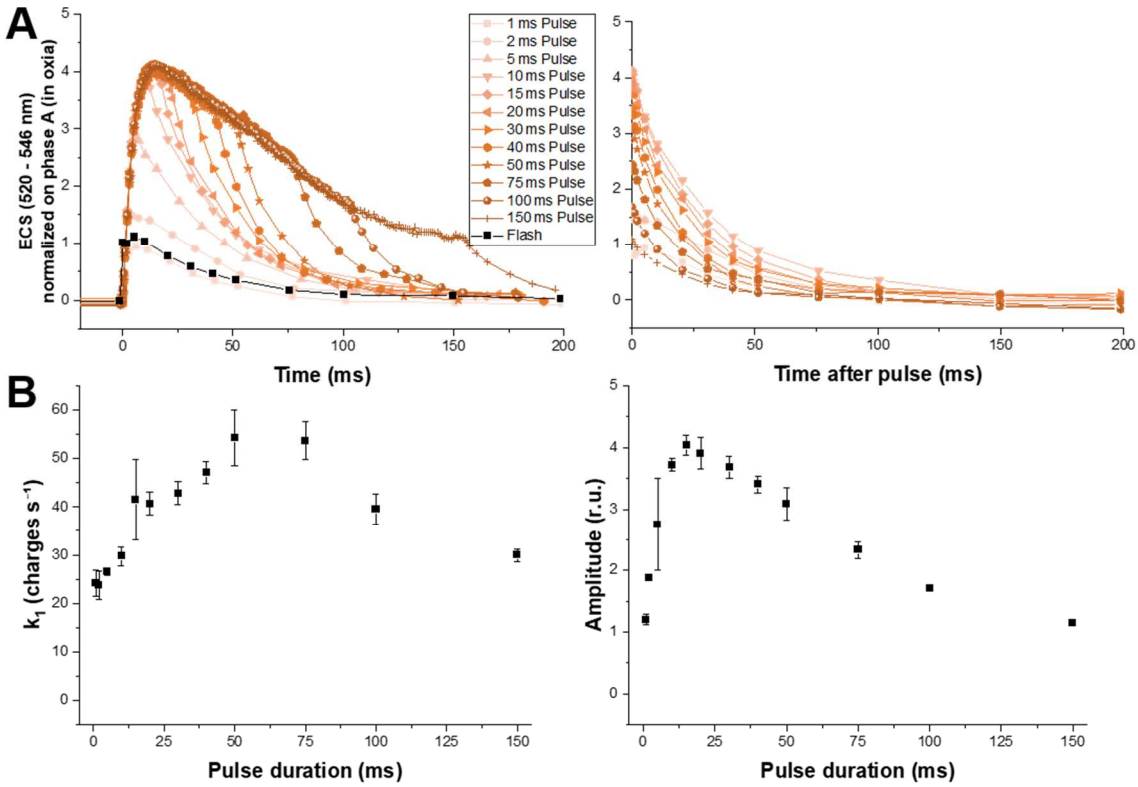

Supplementary Figure 5: Probing the CF_1F_O activation upon high light pulses of different duration in the WT, under oxic conditions.

(A) ECS kinetics of WT exposed to high light pulses of different durations (from 1 to 150 ms) and single turnover flash (left panel) and post-illumination ECS decays (right panel). (B) Parameters obtained through mathematical fit of experimental data shown in (A) with a mono-exponential decay function ($y = A_1.e^{(-k1.t)} + y_0$) with $R^2 > 0{,}99$ for all fits. Left and right panels show respectively constant rate (k_1), and amplitude (A_1). Error bars are standard deviation. n≥ 3.

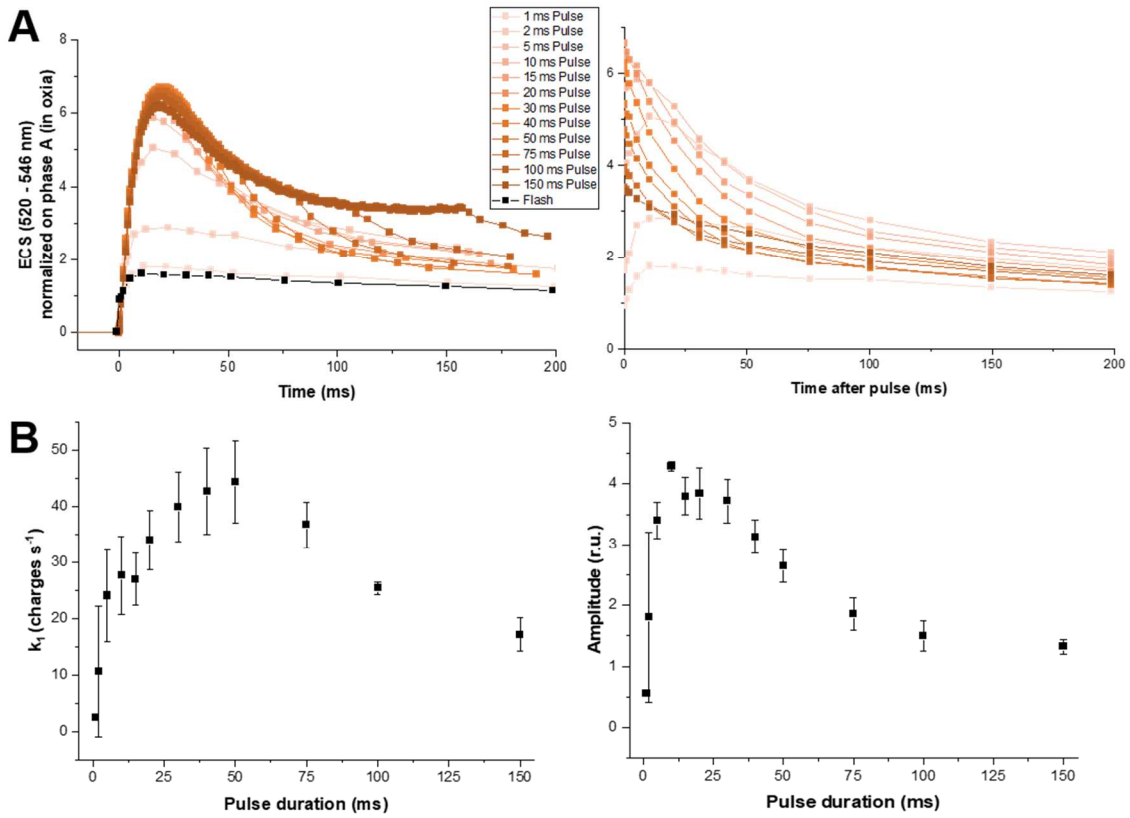

Supplementary Figure 6: Probing the CF_1F_O activation upon high light pulses of different duration in the WT, under anoxic conditions. (A) ECS kinetics of WT exposed to high light pulses of different durations (from 1 to 150 ms) and single turnover flash (left panel) and post-illumination ECS decays (right panel). (B) Parameters obtained through mathematical fit of experimental data shown in (A) with a bi-exponential decay function $y = A_1.e^{(-k1.t)} + A_2.e^{(-k2.t)} + y_0$ with $R^2 > 0{,}99$ for all fits. Left and right panels show respectively constant rate (k_1) and amplitude (A_1) of the fast phase.

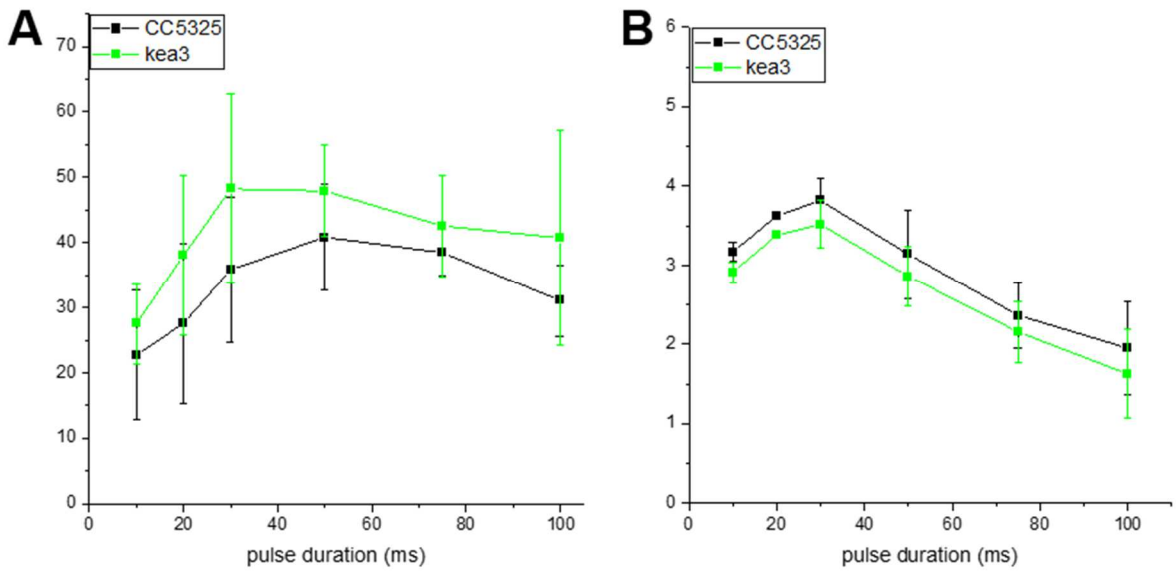

Supplementary Figure 7: Kinetics of ECS decay in the CC5325 and *kea3* mutant.
Constant rate (left panel) and amplitude (right panel) from the mathematical analysis of the ECS decay kinetics of CC5325 (black) and *kea3* mutant (green), exposed to high light pulses of different durations (from 10 to 100 ms) in anoxia. Same analysis as in **Figure 3** anoxia and **Supplementary Figure 6**. Error bars are standard deviation; n ≥ 3.

CONCLUSIONS AND PERSPECTIVES

Ions are critical for all biological processes, and photosynthesis does not break that rule. Every turning point of photosynthetic processes in the thylakoid needs a certain ion to work properly. Yet, the network of chloroplastic ion transport is still poorly known, with many new transporters and their impact on photosynthesis being progressively uncovered (Finazzi et al., 2015; Spetea et al., 2017; Marchand et al., 2018; Li et al., 2021). And for sure, it is quite a struggle to identify the transporters in the chloroplast as photosynthesis is an intricate and complex set of mechanisms, thus, any minor tinkering may greatly impair the whole process. The work presented in this thesis provides precious and novel insights into the regulation of photosynthetic efficiency in view of these ions.

THE MUTANT CGLD1:

A USEFUL CHASSIS FOR MN-RELATED IMPORT AND PHOTOSYNTHETIC PROCESSES.

Our leading question concerned Mn^{2+} delivery and its limitation effect on PSII. In the second chapter of this thesis, the *cgld1-KD* mutant enabled us to demonstrate that, even without the main transporter of Mn^{2+} into the thylakoid, a basal import of Mn^{2+} is present, as the mutant is still able to produce some oxygen under illumination, and our fluorescence data demonstrate PSII activity, although less efficient than in WT. A model accounting for the heterogeneity of Mn-clusters in this strain is proposed. The fluorescence of PSII is a remarkable tool to assess the activity of PSII *in vivo* in different conditions, and it enabled us to show how much time it takes to restore a WT-like PSII activity by supplementing the mutant strain with Mn. From our fluorescence data, it is possible to determine how much of PSII centers are impacted, and we could use this strain to assess the question of the recovery of the altered fraction over a period of Mn^{2+} supplementation or, on the contrary, assess its loss during Mn starvation. This could also become a very useful setup to understand the alternative pathway of Mn intake into the thylakoid by comparing WT and *cgld1* mutant in conditions where we vary the available quantity of Mn and monitor the changes in PSII activity over time; also, we can use the *cgld1* mutant as a chassis for multiple mutagenesis to investigate whether our

hypothesis for Mn^{2+} metallochaperones to be Mn^{2+} carriers is valid, or to investigate the nature of another bivalent cation transporter as was previously suggested. This mutant may also prove a useful tool to deepen our understanding of electron transfer and back-reactions in limited PSII donor side-limited conditions.

ATPase and OPR code unraveling:

A step into deepening the understanding of biogenesis.

In the third chapter, we gained substantial insight in the understanding of CF_1F_O biogenesis. We were able to create the last missing ATP synthase/ase mutant: *atpG-KO* was obtained by CRISPR-Cas9 technology and can be used as a tool, by mutating *atpF* and/or *ATPG* genes, to further investigate the potential spring properties of the peripheral stalks as proposed in (Hahn et al, 2018). Furthermore, this work enabled us to understand that both atpF and ATPG are required for CF_1F_O assembly. But this raises the question of what differs in the CF_1F_O structures of *Chlamydomonas* and green lineage that could explain this heterodimer requirement while cyanobacteria peripheral stalk comprises only homodimers. These *atpF* and *atpG* mutants are also an opportunity to understand these differences. Complementation with modified *atpF* and *ATPG* genes could give some insight to understand the evolutionary differences between homodimers and these heterodimers that led to their differentiation and inter-dependency for CF_1F_O assembly.

Moreover, the MDE1 OPR protein enabled us to deepen our understanding of the OPR code and function, contributing to crack the code. The 5'UTR of *atpE* could be modified to verify our hypothesis that MDE1 protects *atpE* transcripts against 5' to 3' exonuclease activity.

CREATION OF AN AMAZINGLY POWERFUL TOOL TO ASSESS PMF REGULATORS IN THE THYLAKOID.

In the last chapter of this thesis, we were able to develop a biological setup that enabled us to validate and assert some questions left unanswered in previous studies, such as the hypothesis for a leak of protons through the CF_1F_O upon excessive PMF.

The leading interrogation was to understand what happened to PMF when CF_1F_O was absent or impaired. This work reveals an alternative mode of PMF dissipation in the absence of chloroplast ATPase, which could be a photoprotective mechanism under physiological conditions where CF_1F_O activity is impaired. Yet, the existence of a proton leak through CF_1F_O leads to wonder of the particular physiological significance of this additional and alternative dissipation pathway. One would think that when CF_1F_O is impaired, its leaking property would still be a security valve, making the existence of this alternative pathway evolutionary dispensable. As this alternative pathway is also present in *Chlorella* (data not shown), I expect this mechanism to be conserved at least in green algae, and possibly also in other photosynthetic organisms. The identification of the molecular actors in the model organism *Chlamydomonas* would be useful to assess their conservation thanks to genomic comparisons. Mutants impaired in chloroplast ATP synthase/ase in other groups of photosynthetic organisms, like in diatom, will be of great interest to determine whether these organisms also show an alternative pathway of PMF dissipation.

The *ΔatpH* CF_1F_O mutant lacking the CF_O ring proved to be an incredibly powerful tool to investigate the different ion transporters' contribution to PMF regulation or control. Indeed, more and more chloroplast or thylakoid ion transporters are being identified in particular through genomic, proteomic and structural studies and comparisons in various photosynthetic species and lineages.

Additionally, the lab now possesses a variety of mutants from the CLIP library affecting such transporters. Creating double mutants, would be a good opportunity to assess the effect of each transporter on PMF, either by crossing them (what we did to obtain our *kea3 ΔatpH* double mutant), by introducing *ΔatpH* mutation in other transporter mutants, or by mutating other transporters genes by CRISPR-Cas9 targeted mutagenesis (as used for the *atpG-KO* mutant in chapter 3) in a *ΔatpH* context. The characterization of mutant combinations should allow us in the future to learn more about the nature of this mysterious alternative valve.